Cooling of the Building Structure by Night-time Ventilation

Artmann, Nikolai

Publication date:
2009

Document Version
Publisher's PDF, also known as Version of record

Cooling of the building structure by night-time ventilation

PhD thesis by Nikolai Artmann

Defended in public at Aalborg University

(040209)

ISSN 1901-7294

DCE Thesis No. 16

AALBORG UNIVERSITY

Department of Civil Engineering

Aalborg University
Department of Civil Engineering
Indoor Environmental Engineering Research Group

DCE Thesis No. 16

Cooling of the building structure by night-time ventilation

PhD thesis defended in public at Aalborg University (040209)

by

Nikolai Artmann

November 2008

Scientific Publications at the Department of Civil Engineering

Technical Reports are published for timely dissemination of research results and scientific work carried out at the Department of Civil Engineering (DCE) at Aalborg University. This medium allows publication of more detailed explanations and results than typically allowed in scientific journals.

Technical Memoranda are produced to enable the preliminary dissemination of scientific work by the personnel of the DCE where such release is deemed to be appropriate. Documents of this kind may be incomplete or temporary versions of papers—or part of continuing work. This should be kept in mind when references are given to publications of this kind.

Contract Reports are produced to report scientific work carried out under contract. Publications of this kind contain confidential matter and are reserved for the sponsors and the DCE. Therefore, Contract Reports are generally not available for public circulation.

Lecture Notes contain material produced by the lecturers at the DCE for educational purposes. This may be scientific notes, lecture books, example problems or manuals for laboratory work, or computer programs developed at the DCE.

Theses are monograms or collections of papers published to report the scientific work carried out at the DCE to obtain a degree as either PhD or Doctor of Technology. The thesis is publicly available after the defence of the degree.

Latest News is published to enable rapid communication of information about scientific work carried out at the DCE. This includes the status of research projects, developments in the laboratories, information about collaborative work and recent research results.

Published 2008 by
Aalborg University
Department of Civil Engineering
Sohngaardsholmsvej 57,
DK-9000 Aalborg, Denmark

Printed in Aalborg at Aalborg University

ISSN 1901-7294
DCE Thesis No. 16

Preface

This thesis represents a part of the fulfilment for acquiring the Danish PhD degree. The thesis will be presented at Aalborg University on February 4, 2009.

The project was funded by Empa, Swiss Federal Laboratories for Materials Testing and Research, the Hybrid Ventilation Centre, Department of Civil Engineering at Aalborg University and the Swiss Federal Office of Energy (Project no. 101’308). It was also supported by the private sector (WindowMaster, Belimo, SZFF). I acknowledge with thanks all financial support.

The work made in connection to this thesis has been carried out at Empa, Swiss Federal Laboratories for Materials Testing and Research, Laboratory for Building Technologies, Switzerland and at Aalborg University, Hybrid Ventilation Center, Denmark. The work has been supervised by Professor Per Heiselberg, Aalborg University and Dr. Heinrich Manz, Empa.

I would like to thank Heinrich Manz for his continuous guidance, numerous discussions and his highly valuable advice during the whole project. Also, Per Heiselberg I want to thank for his guidance and for the easy and pleasant cooperation despite the long distance. Additionally, I would like to thank Rasmus Lund Jensen for his great help during the experimental work in the laboratory at Aalborg University.

Furthermore I would like to express my thanks to all colleagues at Empa for the very nice and friendly working atmosphere and all members of the Indoor Environmental Engineering Research Group for their hospitality during my stays at Aalborg University.

Nikolai Artmann

November 2008

Abstract

In modern, extensively glazed office buildings, due to high solar and internal loads and increased comfort expectations, air conditioning is increasingly applied even in moderate and cold climates, like in Central and Northern Europe. Particularly in these cases, night-time ventilation is often seen as a promising passive cooling concept. Many successful examples of passively cooled buildings demonstrate the possibility of providing good thermal comfort conditions without the need for energy-intensive air conditioning systems. However, due to uncertainties in the prediction of thermal comfort, architects and engineers are still hesitant to apply passive cooling techniques.

The basic concept of night-time ventilation involves cooling the building structure overnight in order to provide a heat sink during the occupancy period. As this requires a sufficiently high temperature difference between the ambient air and the building structure, the efficiency of night cooling is highly sensitive to climatic conditions and hence also to climate warming. In the first part of this PhD study, the potential for passive cooling of buildings by night-time ventilation was evaluated by analysing climatic data, without considering any building-specific parameters. A method for quantifying the climatic cooling potential (CCP) was developed based on degree-hours of the difference between building and external air temperature. Applying this method to climatic data of 259 stations shows very high night cooling potential over the whole of Northern Europe and still significant potential in Central, Eastern and even some regions of Southern Europe. However, due to the inherent stochastic properties of weather patterns, series of warmer nights can occur at some locations, where passive cooling by night-time ventilation alone might not be sufficient to guarantee thermal comfort.

Possible time-dependent changes in CCP were assessed for the period 1990-2100, with particular emphasis on the *Intergovernmental Panel on Climate Change* (IPCC) “A2” and “B2” scenarios for future emissions of greenhouse gases and aerosols. The study was based on 30 Regional Climate Model (RCM) simulated datasets, as obtained from the European *PRUDENCE* project. Under both emissions scenarios and across all locations and seasons, CCP was found to decrease substantially by the end of the 21st century, so that night-time cooling will cease to be sufficient to assure thermal comfort in many Southern and Central European buildings. In Northern Europe, a significant passive cooling potential is likely to remain, at least for the next few decades.

Because heat gains and night ventilation periods typically do not coincide in time, heat storage is essential for effective night cooling, and thus a sufficient amount of thermal mass is needed in the building. In order to assess the impact of different parameters, such as slab thickness, material properties and the surface heat transfer, the dynamic heat storage capacity of building elements was quantified based on an analytical solution of one-dimensional heat conduction in a slab with convective boundary condition. The potential of increasing thermal mass by using phase change materials (PCM) was also estimated. The results show a significant impact of the heat transfer coefficient on heat storage capacity, especially for thick, thermally heavy elements. For thin, light elements a significant increase in heat capacity due to the use of PCMs was found to be possible.

In order to identify the most important parameters affecting night ventilation performance, a typical office room was modelled using a building energy simulation program (*HELIOS*), and the effect of different parameters such as building construction, heat gains, air change rates, heat transfer coefficients and climatic conditions on the number of overheating degree hours (operative room temperature >26 °C) was evaluated. Besides climatic conditions, the air flow rate during night-time ventilation was found to have the largest effect. However, thermal mass and internal heat gains also have a significant impact on the achievable level of thermal comfort. A significant sensitivity to the surface heat transfer was found for total heat transfer coefficients below about 4 W/m^{2}K.

The convective heat transfer at internal room surfaces is highly affected by the indoor air temperature distribution and the near-surface velocities both of which can vary significantly depending on the air flow pattern in the room. Increased convection is expected due to high air flow rates and the possibility of a cold air jet flowing along the ceiling, but the magnitude of these effects is hard to predict. Heat transfer during night-time ventilation in case of mixing and displacement ventilation has been investigated in a full scale test room. The performance of night time cooling was evaluated based on the temperature efficiency of the ventilation. The results show that for low air flow rates displacement ventilation is more efficient than mixing ventilation. For higher airflow rates the air jet flowing along the ceiling has a significant effect, and mixing ventilation becomes more efficient.

Combining the results of the previous steps, a practicable method for the estimation of the potential for cooling by night-time ventilation during an early stage of design is proposed. In order to assure thermal comfort two criteria need to be satisfied, i.e. (i) the thermal capacity of the building needs to be sufficient to accumulate the daily heat gains within an acceptable temperature variation and (ii) the climatic cooling potential and the effective air flow rate need to be sufficient to discharge the stored heat during the night. The estimation of the necessary amount of thermal mass in the building is based on the dynamic heat storage capacity. The air flow rate needed to discharge the stored heat at a certain climatic cooling potential is assessed based on the temperature efficiency of the ventilation.

Table of contents

List of symbols

A	Surface area	(m^2)
ACR	Air change rate	(ACH)
Ar	Archimedes Number	(-)
c, c_p	Heat capacity	(J/kgK)
c_{dyn}	Dynamic heat storage capacity	(J/m^2K)
CCP	Climatic cooling potential	(Kh)
d	Thickness	(m)
F	View factor	(-)
g	Total solar energy transmittance	(-)
H	Room height	(m)
h	Heat transfer coefficient	(W/m^2K)
I	Solar irradiation	(W/m^2)
$\dot{m}$	Mass flow	(kg/s)
ODH	Overheating degree hours	(Kh)
Q	Heat	(Wh)
$\dot{Q}$	Heat flow	(W)
$\dot{Q}_0$	Reference heat flow	(W)
$\dot{q}$	Heat flux	(W/m^2)
T	Temperature	(K), (°C)
ΔT	Temperature difference	(K)
ΔT_0	Initial temperature difference	(K)
t	Time	(h)
$\dot{V}$	Flow rate	(m^3/s)
x, y, z	Room coordinates	(m)

Greek symbols

γ	Convection ratio	(-)
ε	Emissivity	(-)
η	Temperature efficiency	(-)
θ	Dimensionless temperature	(-)
λ	Thermal conductivity	(W/mK)
ρ	Density	(kg/m^3)
σ	Stefan-Boltzmann constant	(W/m^2K^4)
τ	Dimensionless time	(-)

Subscripts

b	Building	i	Initial
$cond$	Conduction	min	Minimum
$conv$	Convection	out	Outflowing
$crit$	Critical	rad	Radiation
d	Day	tot	Total
e	External	$vent$	Ventilation
f	Final		

1 Introduction

1.1 Increasing cooling energy demand

During the last few decades, a trend towards increasing cooling demand in buildings has been observed in many European countries. Due to high internal and solar heat gains commercial buildings with extensive glazing tend to be overheated in summertime, even in moderate and cold climates like in Central and Northern Europe.

In Switzerland, 46.7 % of the total energy is used in Buildings, i.e. for space heating (35.1 %), domestic hot water (5.5 %), lighting (3.4 %), and for air conditioning and ventilation systems (2.7 %). In private homes until now only 0.1 % of the electric energy is used for air conditioning systems. However, from 2000 till 2006 this number increased by 158 %. In the service sector, the share of the electric energy applied for air conditioning and ventilation systems amounts to 29.1 % already today and increased by 10.6 % during the same period [1].

A study on the energy efficiency of air conditioning systems [2] shows a similar situation for most European countries. Until 2020 the demand for cooled floor area is expected to more than double compared to 2000. Again, office and commercial buildings have the largest share (Figure 1).

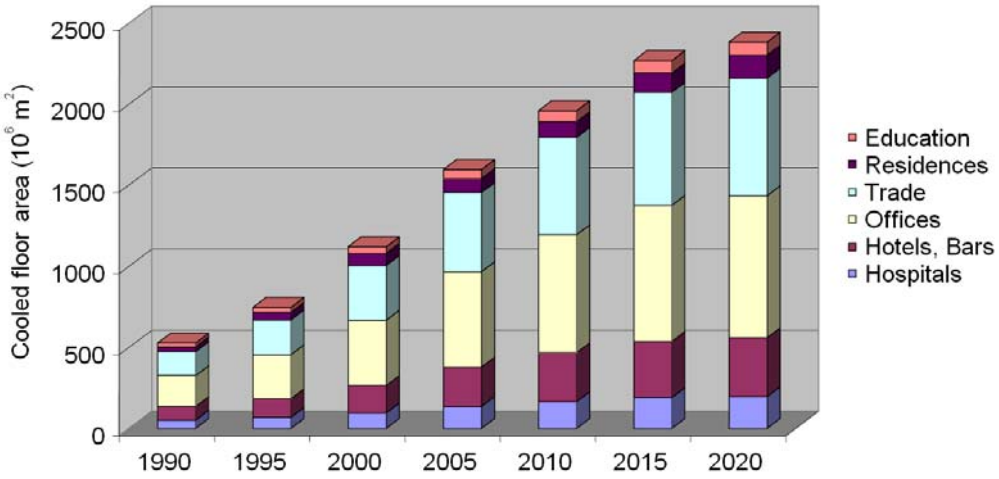

Figure 1. Evolution of cooled floor area in the EU 15 countries by economic sectors from 1990 to 2020 [2].

While the heating requirement can be effectively reduced by installing thermal insulation, cooling plays an increasingly significant role in the overall energy demand of buildings. This trend is enhanced by changes in climatic conditions. In mild winters less energy is needed for heating, but more frequent and longer hot spells result in a significant increase in cooling energy demand. For Switzerland, Christenson et al [3] found a clear increase in cooling degree days during the last century, especially during the last 20 years. Although future climate models are subject to high uncertainties, a continuous increase in cooling degree days is believed to be very likely. Using building energy simulation, Frank [4] observed an increase in cooling energy demand in Swiss office buildings by 223-1050 % for the period 2050-2100 compared to 1961-1990.

Additionally, the urban heat island effect contributes to an increasing cooling demand [5]. In densely populated urban areas, changes in the thermal properties of surface materials (e.g. asphalt or concrete), the lack of evaporation from vegetation and a high density of waste heat sources, result in significantly higher

temperatures compared to surrounding rural areas. As cities tend to become larger and more densely populated, this effect is expected to increase further.

1.2 Passive cooling of buildings

Basically, active cooling can be avoided in well-designed buildings in most Central and Northern European locations. The first step to achieving this is the reduction of internal and solar heat gains. Solar heat gains can be limited by a moderate glazing ratio and effective, preferably exterior, solar shading devices. Also people and electric equipment contribute to the total heat gains in a building. Therefore, next to the direct energy savings, the application of energy efficient office equipment and using daylight instead of electric light helps to reduce the cooling energy demand and to increase thermal comfort.

Besides the reduction of heat gains, passive cooling is based on the utilisation of natural heat sinks including the sky, the atmosphere and the earth. Ventilation to the atmosphere is the most elementary practise of heat removal from buildings and the most widely used passive cooling method. Ventilative cooling includes the direct removal of heat gains during the day and the cooling of the building structure during the night. Heat transfer to the sky, or rather the outer space beyond the atmosphere, is exclusively by radiation. Radiative cooling is most efficient at night under cloudless skies, and therefore in regions having low atmospheric humidity. Evaporative cooling applies to all processes in which the sensible heat in an air stream is exchanged for the latent heat of water droplets or wetted surfaces. Direct evaporative cooling denotes systems where this takes place in the supply air stream. In indirect systems a heat exchanger is used in order to prevent humidification of the supply air. Generally evaporative cooling is most suitable for dry climates. Also the earth can be utilised as a heat sink in different ways. A building can be coupled directly to the earth, or the supply air can be cooled by means of an earth-to-air heat exchanger. These methods are widely applicable, as at most locations earth temperatures fall below or within the comfort range throughout the entire year. Additionally, ground water and also water from the sea, lakes or rivers can be utilised as natural heat sinks. Detailed information on different passive cooling techniques can be found in [6] and [7].

Many of these passive cooling systems have a very long tradition, especially in hot and arid climates, like in Iran [8]. E.g. dome-shaped roofs with air vents were incorporated in buildings as early as 3000 BC. Also very massive constructions were traditionally used in order to minimise daily internal temperature swings. For increased ventilation different types of wind towers were developed in Egypt (malqaf), the Persian Gulf states (badgir) and Pakistan (wind scoops) [9]. Wind towers were also used in combination with underground tunnels and evaporative cooling from damp walls, fountains or underground water streams. Combining different methods yielded very effective cooling systems.

In modern applications the combination of different passive, or passive and active cooling systems is called hybrid cooling. When passive and active systems are combined the passive system is used as long as the natural heat sink is sufficient and therefore the energy consumption of the active system can be reduced significantly. Whenever passive means are not sufficient to provide acceptable thermal comfort conditions, the application of renewable energy sources should be considered for the operation of active air conditioning systems. E.g. an absorption chiller can be powered by using concentrated solar radiation as an energy source.

1.3 Night-time ventilation

During night-time ventilation the relatively cold outdoor air is used as a heat sink to cool the building. Whenever, the outdoor air temperature is below the building temperature, the thermal mass of the building can be cooled by ventilation. During the following day, heat gains are accumulated by the thermal mass

which prevents extensive overheating of the building. The stored heat is then discharged by ventilation during the next night (Figure 2).

Typically solar and internal heat gains occur primarily during the day, but the highest potential for ventilative cooling is available during the night when the outdoor temperature is lowest. Therefore heat storage is an essential requirement for night-time ventilative cooling and a high thermal capacity of building elements (e.g. ceiling, floor, walls) is needed. Furthermore, for an efficient utilisation of the thermal capacity a sufficient heat transfer at the surface and sufficient conduction in the material are needed. An alternative to heavy building elements is the application of phase change materials for increasing the thermal capacity of light-weight structures [10].

Ventilation can be driven by natural forces (thermal buoyancy and wind), or by fans. In case of natural ventilation windows can be operated manually or automatically by a central building management system. As natural ventilation may cause a high variability in the air change rate, hybrid ventilation systems are often used in order to ensure a certain air flow rate. In hybrid ventilation mechanical and natural forces are combined in a two-mode system where the operating mode varies according to the season, and within individual days [11].

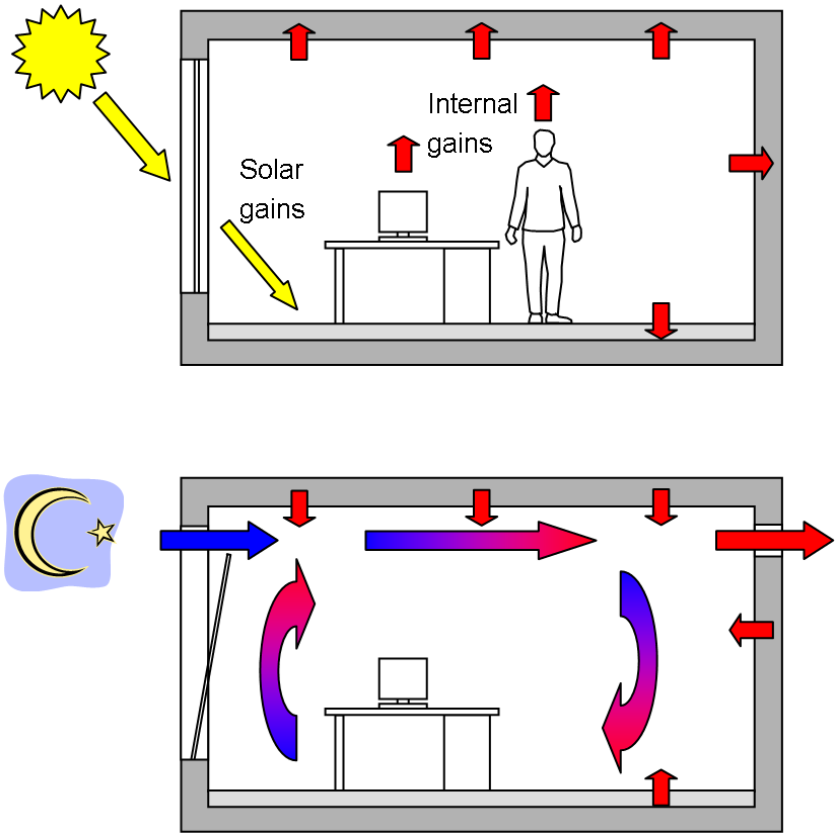

Figure 2. Basic principle of cooling by night-time ventilation.

1.4 Examples of buildings cooled by night-time ventilation

On completion in 2003 the *MIVA* building (*Christophorus Haus*) in Stadl-Paura, Austria [12] was one of the most innovative *Passivhaus* buildings in Europe. The cooling concept includes natural night-time ventilation combined with a ground source heat pump (hybrid cooling). 100 tonnes of thermal mass were included in the building in order to accumulate heat gains and decrease daily temperature variations.

In Switzerland, *Forum Chriesbach* [13] was the first office building applying the *Zero Energy House* standard. In this building passive cooling is achieved by combining natural night-time ventilation with an earth-to-air heat exchanger (hybrid cooling). During night-time ventilation cold outdoor air enters the building through windows in the façade, flows to the central atrium and is exhausted at roof level.

A similar concept is applied in the passively cooled *KfW* office building in Frankfurt, Germany. Night-time ventilation is driven by the stack effect in the atrium, but it is supported by mechanical fans when needed (hybrid ventilation). A monitoring study conducted in this building by Wagner et al. [14] showed, that even under extreme climate conditions acceptable thermal comfort conditions can be reached with passive cooling.

The energy consumption and the internal temperatures and CO_2 levels in the naturally ventilated *Lanchester Library* at Coventry University, UK were recorded by Krausse et al. [15]. Due to the exposed thermal mass and the night ventilation strategy the building meets thermal comfort criteria even during prolonged hot spells, using 51 % less energy than a typical air-conditioned office.

1.5 State-of-the-art and research topics

The international research program *PASCOOL* [16] aimed to develop techniques, tools and design guidelines to promote passive cooling applications in buildings. Within the framework of *PASCOOL* the user-friendly computer code *LESOCOOL* [17] was developed to predict the cooling power and fluctuations of internal temperature during night-time ventilation based on simple models. This tool was validated and a good agreement was found between simulated and experimental indoor air temperature. However, there are some limitations. Firstly, only one single air flow path without branches can be modelled. Secondly, the thermal model is only valid for infinitely thick walls. And thirdly, a constant heat transfer, h = 6 W/m^{2}K is applied for all internal surfaces. Radiative heat transfer between different surfaces is not considered.

IEA ECBCS Annex 28 dealt with low energy cooling systems. A selection chart was provided to help to identify which of the considered cooling technologies are likely to be suitable for a particular application on the basis of key building parameters. This is supported by summary sheets for each of the technologies giving a brief description and key information. For night-time ventilation in cool climates and heavy-weight constructions a possible offset of heat gains in the range of 20 - 30 W/m^2 and a corresponding peak space temperature reduction of 2 - 3 K is given [18].

Often natural or hybrid ventilation is applied for night-time cooling. The *NatVent* project [19] aimed to provide solutions for natural ventilation and low-energy cooling in office-type buildings in countries with moderate and cold climates. A design handbook [20] discusses the basic principles of natural ventilation and provides an overview of prediction methods. *IEA ECBCS* Annex 35 [11] aimed to develop control strategies for hybrid ventilation systems and methods to predict ventilation performance in hybrid ventilated office and educational buildings. An overview of available design methods like simple analytical and empirical methods, single-zone and multi-zone methods, and computational fluid dynamics (CFD) methods is given in [21].

Despite many successful examples and several research projects showing a high potential for cooling by night-time ventilation, architects and engineers continue to be hesitant to apply this technique. This is mainly because of uncertainties in thermal comfort predictions and the lack of simple design tools applicable in an early design stage, when many parameters affecting the performance of night cooling are not known yet. Assumptions made by the user in the input for building simulation leads to uncertainties in comfort predictions [22]. Additionally, the effectiveness of passive and low energy cooling systems is, by their very nature, much more sensitive to climate than is the performance of refrigeration-based systems [23]. For night-time ventilation a sufficiently high temperature difference between ambient air and the building

structure is needed to achieve effective cooling of the building mass. The very high variability of climatic conditions and the uncertain development of global climate warming, therefore might cause discrepancies in thermal comfort conditions in real buildings compared to predictions based on standard climate data.

Some general guidelines for the applicability of ventilative night cooling are given by Givoni [24], [25], [26]. Night-time cooling is recommended mainly in arid and desert regions with a summer diurnal temperature fluctuation of 15 to 20 K and night-time temperatures below about 20 °C. For the maximum daytime temperature a range between 30 and 36 °C is given.

A method to evaluate the climate suitability of a given location for direct ventilative cooling and complimentary night-time ventilative cooling was presented by Axley et al. [27]. The method was applied to four different locations in different climatic zones of the United States. Cooling by natural ventilation was found to be feasible and effective in the cooler locations for moderate to high specific internal gains, but not for hot and humid climates, as for example in Miami, FL, where relatively high night-time ventilation rates would be needed to offset moderate specific internal gains. Estimates of the internal gains that may be offset by night-time cooling are based on the assumption that the building has, essentially, infinite thermal mass thus, as stated by the authors, these results may significantly overestimate the benefit of night-time cooling.

Eicker et al. [28] provided experimental evidence for the limitations of night-time ventilation under climatic conditions currently regarded as extreme. They monitored for 3 years an advanced low-energy office building in Weilheim (Germany), constructed in 1999, that was also equipped with an earth to air heat exchanger. While the building performed excellently during typical German summer conditions (2001, 2002), in 2003, with average summer temperatures more than 3 K higher than usual, nearly 10 % of all office hours were above 26 °C. As the temperatures observed during the exceptionally hot summer of 2003 might correspond to those of a typical summer at the end of this century [29], the findings of Eicker et al. clearly demonstrate that in decades to come cooling by night-time ventilation might cease to work in buildings designed for current climatic conditions.

The impact of climate change on different passive cooling techniques has been analysed by Roaf et al. [23]. For the applicability of night-time ventilation, a monthly mean daily maximum temperature of 31°C was assumed to be the limiting criterion. Based on this and other threshold values, they delineated the regions where different cooling techniques could cease to be viable by 2050. These were found to be extensive enough to conclude that the effects of global warming should be taken into account by designers. Although their approach was suitable to detect first-order effects, the study by Roaf et al. suffers from several shortcomings. Their threshold temperature of 31°C only applies to well-shaded buildings with relatively low internal loads (e.g. residential buildings), as the authors state. The method is also not suitable to quantify gradual changes in cooling potential, e.g. across spatial gradients or over time. Additionally, uncertainties associated with any regional climate projections [30], [31] were not taken into account.

Predictions of thermal comfort in buildings applying night-time ventilation are not only affected by variable climatic conditions, but also by uncertainties in other parameters, like the air change rate, heat gains, effective thermal mass and the heat transfer at internal surfaces. Several studies have been undertaken to investigate the effect of different parameters on the efficiency of night-time cooling.

Using an hourly simulation model, Shaviv et al. [32] analysed the maximum indoor temperature in a residential building in the hot humid climate of Israel as a function of night ventilation air change rate, thermal mass and daily temperature difference. In a heavy mass building, the maximum indoor temperature was found to be reduced by 3 - 6 °C compared to the outdoor maximum.

Finn et al. [33] investigated the effect of design and operational parameters on the performance of a night ventilated library building in the moderate maritime climate of Ireland. Increasing thermal mass by changing

construction materials (from 887 kg/m^2 to 1567 kg/m^2, per unit floor area) was observed to lower peak daily temperature by up to 3 °C. Internal gains (20 to 40 W/m^2) and ventilation rates up to 10 ACH were also found to have a significant effect on internal comfort, with a change in peak temperature of up to 1.0 °C. However, increasing ventilation rates beyond 10 ACH did not lead to significant improvement.

Breesch [34] developed a methodology to predict the performance of natural night ventilation with building simulation (*TRNSYS* [35] coupled with *COMIS* [36]) taking into account the uncertainties in the input. Next to internal heat gains and the air tightness, internal convective heat transfer coefficients were found to have the most important impact on the predicted thermal comfort. It should be noted that increased convection due to high air change rates was not considered in this study. Further investigation of the convective heat transfer in case of natural night ventilation was recommended.

In most of these studies the effect of convective heat transfer at internal surfaces was not considered at all or only in a small range of heat transfer coefficients, even though other studies showed the importance of this parameter for thermal energy storage in building elements. Akbari et al. [37] used an analytical model and numerical simulations to evaluate the effectiveness of massive interior walls. The effectiveness – defined as the ratio of the wall's total diurnal heat storage capacity for a given convective heat transfer coefficient to the maximum storage capacity of the same wall when the coefficient is infinite – of a 0.305 m thick concrete wall was found to be almost doubled by increasing the convective heat transfer coefficient from 2.84 to 5.68 W/m^{2}K. Several authors point out the importance of this finding for the efficiency of night-time ventilation.

Depending on the direction of the heat flow, standard heat transfer coefficients for combined heat transfer (convection and radiation) are in the range from 5.9 to 10 W/m^{2}K [38]. However, during night-time ventilation radiation does not contribute to the heat transfer from room surfaces to the air (as air is virtually transparent for infrared radiation), but in fact transfers heat from one surface to another. For convective heat transfer standard coefficients are 2.5 W/m^{2}K for vertical walls, 5.0 W/m^{2}K for upward heat flow and 0.7 W/m^{2}K for downward heat flow [39]. This means that, especially at the ceiling – a concrete ceiling often represents a significant share of the thermal mass of a room – the convective heat transfer can be very limited (downward heat flow during night-time ventilation).

On the other hand a higher convective heat transfer is expected due to the increased air flow rate and the possibility of a cold air jet flowing along the ceiling [26], [40], [41]. However, Blondeau et al. [42] did not observe any significant difference in predicted indoor air temperature due to various increased convective coefficients during the night-time in their simulation study.

Several studies deal with the heat transfer at internal room surfaces. Different correlations were proposed for natural (e.g. Alamdari and Hammond [43], Khalifa and Marshall [44], Awbi and Hatton [45]) and mixed convection (e.g. Chandra and Kerestecioglu [40], Spitler et al. [46], Awbi and Hatton [47]) from horizontal and vertical surfaces. Based on such empirical correlations Beausoleil-Morrison developed an adaptive algorithm for the simulation of the convective heat transfer at internal building surfaces [48]. However, many of these correlations are based on experiments on small heated plates. A review comparing natural convective heat transfer at isolated surfaces and surfaces in enclosures revealed clear discrepancies [49], [50]. This demonstrates the necessity of considering a room as a whole.

Additionally, the heat transfer obviously depends on the air flow pattern in a room. The effect of different flow patterns on the storage efficiency during night-time ventilation has been investigated by Salmerón et al. [51] using a 2-dimensional computational fluid dynamics model. A variation by a factor of 6 was found between different configurations of air in- and outlet openings. However, radiation between internal room surfaces was not considered in this study. Furthermore, the impact of the air flow rate on the storage efficiency was not investigated.

The aim of this dissertation is to contribute to the improvement of the design methods for cooling by night-time ventilation. It is mainly focused on the effects of climatic conditions and the heat transfer at internal room surfaces. As the work was focused on commercial buildings, no internal heat gains were considered during night time.

1.6 Project phases

In the first part of the project the possibilities and limitations of night-time ventilation under different climatic conditions and the impact of climate warming are evaluated. A degree-hour method for quantifying the climatic potential for night-time ventilation is developed, verified and applied to present and future climate data.

As heat storage is vital for night-time cooling, the impact of different parameters on the dynamic heat storage capacity of building elements is investigated based on the analytical solution of one-dimensional heat conduction.

Subsequently, building energy simulations have been performed to analyse the sensitivity of night cooling performance. The effects of climate, thermal mass, heat gains, air change rate and heat transfer coefficients on thermal comfort conditions in an office building are discussed.

Additionally, the heat transfer in case of mixing and displacement ventilation has been investigated in a full scale test room at Aalborg University. This study provides a detailed analysis of convection and radiation during night-time ventilation depending on the air flow rate and the initial temperature difference between the inflowing air and the room.

Combining the results of the previous steps a new method to evaluate the potential for night-time ventilation during the concept design phase is proposed.

2 Climatic potential for passive cooling of buildings

Night-time ventilation is highly dependent on climatic conditions, as a sufficiently high temperature difference between ambient air and the building structure is needed during the night to achieve efficient convective cooling of the building mass. The purpose of this study was to evaluate the climatic potential for the passive cooling of buildings by night-time ventilation in present and future climates in Europe [52], [53]. A method was developed which is basically suitable for all building types, regardless of building-specific parameters. This was achieved by basing the approach solely on a building temperature variable within a temperature band given by summertime thermal comfort.

2.1 Definition of the climatic cooling potential

Degree-days or degree-hours methods are often used to characterise a climate's impact on the thermal behaviour of a building. The daily climatic cooling potential, CCP_d, was defined as degree-hours for the difference between building temperature, T_b and external air temperature, T_e (Figure 3):

$$CCP_d = \sum_{t=t_i}^{t_f} m_{d,t} \left(T_{b(d,t)} - T_{e(d,t)}\right) \quad \begin{cases} \mathrm{m} = 1\,\mathrm{h} & \text{if } T_b - T_e \geq \Delta T_{crit} \\ \mathrm{m} = 0 & \text{if } T_b - T_e < \Delta T_{crit} \end{cases} \tag{1}$$

where t stands for the time of day, with $t \in \{0, \ldots, 24\ \mathrm{h}\}$; t_i and t_f denote the initial and the final time of night-time ventilation, and ΔT_{crit} is the threshold value of the temperature difference, when night-time ventilation is applied. In the numerical analysis, it was assumed that night-time ventilation starts at t_i = 19 h and ends at t_f = 7 h. As a certain temperature difference is needed for effective convection, night ventilation is only applied if the difference between building temperature and external temperature is greater than 3 K.

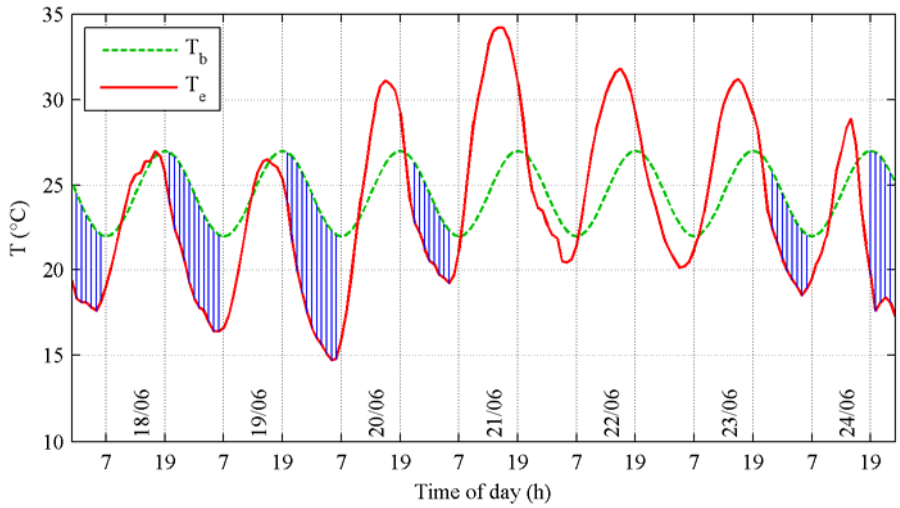

Figure 3. Building temperature, T_b and external air temperature, T_e during one week in summer 2003 for Zurich SMA (ANETZ data). Shaded areas illustrate graphically the climatic cooling potential, CCP.

As heat gains and night-time ventilation are not simultaneous, energy storage is an integral part of the concept. In the case of sensible energy storage, this is associated with a variable temperature of the building structure. This aspect is included in the model by defining the building temperature as a harmonic oscillation around 24.5°C with an amplitude of 2.5 K:

$$T_{b(t)} = 24.5 + 2.5\cos\left(2\pi\frac{t - t_i}{24}\right) \quad (2)$$

The maximum building temperature occurs at the starting time of night ventilation, and given a ventilation time of 12 hours, the minimum building temperature occurs at the end time (Figure 3). The temperature range T_b = 24.5 °C ± 2.5 °C corresponds to that recommended for thermal comfort in offices [54].

2.2 Practical Significance of CCP

To discuss the practical significance of the calculated degree-hours, an example shall be given. It is assumed that the thermal capacity of the building mass is sufficiently high and therefore does not limit the heat storage process. If the building is in the same state after each 24 h cycle, the daily heat gains Q_d (Wh) stored to the thermal mass, equal the heat which is discharged by night ventilation:

$$Q_d = \dot{m} \cdot c_p \cdot CCP_d \quad (3)$$

The effective mass flow rate $\dot{m}$ is written as $\dot{m} = A_{Floor} \cdot H \cdot \eta \cdot ACR \cdot \rho$, where A_{Floor} is the floor area and H the height of the room, ACR the air change rate and η a temperature efficiency, which is defined as $\eta = (T_{out} - T_e)/(T_b - T_e)$ and takes into account the fact that the temperature of the outflowing air T_{out} is lower than the building temperature T_b. The density and the specific heat of the air are taken as $\rho = 1.2\,\mathrm{kg/m^3}$ and $c_p = 1000\,\mathrm{J/(kg\,K)}$. Assuming a room height of H = 2.5 m and a constant effective air change rate of $\eta \cdot ACR = 6\,\mathrm{h^{-1}}$ yields:

$$\frac{Q_d}{A_{Floor}} = H \cdot \eta \cdot ACR \cdot \rho \cdot c_p \cdot CCP_d = \frac{2.5\,\mathrm{m} \cdot 6\,\mathrm{h^{-1}} \cdot 1.2\,\mathrm{kg/m^3} \cdot 1000\,\mathrm{J/kgK}}{3600\,\mathrm{s/h}} CCP_d = 5\frac{W}{m^2K} CCP_d \quad (4)$$

For the climatic cooling potential needed to discharge internal heat gains of 20 W/m^{2}K and solar gains of 30 W/m^{2}K during an occupancy time of 8 h follows:

$$CCP_d = \frac{Q_d}{A_{Floor}} \Big/ 5\frac{W}{m^2K} = \frac{(20+30)\cdot 8}{5}\,\mathrm{Kh} = 80\,\mathrm{Kh} \quad (5)$$

This example should be seen as a rough estimation only, as solar and internal gains of an office room can vary substantially depending on the type of building use, local climate, and the solar energy transmittance and orientation of the façade.

2.3 Climatic cooling potential in Europe

The degree-hour method was applied for a systematic analysis of the potential for night time cooling in different climatic zones of Europe. Semi-synthetic climate data [55] from 259 weather stations was used to map the climatic cooling potential (Figure 4). Additionally the cumulative frequency distribution of CCP was plotted for 20 European locations (Figure 5). These charts show the number of nights per year when CCP exceeds a certain value.

In the whole of Northern Europe (including the British Isles) a very significant climatic cooling potential was found, and therefore passive cooling of buildings by night-time ventilation seems to be applicable in most cases. In Central, Eastern and even in some regions of Southern Europe, the climatic cooling potential is still

significant, but due to the inherent stochastic properties of weather patterns, series of warmer nights can occur at some locations, where passive cooling by night-time ventilation might not be sufficient to guarantee thermal comfort. If lower thermal comfort levels are not accepted during short periods of time, additional cooling systems are required. In regions such as southern Spain, Italy and Greece climatic cooling potential is limited and night cooling alone might not be sufficient to provide good thermal comfort during all the year. Nevertheless, night-time ventilation can be used in hybrid cooling systems during spring and fall.

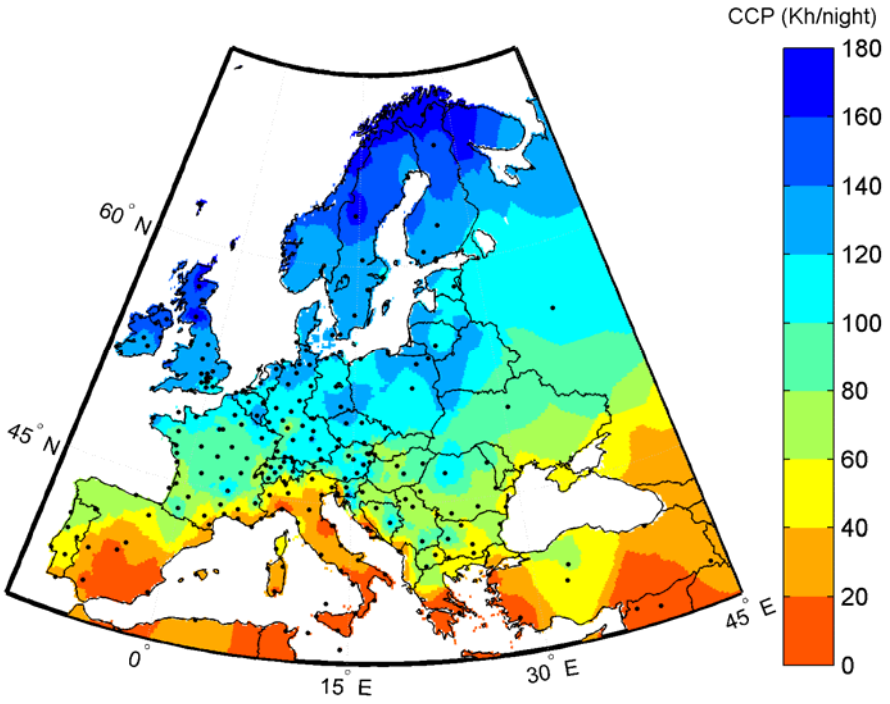

Figure 4. Map of mean climatic cooling potential (Kh/night) in July based on Meteonorm data [55].

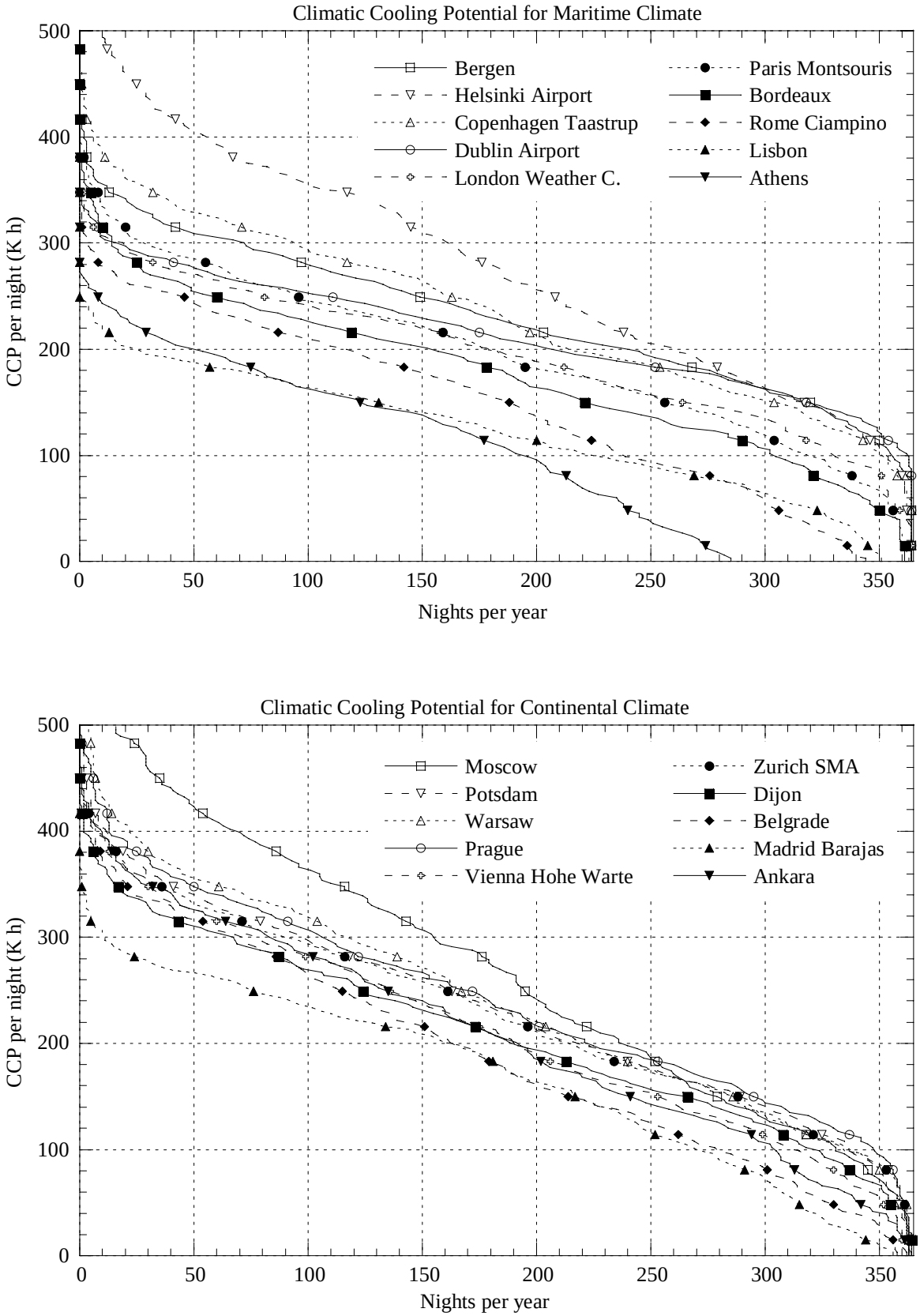

Figure 5. Cumulative frequency distribution of CCP for maritime (top) and continental (bottom) locations.

2.4 Impact of climate warming on climatic cooling potential

In order to quantify the impact of climate warming on the potential for night cooling, linear regression models were developed to estimate the daily climatic cooling potential (CCP_d) from the minimum daily air temperature, T_{min}. For eight case study locations representing different climatic zones across a North-South transect in Europe, CCP was computed for present conditions (1961 - 1990) using measured T_{min} data from the *European Climate Assessment* (ECA) database. Possible future changes in CCP were assessed for the period 2071 - 2100 under the *Intergovernmental Panel on Climate Change* (IPCC) "A2" and "B2" scenarios for future emissions of greenhouse gases and aerosols defined in the *Special Report on Emission Scenarios* (SRES, [56]). The "A2" storyline and scenario family describes a very heterogeneous world. The underlying theme is self-reliance and preservation of local identities. Fertility patterns across regions converge very slowly, which results in continuously increasing population. Economic development is primarily regionally oriented and per capita economic growth and technological change more fragmented and slower than in other storylines. The "B2" storyline and scenario family describes a world in which the emphasis is on local solutions to economic, social and environmental sustainability. It is a world with continuously increasing global population, at a rate lower than "A2", intermediate levels of economic development, and less rapid and more diverse technological change than in the "A1" and "B1" storylines. While the scenario is also oriented towards environmental protection and social equity, it focuses on local and regional levels. The SRES scenarios do not include additional climate initiatives, which means that no scenarios are included that explicitly assume implementation of the United Nations Framework Convention on Climate Change or the emissions targets of the Kyoto Protocol.

The analysis of climate change impacts was based on 30 *Regional Climate Model* (RCM) data sets obtained from the European *PRUDENCE* project [57]. This project represents an attempt to integrate European climate projections of different institutions, and its website provides a large database of RCM simulation results for Europe. These were based on boundary conditions from 6 global simulations with two *Atmosphere-Ocean General Circulation Models* (AOGCM), Arpege/OPA and ECHAM4/OPYC, plus three atmosphere-only *Global Climate Models* (GCM), ECHAM5, HadAM3H and HadAM3P that were driven with sea-surface temperature and sea-ice boundary conditions taken from simulations with the HadCM3 AOGCM. More information about the climate simulation models can be found on the PRUDENCE website.

For Zurich and Madrid Figure 6 shows significant changes in the percentage of nights per season when the daily cooling potential, CCP_d exceeds a certain value. For Zurich, under current climate conditions CCP_d is higher than 80 Kh (roughly necessary to discharge heat gains of 50 W/m^2, see section 2.2) throughout most of the year, except for about 10 % of summer nights. Under the "A2" scenario CCP_d was found to fall below 80 Kh in more than 50 % ("B2": 45 %) of summer nights.

For the studied locations in Southern Europe CCP_d values under present climatic conditions were found to be below 80 Kh throughout almost the entire summer, but a considerable cooling potential was revealed in the transition seasons. For the whole year the percentage of nights when CCP_d exceeds 80 Kh in Madrid was found to decrease from 70 % under present conditions to 52 % under "A2" conditions.

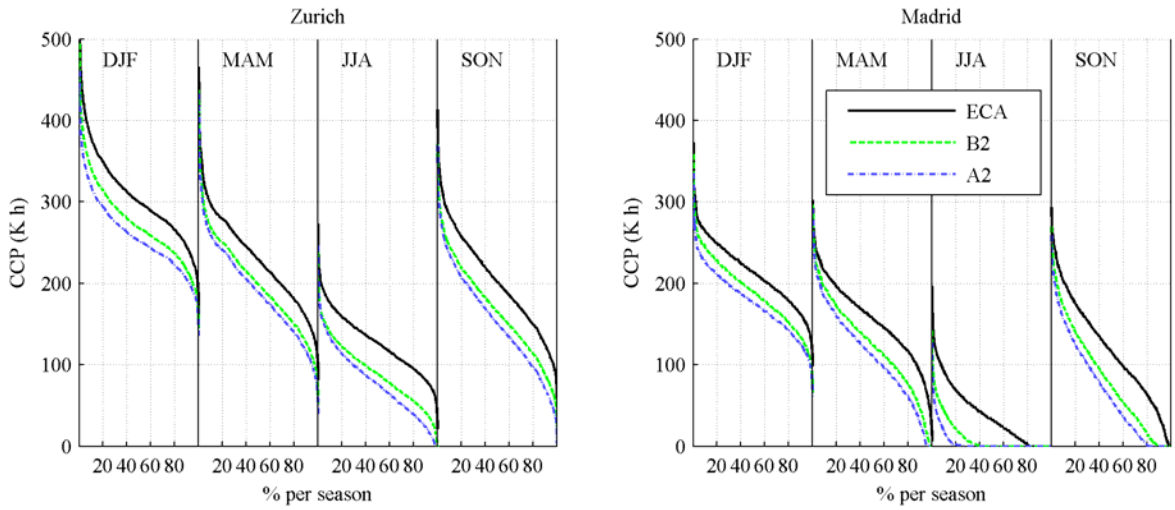

Figure 6. Seasonal cumulative distributions of CCP_d in Zurich (left) and Madrid (right) for current climate (ECA) and averages for forcing scenarios "A2" and "B2".

Transient scenarios were based on upper and lower bounds for the change in global temperature as provided by Cubash et al. [58] (their Figure 9.14, "several models, all SRES envelope"). These bounds accounted for a much broader range of radiative forcing scenarios and possible global temperature responses to a given forcing (climate sensitivities) than the PRUDENCE scenarios. However, it should be noted that these do still not account for the full range of possible future development.

Figure 7 shows a range of the possible development of the mean climatic cooling potential, *CCP* during the summer (June July August) from 1990 to 2100 for three European locations. The lower limit indicates a rapid decrease in night cooling potential, especially after 2030. In the case of Madrid the slope of the lower limit tails out as it approaches zero. The upper limit shows a flatter slope and levels to a constant value at the end of the 21st century.

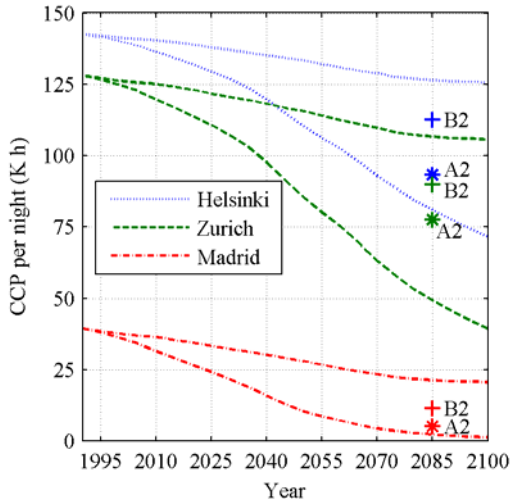

Figure 7. Time-dependent change in mean climatic cooling potential during summer (JJA); upper and lower scenario based on mean global temperature scenarios ([58] Figure 9.14, "several models, all SRES envelope") and mean values of selected PRUDENCE models for "A2" and "B2".

The decreases found in mean cooling potential have regionally varying implications. In Northern Europe the risk of thermal discomfort for buildings that use exclusively ventilative night cooling is expected to steadily increase up to possibly critical levels in the second half of the 21st century. In Central Europe extended periods with very low night cooling potential – where thermal comfort cannot be assured based on night-time ventilation only – could already become more frequent in the next few decades, if a strong warming scenario became real. For Southern Europe the potential for ventilative night cooling will sooner or later become negligible during summer and will decrease to critical levels in the transition seasons.

2.5 Concluding remarks

Additionally to climate warming the heat island effect causes a decrease in the potential for night-time ventilation in urban areas compared to surrounding rural areas. Williamson and Erell [59] applied the CCP concept to assess the implications of heat islands for building ventilation. For London they found a reduction in CCP during summer of about 9 %. Even larger effects were found for Adelaide, Australia (up to 26 %) and Sde Boqer, Israel (up to 61 %).

In order to avoid heavily increased energy consumption by mechanical cooling systems there is a great need for additional passive cooling techniques, such as radiant or evaporative cooling, and/or hybrid approaches. However, it should be noted that although cooling by night-time ventilation is expected to become increasingly ineffective during summer, it is likely to remain an attractive option in the transition seasons. This will be even more the case, if it is considered that under general warming the cooling season will tend to start earlier in spring and end later in autumn. In fact, the decreasing cooling potential and the simultaneously increasing cooling demand result in a shift of possible applications of night-time ventilation in Europe from South to North and from summer to the transition seasons.

Any assessment of possible changes in future climate is subject to large uncertainties. Nevertheless, the extent and rate of the expected climatic changes and the long service life of buildings imply the need for designing buildings capable of providing comfortable thermal conditions under more extreme climatic conditions.

3 Dynamic heat storage capacity of building elements

As heat gains and night ventilation periods do normally not coincide in time, the energy of daily heat gains needs to be stored until it can be discharged by ventilation during the following night. A sufficient amount of thermal mass is therefore needed for a successful application of night-time ventilation. For effective utilisation of the thermal mass both a sufficient heat transfer to the surface and sufficient conduction within the element are needed. The purpose of this study was to evaluate the impact of different parameters such as material properties, slab thickness and heat transfer coefficient on the heat storage capacity of building elements [60].

3.1 Model of a building element

A building element was represented by a homogeneous slab with half-thickness *d*. One surface of the slab was exposed to a varying temperature, while the other surface was considered adiabatic. The analytical solution to the heat transfer problem in a slab with convective boundary condition and sinusoidally varying air temperature ([37], [61]) was used to determine the spatial and temporal temperature profile in the element. Integrating the positive (charging) or negative (discharging) heat flow at the surface over one periodic cycle yields the dynamic heat storage capacity c_{dyn} of the element. This corresponds to the dynamic heat storage capacity as defined in the European standard EN ISO 13786 [62]. A method to calculate the dynamic heat storage capacity of an element composed of layers with different thermal properties is also presented in EN ISO 13786. The dynamic heat storage capacity depends on the time period of the temperature variation. As the performance of night-time ventilation mostly depends on the diurnal heat storage, the capacity was calculated based on a 24 h temperature variation.

3.2 Impact of different Parameters

Figure 8 shows the diurnal heat storage capacity, c_{dyn} of different building elements depending on the heat transfer coefficient *h*. The properties of the materials are given in Table 1. The impact of the heat transfer coefficient depends greatly on slab thickness and the thermal properties of the material. For thin slabs (d = 15 mm) the heat storage capacity is almost constant for heat transfer coefficients higher than h = 3 W/m^{2}K. In contrast, for thick slabs increasing the heat transfer coefficient up to h = 30 W/m^{2}K significantly increases the diurnal heat storage capacity. Generally, the storage capacity of thin elements, such as gypsum boards used for light-weight wall constructions or medium density fibreboards (MDF) used for furniture is rather small compared to thick and heavy elements such as a concrete ceiling or sand-lime brick walls (bricks made from sand and slaked lime). However, especially at a low heat transfer coefficient and in consideration of its large surface area, furniture might still make a notable contribution to the total heat storage capacity of a room.

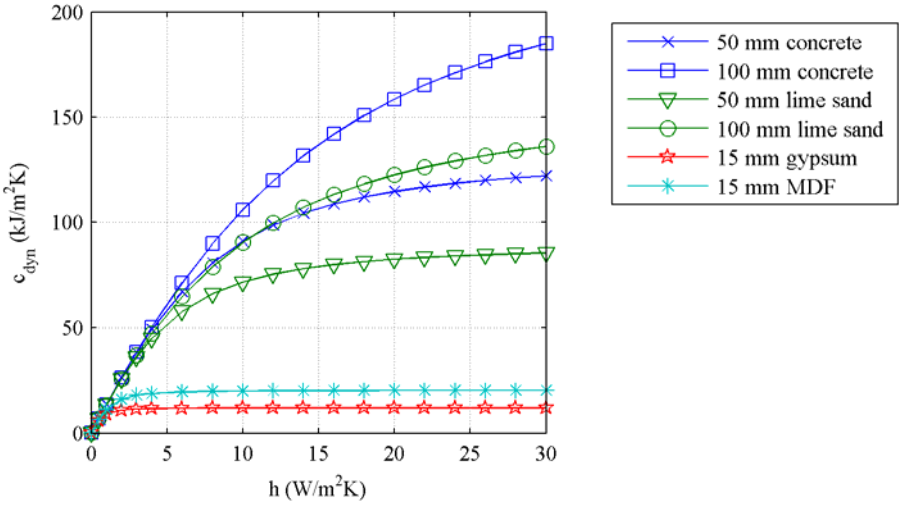

Figure 8. Diurnal heat storage capacity, c_{dyn} of different building elements depending on the heat transfer coefficient h.

Table 1. Material properties.

	λ (W/m^{2}K)	ρ (kg/m^3)	c (kJ/kgK)
Concrete	1.80	2400	1.1
Sand-lime	1.10	2000	0.9
Gypsum	0.40	1000	0.8
MDF	0.18	800	1.7
Gypsum, 20% PCM	0.36	960	9.0*
Gypsum, 40% PCM	0.32	920	17.3*

* In the melting temperature range.

Increasing the slab thickness clearly raises the diurnal heat storage capacity until a maximum is reached. Beyond the maximum the capacity decreases slightly and converges to a constant value as the thickness approaches infinity (Figure 9). This somewhat surprising effect has been described previously (e.g. [63]) and is explained by the superposition of an incident wave and a reflected wave. With increasing heat transfer coefficient the maximum becomes more distinct. Additionally the optimum thickness of a concrete slab increases from about d = 90 mm to 140 mm if the heat transfer coefficient increases from h = 5 W/m^{2}K to h = 30 W/m^{2}K.

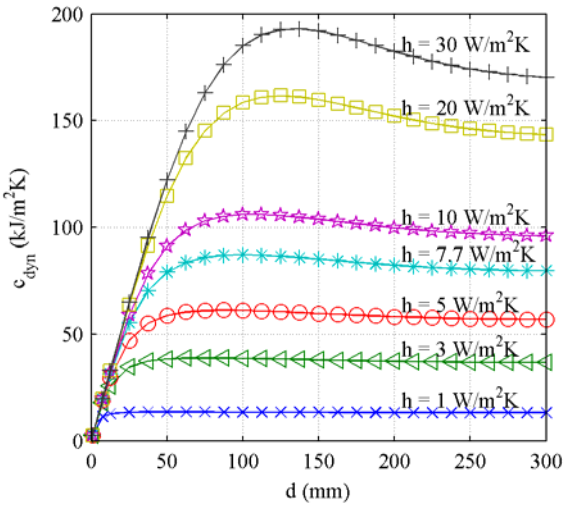

Figure 9. Diurnal heat storage capacity, c_{dyn} of a concrete slab depending on the thickness, d for different heat transfer coefficients, h.

Analysing the impact of the thermal conductivity, λ of the slab material showed that in most cases the storage capacity increases only slightly for conductivities above 1.8 W/mK (concrete). For thin slabs (d = 15 mm) there is almost no impact of the conductivity in the range from λ = 0.05 W/mK to λ = 50 W/mK. Only in the case of a very thick slab (d = 100 mm) in combination with a high heat transfer coefficient (h = 20 W/m^{2}K) does the storage capacity increase with conductivities up to 50 W/mK (Figure 10).

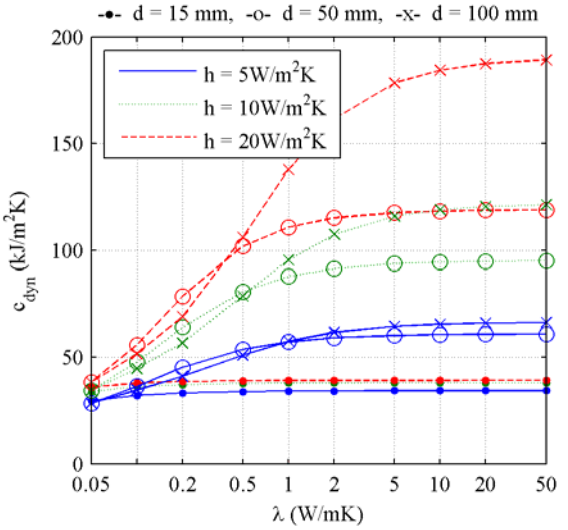

Figure 10. Diurnal heat storage capacity, c_{dyn} depending on the thermal conductivity, λ for different heat transfer coefficients, h and slab thicknesses, d; ρc = 2.6 MJ/m^{3}K.

The impact of the volumetric heat capacity, ρc is displayed in Figure 11. The heat storage capacity of very light materials such as insulation materials with ρc < 0.1 MJ/m^{3}K is generally very small. Even for a slab with half-thickness d = 100 mm and a high heat transfer coefficient, h = 20 W/m^{2}K, the heat storage capacity is only 10 kJ/m^{2}K. Increasing the thermal capacity to the value of concrete (ρc = 2.6 MJ/m^{3}K) significantly improves the storage capacity, especially at high heat transfer coefficients (h = 10 to 20 W/m^{2}K) to maximum

158 kJ/m^{2}K. Further improvement for capacities above ρc = 2.6 MJ/m^{3}K is only achieved for thin slabs (d = 15 mm) or at very high heat transfer coefficients (h = 20 W/m^{2}K).

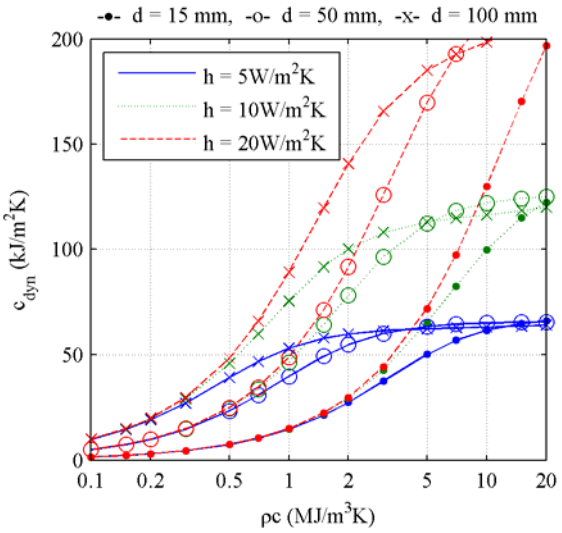

Figure 11. Diurnal heat storage capacity, c_{dyn} depending on the heat capacity, ρc for different heat transfer coefficients, h and slab thicknesses, d; λ = 1.8 W/mK.

A possibility for increasing the thermal heat capacity is the integration of micro-encapsulated phase change materials (PCM) into gypsum plaster boards or plaster [10]. For a rough estimation of the effect of PCMs on the dynamic heat storage capacity a very simple model, assuming a constant heat capacity in the melting temperature range, was used in this study. The estimated thermal properties are given in Table 1. Applying this model, the dynamic heat capacity of 15 mm thick gypsum plaster boards with 20 % and 40 % PCM content was found to be similar to a 50 mm and 100 mm thick concrete slab, respectively (Figure 12).

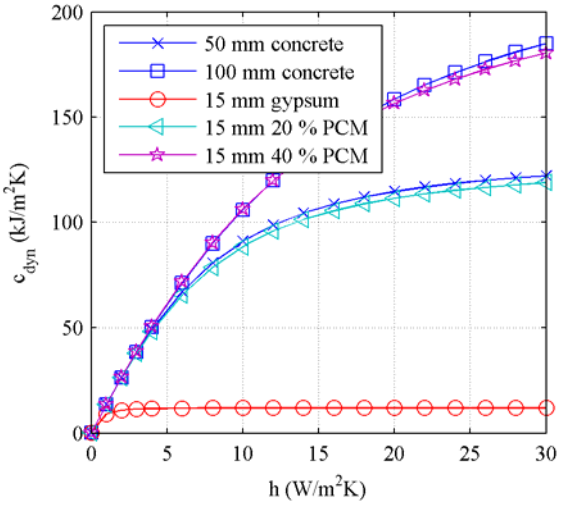

Figure 12. Effect of integrated PCM on the diurnal heat storage capacity, c_{dyn} depending on the heat transfer coefficient, h. Gypsum plaster board with different PCM contents compared to concrete slabs.

3.3 Conclusion

The dynamic heat storage capacity of building elements is affected by many parameters, like material properties, thickness and surface heat transfer coefficient. However, the sensitivity to each parameter depends on other parameters. In many cases the capacity is limited by one parameter and changing the limiting parameter has the largest effect. For example, the dynamic heat storage capacity of thin, light-weight elements, like gypsum plaster boards, is limited by the total heat capacity. In this case, the integration of phase change materials can significantly improve the dynamic heat storage capacity.

On the other hand, for massive elements, like a concrete floor slab or sand-lime brick walls, the thermal properties of common building materials are sufficient, but the dynamic heat storage capacity is mainly limited by the heat transfer at the surface. In this case the penetration depth of the temperature variation is limited and the total heat capacity of the element is only partially utilised. Therefore, for massive elements the dynamic heat storage capacity highly depends on the heat transfer coefficient.

4 Simulation study on performance of night-time ventilation

The heat storage capacity of building elements is an important precondition for the application of night cooling. However, the effectiveness of night-time ventilation also depends on other parameters such as internal and solar heat gains, climatic conditions (outdoor air temperature) and ventilation air change rate. Additionally, several building elements with different properties are typically present in a real room. The impact of different parameters and the interaction of different building elements were investigated in detail by building energy simulation [64].

4.1 Simulation model

A typical office room with 20 m^2 floor area (Table 2) was modelled using the building energy simulation programme *HELIOS* [65]. Starting from a base case, different parameters were varied to assess their effect on night ventilation performance. In order to assess the impact of thermal mass, three different building types, representing a light-weight (suspended ceiling, gypsum board walls), medium-weight (exposed concrete ceiling, gypsum board walls), and heavy-weight (exposed concrete ceiling, solid sand-lime brick walls) construction. The detailed composition of the building elements and the thermal properties of the building materials are given in Table 3. The resulting dynamic heat storage capacity per unit floor area is illustrated in Figure 13.

Table 2. Main parameters of the modelled office room.

Floor area	20	m^2
Room height	2.6	m
Volume	52	m^3
Facade area	10.4	m^2
Facade area/volume ratio	0.2	m^{-1}
Internal surface area	86.8	m^2
Ceiling area	20	m^2
Internal wall area	36.4	m^2
External wall area	4.8	m^2
Window area	5.6	m^2
Glazed area (aperture)	4.05	m^2
Glazed area/facade area ratio	38.9	%

Additionally three different levels of internal heat gains (low: 159 Wh/m^2d, medium: 229 Wh/m^2d and high: 313 Wh/m^2d) were defined to show their impact on night ventilation performance. In all cases the office was occupied by two people, with a heat gain of 126 W/person (60 % conv. / 40 % rad.). Heat gains from equipment (80 % conv. / 20 % rad.) were assumed to be 50 W/person (low) or 150 W/person (medium and high). Lighting power was 10 W/m^2 (40 % conv. / 60 % rad.) with different schedules representing an office with (low and medium) and without (high) daylight utilisation (Figure 14). No heat gains were assumed during weekends.

Table 3. Composition of building elements and thermal properties of building materials

Element	Material	*d* (m)	λ (W/mK)	ρ (kg/m^3)	*c* (kJ/kgK)
Floor slab (light-, medium-, heavy-weight)	Carpet	0.005	0.05	80	930
	Plaster Floor	0.08	1.5	2200	1080
	Sound insulation	0.04	0.04	30	1404
	Concrete	0.18	1.8	2400	1080
Suspended ceiling (light-weight)	Air gap	0.25	R = 0.160 m^{2}K/W		
	Acoustic panel	0.02	0.21	800	900
Internal wall (light-, medium-weight)	Gypsum board	0.025	0.4	1000	792
	Mineral wool	0.07	0.036	90	612
	Gypsum board	0.025	0.4	1000	792
Internal wall (heavy-weight)	Plaster	0.015	0.7	1400	936
	Sand-lime brick *	0.15	1.1	2000	936
	Plaster	0.015	0.7	1400	936
External wall (light-, medium-weight)	Concrete	0.18	1.8	2400	1080
	Exp. polystyrene	0.12	0.035	40	1200
	Gypsum board	0.025	0.4	1000	792
External wall (heavy-weight)	Plaster ext.	0.02	0.87	1600	1000
	Exp. polystyrene	0.12	0.035	40	1200
	Sand-lime brick *	0.15	1.1	2000	936
	Plaster	0.015	0.7	1400	936

* Sand-lime brick: Bricks made from sand and slaked lime.

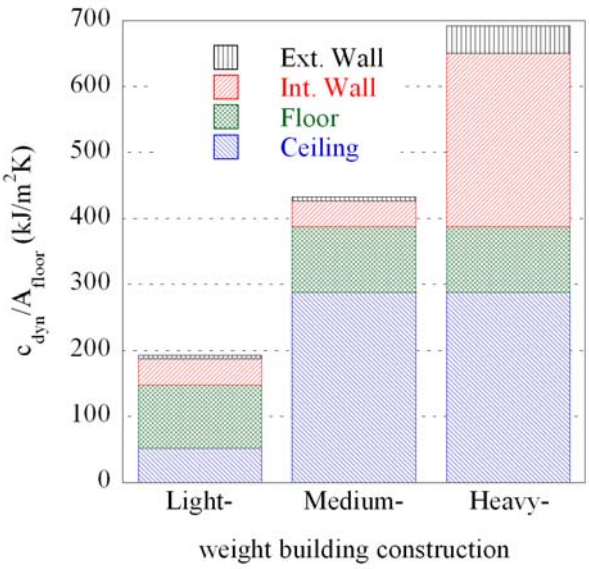

Figure 13. Dynamic heat storage capacity of building elements for three different levels of thermal mass (EN ISO 13786 [62]; excluding surface resistance).

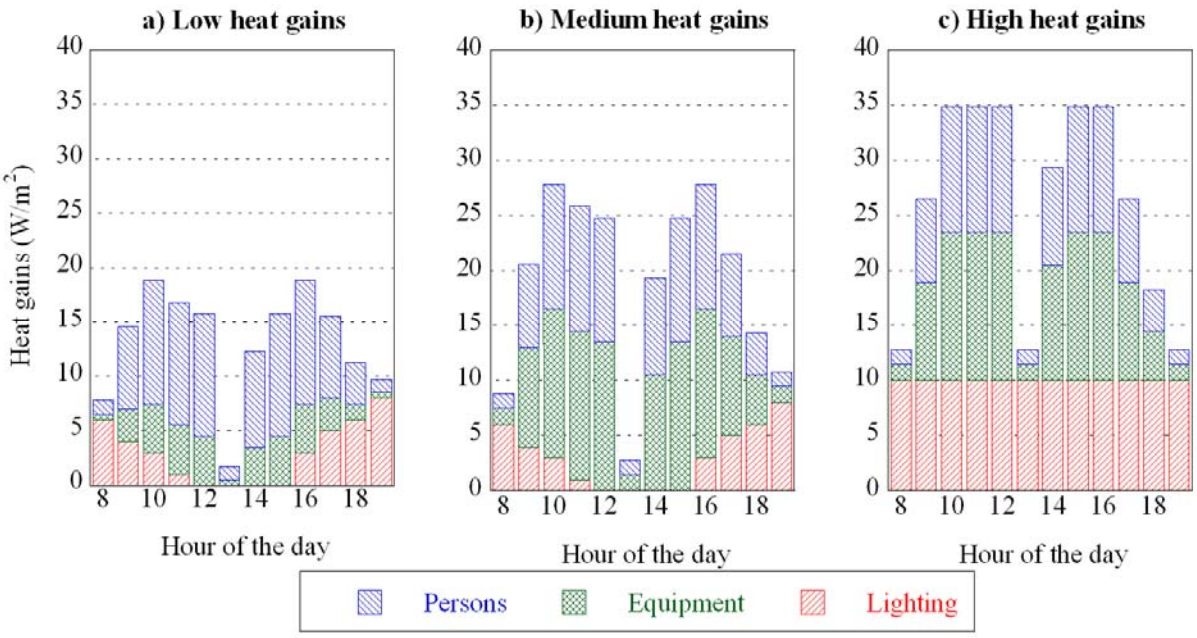

Figure 14. Low (159 Wh/m²d), medium (229 Wh/m²d) and high (313 Wh/m²d) internal heat gains over the course of a day.

Night-time ventilation was assumed from 7 pm to 7 am at a fixed air change rate (base case: 6 ACH). The increased air change rate was applied if the external temperature was at least ΔT_{crit} = 3 K below the average room surface temperature, $T_{Surface}$. To prevent over-cooling, night ventilation was terminated as soon as the average room surface temperature, $T_{Surface}$ fell below 20 °C.

Different climatic data sets were applied to assess the impact of local and annual climatic variability. In addition to semi-synthetic data for different locations (*Meteonorm* and *Design Reference Year*, DRY), long-term measured data for Zurich (*ANETZ*) were used.

In order to evaluate the impact of the heat transfer between building elements and the room air, a wide range of surface heat transfer coefficients was investigated. In *HELIOS* convective and radiative heat transfer is modelled using combined heat transfer coefficients. In the base case, all combined heat transfer coefficients were set to h = 7.7 W/m²K in accordance with DIN 4701 [66].

Night-time ventilation performance was rated by evaluating overheating degree hours of the operative room temperature above 26 °C. Different standards (e.g. [54], [67], [68]) give limits of acceptable overheating corresponding to a range from about 100 to 400 Kh above 26 °C per year. The limit to be applied for a certain application mainly depends on the building usage. Generally a wider temperature range will be accepted in residential buildings than in commercial buildings. Furthermore, the tolerated extent of overheating also depends on the occupants' possibilities to adapt themselves, (e.g. by changing clothing) and control their environment (operation of windows, access to building controls, etc.). In order to account for the ability to adaptation the concept of adaptive thermal comfort has been proposed which relates the comfort temperature to the external temperature [69], [70]. In this study 100 Kh above 26 °C was considered good thermal comfort, while up to 400 Kh was still considered acceptable.

4.2 Impact of different parameters

Figure 15 shows the overheating degree hours above 26 °C (ODH_{26}) in a medium thermal mass office with high internal heat gains based on different climatic data for Zurich SMA. In the period from 1981 to 2005

(excluding 2003), overheating degree hours exceeding 26 °C varied in the range from 20 to 400 Kh if measured weather data (ANETZ) was used. In 2003, exceptionally high summer temperatures resulted in nearly 900 Kh above 26 °C, while the mean value from 1981 to 2005 was 142 Kh/a.

Simulations based on Meteonorm or DRY data resulted in a far lower extent of overheating. Overheating degree hours amounted to 2.3 Kh/a if the Meteonorm standard data were applied, and 79 Kh/a when Meteonorm data based on 10-year maximum monthly mean values were used. Applying DRY data (based on measurements from 1981-1990) resulted in 25 Kh/a, while ANETZ data averaged over the same period yielded 82 Kh/a. For the following simulations ANETZ data from the period 1996 to 2005 were applied.

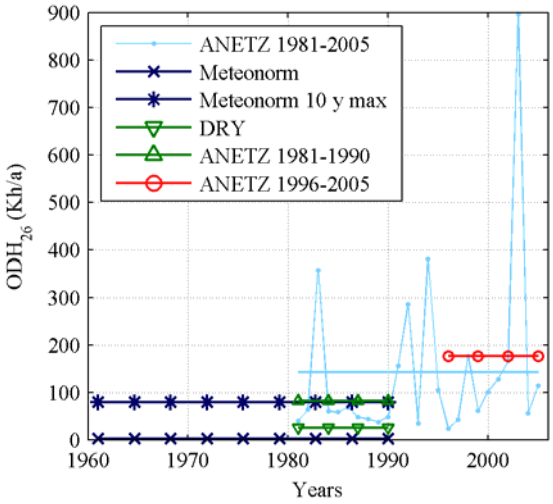

Figure 15. Overheating degree hours above 26 °C (ODH_{26}) based on different climatic data for Zurich SMA: ANETZ 1981-2005, Meteonorm (standard and 10-year maximum), DRY, ANETZ 1981-1990 (mean) and ANETZ 1996-2005 (mean); medium thermal mass, high level of internal heat gains, air change rate 6 ACH, all heat transfer coefficients h = 7.7 W/m²K.

Significant effects of both different building constructions (thermal mass) and different levels of internal heat gains are shown in Figure 16. While in most cases thermal conditions were quite comfortable with less than 200 Kh/a, hardly acceptable overheating (ODH_{26} = 416 Kh/a) resulted for the extreme case of a light weight office with high internal loads. A 180 mm thick concrete ceiling in direct contact with the room air reduced overheating by a factor of two compared to a suspended ceiling. The additional application of solid sand-lime brick walls instead of gypsum board walls reduced overheating by a factor of three.

Internal heat gains had an effect of similar magnitude. Both increasing the heat gains of office equipment from 50 W to 150 W per person and using artificial light instead of daylight, respectively, increased overheating degree hours by a factor of 2 to 2.5. These factors depended on thermal mass, with a smaller sensitivity in heavier buildings. Especially in light-weight buildings, heat gains should be reduced as far as possible by applying energy-efficient office equipment, daylight utilisation, and the installation of effective solar shading devices.

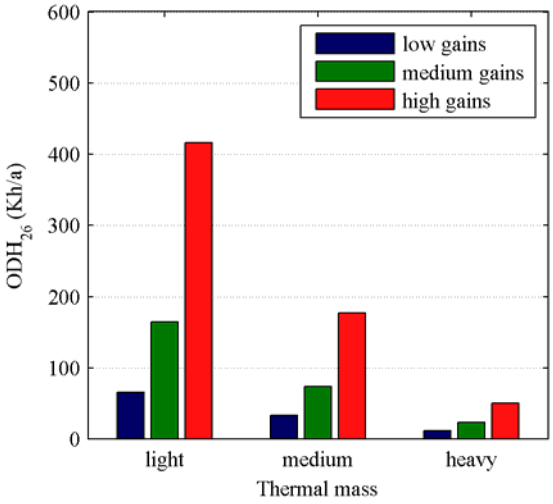

Figure 16. Overheating degree hours above 26 °C for different building constructions (light, medium and heavy mass) and different levels of internal heat gains (low, medium and high), Zurich (ANETZ 1996-2005), 6 ACH, all heat transfer coefficients h = 7.7 W/m²K.

Figure 17 (left) shows the overheating degree hours above 26 °C as a function of air change rate during night-time ventilation (0.5 - 32 ACH) for high heat gains and different building constructions. In case of a medium- and heavy weight building, a relatively low air change rate below 4 ACH was sufficient to maintain the limit of thermal comfort (prEN 15251 [54], category III; about 400 Kh). In the light-weight building an air change rate of about 7 ACH is needed to keep this limit.

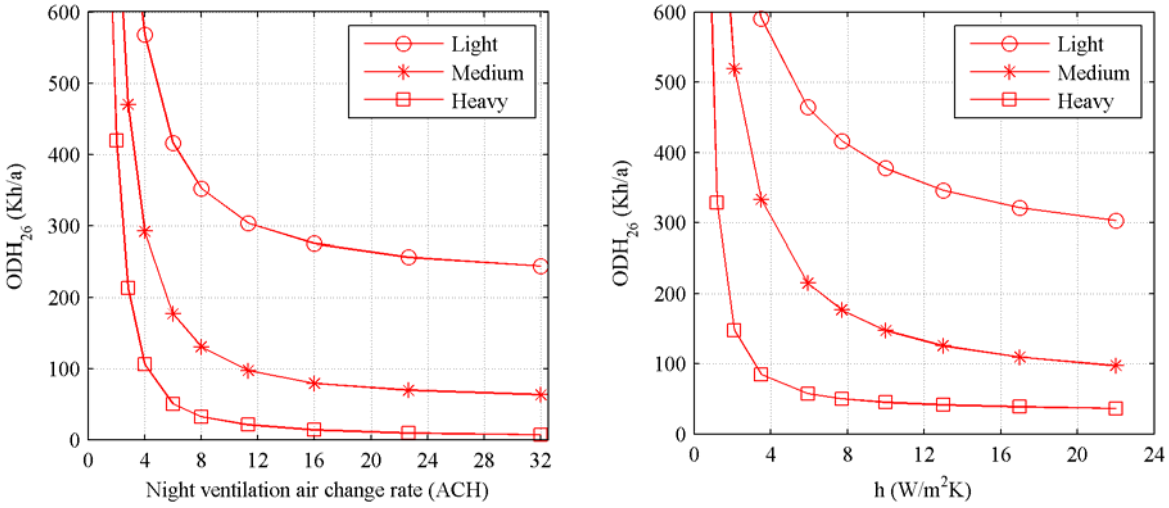

Figure 17. Overheating degree hours above 26 °C (ODH_{26}) for high internal heat gains and different building constructions; Zurich, ANETZ 1996-2005; left: depending on the air change rate, h = 7.7 W/m²K; right: depending on the heat transfer coefficients (all surfaces, day and night), air change rate: 6 ACH.

Increasing the night ventilation air change rate improved thermal comfort significantly. For the example of a heavy-weight building with high internal heat gains, overheating was reduced from 419 to 32 Kh/a when the air change rate was increased from 2 to 8 ACH. However, applying a higher air change rate than 8 ACH did not improve thermal comfort significantly. The critical air change rate beyond which no significant improvement in absolute ODH_{26} values occurred, increased with decreasing thermal mass.

Variation of the combined heat transfer coefficients (convection and radiation) in the range from 5.9 to 10 W/m^{2}K (EN ISO 6946 [38]) generally had a minor effect on overheating degree hours (Figure 17, right). The most significant effect was found for a light-weight office, where overheating degree hours were reduced from 464 to 377 Kh/a. Only little improvement was found for increased heat transfer coefficients (HTC) in the range from 10 to 22 W/m^{2}K. However, night-time ventilation becomes increasingly inefficient for HTCs below about h = 4 W/m^{2}K.

Changing the air flow rate during the day mainly affected thermal comfort in cases where night-time ventilation is not very effective, i.e. in light or medium-weight buildings together with a high or medium level of internal heat gains (Figure 18). In such cases, heat gains were partly discharged during the day and overheating decreased with increasing air change rate. In contrast, overheating increased slightly in cases with very good thermal comfort (ODH_{26} < 50 Kh/a), when the air flow rate during the day was increased. In cases with good night ventilation performance with daytime indoor air temperatures below the ambient temperature, an increased air flow rate during the day causes additional heat gains.

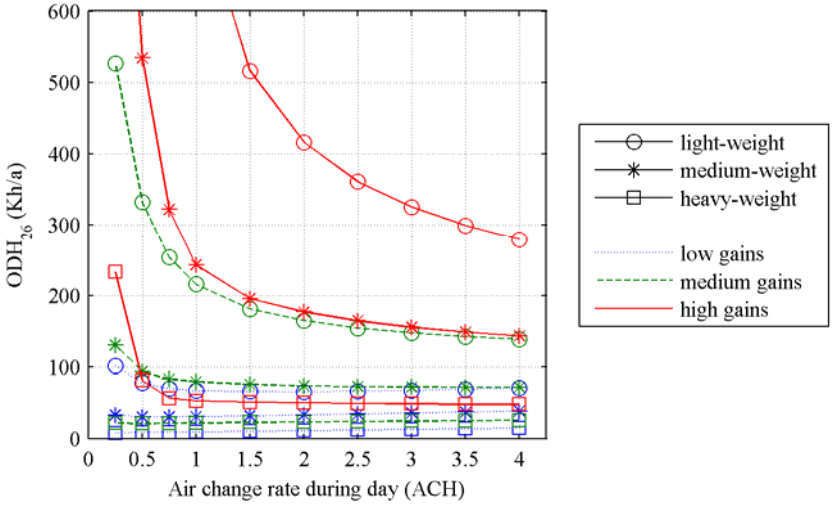

Figure 18. Overheating degree hours (ODH) above 26 °C as a function of air change rate during the day for different building constructions and different levels of internal heat gains; 6 ACH; heat transfer coefficients h = 7.7 W/m^{2}K (all surfaces, day and night); Zurich, ANETZ 1996-2005.

4.3 Discussion and conclusions

Night-time ventilation performance was found to be highly sensitive to climatic conditions, which demonstrates the significance of high-quality climatic data for building energy simulations. Furthermore, simulations based on commonly-used semi-synthetic one year data sets such as Meteonorm or DRY data tend to underestimate the extent of overheating compared to weather data measured in recent years. Therefore, for reliable thermal comfort predictions the application of up-to-date climatic data from long-term measurements including extreme weather conditions is recommended. Because of the gradually warming of the global climate, continuous updating of weather data for building simulation is needed.

Simulations with different night ventilation air change rates clearly demonstrated the effectiveness of night-time ventilation, as increased flow rates significantly reduced overheating degree hours. However, increasing the air flow rate above a certain value – a critical air flow rate depending on building construction and heat gains – did not lead to further improvement worth mentioning. On the other hand, the very high sensitivity to

night ventilation air change rates up to about 4 ACH makes predictions of thermal comfort very uncertain. This is especially true for buildings using natural night ventilation, where the air change rate depends on ambient temperature and wind conditions. If natural ventilation is driven by buoyancy forces, low air flow rates coincide with a high external temperature, and the cooling effect is smallest during warm periods. In cases where air change rates in a range of high sensitivity are to be expected, the application of a hybrid ventilation system should be considered. A shortfall of the critical air flow rate can thus be prevented and the risk of overheating can be reduced.

Due to high air change rates and high air flow velocities, increased heat transfer is expected during night-time ventilation. However, only little improvement of thermal comfort was found for heat transfer coefficients in the range from 10 up to 22 W/m^{2}K. On the other hand, if all surfaces have a similar temperature which is higher than the room temperature – a typical situation during night-time ventilation – a combined heat transfer model overestimates the radiative heat flow. Heat transfer coefficients for convection alone, however, can be as low as 0.7 W/m^{2}K (EN ISO 13791 [39]; downward heat-flow at horizontal surfaces). Especially at the ceiling (downward heat-flow during night-time ventilation) free convection might be very limited and the reduced heat transfer could impair the efficiency of night-time ventilation. The simulation study showed a very high sensitivity for heat transfer coefficients below about h = 4 W/m^{2}K. The wide range of possible heat transfer coefficients and the partially high sensitivity can cause major uncertainties in thermal comfort predictions. Therefore, convective and radiative heat transfer during night-time ventilation needs to be investigated in more detail.

5 Experiments on heat transfer during night-time ventilation

The convective heat transfer at internal room surfaces is highly affected by the indoor air temperature distribution and the near-surface velocities both of which can vary significantly depending on the air flow pattern in the room. Additionally, if the surfaces of a room differ in thermal capacity or heat transfer, their temperature will also differ and radiation becomes significant. This study provides a detailed analysis of convection and radiation during night-time ventilation depending on the air flow rate and the initial temperature difference between the inflowing air and the room. Heat transfer in case of mixing and displacement ventilation has been investigated in a full scale test room. The main active thermal mass of the test room was located in the ceiling which represents a typical situation in offices [71].

5.1 Setup of the test room

A test room at Aalborg University – a wooden construction insulated with 100 mm rock wool – was rebuilt for the experimental investigation of the heat transfer during night-time ventilation. For increased thermal mass a heavy ceiling element consisting of 7 layers of 12.5 mm gypsum boards was installed [72]. The walls and the floor were insulated with 160 mm (floor: 230 mm) expanded polystyrene (EPS). After installation of the insulation the internal dimensions were 2.64 m x 3.17 m x 2.93 m (width x length x height) resulting in a volume of 24.52 m^3. A detailed description of the test room can be found in [73].

A mechanical ventilation system was installed to supply air at a defined temperature to the test room, providing an air flow rate ranging from 2.3 to 13 air changes per hour (ACH). Two different air distribution principles representing mixing and displacement ventilation were investigated (Figure 19).

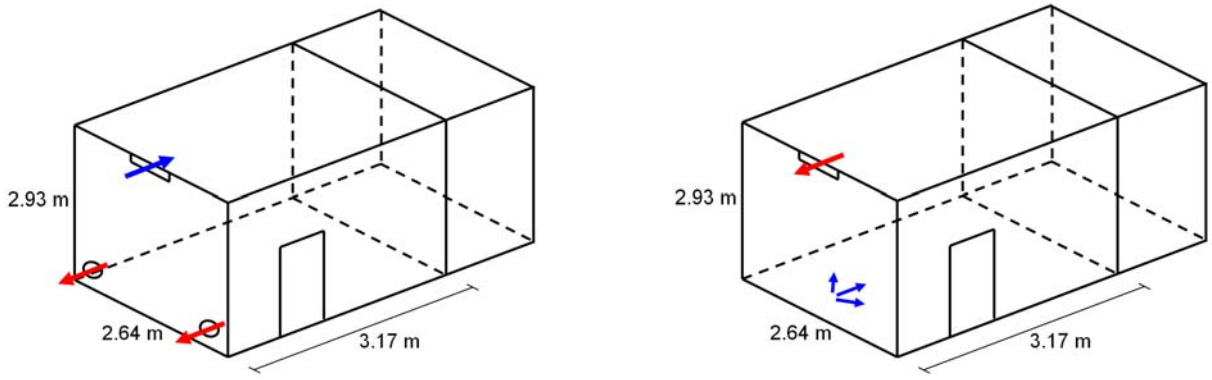

Figure 19. Configurations of the air in- and outlet openings of the test room for mixing (left) and displacement ventilation (right).

In total 110 thermocouples were installed in the ceiling element to measure the temperature at 22 positions and 5 different layers (including the internal surface). 18 hot sphere anemometers were installed to measure the air flow velocity close to the ceiling. At the wall and floor surfaces temperatures were measured at 3 positions each. Additional thermocouples were installed to measure air temperatures close to the surfaces and in the symmetric plane of the room. Also the in- and outflowing air temperatures were measured by thermocouples. The air flow rate was measured using an orifice and a micro-manometer.

5.2 Procedure for experiments and data evaluation

In each experiment the response of the test room to a step in the air flow rate (inflow temperature below room temperature) was measured for at least 12 hours. In total 16 experiments with different air distribution modes, air change rates (*ACR*) and initial temperature differences (ΔT_0) were conducted (Table 4).

Table 4. List of experiments.

No	Air distribution mode	*ACR* (ACH)	ΔT_0 (K)
1	Mixing ventilation	2.3	7.9
2	Mixing ventilation	3.3	4.3
3	Mixing ventilation	3.3	10.2
4	Mixing ventilation	6.7	2.9
5	Mixing ventilation	6.8	6.1
6	Mixing ventilation	6.6	8.9
7	Mixing ventilation	13.1	2.9
8	Mixing ventilation	13.2	4.0
9	Mixing ventilation	13.1	5.3
10	Mixing ventilation	13.3	9.2
11	Displacement ventilation	3.1	10.1
12	Displacement ventilation	6.7	5.8
13	Displacement ventilation	6.7	11.3
14	Displacement ventilation	12.6	3.6
15	Displacement ventilation	12.6	6.0
16	Displacement ventilation	12.7	12.7

By way of example, Figure 20 shows temperature profiles measured during experiment no. 4, with mixing ventilation with 6.7 ACH and an initial temperature difference of ΔT_0 = 2.9 K. Profiles A to E correspond to different layers of the ceiling element, where A is the internal surface and E is the external surface of the gypsum boards.

For the evaluation of the heat transfer at the internal room surfaces, first the total surface heat flow (conduction in the material) for each section (22 at the ceiling and 3 at the other surfaces) was calculated. The conductive surface heat flow was determined by applying the measured boundary conditions (A and E in Figure 20) to a transient 1-dimensional finite difference model using an explicit scheme. Running the model resulted in the spatial temperature profile for each time step. For each section, *i*, the conductive heat flux, $\dot{q}_{cond,i}$ at the surface was calculated from the spatial temperature gradient. The radiative heat flux, $\dot{q}_{rad,i}$ between the surfaces was determined from the measured surface temperatures and the view factors. The difference between conduction and radiation then yielded the convective heat flux, $\dot{q}_{conv,i}$ for each section. The total convective heat flow, $\dot{q}_{conv,tot}$ was then yielded from integrating $\dot{q}_{conv,i}$ over all surfaces.

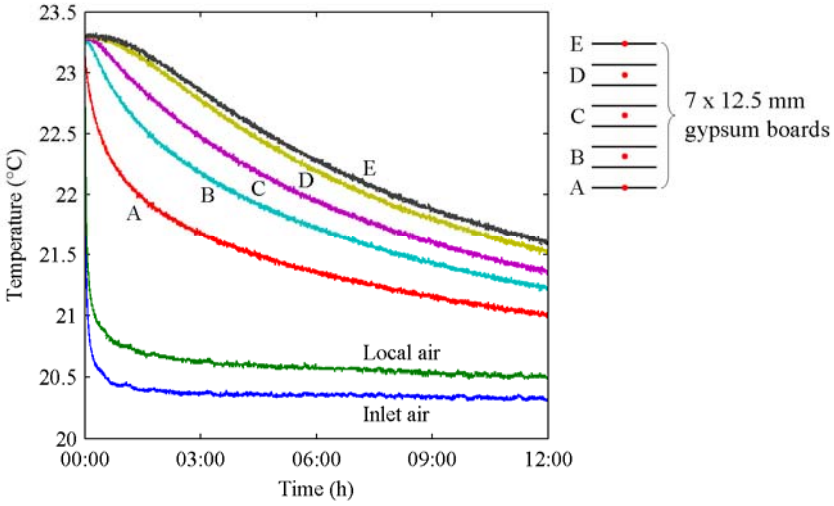

Figure 20. Temperatures measured at the ceiling during the experiment no. 4 with mixing ventilation with 6.7 ACH and an initial temperature difference of ΔT_0 = 2.9 K (A-E: different layers of the ceiling, A: internal surface, E: external surface).

5.3 Experimental results

To compare temperature profiles in different experiments the dimensionless Temperature, θ was defined as,

$$\theta = \frac{T - T_{Inlet}}{\Delta T_0}, \tag{6}$$

so that θ = 0 corresponds to the inlet air temperature and θ = 1 to the initial room temperature.

To characterises the flow pattern of the inflowing air jet the 'dimensional' Archimedes number, *Ar'* was defined as,

$$Ar' = \left(\overline{T}_{Surface} - T_{Inlet}\right) / \dot{V}^2, \qquad \left(Ks^2/m^6\right). \tag{7}$$

In mixing ventilation with a small Archimedes number (small temperature difference, high flow rate) the inlet air jet is attached to the ceiling, while for a high Archimedes number (large temperature difference, low flow rate) the air tends to drop down when entering the room.

Figure 21 shows vertical temperature profiles and horizontal temperature profiles 30 mm below the ceiling in experiments with mixing and displacement ventilation, and each with a low and high Archimedes number. For small Archimedes numbers, due to the higher air flow rate the dimensionless room air temperature is generally lower, i.e. closer to the inlet air temperature.

In the experiment with mixing ventilation and low Archimedes number (experiment no. 7) the temperature profiles clearly show the cold air jet close to the ceiling. Along the centre line the temperature increases almost linearly (Figure 21, c)). In the lower part of the room the air is mixed well, i.e. the temperature distribution is homogeneous.

In case of mixing ventilation and a high Archimedes number (experiment no. 3) the cold inflowing air drops down. Except for a small area close to the inlet opening, the air temperature close to the ceiling is very high and homogeneously distributed.

In the experiments with displacement ventilation (experiments no. 11 and 14) the temperature profiles are similar, showing a clear stratification with the largest gradient close to the ceiling. Along the ceiling the air temperature is distributed homogeneously with a slight decrease towards the outlet opening.

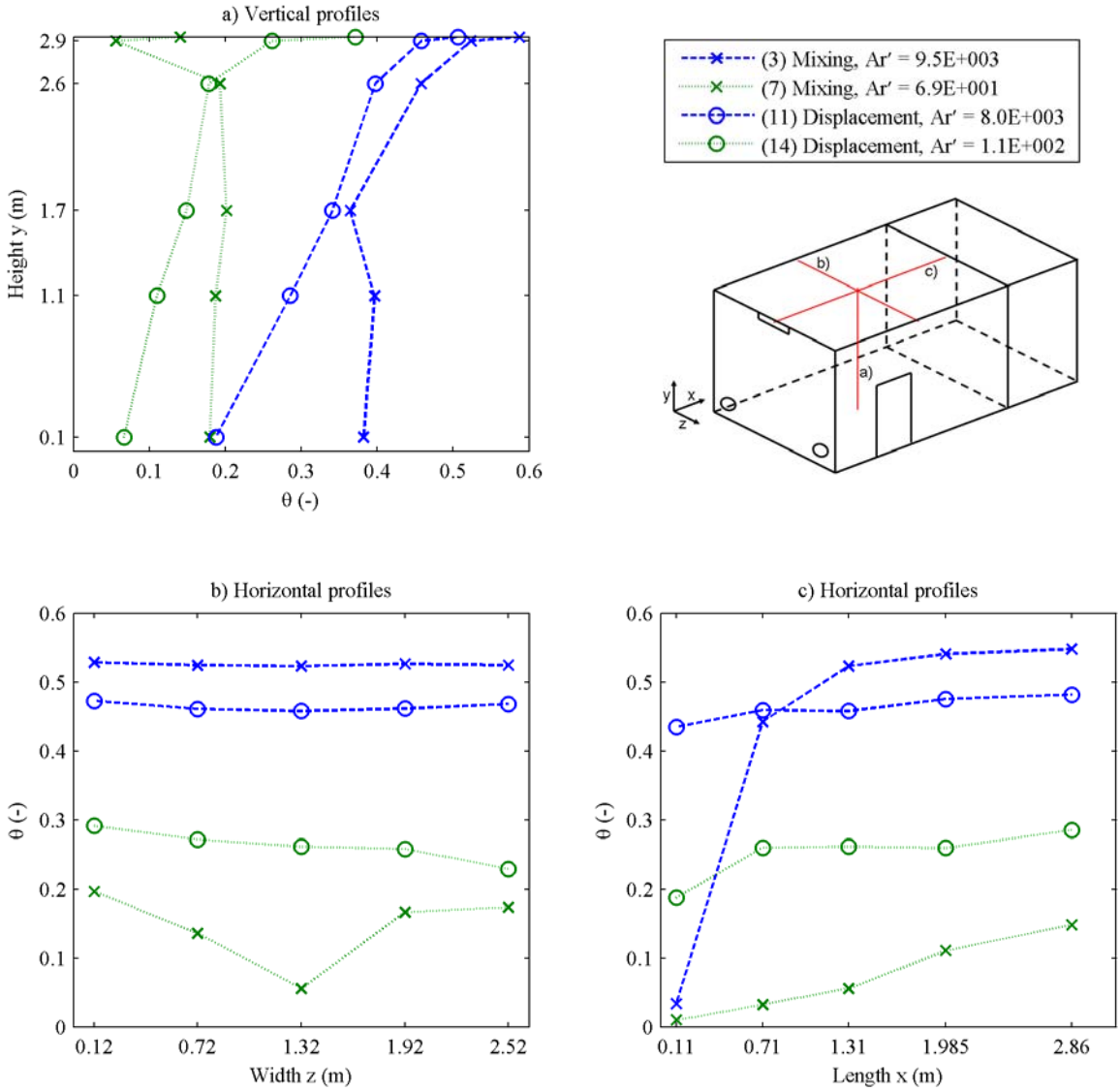

Figure 21. Temperature profiles (dimensionless temperature θ) comparing experiments no. 3, 7, 11 and 14; a) Vertical profiles (x = 1.31 m, z = 1.32 m); b), c) Horizontal profiles close to the ceiling (y = 2.9 m, b) x = 1.31 m, c) z = 1.32 m); mean values of the 12th hour.

The different air flow pattern and the development of the air jet also affect the heat transfer at the ceiling. To demonstrate this, the ratio of the convective and the total heat flow from the ceiling was defined as,

$$\gamma = \frac{\dot{Q}_{conv,\,Ceiling}}{\dot{Q}_{cond,\,Ceiling}}. \qquad (8)$$

Figure 22 shows the convection ratio, γ depending on the 'dimensional' Archimedes number, *Ar'*. During experiments with mixing ventilation, for small Archimedes numbers the inlet air jet is attached to the ceiling and the convection ratio is large. For higher Archimedes numbers the jet tends to drop down. In this case a smaller proportion of the total heat flow is due to convection and radiation becomes dominant. In

displacement ventilation, the air flow pattern does not change depending on buoyancy effects and the impact of *Ar'* is small. In all experiments with displacement ventilation less than 32 % of the heat flow from the ceiling is due to convection.

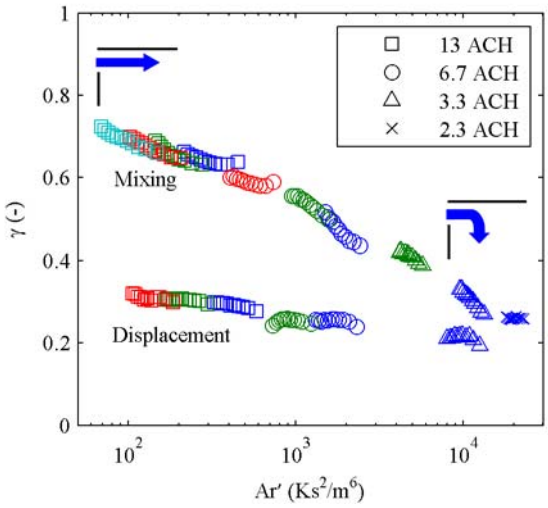

Figure 22. Ratio γ of convective to total heat flow from the ceiling depending on Ar' for mixing and displacement ventilation; hourly values, first hour excluded. Uncertainty estimate for γ: ± 0.11 [73].

Comparing different experiments shows that the mean convective heat flux from all internal room surfaces scales linearly with the difference between the mean surface temperature and the inflowing air temperature. This means, that the average heat transfer coefficient, $h' = \dot{q}_{conv,tot} / \left(\overline{T}_{Surface} - T_{Inlet}\right)$, defined using the inlet air temperature instead of the room air temperature, is almost constant during each experiment and for experiments with different inflowing air temperatures (Figure 23).

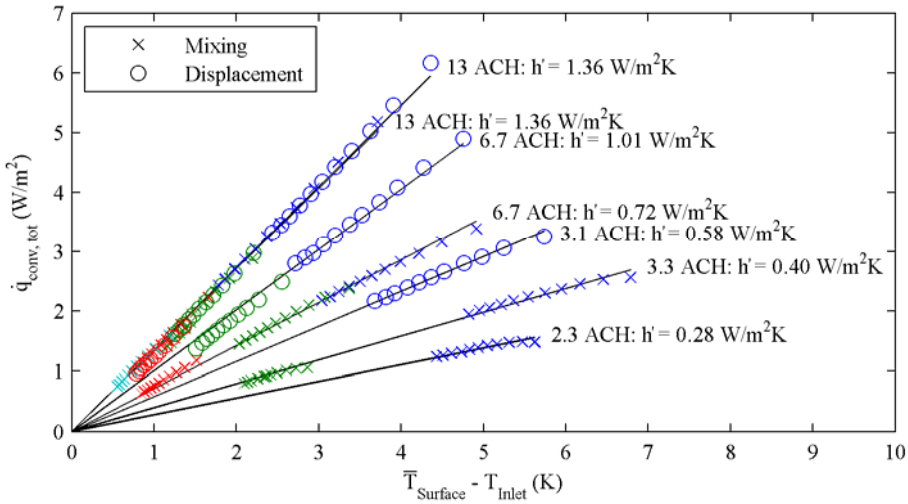

Figure 23. Mean convective heat flux from all surfaces depending on the difference between the mean surface temperature and the inlet air temperature; hourly values, first hour excluded; different colours relate to different experiments. Uncertainty estimate for $\dot{Q}_{conv,tot}$: ± 16 % [73].

The performance of night-time ventilation can be described by the temperature efficiency of the ventilation:

$$\eta = \frac{T_{Outlet} - T_{Inlet}}{\overline{T}_{Surface} - T_{Inlet}} \tag{9}$$

The temperature efficiency yielded from the measurements mainly depends on the air distribution mode and the air change rate (Figure 24). During each experiment (excluding the first hour) and for different inlet air temperatures the efficiency is almost constant.

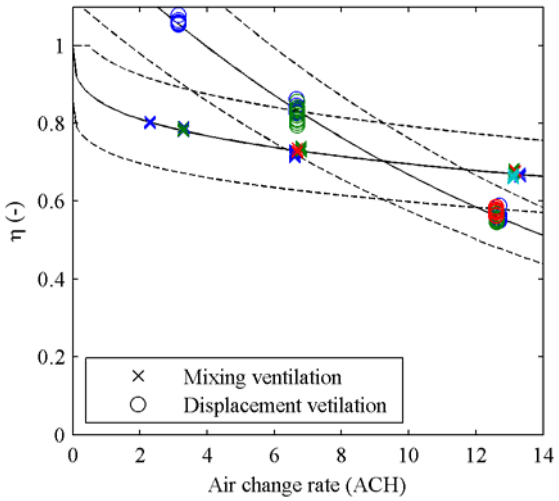

Figure 24. Temperature efficiency η depending on the air change rate for mixing and displacement ventilation; hourly values, first hour excluded. Fitted curves with estimated uncertainty bands (± 14 % [73])

In a perfectly mixed room, during night-time cooling ($T_{Inlet} < \overline{T}_{Surface}$ and without internal heat sources) the temperature efficiency is limited to 1. The values found in experiments with mixing ventilation decrease slightly with increasing air change rate. In displacement ventilation at small air flow rates, the temperature stratification can result in an efficiency exceeding 1. For higher air change rates, the decrease in the efficiency is more distinct for displacement ventilation than for mixing ventilation.

5.4 Conclusion

The experimental results clearly demonstrated the interaction of convective and radiative heat flows contributing to the total heat flow discharged from a room during night-time ventilation. For mixing ventilation, different flow characteristics significantly affect the ratio of the convective to the total heat flow from the ceiling. In cases with low convective heat transfer at the ceiling (mixing ventilation at high Archimedes number or displacement ventilation) large differences in surface temperatures cause higher radiative heat flows from the ceiling to the floor.

Nonetheless, it is beneficial to prevent warm air from accumulating below the ceiling. In displacement ventilation this is achieved through the location of the outlet opening close to the ceiling. At low air flow rates, the temperature stratification and the high location of the outlet opening results in a very high temperature efficiency ($\eta > 1$). In mixing ventilation warm air should be removed from the ceiling by the inflowing air jet. However, only at a relatively high air change rate (above about 10 ACH) the effect of the air jet flowing along

the ceiling becomes significant and mixing ventilation is more efficient. Therefore, if a low air flow rate is expected, the outlet opening should be placed as close to the ceiling as possible.

6 Design method for concept design phase

The findings from the previously described studies shall be combined to develop a practicable method for the estimation of the potential for cooling by night-time ventilation during an early stage of design.

6.1 Design method

The climatic conditions can be characterised by the climatic cooling potential, *CCP* (Kh), the thermal mass of the building can be estimated by the dynamic heat storage capacity, c_{dyn} (kJ/m^{2}K), and the air flow pattern including the resulting heat transfer can be described by the temperature efficiency of the ventilation, η.

In order to assure thermal comfort two criteria need to be satisfied:

1. The thermal capacity of the building needs to be sufficient to accumulate the daily heat gains within an acceptable temperature variation.
2. The climatic cooling potential and the effective air flow rate need to be sufficient to discharge the stored heat during the night.

If both criteria are satisfied for each day of the year, the building temperature will stay within the comfort range which was defined to assess the amount of thermal mass and the climatic cooling potential. As the heat gains and the climatic cooling potential are highly variable, it might not be possible to satisfy both criteria for every day of the year. In this case a certain extent of overheating will occur especially during hot periods, when high heat gains coincide with a low cooling potential. Assessing the extent of overheating during hot spells requires a dynamic model considering all parameters jointly. However, for a first estimation during the concept design phase, the two criteria can be considered separately. Furthermore each day/night cycle is considered separately, and therefore dynamic effects with time periods longer than 24 hours are not taken into account.

To assess the necessary amount of thermal mass, the daily heat gains, Q_d (Wh) need to be estimated and the maximum acceptable daily temperature variation, ΔT (K) needs to be determined. For the internal heat gains, the heat from people, equipment and lighting need to be considered. The solar heat gains can be estimated from the solar irradiation, the glazed area and the total solar energy transmittance (g-value) of the facade. If the outdoor temperature is higher than the indoor temperature, additional heat gains arise from thermal transmission and ventilation during the day.

The total amount of dynamic heat storage capacity, C_{dyn} (J/K) can then be estimated as,

$$C_{dyn} = \sum_i c_{dyn,i} \cdot A_i > \frac{Q_d \cdot 3600\,s/h}{\Delta T} \qquad (10)$$

In the calculation of the heat storage capacity, c_{dyn} of the building elements in the room, the surface heat transfer during the day needs to be considered (see Figure 8). In the European Standard prEN 15251 [54] ranges for thermal comfort are given in three categories, A: 2 K, B: 3 K and C: 5 K. According to the ASHRAE Standard 55 [70] the thermal comfort range is 5 K (PPD: 10 %) to 7 K (PPD: 20 %). Additionally, the maximum temperature drift for a 4 h period is given as 3.3 K. Generally broader temperature ranges are acceptable in non-air-conditioned buildings [74].

The estimation of the air change rate and daily cooling potential, CCP_d necessary to discharge daily heat gains, Q_d is based on the conservation of energy during one daily cycle of charging and discharging the thermal mass:

$$Q_d = \eta \cdot A_{Floor} \cdot H \cdot \frac{ACR}{3600\,s/h} \cdot \rho_{Air} \cdot c_{p,\,Air} \cdot CCP_d \qquad (11)$$

where η is the temperature efficiency of the ventilation, A_{Floor} the floor area, H the room height, ρ_{Air} the density of air and $c_{p,\,Air}$ the heat capacity of air. The daily cooling potential, CCP_d available at a certain location can be determined from cumulative distributions as presented in Figure 5.

Rearranging equation 11 yields the daily heat gains per unit floor area and CCP_d (Wh/m^{2}Kh), which can be discharged at a given air change rate (ACH) depending on the temperature efficiency, η:

$$\frac{Q_d}{A_{Floor} \cdot CCP_d} = \eta \cdot H \cdot \frac{ACR}{3600\,s/h} \cdot \rho_{Air} \cdot c_{p,\,Air} \qquad (12)$$

For the temperature efficiency, found in the experiments with mixing and displacement ventilation (section 5) this correlation is shown in Figure 25. This diagram provides a descriptive illustration of night-time ventilation performance. Additionally, such a diagram can be used as design chart to estimate the air flow rate, necessary to discharge daily heat gains at a given CCP_d. However, in order to make this method more generally applicable, further work is needed to determine the temperature efficiency for various room geometries, constructions (amount and location of thermal mass) and air distribution principles (location of inlet and outlet openings). A catalogue of design charts for various cases will be of immediate use for estimating the performance of night-time ventilation during the concept design phase.

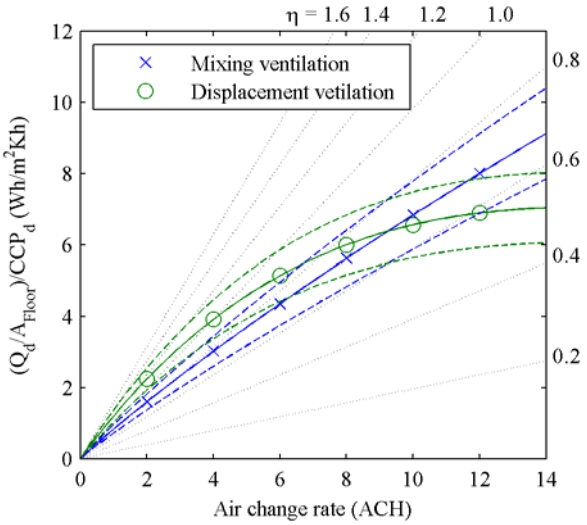

Figure 25. Heat discharged during night-time ventilation per unit floor area and daily CCP depending on the air change rate; based on experimental results for mixing and displacement ventilation (including range of uncertainty [73]) and lines of constant efficiency η; room height H = 2.93 m.

6.2 Example of application

An example shall be given to illustrate the application of the previously described design method for the office room defined for the simulation study (see section 4) located in Zurich:

1. Heat gains

Three different levels of internal heat gains, low (159 Wh/m^2), medium (229 Wh/m^2) and high (313 Wh/m^2) were defined for the parameter study.

Additionally, solar heat gains need to be considered. In the simulation model, the office room had two windows (total glazed area, A_{Glass} = 4.05 m^2) on the South façade. With the solar shading device closed, the total solar energy transmittance, g was 16 %. Assuming solar irradiation on a sunny day in July of I = 2000 Wh/m^2 yields:

$$\frac{Q_{d,Solar}}{A_{Floor}} = \frac{A_{Glass}}{A_{Floor}} \cdot g \cdot I = \frac{4.05\ m^2}{20\ m^2} \cdot 0.16 \cdot 2000 \frac{Wh}{m^2} = 65 \frac{Wh}{m^2} \quad (13)$$

For the total daily heat gains follows:

- Low gains: Q_d / A_{Floor} = 224 Wh/m^2
- Medium gains: Q_d / A_{Floor} = 294 Wh/m^2
- High gains: Q_d / A_{Floor} = 378 Wh/m^2

2. Thermal mass

For the calculation of the dynamic heat storage capacity of the building elements the heat transfer coefficient was assumed as h = 7.7 W/m^{2}K. For the three cases defined for the simulation study the dynamic heat storage capacity per unit floor area amounts to [62]:

- Light-weight: C_{dyn} / A_{Floor} = 131 kJ/m^{2}K
- Medium-weight: C_{dyn} / A_{Floor} = 180 kJ/m^{2}K
- Heavy-weight: C_{dyn} / A_{Floor} = 287 kJ/m^{2}K

Applying equation 10, the maximum daily temperature variation, ΔT resulting for the different cases can be determined (Table 5). Aiming a maximum daily temperature variation of 5 to 6 K leads to the following conclusions:

- Low gains: Light- or medium-weight construction
- Medium gains: Medium-weight construction
- High gains: Heavy-weight construction

Table 5. Maximum daily temperature variation ΔT (K) depending on building construction and daily heat gains.

	Low gains (224 Wh/m^2)	Medium gains (294 Wh/m^2)	High gains (378 Wh/m^2)
Light-weight (131 kJ/m^{2}K)	6.2 K	8.1 K	10.4 K
Medium-weight (180 kJ/m^{2}K)	4.5 K	5.9 K	7.6 K
Heavy-weight (287 kJ/m^{2}K)	2.8 K	3.7 K	4.7 K

3. Temperature efficiency

For this example the temperature efficiency found in the experiments (section 5) during mixing ventilation was assumed. The equation for the fitted curve is

$$\eta = 1 - 0.1538 \cdot ACR^{0.2966} \,. \tag{14}$$

4. Climatic cooling potential

The climatic cooling potential is computed according to the definition in section 2.1 (equation 1) based on ANETZ data measured at Zurich SMA for the 10 years period 1996 to 2005. Figure 26 shows the cumulative frequency of *CCP* during the 50 warmest nights per year. In 15 nights per year *CCP* is below 60 Kh and there are 2 - 3 nights per year without any cooling potential.

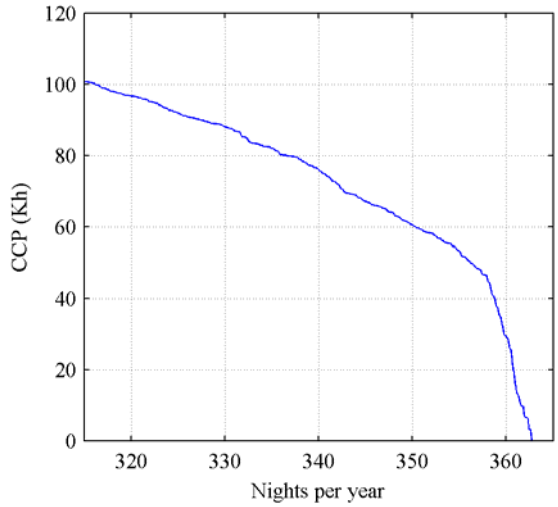

Figure 26. Climatic cooling potential, CCP for the period 1996-2005 at Zurich SMA (based on ANETZ data).

The *CCP* needed to discharge the daily heat gains is assessed as (cf. equation 11):

$$CCP = \frac{Q_d}{A_{Floor}} \cdot \frac{3600\,\mathrm{s/h}}{\eta \cdot ACR \cdot H \cdot \rho_{Air} \cdot c_{p,\,Air}} \,, \tag{15}$$

with room height *H* = 2.6 m and $\rho_{Air} \cdot c_{p,\,Air} = 1142\ \mathrm{J/kgK}$.

5. Night ventilation air change rate

Depending on the air change rate the number of days per year with insufficient *CCP* can be assessed from the cumulative frequency distribution. For the three levels of heat gains Figure 27 shows the risk for overheating depending on the air change rate. In all cases the risk for overheating is reduced rapidly with increasing air change rate to about 7 to 8 days per year. However, even at 30 ACH a risk of overheating on 4 to 5 days per year remains.

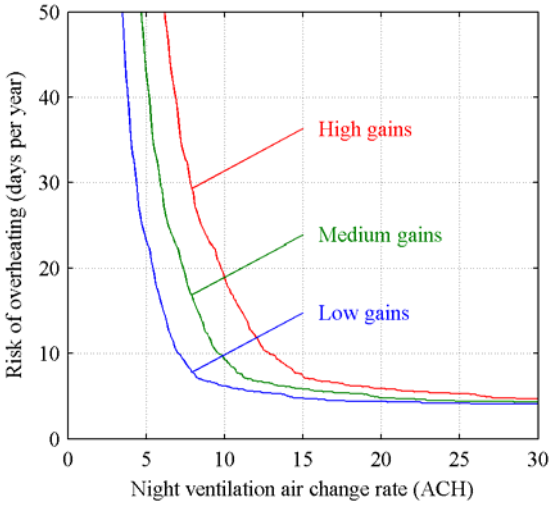

Figure 27. Number of days per year with a risk of overheating depending on the air change rate for low, medium and high heat gains.

For the three levels of heat gains, the air change rates needed to limit the risk of overheating to 7 days per year are:

- Low gains: *ACR* = 9 ACH
- Medium gains: *ACR* = 12 ACH
- High gains: *ACR* = 16 ACH

6.3 Comparison with simulation results

In order to verify the design method, the different case examples were simulated with the suggested air change rates (low gains: 9 ACH, medium gains: 12 ACH, high gains: 16 ACH). Table 6 gives the number of days when the operative room temperature exceeds 27 °C which was the maximum of the building temperature in the definition of *CCP*. In the recommended cases the operative room temperature exceeds 27 °C on 3.8 (low gains/light-weight), 2.7 (medium gains/medium weight) and 0.7 (high gains/heavy-weight) days per year, while the design method predicted a risk of overheating on 7 days per year in all cases.

Table 6. Number of overheating days with operative room temperature exceeding 27 °C (days per year) based on simulations.

	Low gains (224 Wh/m^2) 9 ACH	Medium gains (294 Wh/m^2) 12 ACH	High gains (378 Wh/m^2) 16 ACH
Light-weight (131 kJ/m^{2}K)	3.8 d/y*	8.6 d/y	22.0 d/y
Medium-weight (180 kJ/m^{2}K)	1.5 d/y	2.7 d/y*	5.8 d/y
Heavy-weight (287 kJ/m^{2}K)	0.5 d/y	0.7 d/y	0.7 d/y*

* Cases recommended based on the design method

This comparison suggests that the design method overestimates the risk for overheating. There are various possible reasons to explain this:

- As discussed in [52], in some cases the assumption of a harmonically oscillating building temperature results in an underestimation of *CCP*. Due to its definition the building temperature starts to decrease at 7 pm even if the external temperature is not low enough for effective night-time ventilation. This results in *CCP* = 0, although there might be a cooling potential during the late night hours if the building temperature would remain at a constant level until ventilation starts (cf. Figure 3).

- In the simulations ventilation with 2 ACH was considered during the day to ensure indoor air quality. In the mild climate of Zurich the external temperature is mostly below the indoor temperature, and therefore the heat gains are partially discharged by ventilation during the day. To account for this effect it could be assumed, that only a certain fraction of the heat gains needs to be discharged by night-time ventilation. However, the discharge of heat during the day highly depends on climatic conditions. To be on the safe side, it is recommended to design night-time ventilation for the total daily heat gains. Additionally in the simulation no heat gains were assumed during weekends.

- In the example the temperature efficiency measured in the experiments during mixing ventilation was applied, while in the simulations the coefficient for combined heat transfer was assumed as 7.7 W/m^{2}K. As discussed in section 4.2 a combined heat transfer model might overestimate radiation during night-time ventilation.

- In the simulation night-time ventilation was terminated when the mean surface temperature fell below 20 °C, i.e. the maximum daily temperature variation without exceeding 27 °C was 7 K. In the suggested case examples the temperature variation was in the range from 4.7 to 6.2 K. Comparing the case examples shows that the overestimation of overheating by the design method is highest in cases with a small daily temperature variation. This means that increasing the thermal mass does not only decrease the daily temperature variation but also gives additional safety in the ventilation rate.

- In case of oversized thermal mass (daily temperature variation smaller than the acceptable thermal comfort range), insufficient cooling potential in one single night will not cause overheating on the next day. Only after several consecutive nights of insufficient *CCP* the temperature of the thermal mass will gradually increase and finally the room temperature will exceed the limit for thermal comfort. In the design method based on daily *CCP* this dynamic effect can not be accounted for. Therefore, in the detailed design phase a dynamic building simulation should be performed.

6.4 Concluding remarks

Although there are some limitations, the example showed that the proposed design method gives valuable results for the estimation of the thermal capacity and the airflow rate needed to ensure thermal comfort by night-time cooling. This method is recommended for a first estimation during the concept design phase and is not meant to replace a detailed analysis by means of dynamic building energy simulations.

The model most commonly used in building energy simulation assumes a homogeneous room air temperature and the outflowing air temperature being equal to the room air temperature. During displacement ventilation, due to the temperature stratification, some of the internal room surfaces (e.g. the floor) can be colder than the outflowing air. As the temperature of this surface, $T_{Surface,\,i}$ is still higher than the air close to it, the surface releases heat to the air ($\dot{q}_{conv,\,i} > 0$). For a one-air-node model this results in a negative heat transfer coefficient:

$$h_i = \frac{\dot{q}_{conv,i}}{T_{Surface,i} - T_{Room\ air}} = \frac{\dot{q}_{conv,i}}{T_{Surface,i} - T_{Outlet}} < 0 \quad (16)$$

An alternative approach could be to use the temperature efficiency, η to calculate the total heat flow discharged from a room in a dynamic model. In this model, the efficiency represents the heat transfer at all room surfaces (including radiation), which supersedes the definition of heat transfer coefficients for single surfaces. However, such a model does not give the heat flows from different room surfaces separately. Therefore the entire thermal mass of the room needs to be modelled as one element with a homogeneous surface temperature. A possible approach for representing the thermal mass of a room (or building) using a virtual sphere model has been proposed by Li and Yam [75]. The applicability of the temperature efficiency and the virtual sphere model in a dynamic building energy simulation, however, needs further investigation.

7 Conclusions

For quantifying the climatic potential for night-time cooling a degree-hours method was developed, evaluating the utilisable difference between the building and the ambient temperature. The method for calculating the climatic cooling potential (CCP) is basically suitable for all building types, regardless of building-specific parameters. This was achieved by basing the approach solely on a building temperature variable within a temperature band given by summertime thermal comfort.

Applying this method to European climate data displayed an obvious gradient in CCP decreasing from North to South. Under current climatic conditions, the potential for passive cooling by night-time ventilation was found to be very significant in Northern Europe (including the British Isles), and still sufficient in most nights of the year in Central and Eastern Europe. However, a risk of thermal discomfort on a few days per year exists, depending on building design and heat gains. In Southern Europe passive night-time cooling might not be sufficient the whole year round, but can still be used in hybrid cooling systems.

A detailed analysis of data from future climate projections until the end of the 21st century showed that night-time cooling potential will cease to be sufficient to assure thermal comfort in many Southern and Central European buildings. In Northern Europe, a significant cooling potential is likely to remain, at least for the next few decades. At the same time the cooling demand increases which results in a shift of possible applications from South to North and from summer to spring and autumn. Due to uncertainties in climate projections, upper and lower bound estimates for future CCP were found to diverge strongly in the course of the 21st century. Therefore, the need for adaptive building design taking into account a wide range of possible climatic boundary conditions becomes evident.

The high sensitivity of night cooling to climatic conditions was confirmed in a parameter study based on building energy simulation (*HELIOS*). Simulations based on commonly-used semi-synthetic one year data sets such as *Design Reference Year* (DRY) or *Meteonorm* [55] data were found to underestimate the extent of overheating compared to measured weather data. Therefore, for reliable summer thermal comfort predictions the application of long term measured climate data including extreme periods is recommended.

The building energy simulation study also revealed a high sensitivity to the surface heat transfer, if heat transfer coefficients were below about 4 W/m^{2}K. Convective heat transfer coefficients at internal room surfaces however vary in a wide range from 0.7 W/m^{2}K given for downward heat flow at horizontal surfaces [39], to values above 20 W/m^{2}K in cases with high air flow velocities. Applying the standard definition of heat transfer coefficients – based on the difference between the surface temperature and the average room air temperature – the temperature stratification in case of displacement ventilation can even result in negative heat transfer coefficients at individual surfaces.

A practicable method to evaluate the potential for night cooling was proposed. In order to assure thermal comfort two criteria need to be satisfied, i.e. (i) the thermal capacity of the building needs to be sufficient to accumulate the daily heat gains within an acceptable temperature variation and (ii) the climatic cooling potential and the effective air flow rate need to be sufficient to discharge the stored heat during the night. The amount of thermal mass needed to accumulate daily heat gains can be assessed based on the dynamic heat capacity of the building elements. Using a design chart, the minimum air flow rate necessary to discharge the stored heat can be estimated based on the climatic cooling potential and the temperature efficiency. This approach might mainly be helpful during the concept design phase of a building. For a more detailed analysis of the summertime transient thermal behaviour, the temperature efficiency can also be applied to determine the total heat flow in a dynamic simulation.

Experimental results showed, that for displacement ventilation at low air flow rates, the temperature stratification and the high location of the outlet opening results in a very high temperature efficiency ($\eta > 1$). In mixing ventilation warm air is supposed to be removed from the ceiling by the inflowing air jet. However, only at a relatively high air change rate (above about 10 ACH) the effect of the air jet flowing along the ceiling becomes significant and mixing ventilation is more efficient. Therefore, if a low air flow rate is expected, the outlet opening should be placed as close to the ceiling as possible.

Considering higher comfort expectations, increasing heat gains and the gradually warming climate, a rapid increase in cooling energy demand is expected if mechanical air conditioning systems are applied. As peak cooling loads occur coincidentally over large areas, a very high peak load capacity would be needed to prevent extensive breakdowns of electric power supply. Additionally, substantial greenhouse gas emissions are related to the increased energy demand, while actually a significant reduction of emissions will be necessary to restrain climate warming to an acceptable limit. This demonstrates the great need for the application of passive and low energy cooling methods. Overall, this PhD study showed that night-time ventilation holds a high potential to reduce cooling energy demand in Central, Eastern and Northern Europe. It is hoped, that the findings of this study will contribute to a more frequent application of passive cooling methods.

8 Recommendations for future work

The method proposed for assessing the heat flow discharged during night-time ventilation is based on the temperature efficiency of the ventilation. In the experiments conducted, the temperature efficiency during mixing and displacement ventilation was determined for a test room with a heavy ceiling and light-weight walls and floor. In order to make this method more generally applicable, further work is needed to determine the temperature efficiency for various room geometries, constructions (amount and location of thermal mass) and ventilation systems (location of inlet and outlet openings).

Additionally the presence of furniture might have a significant impact on the air flow, the heat transfer, and the resulting temperature efficiency. On the one hand, furniture might constrain the heat transfer at the floor and wall surfaces. On the other hand, the large surface area of furniture might increase the total convective heat flow. Even if furniture does not contribute much to the total heat storage capacity of a room, the temperature of its surfaces drops quickly and heat is transferred from heavy-weight building elements by radiation. Furthermore the presence of furniture might completely change the air flow pattern in a room.

A possible approach to investigate a large number of different cases could be the application of computational fluid dynamics (CFD). As the time constant of building elements is typically much longer than the time constant of the room air, a steady state CFD model is believed to be sufficient to determine the temperature efficiency. To induce a temperature gradient between the thermal mass and the supply air a heat source is needed in a steady state model. In order to achieve a realistic surface temperature distribution, a heat source (constant temperature or constant heat flow density) at the external surface of heavy-weight building elements is suggested. Initial CFD simulations using such a model appeared to be promising.

In case of displacement ventilation the temperature stratification can result in negative heat transfer coefficients according to the standard definition based on the difference between the surface temperature and the average room air temperature. In order to avoid a physically meaningless definition of negative heat transfer coefficients, the temperature efficiency of the ventilation could possibly be used to model the total heat flow discharged during night-time ventilation. Furthermore, the temperature efficiency is based on the difference between the average internal surface temperature and the inflowing air temperature, and thus the assumption of a homogeneous room air temperature can be avoided. The applicability of this approach could be investigated by comparing simulation results from different models to experimental data.

References

[1] Swiss Federal Office of Energy. Analyse des Schweizerischen Energieverbrauchs 2000-2006 nach Verwendungszwecken. Bundesamt für Energie, Bern, 2008 (in German).

[2] Energy Efficiency and Certification of Central Air Conditioners (EECCAC) Final Report - April 2003, Co-ordinator: Adnot J, Armines, France.

[3] Christenson M, Manz H, Gyalistras D. Climate warming impact on degree-days and building energy demand in Switzerland. Energy Conversion and Management 2005, 47, pp. 671-686.

[4] Frank T. Climate change impacts on building heating and cooling energy demand in Switzerland. Energy and Buildings 2005, 37 pp. 1175-1185.

[5] Kolokotroni M, Giannitsaris I, Watkins R. The effect of the London urban heat island on building summer cooling demand and night ventilation strategies. Solar Energy 2006, 80 pp. 383-392.

[6] Cook J (ed.). Passive cooling. MIT Press, Cambridge, MA, 1989.

[7] Santamouris M, Asimakopolous D (ed). Passive cooling of buildings. James & James, London, UK, 1996

[8] Bahadori M N. Passive cooling systems in Iranian architecture, Scientific American 1978, 283 (2), pp. 144-154.

[9] McCarthy B. Wind Towers: Detail in Building. Academy Editions, Wiley, West Sussex, UK 1999.

[10] Schossig P, Henning H M, Gschwander S, Haussmann T. Micro-encapsulated phase-change materials integrated into construction materials. Solar Energy Materials & Solar Cells 2005, 89, pp. 297-306.

[11] P Heiselberg (ed.). Principles of hybrid ventilation. IEA ECBCS Annex 35. Design of energy efficient hybrid ventilation (HybVent). Aalborg University, Denmark, 2002.

[12] AEE - Institute for Sustainable Technologies (AEE INTEC). Office building MIVA “Christophorus House”, Austria. KeepCool WP 1: Best Practice Project (retrieved from http://www.energyagency.at, October 2008).

[13] Eawag Forum Chriesbach - A sustainable new building. Baumonographie (retrieved from http://www.forumchriesbach.eawag.ch, October 2008).

[14] Wagner A, Kleber M, Parker C. Monitoring results of a naturally ventilated and passively cooled office building in Frankfurt, Germany. International Journal of Ventilation 2007, 6 (1), pp. 3-20.

[15] Krausse B, Cook M, Lomas K. Environmental performance of a naturally ventilated city centre library. Energy and Buildings 2007, 39, pp. 792-801.

[16] Santamouris M, Argiriou A, Balaras, C. Developments on passive cooling in buildings – results from recent research. ASHRAE Transactions 1997, 103 (1), pp. 983-992.

[17] Flourentzos F, Van der Maas J, Roulet C A. Lesocool Manual. EPFL Lausanne, 1996, LESO-PB-REPORT-1996-1013.

[18] Barnard N, Jaunzens D (ed.). Technology selection and early design guidance. IEA ECBCS Annex 28. Low energy cooling systems. Building research establishment Ltd 2001.

[19] NatVent. Final monitoring report. BRE Trust Companies, UK, 1998 (retrieved from http://www.bre.co.uk/natvent, October 2008).

[20] Allard F (ed.). Natural ventilation in Buildings: A design handbook. James & James, London, UK, 1998.

[21] Delsante A, Vik T A (ed.). Hybrid Ventilation: State-of-the-Art Review. IEA ECBCS Annex 35. Design of energy efficient hybrid ventilation (HybVent). 2000.

[22] Breesch H, Janssens A. Uncertainty and sensitivity analysis to evaluate natural night ventilation design in an office building. 26th AIVC conference 2005, Brussels, Belgium.

[23] Roaf S, Haves P, Orr J. Climate change and passive cooling in Europe, in Proceedings of 'Environmentally Friendly Cities', PLEA '98 (Passive and Low Energy Architecture) Conference, Lisbon, Portugal, June 1998, pp. 463-466.

[24] Givoni B. Passive and low energy cooling of buildings. Van Nostrand Reinhold, New York, 1994.

[25] Givoni B. Comfort, climate analysis and building design guidelines. Energy and Buildings 1992, 18 (1), pp. 11-23.

[26] Givoni B. Performance and applicability of passive and low-energy cooling. Energy and Buildings 1991, 17 (3), pp. 177-199.

[27] Axley J W, Emmerich S J. A method to assess the suitability of a climate for natural ventilation of commercial buildings. Proceedings: Indoor Air 2002, Monterey, CA.

[28] Eicker U, Huber M, Seeberger P, Vorschulze C. Limits and potentials of office building climatisation with ambient air. Energy and Buildings 2006, 38, pp. 574-581.

[29] Schaer C, Vidale P L, Luethi D, Frei C, Haeberli C, Liniger M A, Appenzeller C. (2004) The role of increasing temperature variability in European summer heatwaves, Nature 2004, 427, pp. 332-336.

[30] Gyalistras D, Schär C, Davies H C, Wanner H. Future Alpine climate. In: Cebon P, Dahinden U, Davies H C, Imboden D, Jäger C G (eds). Views from the Alps: Regional Perspectives on Climate Change, MIT Press 1998, Boston, pp. 171-223.

[31] Mearns L O, Hulme M, Carter T R, Leemans R, Lal M, Whetton, P et al. (2001) Climate scenario development. In: Houghton J T, Ding Y, Griggs D J, Noguer M, van der Linden P J, Dai X D, Maskell K, Johnson C A (eds). Climate Change 2001: The Scientific Basis. Contribution of Working Group I to the Third Assessment Report of the Intergovernmental Panel on Climate Change (IPCC), Cambridge UK and New York USA: Cambridge University Press 2001, pp. 739-768.

[32] Shaviv E, Yezioro A, Capeluto I G. Thermal mass and night ventilation as passive cooling design strategy. Renewable Energy 2001, 24, pp. 445-454.

[33] Finn D, Connolly D, Kenny P. Sensitivity analysis of a maritime located night ventilated library building. Solar Energy 2007, 81, pp. 697-710.

[34] Breesch H. Natural night ventilation in office buildings. PhD thesis, Gent University, Belgium, 2006.

[35] TRNSYS Transient system simulation programme. Solar Energy Lab, University of Wisconsin, Madison, USA.

[36] Dorer V, Weber A. Multizone air flow model COMIS as Type 57 for TRNSYS. IEA-ECB Annex 23 'Multizone air flow modelling' Technical Note, 1994.

[37] Akbari H, Samano D, Mertol A, Baumann F, Kammerud R. The effect of variations in convection coefficients on thermal energy storage in buildings Part I – Interior Partition Walls. Energy and Building 1986, 9, pp. 195-211.

[38] EN ISO 6946. Building components and building elements – thermal resistance and thermal transmittance – calculation method. European Committee for Standardization (CEN), Brussels, 1996.

[39] EN ISO 13791. Thermal performance of buildings – internal temperatures in summer of a room without mechanical cooling – general criteria and calculation procedures. European Committee for Standardization (CEN), Brussels, 2004.

[40] Chandra S, Kerestecioglu A A. Heat transfer in naturally ventilated rooms data from fullscale measurements. ASHRAE Transformation 1984, 90 (1), pp. 211-224.

[41] Clark G. Passive cooling systems. In: Cook J. (ed.). Passive Cooling. MIT Press, 1989, pp. 347-538.

[42] Blondeau P, Sperandio M, Allard F. Night ventilation for building cooling in summer. Solar Energy 1997, 61, pp. 327-335.

[43] Alamdari F, Hammond G P. Improved data correlations for buoyancy driven convection in rooms, Building Services Engineering Research & Technology 1983, 4, pp. 106-112.

[44] Khalifa A J, Marshall R H. Validation of heat transfer coefficients on interior building surfaces using a real-sized indoor passive test cell. International Journal of Heat and Mass Transfer 1990, 33, pp. 2219-2236.

[45] Awbi H B, Hatton A. Natural convection from heated room surfaces, Energy and Buildings 1999, 30, pp. 233-244.

[46] Spitler J D, Pedersen C O, Fisher D E, Interior convective heat transfer in buildings with large ventilative flow rates, ASHRAE Transactions 1991, 97, pp. 505-515.

[47] Awbi H B, Hatton A. Mixed convection from heated room surfaces, Energy and Buildings 2000, 32, pp. 153-166.

[48] Beausoleil-Morrison I. The adaptive simulation of convective heat transfer at internal building surfaces, Building Environment 2002, 37, pp. 791-806.

[49] Khalifa A J. Natural convective heat transfer coefficient – a review I. Isolated vertical and horizontal surfaces. Energy Conversion and Management 2001, 42, pp. 491-504.

[50] Khalifa A J. Natural convective heat transfer coefficient – a review II. Surfaces in two- and three-dimensional enclosures. Energy Conversion and Management 2001, 42, pp. 505-517.

[51] Salmerón J M, Sanz J A, Sánchez F J, Álvarez S, Pardo Á. Flow pattern effects on night cooling ventilation. International Journal of Ventilation 2007, 6 (1), pp. 21-30.

[52] Artmann N, Manz H, Heiselberg P. Climatic potential for passive cooling of buildings by night-time ventilation in Europe. Applied Energy 2007, 84, pp. 187-201.

[53] Artmann N, Gyalistras D, Manz H, Heiselberg P. Impact of climate warming on passive night cooling potential. Building Research & Information 2008, 36 (2), pp. 111-128.

[54] prEN 15251. Criteria for the indoor environment including thermal, indoor air quality, light and noise. European Committee for Standardization (CEN), Brussels, 2005.

[55] Meteonorm, Global meteorological database for engineers, planners and education. Version 5.1 – Edition 2005, Software incl. Manual (www.meteonorm.com).

[56] Nakicenovic N, Alcamo J, Davis G, De Vries B, Fenhann J, Gaffin S, Gregory K, Grübler A, Jung T Y, Kram T, La Rovere E L, Michaelis L, Mori S, Morita T, Pepper W, Pitcher H, Price L, Raihi K, Roehrl A , Rogner H H, Sankovski A, Schlesinger M, Shukla P, Smith S, Swart R, Van Rooijen S, Victor N, Dadi Z. IPCC Special Report on Emissions Scenarios. Cambridge University Press, Cambridge, 2000.

[57] PRUDENCE. Prediction of Regional scenarios and Uncertainties for Defining European Climate Change risks and Effects, Final Report 2005, (available at: http://prudence.dmi.dk).

[58] Cubasch U, Meehl G A, Boer G J, Stouffer R J, Dix M, Noda A, Senior C A, Raper S, Yap K S et al. Projections of Future Climate Change. In: Houghton J T, Ding Y, Griggs D J, Noguer M, van der Linden P J, Dai X D, Maskell K, Johnson C A, editors. Climate Change 2001: The Scientific Basis. Contribution of Working Group I to the Third Assessment Report of the Intergovernmental Panel on Climate Change (IPCC), Cambridge UK and New York USA: Cambridge University Press; pp 525-582, 2001.

[59] Williamson A, Erell E. The implications for building ventilation of the spatial and temporal variability of air temperature in the urban canopy layer. International Journal of Ventilation 2008, 7 (1), pp. 23-35.

[60] Artmann N, Manz H, Heiselberg P. Parametric study on the dynamic heat storage capacity of building elements. 2nd PALENC and 28th AIVC Conference, Building Low Energy Cooling and Advanced Ventilation Technologies in the 21st Century, Crete Island, Greece, 27-29 September 2007.

[61] Carslaw H S, Jaeger J C. Conduction of heat in solids. Oxford University Press, Oxford, UK, 2nd edn, 1959.

[62] EN ISO 13786. Thermal performance of building components – Dynamic thermal characteristics – Calculation methods. European Standard 1999.

[63] Gruber P, Toedtli J. On the optimal thermal storage capacity of a homogeneous wall under sinusoidal excitation. Energy and Buildings 1989, 13, pp. 177-186.

[64] Artmann N, Manz H, Heiselberg P. Parameter study on performance of building cooling by night-time ventilation. Renewable Energy 2008, 33, pp. 2589-2598.

[65] HELIOS Software. Building energy simulation code. Swiss Federal Laboratories for Materials Testing and Research (Empa). Switzerland, Duebendorf, 2007.

[66] DIN 4701. Energy efficiency of heating and ventilation systems in buildings, German Institute of Standardization, Berlin, Germany, 2003.

[67] DIN 4108. Thermal protection and energy economy in buildings. German Standard, Beuth Verlag, 2003.

[68] DS474. Specifikation af termisk indeklima. Danish Standard, 1995 (in Danish).

[69] Nicol J F and Humphreys M A. Adaptive thermal comfort and sustainable thermal standards for buildings. Energy and Buildings 2002, 34, p. 563-572.

[70] ASHRAE Standard 55. Thermal environmental conditions for human occupancy. American Society of Heating, Refrigerating, and Air-Conditioning Engineers (ASHRAE), 2004.

[71] Artmann N, Jensen R L, Manz H, Heiselberg P. Experimental investigation of heat transfer during night-time ventilation. Submitted to Energy and Buildings, October 2008.

[72] Jensen R L. Modelling of natural ventilation and night cooling – by the loop equation method. PhD-thesis, Aalborg University, Department of Civil Engineering, Hybrid Ventilation Centre, 2005 (in Danish).

[73] Artmann N, Jensen R L. Night-time ventilation experiments – Setup, data evaluation and uncertainty assessment. DCE Technical Report No. 053, Aalborg University, Department of Civil Engineering, 2008.

[74] Olesen B W, Parsons K C. (2002) Introduction to thermal comfort standards and to the proposed new version of EN ISO 7730. Energy and Buildings 2002, 34, pp. 537-548.

[75] Li Y, Yam J C W. Designing thermal mass in naturally ventilated buildings. International Journal of Ventilation 2004, 2 (4), pp. 313-324.

Publications

International journal papers

Artmann N, Manz H, Heiselberg P. Climatic potential for passive cooling of buildings by night-time ventilation in Europe. Applied Energy 2007; 84 pp. 187-201.

Artmann N, Gyalistras D, Manz H, Heiselberg P. Impact of climate warming on passive night cooling potential. Building Research & Information 2008, 36:2, pp. 111-128.

Artmann N, Manz H, Heiselberg P. Parameter study on performance of building cooling by night-time ventilation. Renewable Energy 2008, 33, pp. 2589-2598.

Artmann N, Jensen R L, Manz H, Heiselberg P. Experimental investigation of heat transfer during night-time ventilation. Submitted to Energy and Buildings, October 2008.

Conference papers

Artmann N, Manz H, Heiselberg P. Potential for passive cooling of buildings by night-time ventilation in present and future climates in Europe. PLEA2006 - The 23rd Conference on Passive and Low Energy Architecture, Geneva, Switzerland, 6-8 September 2006.

Artmann N, Manz H, Heiselberg P. Parametric study on the dynamic heat storage capacity of building elements. 2nd PALENC and 28th AIVC Conference, Building Low Energy Cooling and Advanced Ventilation Technologies in the 21st Century, Crete Island, Greece, 27-29 September 2007.

Technical reports

Artmann N, Vonbank R, Jensen R L. Temperature measurements using type K thermocouples and the Fluke Helios Plus 2287A data logger. DCE Technical Report No. 052, Aalborg University, 2008.

Artmann N, Jensen R L. Night-time ventilation experiments – Setup, data evaluation and uncertainty assessment. DCE Technical Report No. 053, Aalborg University, 2008.

National Journal papers

Artmann N. Passive Gebäudekühlung. Baublatt 2008, 32, pp. 16-19.

Artmann N. Passive Gebäudekühlung mit Nachtlüftung. Fassade, Schweizerische Zentrale Fenster und Fassaden, SZFF. Accepted, November 2008.

Artmann N, Manz H, Heiselberg P, Gyalistras D. Impact of climate warming on passive night cooling potential in Europe. Empa Activity Report 2008.

Presentations

Artmann N. Climatic potential for passive cooling of buildings by night-time ventilation in Europe. IEA, 4th Annex 44 Forum, Torino, 29 March 2006.

Artmann N. A parametric study on the performance of building cooling by night-time ventilation. IEA, 6th Annex 44 Forum, Lisbon,16 April 2007.

Artmann N. Passive cooling of buildings by night-time ventilation. Empa PhD Seminar, Duebendorf, 9 January 2008.

Artmann N. Passive Gebäudekühlung mit Nachtlüftung. SZFF Fachtagung, Zurich, 5 June 2008.

Artmann N. Parameter study on performance of building cooling by night-time ventilation. Empa PhD Symposium, St Gallen, 13 November 2008

Available online at www.sciencedirect.com
ScienceDirect
Applied Energy 84 (2007) 187–201
APPLIED ENERGY
www.elsevier.com/locate/apenergy

Climatic potential for passive cooling of buildings by night-time ventilation in Europe

N. Artmann [a,*], H. Manz [a], P. Heiselberg [b]

[a] *Swiss Federal Laboratories for Materials Testing and Research (EMPA), Laboratory for Building Technologies, Ueberlandstr. 129, CH-8600 Duebendorf, Switzerland*
[b] *Hybrid Ventilation Centre, Department of Civil Engineering, Aalborg University, Sohngaardsholmsvej 57, DK-9000 Aalborg, Denmark*

Received 18 February 2006; received in revised form 20 May 2006; accepted 28 May 2006
Available online 24 August 2006

Abstract

Due to an overall trend towards less heating and more cooling demands in buildings in many European countries over the last few decades, passive cooling by night-time ventilation is seen as a promising technique, particularly for commercial buildings in the moderate or cold climates of Central, Eastern and Northern Europe. The basic concept involves cooling the building structure overnight in order to provide a heat sink that is available during the occupancy period. In this study, the potential for passive cooling of buildings by night-time ventilation was evaluated by analysing climatic data, without considering any building-specific parameters. An approach for calculating degree–hours based on a variable building temperature – within a standardized range of thermal comfort – is presented and applied to climatic data of 259 stations all over Europe. The results show a high potential for night-time ventilative cooling over the whole of Northern Europe and still significant potential in Central, Eastern and even some regions of Southern Europe. However, due to the inherent stochastic properties of weather patterns, a series of warmer nights can occur at some locations, where passive cooling by night-time ventilation alone might not be sufficient to guarantee thermal comfort.

Keywords: Passive cooling; Night-time ventilation; Climatic cooling potential

* Corresponding author. Tel.: +43 44 823 4620; fax: +43 44 823 4009.
E-mail address: nikolai.artmann@empa.ch (N. Artmann).

0306-2619/$ - see front matter © 2006 Elsevier Ltd. All rights reserved.
doi:10.1016/j.apenergy.2006.05.004

1. Introduction

During the last few decades, a trend towards increasing cooling demand in buildings has been observed in Europe. Especially in commercial buildings, more and more air-conditioning systems are being installed, even in moderate and cold climates such as in Central or Northern Europe. This increase in cooling demand is due to higher internal loads and – particularly in modern buildings with extensive glazing – higher solar gains. Additionally, increased comfort expectations in summer time and the gradual warming of our climate are contributing to the rise in cooling demand. Mainly in Southern European residential buildings, cooling is also becoming more popular. While the heating demand can be effectively reduced by installing thermal insulation, cooling plays a more significant role in the overall energy demand of buildings.

Particularly in moderate climates, such as in Switzerland, Germany or the UK, and cold climates such as in Scandinavia, with relatively low night-time temperatures even in summer, passive cooling of buildings by night-time ventilation seems to be a promising technique. The basic concept involves cooling the building structure overnight in order to provide a heat sink that is available during occupancy periods [1–3]. Such a strategy could guarantee the daytime thermal-comfort of building occupants without mechanical cooling or, at least, with a lower daytime cooling energy requirement.

The ventilation can be achieved by mechanically forcing air through ventilation ducts, but as well by natural ventilation through the windows. Also hybrid systems combining the two methods are often used. Thereby fans are only used if natural forces – thermal buoyancy and wind – are not strong enough to ensure sufficient ventilation rates.

However, night-time ventilation is highly dependent on climatic conditions, as a sufficiently high temperature-difference between ambient air and the building structure is needed during the night to achieve efficient convective cooling of the building mass. Givoni [4–6] recommends the application of night-time cooling mainly for arid regions, where comfortable indoor conditions cannot be achieved by daytime ventilation and where night-time temperatures are below about 20 °C. For the daytime temperature, a range between 30 and 36 °C is given.

In order to analyse the potential of different passive cooling strategies, Roaf et al. [7] also suggest, as a criterion for building cooling by night-time ventilation, a minimum night-time temperature of 20 °C in combination with a mean maximum temperature of less than 31 °C. The mean maximum temperature was found to be the limiting criterion. Maps of the July mean maximum temperature for the current epoch as well as for 2050, taking into account temperature increases due to climate warming, are presented.

Another approach to the analysis of climate suitability for natural ventilation of commercial buildings is presented by Axley and Emmerich [8]. Night-time ventilation is calculated on the basis of the assumption of a constant building-temperature (infinite building mass), and is only applied when daytime comfort ventilation is not efficient. This approach is applied to four different locations in different climatic zones of the United States. Cooling by natural ventilation was found to be feasible and effective in the cooler locations for moderate to high specific internal-gains, but not for hot and humid climates, as for example in Miami, FL, where relatively high night-time ventilation rates would be needed to offset moderate specific internal-gains.

Many of these studies focus on residential buildings, where cooling is usually only needed in hot climates. However, given the increasing cooling demand in commercial

buildings in moderate and even in cold climates, night-time ventilation is also seen as a valuable alternative to air-conditioning in these kinds of buildings. In these buildings, windows often cannot be opened during the occupancy period because of traffic noise or wind speed at high elevation and, therefore, daytime ventilation is not feasible.

The purpose of this study is to evaluate the climatic potential for passive cooling of buildings by night-time ventilation in all climatic zones of Europe by analysing climatic data.

2. Method

A method was developed, verified and applied which is basically suitable for all building types, regardless of building-specific parameters. This is because the approach is just based on a building temperature variable within a temperature band given by summer time thermal comfort.

2.1. Climatic data

Hourly air-temperature data are needed to analyse the climatic potential for passive cooling of buildings by night-time ventilation. In order to analyse the European climate, the potential for night-time cooling has to be calculated for many locations. Two sources of temperature data were employed in this study.

For Switzerland, high-quality long time-series of measured hourly-temperature data are available. The automatic measurement network (ANETZ) consisting of 72 stations was launched in the early 1980s. ANETZ is operated by the National Weather Service (MeteoSwiss) and measures, in addition to air temperatures 2 m above ground level, a range of meteorological parameters.

The commercial database Meteonorm [9] provides semi-synthetic meteorological data for 7400 stations around the world. Hourly air temperature data are generated on the basis of measured long-term monthly mean values (mainly 1961–1990). The model used to generate hourly data is based on the assumption that the amplitude of the temperature variation during daytime is approximately proportional to the amplitude of the daily global radiation profile and thus the temperature profile is calculated by transforming the radiation profile. The method was validated for different locations [9]. For this study, 259 meteorological stations in densely-populated locations all over Europe were selected to map the climatic potential for cooling of buildings by night-time ventilation. Stations at very high elevations, e.g. in the Alps, were not considered because these data do not represent climates that many buildings are exposed to.

To give an overview of the European climatic conditions in summer, temperature maps are presented. As night ventilation is only effective if the ambient temperature is well below the inside temperature of a building, the most important climatic parameter for the applicability of night-time ventilative cooling is the minimum night-temperature. Mapping of temperature data was done by means of a commercial software package (Matlab Mapping Toolbox). For each grid point, the three nearest weather stations were selected and an interpolation algorithm employed that was based on weighted mean values using quadratic distances between grid point and location of weather stations. Fig. 1 shows the mean values of the daily minimum temperatures in July. Considering a minimum night temperature of 20 °C as a threshold, as stated by Givoni [4], night-time ventilative cooling

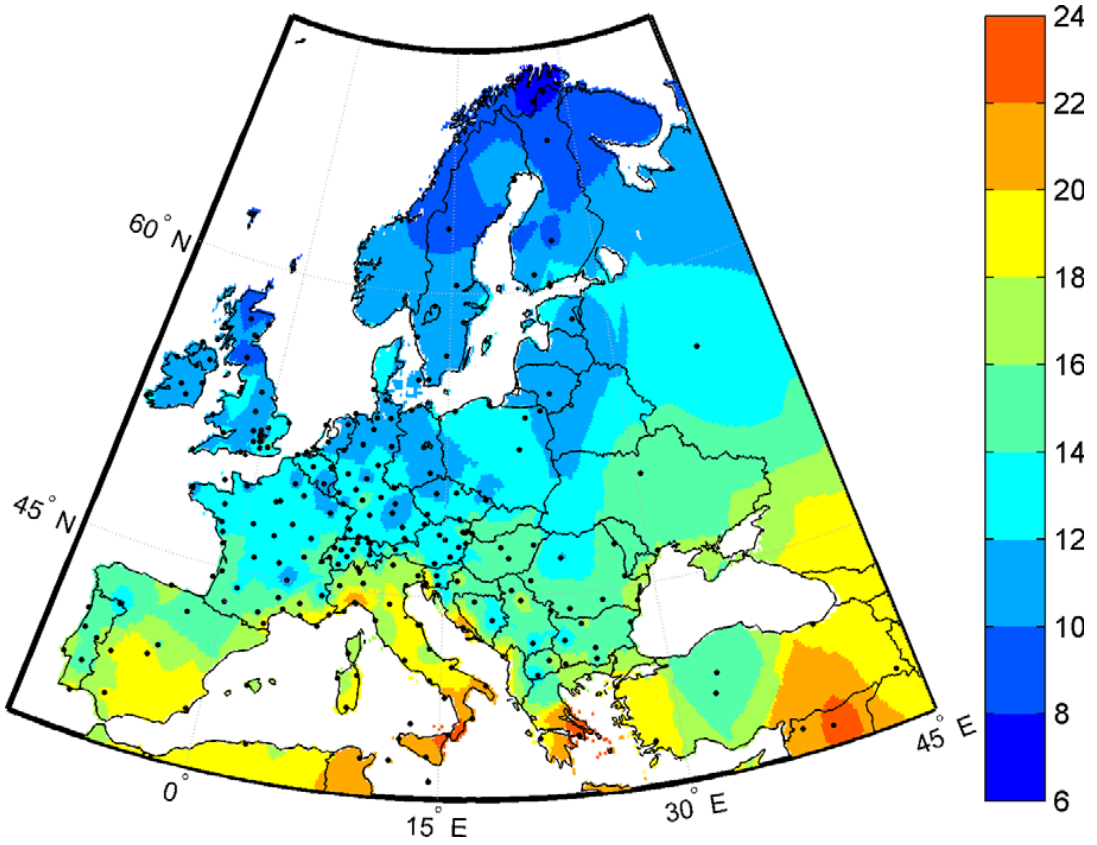

Fig. 1. Mean daily minimum temperatures (°C) for July based on Meteonorm data [9].

seems to be applicable, except for most southern regions, over the whole of Europe. However, due to the inherent stochastic properties of weather patterns, nights with much higher minimum temperatures can occur in regions where the monthly mean value of daily minimum temperatures is below 20 °C.

Passive cooling by night-time ventilation seems to be of most interest in climates with high maximum temperatures (high cooling demand) and low minimum temperatures (high cooling potential). Therefore, the mean difference between minimum and maximum temperature in July was computed for the same locations as described above and is displayed in Fig. 2. The highest mean differences of 14–18 K can be found in continental regions in Southern Europe. Here moderate night temperatures, together with very high temperatures during the day, lead to high daily differences. On the other hand, very small differences of only 4–8 K can be observed at some locations on the west coasts of the British Isles, Northern Europe and Italy. In these regions the climate is influenced by a maritime airflow from the Atlantic Ocean or the Mediterranean Sea, which leads to equalised temperatures.

2.2. Definition of the 'climatic cooling potential' (CCP)

For the characterisation of a climate's impact on the thermal behaviour of a building, degree–days or degree–hours methods are often used. In this study, the mean climatic potential for ventilative cooling during a time period of N nights, the CCP is defined as a summation of products between building/external air temperature-difference, $T_b - T_e$, and time interval:

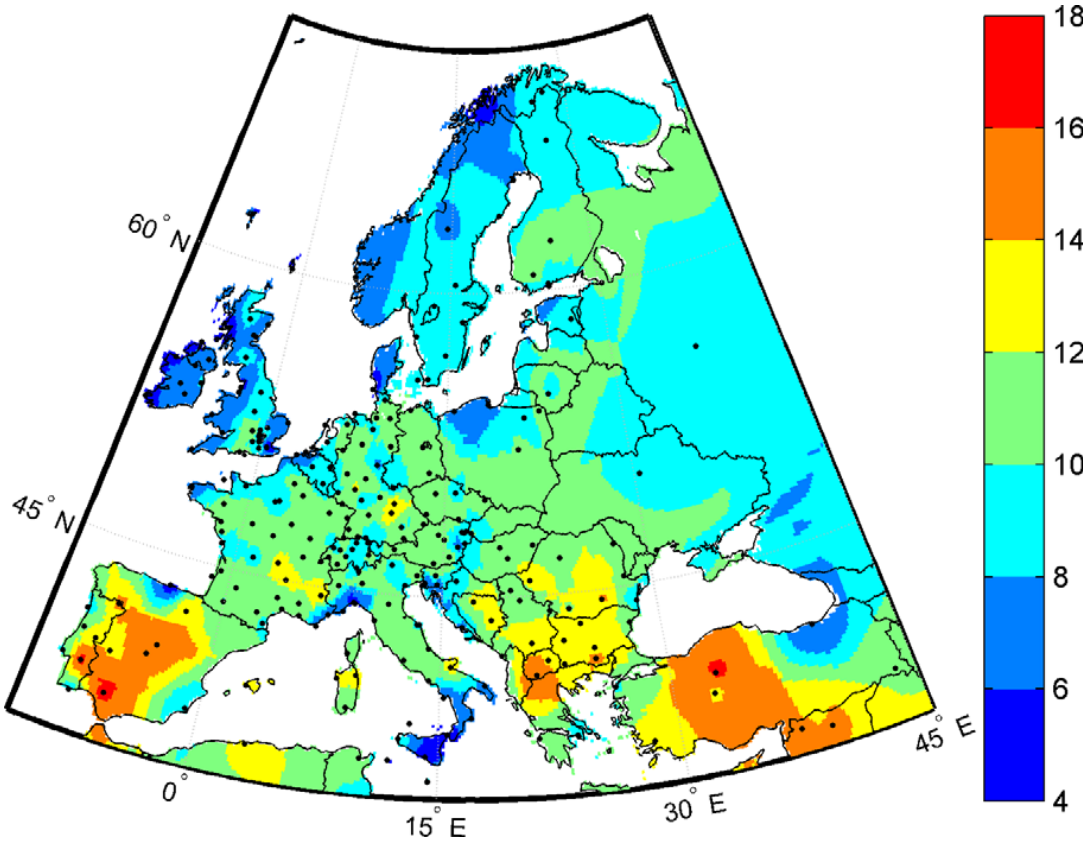

Fig. 2. Mean differences between minimum and maximum temperatures (K) in July based on Meteonorm data [9].

$$\mathrm{CCP} = \frac{1}{N}\sum_{n=1}^{N}\sum_{h=h_i}^{h_f} m_{n,h}(T_{\mathrm{b},n,h} - T_{\mathrm{e},n,h}) \quad \begin{cases} m = 1\ \mathrm{h} & \text{if } T_\mathrm{b} - T_\mathrm{e} \geqslant \Delta T_\mathrm{crit} \\ m = 0 & \text{if } T_\mathrm{b} - T_\mathrm{e} < \Delta T_\mathrm{crit} \end{cases} \tag{1}$$

h stands for the time of day, where $h \in \{0, \ldots, 24\ \mathrm{h}\}$, h_i and h_f denote the initial and the final time of night-time ventilation, and ΔT_crit is the threshold value of the temperature difference, when night-time ventilation is applied. In the numerical analysis, it was assumed that night-time ventilation starts at $h_\mathrm{i} = 19$ h and ends at $h_\mathrm{f} = 7$ h. As a certain temperature-difference is needed for effective convection, night ventilation is only applied if the difference between building and ambient temperature is greater than $\Delta T_\mathrm{crit} = 3$ K.

2.3. Building temperature

Because heat gains and night-time ventilation do not coincide in time, energy storage is an inherent part of the concept. As building structures are almost always made of materials which are suitable for sensible energy storage only, such as concrete or brick, the temperature of the building structure varies when energy is stored or released. To take this fact into account, a variable building temperature is therefore used for the calculation of the climatic cooling potential. In order to develop a model, which is as general as possible, no building-specific parameters are employed. The building temperature T_b in °C is assumed to oscillate harmonically:

$$T_{b,h} = 24.5 + 2.5\cos\left(2\pi\frac{h - h_i}{24}\right) \quad (2)$$

Applying this definition, the maximum building temperature occurs at the initial time of night-ventilation, h_i, and as the ventilation time is 12 h, the minimum building temperature occurs at the final time h_f (Fig. 3). Depending on the direction of the building façade and the ratio of internal and solar gains, the maximum building temperature typically occurs between 2 pm ($h = 14$ h) and 6 pm ($h = 18$ h). Especially for high thermal-mass buildings with high internal gains, a shift of the maximum to later hours is expected.

The temperature range of $T_b = 24.5 \pm 2.5$ °C reflects the temperature range recommended for thermal comfort in offices. In the CEN report CR 1752 [10], three different categories of thermal comfort are defined, each based on a mean temperature of 24.5 °C (category A ± 1 °C, category B ± 1.5 °C, category C ± 2.5 °C). The international standard ISO 7730 [11] also recommends a temperature range of $T = 24.5 \pm 1.5$ °C. However, recent studies have shown that broader temperature ranges seem to be acceptable in non-air-conditioned buildings [12]. Category C of CR 1752, corresponding to an extension of the temperature range stated in ISO 7730, was therefore employed.

2.4. Practical significance of CCP

To discuss the practical significance of the calculated degree–hours, an example will be given. The following simple calculation should be seen as a rough analysis only and is not intended to replace a detailed simulation of a specific building at a given location by means of a building energy-simulation code.

It is assumed that the thermal capacity of the building mass is sufficiently high and therefore does not limit the heat storage process. If the building is in the same state after one cycle, the heat Q_{charge}, which charges the building structure during the occupancy period t_{occ}, is equal to the heat $Q_{release}$, which is released by night ventilation. The mean heat-flux during the storage process $\dot{q}$, per room area A, can then be calculated as follows:

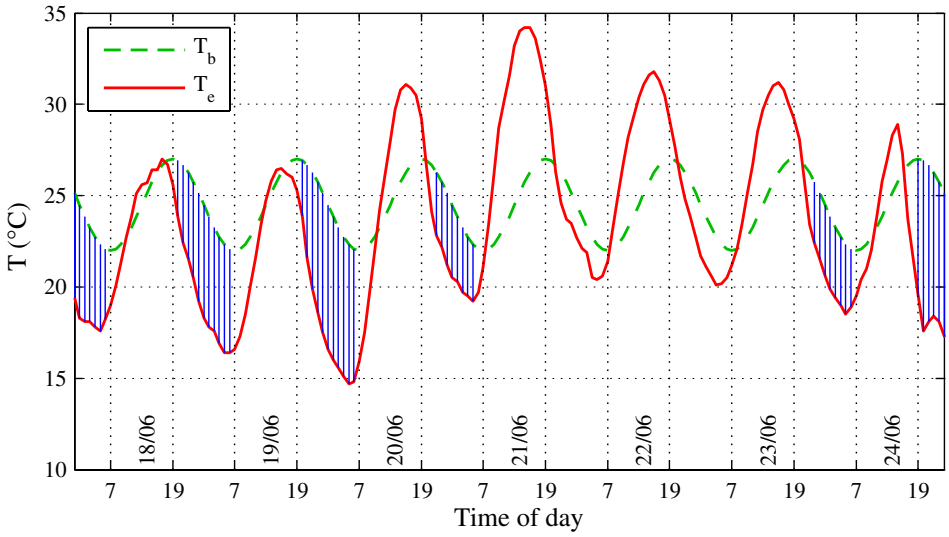

Fig. 3. Building temperature T_b and external air temperature T_e during one week in summer 2003 for Zurich SMA (ANETZ data). Shaded areas illustrate graphically the climatic cooling potential.

$$\dot{q} = \frac{Q_{\text{charge}}}{At_{\text{occ}}} = \frac{Q_{\text{release}}}{At_{\text{occ}}} = \frac{\dot{m}c_p}{At_{\text{occ}}}\text{CCP} \tag{3}$$

The effective mass flow rate $\dot{m}$ is written as $\dot{m} = AHR\eta\rho$, where H is the height of the room, R the air change rate and η a temperature efficiency, which is defined as $\eta = (T_{\text{out}} - T_{\text{e}})/(T_{\text{b}} - T_{\text{e}})$ and takes into account the fact that the temperature of the outflowing air T_{out} is lower than the building temperature T_{b}. The density and the specific heat of the air are taken as $\rho = 1.2\ \text{kg/m}^3$ and $c_p = 1000\ \text{J/(kg K)}$.

Assuming a room height of $H = 2.5$ m, a constant effective air change rate of $R\eta = 6\ \text{h}^{-1}$, and an occupancy time of $t_{\text{occ}} = 8$ h, the heat flux $\dot{q}$, which is absorbed per degree–hour of the cooling potential CCP, can be calculated as

$$\frac{\dot{q}}{\text{CCP}} = \frac{HR\eta\rho c_p}{t_{\text{occ}}} = \frac{2.5\ \text{m} \cdot 6\frac{1}{\text{h}} \cdot 1.2\frac{\text{kg}}{\text{m}^3} \cdot 1000\frac{\text{J}}{\text{kg K}}}{8 \cdot 3600\ \text{s}} = 0.625\frac{\text{W/m}^2}{\text{Kh}} \tag{4}$$

Depending on local climate, orientation and total solar energy transmittance of a façade, geometry and type of building use, solar and internal gains of an office room can vary substantially. Assuming e.g. internal heat-gains of $20\ \text{W/m}^2$ and solar gains of $30\ \text{W/m}^2$ – both values refer to the time period of 8 h – a climatic cooling potential of about 80 Kh per night is needed to discharge the stored heat.

3. Verification of the method

To verify the applicability of the presented method, the climatic cooling potential was calculated on the basis of measured hourly temperature data for Zurich SMA. ANETZ data downloaded from the data centre of the National Weather Service (MeteoSwiss) were employed. The data of 2003 with its exceptionally high temperatures in July and August [13] were used. The impact of different parameters on the CCP is discussed.

3.1. Building temperature

Fig. 3 shows the building temperature (Eq. (2)), the measured external-air temperature in Zurich SMA and the resulting climatic cooling potential (hatched area) for one week in June. In most cases, the theoretical building temperature appears to be reasonable, as it corresponds to the outdoor temperature quite well. However, in the two nights from June 21st to 23rd, the temperature difference stays below 3 K during the whole night and therefore no ventilation is applied. Due to its definition, the building temperature although decreases, which is, strictly speaking, physically incorrect. There might actually be a cooling potential during the late-night hours if the building temperature would remain at a constant level until ventilation starts. A more 'realistic', non-harmonic building temperature could obviously be obtained using a building energy simulation code, with the drawback of having to define numerous building parameters and therefore losing generality.

3.2. Sensitivity of CCP

In order to analyse the impact of the buildings temperature-amplitude ΔT_{b}, the threshold value of the temperature difference ΔT_{crit} and the initial time of night ventilation h_{i},

the daily climatic cooling potential CCP was calculated with different values of these parameters and plotted as cumulative frequency charts. This type of charts displays the number of nights, when the cooling potential exceeds a certain value. Fig. 4 shows the cumulative frequency of CCP for the 165 warmest nights of the year, where the sensitivity is highest. An impact of the building temperature amplitude on CCP can only be seen for nights with a very low CCP. In most cases, the lowest cooling potential is obtained if an amplitude of 2.5 K is assumed. An impact of the threshold temperature difference ΔT_{crit} can be found for nights with a cooling potential less than 100 Kh. Mechanical night-time

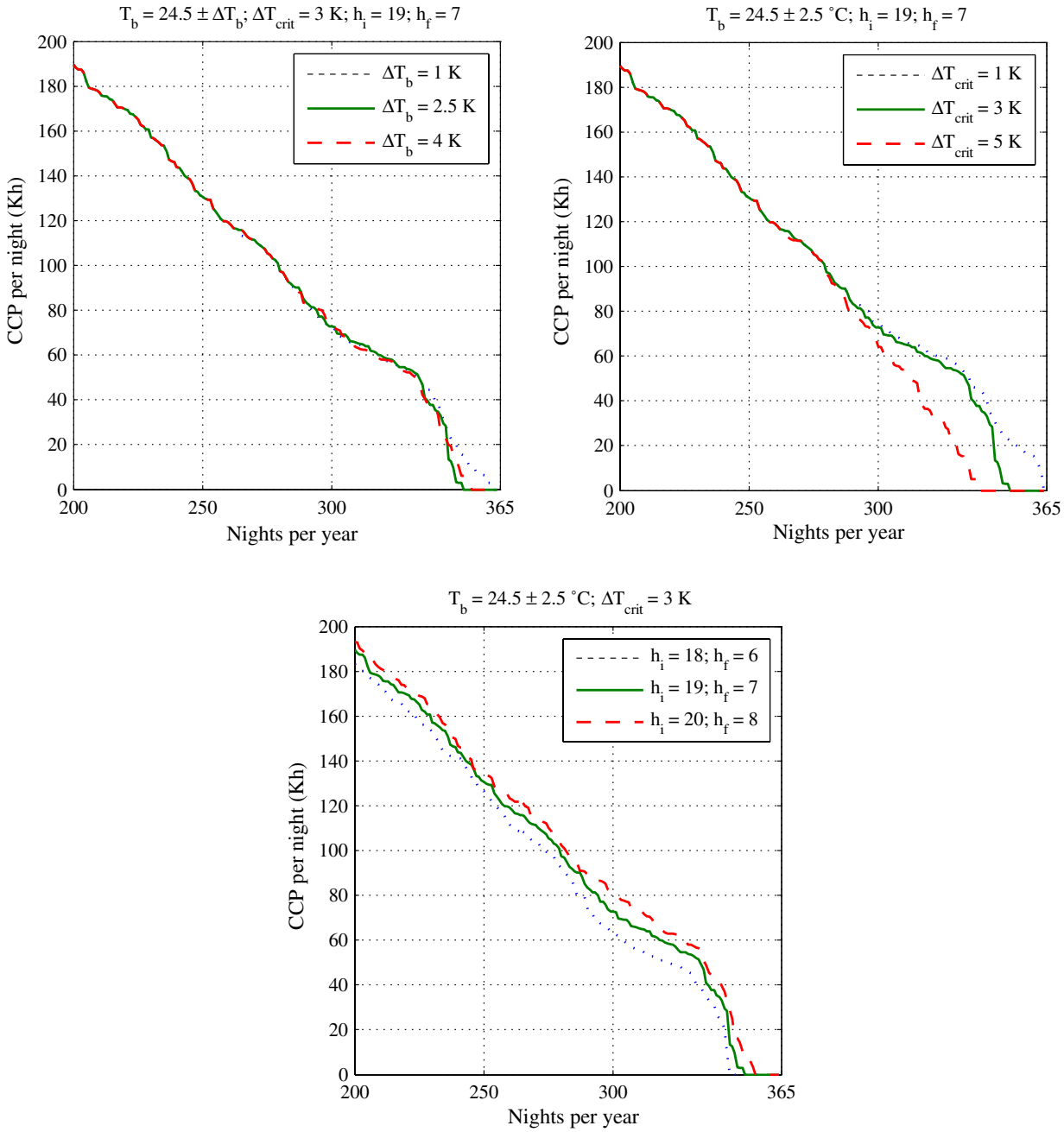

Fig. 4. Cumulative frequency of climatic cooling potential calculated with different building-temperature amplitudes ΔT_b (top left), threshold values of the temperature difference ΔT_{crit} (top right) and the initial time of night-ventilation h_i (bottom) for Zurich SMA in summer 2003 (ANETZ data).

ventilation experiments performed by Blondeau et al. [14] showed that a useful ratio between electrical energy and cooling energy is achieved for a critical temperature-difference greater than 2–3 K. Although the air-flow rate and the convective heat-transfer obviously increase with a higher temperature-difference, the threshold value of the temperature difference is not as crucial for natural ventilation as it is for mechanical ventilation because no electric energy input is required. But as the air-flow rate caused by thermal buoyancy is very dependent on the temperature difference, a certain difference is needed to achieve high air-change rates by natural ventilation. The impact of the initial time of night-ventilation h_i is seen over a wider range of the CCP. A shift of ±1 h results in a variation of maximum ±10 Kh in the CCP.

3.3. Cooling potential in different time-intervals

To compare different climates, the cooling potential has to be averaged over a certain time period. Fig. 5 shows the climatic cooling potential per night together with weekly and monthly mean values. Due to the inherent stochastic properties of weather patterns, nightly values reveal a wide fluctuation within a bandwidth of up to 200 Kh within a few days; weekly mean values still vary by about 50–100 Kh within a month.

In Fig. 5, the monthly mean value in August exceeds 50 Kh, although there is a whole week in this exceptionally-hot summer [13] without any noteworthy potential for night cooling. Attention should be paid to this fact, especially as a low night-cooling potential is associated with a high cooling-demand.

There is not only a variability of cooling potential per night within a month, the monthly mean values also vary over the years. For the period of 1981–2002, standard deviation, minimum and maximum of monthly mean values were computed for all calendar months. Fig. 6 also shows the impact of the hot summer in the year 2003 on the climatic potential for night cooling; mean values for June and August are far below all the data of the previous 22 years.

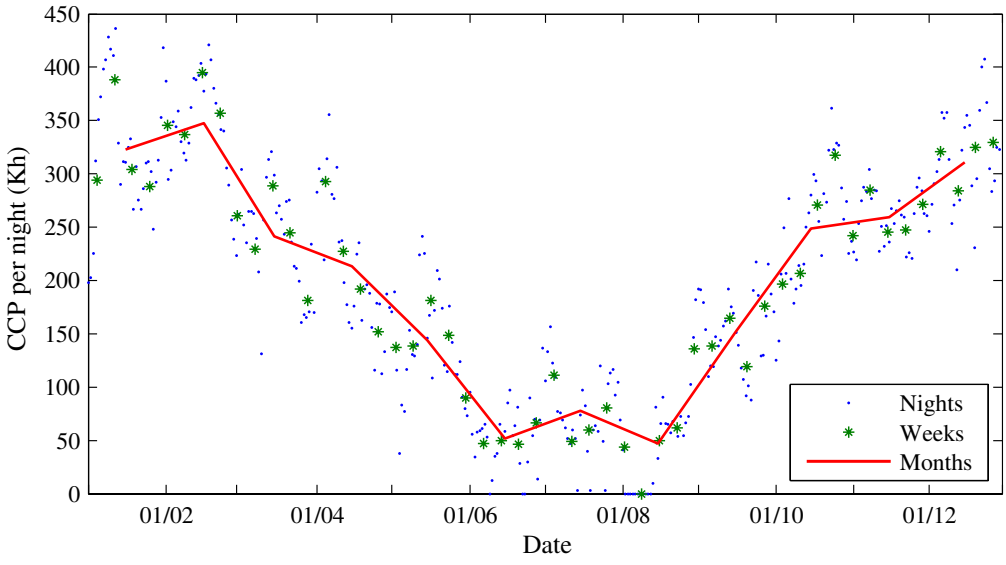

Fig. 5. Climatic cooling potential for nights, weeks, and months for Zurich SMA in 2003 (ANETZ data).

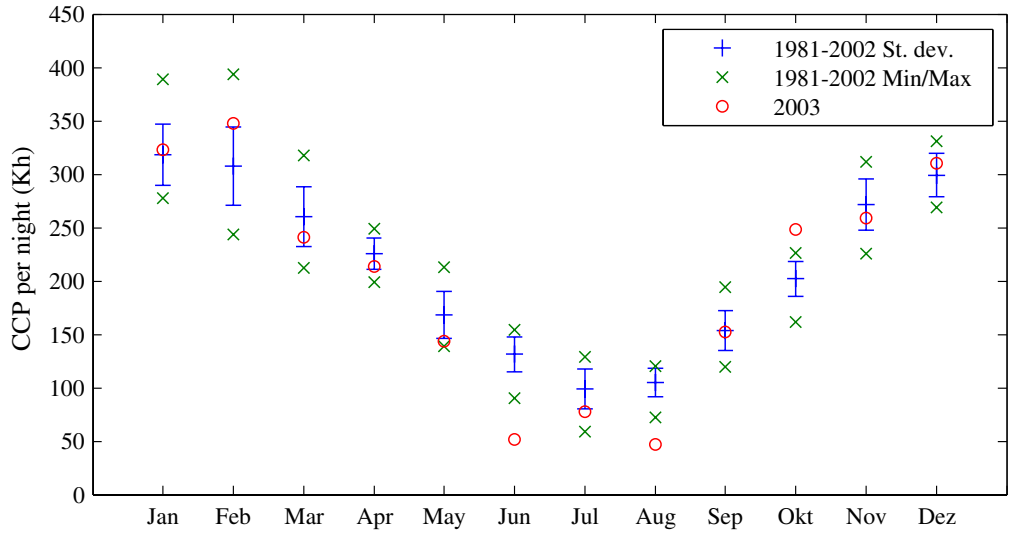

Fig. 6. Mean value and standard deviation, minimum and maximum of monthly mean climatic cooling potential for Zurich SMA 1981–2002 and monthly mean CCP for 2003 (ANETZ data).

3.4. Applicability of semi-synthetic climatic data

As the hourly temperature data provided by the meteorological database Meteonorm [9] are semi-synthetic values generated from monthly mean values (see Section 2.1), the applicability of these data for calculating the cooling potential was verified by comparing Meteonorm data with Swiss ANETZ data from Zurich SMA (1983–1992) and Danish Design Reference Year (DRY) [15] data from Copenhagen Vaerlose, respectively. The Copenhagen Vaerlose DRY is based on measured data for the period 1975–1989. Zurich SMA data represent a climate typical of the Swiss Plateau north of the Alps and Vaerlose data represent a climate heavily influenced by the sea. For the comparison of data

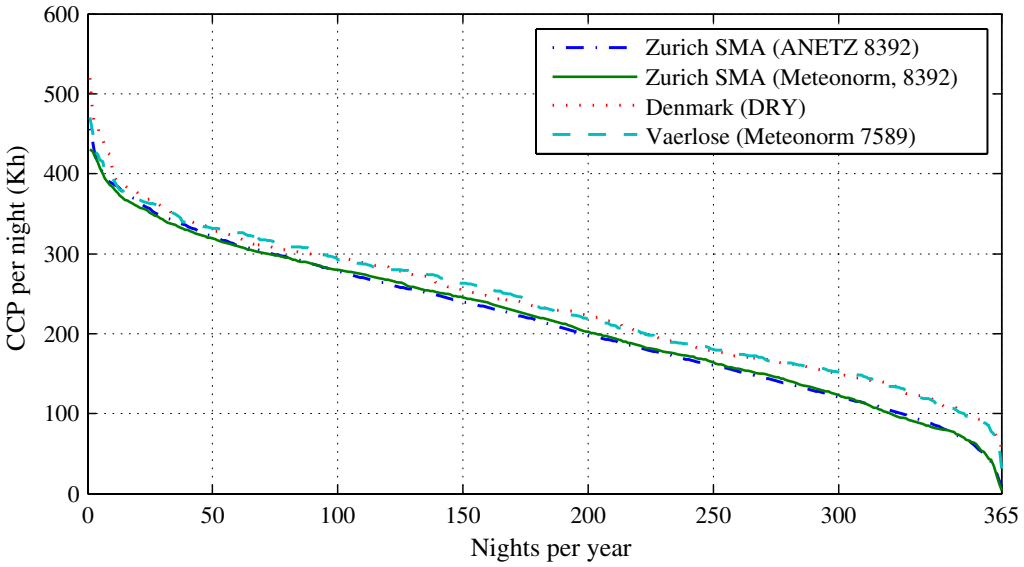

Fig. 7. Comparison of climatic cooling potential calculated from Meteonorm data with ANETZ data from Zurich SMA and the DRY of Copenhagen Vaerlose.

from the same period, monthly mean values of the ANETZ and DRY data were used to generate hourly temperature-data by Meteonorm. The cumulative frequency of the CCP obtained from these data was then compared with the one computed directly on the basis of hourly ANETZ and DRY temperature data. Fig. 7 shows good agreement of the CCP data obtained by the two different methods, especially for the more critical warm season with low cooling potential. It was therefore concluded that the algorithms used in the Meteonorm software in generating hourly data have a negligible effect on the calculation of climatic cooling potential.

4. Results

To give an overview of the climatic potential for night-time cooling in Europe, the July mean values of the CCP were plotted on a map (Fig. 8). As expected, a clear gradation from north to south can be seen. Even in the hottest month of the year, a very high cooling potential of 120–180 Kh occurs in Northern Europe (including the British Isles). In Central and Eastern Europe, but also, in the northern parts of Portugal, Spain, Greece and Turkey, the cooling potential is still 60–140 Kh.

To analyse the potential of night-time ventilative cooling during a whole year, monthly mean values per night and cumulative frequency distribution of the CCP were plotted for four locations in different European climatic regions (Fig. 9). It can be observed that there is usable potential during the colder periods in locations where only a very low potential was displayed in Fig. 8. For example, in Lisbon, where the climatic

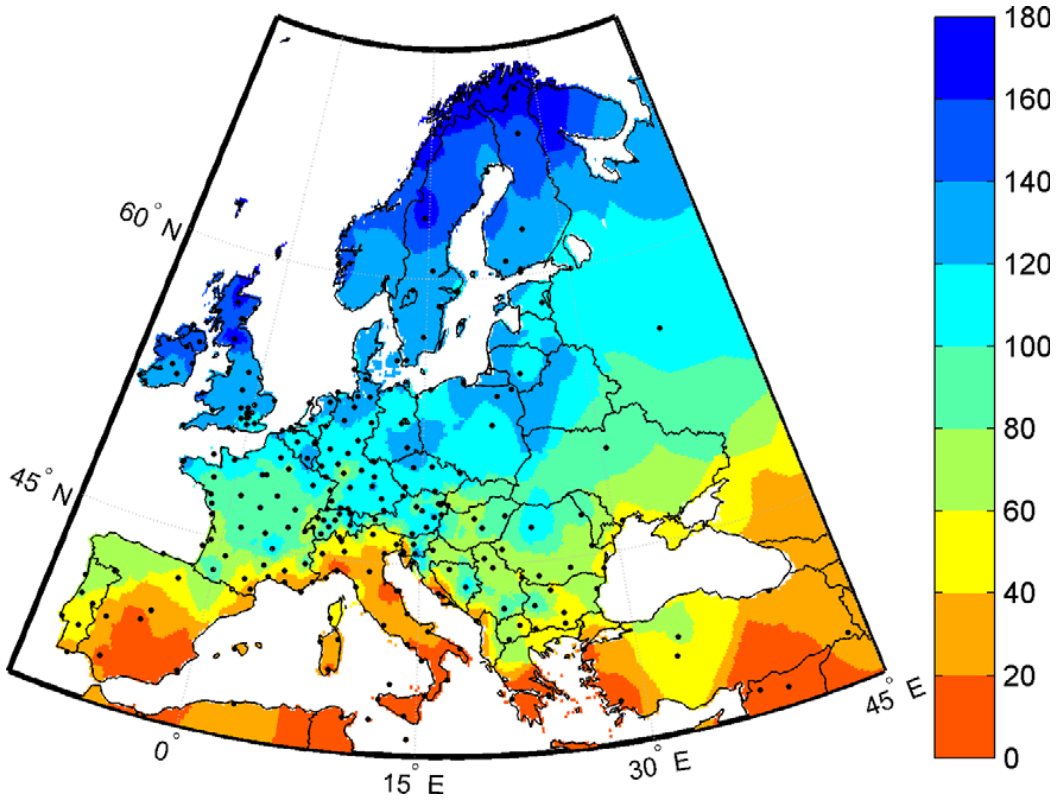

Fig. 8. Map of mean climatic cooling potential (Kh/night) in July based on Meteonorm data [9].

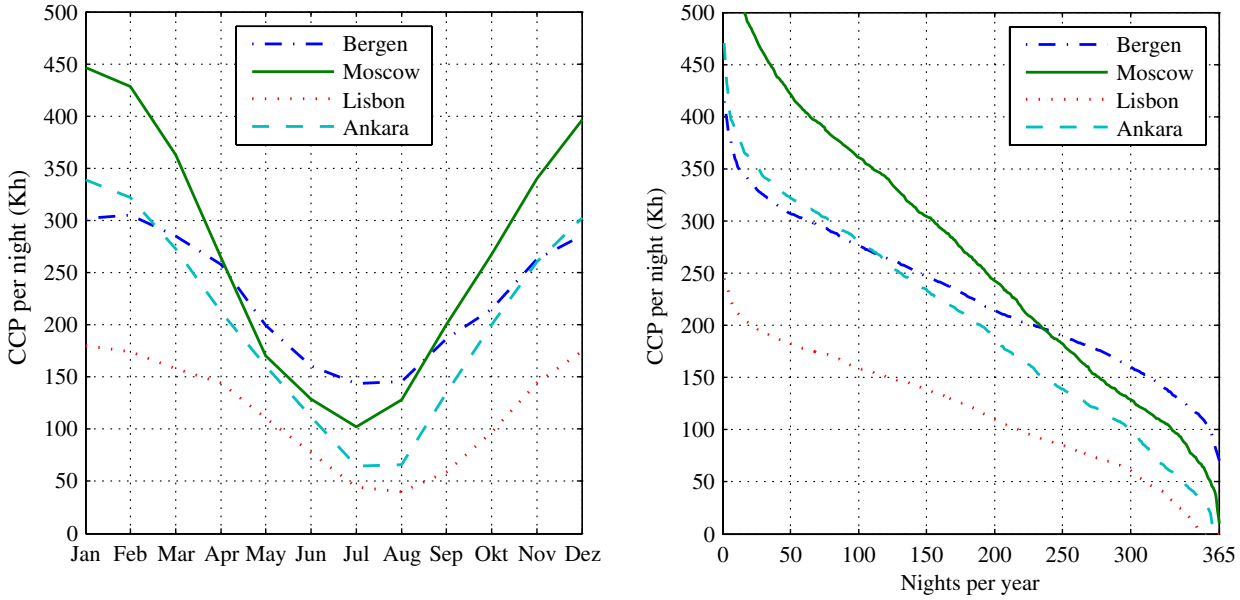

Fig. 9. Monthly mean climatic cooling potential per night (left) and cumulative frequency distribution (right) of climatic cooling potential for different locations based on Meteonorm [9] data.

potential is lowest, the CCP is between 70 and 180 Kh per night from October to June (Fig. 9, left).

Fig. 9 also demonstrates the difference between a continental climate such as in Moscow, which leads to a high variation in the monthly cooling potential (100–450 Kh) and a maritime climate such as in Bergen, where the potential only varies between 150 and 300 Kh. In the cumulative frequency chart, the maritime climates of Bergen and Lisbon show a kind of plateau of almost constant CCP values, while the curves for the continental climates of Moscow and Ankara, covering a wider range of CCP, are represented by a more constant slope.

Due to the inherent stochastic properties of weather patterns, individual CCP values per night can fall far below the monthly mean values. On further examination, cumulative frequency distributions of the CCP per night are therefore helpful (Fig. 9, right). For 20 different locations, two cumulative frequency charts of the climatic potential for night-time cooling in maritime (Fig. A1) and continental (Fig. A2) climates are presented in the Appendix.

5. Discussion

In the whole of Northern Europe (including the British Isles), mean CCP per night in July is roughly 120–180 Kh. Taking into account variations of nightly values around the monthly mean value, a sufficient cooling potential to assure thermal comfort in this region throughout the year appears very likely for most applications.

In Central, Eastern and some regions of Southern Europe, a mean monthly CCP of 60–140 Kh was found. In these regions, cooling by night-time ventilation is a promising technique for most applications. But it has to be borne in mind that nightly values can fall far below the monthly mean values, and that a few nights with a very low cooling potential may occur per year. As the case arises, it has to be examined whether the resulting discomfort is acceptable.

In regions such as southern Spain, Italy and Greece with a mean CCP per night for July of less than 60 Kh, night-time ventilation alone might not be sufficient throughout the year. For buildings where a high level of thermal comfort is expected, other passive-cooling techniques, such as radiant or evaporative cooling, might therefore be of interest. Whenever passive systems cannot provide a sufficient cooling effect, hybrid systems should be considered. For example, even in air-conditioned buildings night-time ventilation could be used in order to reduce the energy demand of the mechanical cooling system.

There are buildings, mainly commercial buildings with high internal and/or solar loads, that need to be cooled even if the outdoor temperature is well below the thermal comfort limit. Thus, especially in the warmer climates of Southern Europe, cooling is not only needed in summer, but also during the transitional periods and for some buildings even in winter. In such cases, night-time ventilative cooling can be used in hybrid systems to reduce the energy demands of air-conditioned buildings. Night-time ventilation is applied whenever the outside air temperature is significantly below the building temperature and mechanical cooling has to be used only if thermal comfort cannot be achieved.

The information available in cumulative frequency charts might be of special interest for planning engineers who wish to estimate the potential for cooling by night-time ventilation. For example, in Bergen (Fig. 9, right), the climatic cooling potential never falls below around 75 Kh and exceeds 100 Kh on 355 days per year. By contrast, there are about 15 days per year without any potential for night-time cooling in Lisbon.

6. Conclusions

In this study, a method was developed to compute the climatic potential for passive cooling of buildings by night-time ventilation. This method is based on a variable building temperature, variable within a temperature range of thermal comfort as specified in international standards, without assuming any building-specific parameters. The floating building temperature is an inherent necessity of this passive-cooling concept. The robustness of the degree–hours approach was tested and the impact of the assumed building temperature function and the threshold value of the temperature difference between building and ambient air investigated. This method was employed for a systematic analysis of European climate, with regard to passive cooling by night-time ventilation, using 259 stations.

It was shown that, in the whole of Northern Europe (including the British Isles), there is very significant potential for passive cooling of buildings by night-time ventilation and this method therefore seems to be applicable in most cases. In Central, Eastern and even in some regions of Southern Europe, the climatic cooling potential is still significant, but due to the inherent stochastic properties of weather patterns, a series of warmer nights can occur at some locations, where passive cooling by night-time ventilation might not be sufficient to guarantee thermal comfort. If lower thermal-comfort levels are not accepted during short time periods, additional cooling systems are required. In regions such as southern Spain, Italy and Greece, climatic cooling potential is limited. Nevertheless, passive cooling of buildings by night-time ventilation might be promising for hybrid systems.

The presented method is valuable to discuss the cooling potential for a given climate and might mainly be helpful in the first design phase of a building at a given location. However, it has to be stressed that a more thorough analysis of the summer time transient thermal behaviour of a building has to be based on building-energy simulation, taking into account all building-specific parameters, such as time-dependent internal and solar gains, active building thermal mass, but also air-flow patterns and air-flow rates. The latter may even require a computational fluid dynamics analysis because room geometry, window type and positioning may significantly affect the air-flow rate and, therefore, the cooling effect.

More work is needed to show the impact of future gradual climate warming on the cooling potential in order to better understand the long-term potential of this technology. Additionally, more knowledge and improved modelling algorithms in building energy simulation codes are required in the field of air exchange and the resulting cooling effect.

Acknowledgements

This work was partially funded by the Hybrid Ventilation Centre, The Department of Civil Engineering at Aalborg University and the Swiss Federal Office of Energy (Project No. 101'308). The project is also supported by the private sector (WindowMaster, Belimo, SZFF). We acknowledge with thanks all financial support.

Appendix

See Figs. A1 and A2.

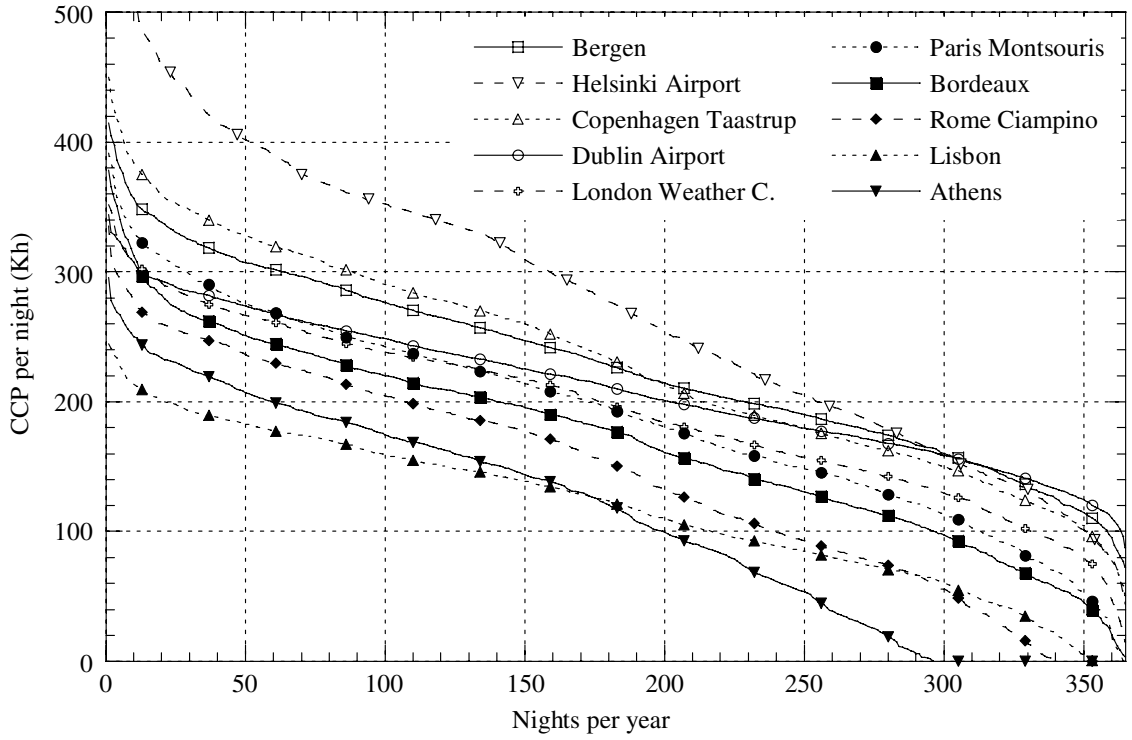

Fig. A1. Climatic cooling potential for a maritime climate.

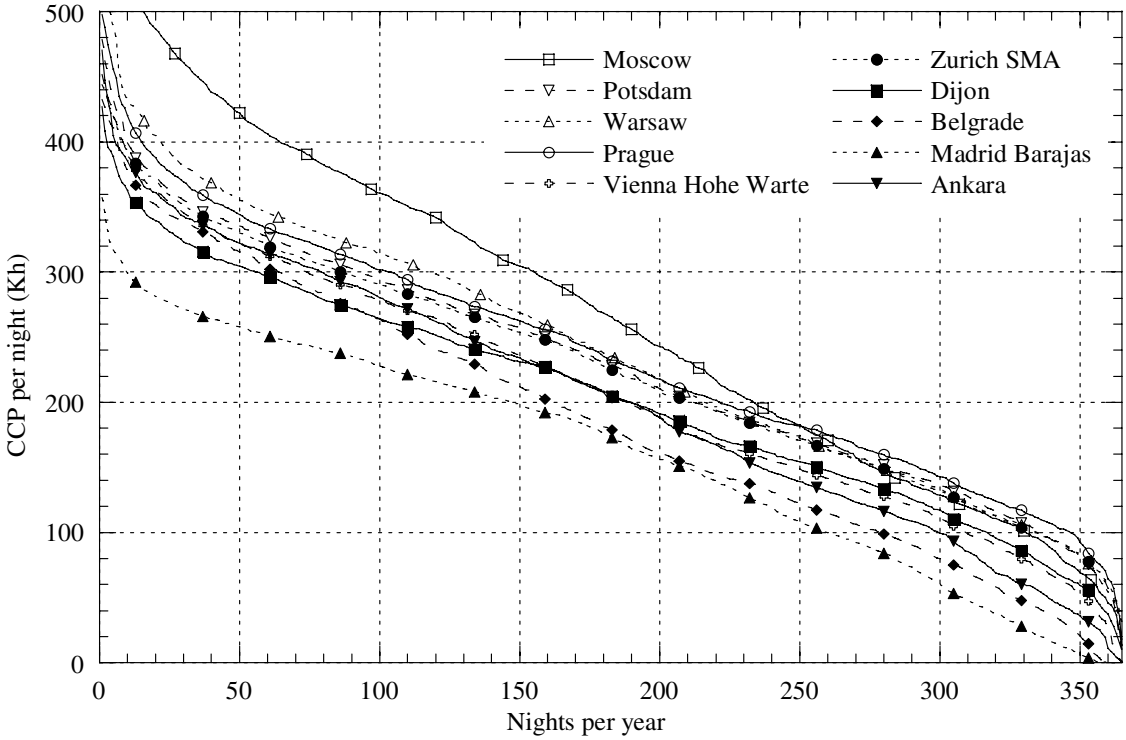

Fig. A2. Climatic cooling potential for a continental climate.

References

[1] Allard F. Natural ventilation in buildings. London: James & James; 1998.
[2] Chandra S. Ventilative cooling. In: Cook J, editor. Passive cooling. Cambridge (MA): The MIT Press; 1989. p. 70.
[3] Santamouris M, Asimakopoulos D. Passive cooling of buildings. London, UK: James & James; 1996.
[4] Givoni B. Passive and low energy cooling of buildings. New York: Van Nostrand Reinhold; 1994.
[5] Givoni B. Comfort, climate analysis and building design guidelines. Energ Build 1992;18(1):11–23.
[6] Givoni B. Performance and applicability of passive and low-energy cooling. Energ Build 1991;17(3):177–99.
[7] Roaf S, Haves P, Orr J. Climate change and passive cooling in Europe. In: Proceedings of "Environmentally friendly cities", PLEA 98 (passive and low energy architecture) conference, held Lisbon, Portugal, June 1998. UK: James & James Ltd.; 1988. p. 463–6.
[8] Axley JW, Emmerich SJ. A method to assess the suitability of a climate for natural ventilation of commercial buildings. In: Proceedings: indoor air, 2002, Monterey (CA).
[9] Meteonorm, Global meteorological database for engineers, planners and education. Version 5.1 – Edition 2005, Software incl. Manual [www.meteonorm.com].
[10] CR 1752 Ventilation for buildings: design criteria for the indoor environment. CEN, Brussels; 1998.
[11] ISO 7730 Moderate thermal environments – Determination of the PMV and PPD indices and specification of the conditions for thermal comfort. International Standard; 1994.
[12] Olesen BW, Parsons KC. Introduction to thermal-comfort standards and to the proposed new version of EN ISO 7730. Energ Build 2002;34:537–48.
[13] Schaer C, Vidale PL, Luethi D, Frei C, Haeberli C, Liniger MA, et al. The role of increasing temperature variability in European summer heat-waves. Nature 2004;427:332–6.
[14] Blondeau P, Spérandino M, Allard F. Night ventilation for building cooling in summer. Sol Energ 1997;61(5):327–55.
[15] Moller Jensen J, Lund H. Design Reference Year, DRY. Meddelelse Nr 281, Technical University of Denmark; 1995 [in Danish].

Building Research & Information (2008) 36(2), 111–128

Routledge
Taylor & Francis Group

Impact of climate warming on passive night cooling potential

N. Artmann[1], D. Gyalistras[2], H. Manz[1] and P. Heiselberg[3]

[1]Empa, Swiss Federal Laboratories for Materials Testing and Research, Laboratory for Building Technologies, CH-8600 Duebendorf, Switzerland
E-mails: nikolai.artmann@empa.ch and heinrich.manz@empa.ch

[2]Institute for Integrative Biology, ETH Zurich, CH-8092 Zurich, Switzerland
E-mail: gyalistras@env.ethz.ch

[3]Hybrid Ventilation Centre, Department of Civil Engineering, Aalborg University, DK-9000 Aalborg, Denmark
E-mail: ph@civil.aau.dk

Night-time ventilation is often seen as a promising passive cooling concept. However, as it requires a sufficiently high temperature difference between ambient air and the building structure, this technique is highly sensitive to changes in climatic conditions. In order to quantify the impact of climate warming on the night-time ventilative cooling potential in Europe, eight representative locations across a latitudinal transect were considered. Based on a degree-hours method, site-specific regression models were developed to predict the climatic cooling potential (CCP) from minimum daily air temperature (T_{min}). CCP was computed for present conditions (1961–90) using measured T_{min} data from the European Climate Assessment (ECA) database. Possible time-dependent changes in CCP were assessed for 1990–2100, with particular emphasis on the Intergovernmental Panel on Climate Change (IPCC) 'A2' and 'B2' scenarios for future emissions of greenhouse gases and aerosols. Time-dependent, site-specific T_{min} scenarios were constructed from 30 Regional Climate Model (RCM) simulated data sets, as obtained from the European PRUDENCE project. Under both emissions scenarios and across all locations and seasons, CCP was found to decrease substantially by the end of the 21st century. For the six Central and Northern European locations (>47°N) CCP was found to decrease in summer (June–August) by 20–50%. For the two Southern European locations (Madrid and Athens), future CCP was found to become negligible during the summer and to decrease by 20–55% during the spring and the autumn. The study clearly shows that night-time cooling potential will cease to be sufficient to ensure thermal comfort in many Southern and Central European buildings. In Central and Northern Europe, a significant passive cooling potential is likely to remain, at least for the next few decades. Upper and lower bound estimates for future CCP were found to diverge strongly in the course of the 21st century, suggesting the need for flexible building design and for risk assessments that account for a wide range of emissions scenarios and uncertainty in climate model results.

Keywords: climate change, climate scenarios, climatic cooling potential, night-time ventilation, passive cooling, Europe

La ventilation nocturne est souvent considérée comme un concept de refroidissement passif prometteur. Toutefois, cette technique nécessitant une différence de température suffisamment élevée entre l'air ambiant et la structure du bâtiment, elle est très sensible aux changements des conditions climatiques. Pour quantifier l'impact du réchauffement climatique sur les possibilités de refroidissement par ventilation nocturne, on a considéré huit emplacements représentatifs sur une transversale latitudinale en Europe. Sur la base d'une méthode 'degrés-heures', on a développé des modèles de régression spécifiques à des sites pour prévoir le potentiel de refroidissement climatique (CCP) à partir de la température quotidienne minimale de l'air (T_{min}). On a calculé le CCP pour les conditions présentes pendant la période 1961–90

Building Research & Information ISSN 0961-3218 print/ISSN 1466-4321 online
http://www.tandf.co.uk/journals
DOI: 10.1080/09613210701621919

en utilisant les données T_{min} de la base de données ECA (Evaluation du climat européen). On a évalué de possibles changements du CCP liés à la durée pour la période 1990–2100, en mettant l'accent sur les scénarios A2 et B2 du GIEC (Groupe d'experts intergouvernemental sur l'évolution du climat) relatifs aux futures émissions de gaz à effet de serre et aux aérosols. Des scénarios liés à la durée, avec T_{min} spécifiques aux sites ont été élaborés à partir de 30 ensembles de données de modèles de climats régionaux simulés obtenus dans le cadre du projet européen PRUDENCE. Pour les deux scénarios d'émission et pour tous les emplacements et saisons, on a constaté que le CCP diminuait de façon substantielle dès la fin du XXIe siècle. Pour les six emplacements en Europe centrale et en Europe du Nord (>47° nord), on a constaté que le CCP diminuait de 20–50% (juin–août). Pour les deux emplacements en Europe du Sud (Madrid et Athènes), on a constaté que le futur CCP devenait négligeable pendant l'été et diminuait de 20–55% pendant le printemps et l'automne. Cette étude montre clairement que le potentiel de refroidissement nocturne cessera d'être suffisant pour assurer le confort thermique dans de nombreux bâtiments construits en Europe du Sud et en Europe centrale. En Europe centrale et en Europe du Nord, un potentiel significatif de refroidissement passif va vraisemblablement durer pendant au moins les prochaines décennies. Il s'est avéré que les estimations supérieures et inférieures du futur CCP divergeaient nettement dans le courant du XXIe siècle, ce qui suggère la nécessité de concevoir les bâtiments avec souplesse et d'évaluer le risque en tenant compte d'une large gamme de scénarios d'émission et de l'incertitude des résultats des modèles climatiques.

Mots clés: changements climatiques, scénarios climatiques, potentiel de refroidissement climatique, ventilation nocturne, refroidissement passif, Europe

Introduction

As a consequence of increasing atmospheric concentrations of greenhouse gases, significant changes in the global climate are expected. The globally and annually averaged near-surface temperature has been estimated to have increased by 0.74 ± 0.18°C over the last century (1906–2005), with the rate of warming over the last 50 years being almost double that over the last century (Trenberth *et al.*, 2007). Applying six different marker scenarios for possible future emissions of radiatively active gases and aerosols, projections from a range of climate models suggest by the end of the 21st century a warming rise of 1.1–6.4°C will occur as compared with 1980–99 (Meehl *et al.*, 2007). This warming trend will be accompanied by complex and significant changes in regional climates that nowadays can be studied in increasing spatio-temporal detail with the aid of regional climate models (Giorgi *et al.*, 2001).

Climate change will impact in a variety of ways on the built environment and buildings (Engineering and Physical Sciences Research Council (EPSRC), 2003; Chartered Institution of Building Services Engineers (CIBSE), 2005). In particular, rising ambient temperatures imply a decrease in heating energy demand for buildings, but also an increasing demand for cooling. For Switzerland, for example, recent studies employing a degree-days method (Christenson *et al.*, 2005) and transient building energy simulations (Frank, 2005) demonstrated significant 20th-century trends in building energy demand that are likely to continue throughout the 21st century due to ongoing climate warming.

Even for the colder climate of the UK an increased risk of summertime overheating is expected as the occurrence of times with temperatures over 28°C was found to rise from 1 to 6% by the 2080s. Simulation studies revealed the application of thermal mass for building cooling to be very helpful, but due to a more frequent occurrence of hot spells, an effective way to dissipate the heat from the mass is seen to be essential (CIBSE, 2005).

Not only climate change, but also increased comfort expectations in summertime, high internal loads, and, especially in modern, extensively glazed buildings, higher solar gains (Manz, 2004; Manz and Frank, 2005) contribute to an increasing demand for cooling of buildings. Thus, commercial buildings in particular have experienced an upward trend in cooling energy demand over the last few decades, and the installation of air-conditioning systems is becoming more common even in the moderate and cool climates of Central and Northern Europe.

Particularly in this case – commercial buildings with high cooling loads in moderate climates with relatively low night-time temperatures even in summer – passive cooling by night-time ventilation appears to offer considerable potential. The basic concept involves cooling the building structure overnight in order to provide a heat sink, which absorbs heat gains during occupancy periods, and to guarantee thermal comfort without mechanical cooling or, at least, with a lower daytime cooling energy requirement (Chandra, 1989; Santamouris and Asimakopoulos, 1996; Allard, 1998). Night-time ventilation can be driven by natural forces (thermal buoyancy and wind), mechanical fans or hybrid ventilation systems. However, as in any case a sufficiently large temperature difference between ambient air and the building structure is needed during the night to achieve efficient convective cooling

of the building mass; this concept is highly dependent on climatic conditions and its potential could be jeopardized by climate warming.

For current European climatic conditions, the potential of passive cooling by night-time ventilation was investigated using a degree-hours method (Artmann *et al.*, 2007). The potential was found to be very significant in Northern Europe (including the British Isles), and still sufficient on most nights of the year in Central and Eastern Europe. In Southern Europe passive night-time cooling might not be sufficient the whole year round, but could still be used in hybrid systems.

Eicker *et al.* (2006) provided experimental evidence for the limitations of night-time ventilation under climatic conditions currently regarded as extreme. They monitored for three years an advanced low-energy office building in Weilheim, Germany, which was constructed in 1999, that was also equipped with an earth-to-air heat exchanger. While the building performed excellently during typical German summer conditions (2001 and 2002), in 2003, with average summer temperatures more than 3 K higher than usual, nearly 10% of all office hours were above 26°C. As the temperatures observed during the exceptionally hot summer of 2003 might correspond to those of a typical summer at the end of this century (Schaer *et al.*, 2004), the findings of Eicker *et al.* clearly demonstrate that in decades to come cooling by night-time ventilation might cease to work in buildings designed for current climatic conditions.

The impact of climate change on different passive cooling techniques has been analysed by Roaf *et al.* (1998). For the applicability of night-time ventilation, a monthly mean daily maximum temperature of 31°C was assumed to be the limiting criterion. Based on this and other threshold values, they delineated the regions where different cooling techniques could cease to be viable by 2050. These were found to be extensive enough to make them conclude that the effects of global warming should be taken into account by designers.

However, the study of Roaf *et al.* (1998) suffers from several shortcomings. First, their threshold temperature of 31°C only applies to well-shaded buildings with relatively low internal loads (e.g. residential buildings), as the authors state. Second, their threshold-based method is not suitable for quantifying gradual changes in cooling potential, e.g. across spatial gradients or over time. Although their approach was suitable to detect first-order effects, the 'cascade of uncertainty' associated with any regional climate projections (Gyalistras *et al.*, 1998; Mearns *et al.*, 2001) should also be taken into account for the elaboration of guidelines.

Uncertainty in climate projections arises, first of all, from the basic unpredictability of the socio-economic system and technological development. This makes it necessary to formulate a wide range of scenarios for the future emission of radiatively active gases and aerosols (Nakicenovic *et al.*, 2000). Further uncertainties are added in the process of estimating concentrations from emissions, radiative forcing from concentrations, and global climate changes from forcing. The most sophisticated tools available to accomplish the last step are what are known as Atmosphere–Ocean General Circulation Models (AOGCM) – global models with a rather coarse horizontal resolution of 200–300 km (Cubasch *et al.*, 2001). AOGCM results can be used as initial and boundary conditions for Regional Climate Models (RCM), to simulate local climatic effects for smaller areas, e.g. Europe, on a finer grid of about 50 km (Christensen *et al.*, 2002). This last 'downscaling' step again introduces additional uncertainty related to limitations of the available data, knowledge and AOGCMs/RCMs.

Nonetheless, it is assumed in this work that careful analysis of a wider range of regional climate scenarios can be used to provide upper and lower limits on the future space–time evolution of the cooling potential by night-time ventilation. Specifically, in this study the implications of two selected global emissions scenarios on cooling potential across eight representative sites in Europe are explored. This is accomplished by combining the degree-hours method of Artmann *et al.* (2007) with state-of-the-art temperature scenarios for 2071–2100, as derived from simulations with 12 RCMs driven by six different AOGCMs. The significant impact of climate warming on the potential for cooling by night-time ventilation is assessed, uncertainties associated with the applied scenarios and method are quantified, and consequences for building design are discussed.

Materials and methods

Case study locations

In the wake of inherent stochastic weather patterns, the potential for night-time cooling is subject to wide fluctuation in space and time (Artmann *et al.*, 2007). Moreover, it depends non-linearly on meteorological conditions, and this makes the use of coarse weather data (e.g. averages over a month or larger regions) problematic. Therefore, in this study representative locations were chosen for a more detailed analysis using hourly and daily weather data. The considered locations represent different climatic zones across a North–South transect in Europe (Table 1 and Figure 1). Table 1 also includes daily minimum temperature statistics based on long-term measurement data (1961–90) provided by the European Climate Assessment (ECA).

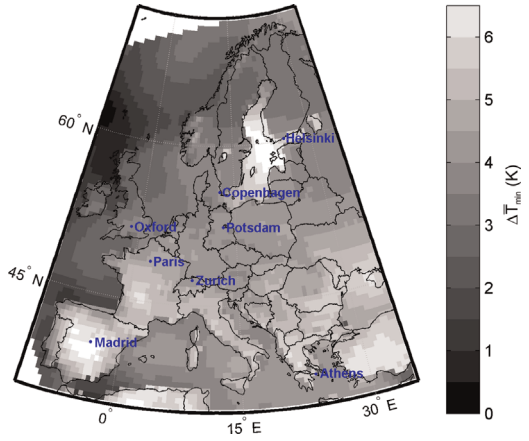

Figure 1 Change in long-term mean daily minimum temperature, $\Delta\overline{T}$, in summer (June–August) over Europe under the 'A2' emissions scenario for 2071–2100 relative to the baseline 1961–90, as simulated by the Danish Meteorological Institute regional climate model. Simulations were based on boundary conditions from the HadAM3H atmospheric general circulation model (Table A1, scenario No S1). Data are from PRUDENCE (2006)

Observed weather and climate data

Two sources of observed weather and climate data were used. The first was the commercial Meteonorm (2005) database that contains measurements from 7400 stations around the world. The database comes with software to generate semi-synthetic hourly weather data from measured long-term monthly mean values of weather variables (mainly representative of the period 1961–90) by means of stochastic simulation. Data for all case study locations were available in the Meteonorm database. Five different sets of random numbers were used at each location to generate a one-year data set of hourly mean temperature. The resulting sample size was 5 × 365 days × 24 hours. The applicability of these data for the calculation of the climatic cooling potential has been shown previously (Artmann *et al.*, 2007).

The second source of measured weather data was daily minimum temperatures (T_{min}) for 1961–90 as provided by the ECA (Klein Tank *et al.*, 2002). For easier handling the data sets were reduced to 360 days per year. This was accomplished by excluding all values for 29 February and 31 March, May, July, August and October. This procedure yielded 90 values per season. Winter was defined as December–February, spring as March–May, summer as June–August, and autumn as September–November. The resulting sample size for the 30-year period was 2700 daily values per season.

Model-simulated temperature data

All calculations of climate change effects were based on changes in the seasonal statistics of daily minimum temperatures (T_{min}) as simulated by a range of state-of-the-art RCMs. All RCM data were obtained from the PRUDENCE project (Christensen *et al.*, 2002, 2007; PRUDENCE, 2005). This project represented an attempt to integrate European climate projections of different institutions, and its website (PRUDENCE, 2006) provides a large database of RCM simulation results for Europe. These were based on boundary conditions from six global simulations with two AOGCMs (Arpege/OPA and ECHAM4/OPYC), plus three atmosphere-only GCMs (ECHAM5, HadAM3H and HadAM3P) that were driven with sea-surface temperature and sea-ice boundary conditions taken from simulations with the HadCM3 AOGCM. More information about the climate simulation models can be found on the PRUDENCE website.

Two kinds of RCM-simulated T_{min} data were used: 'control' data from regional climate RCM simulations under present-day (1961–90) conditions, and 'scenario' data for 2071–2100 under the emissions scenarios 'A2' and 'B2', as described in the Intergovernmental Panel on Climate Change's (IPCC) Special Report on Emission Scenarios (SRES) (Nakicenovic *et al.*, 2000; Intergovernmental Panel on Climate Change (IPCC), 2006).

All T_{min} data available from the PRUDENCE website, in total 20 control and 30 scenario runs, were initially considered (Table A1). This yielded a total of $n_{Ctrl} = 636$ and $n_{Scen} = 956$ seasonal data sets (=20 or 30 × eight locations × four seasons, minus four cases with no RCM data available for Madrid).

The RCM data were provided on varying model grids. For all calculations in this study the near-surface temperature data from the land gridpoint closest to the respective case study location were used for each RCM.

RCM control climates may deviate substantially from observations due to errors in the driving GCMs and to RCM deficiencies or omissions regarding the representation of the topography (e.g. inland bodies of water, mountains), and relevant processes (such as sea-ice or vegetation dynamics). In order to exclude 'unrealistic' RCM data sets the control data from all RCMs were first compared with the corresponding ECA measurements. To account for regional and seasonal variation in model performance for each selected grid point and season the 30-year long-term means ($\overline{T}_{min}$) and standard deviations (S) of the measured (subscript 'Obs' in the following equations; S in Table 1) and under present-day conditions simulated (subscript Ctrl) T_{min} data were computed. The simulated $\overline{T}_{min}$ were then corrected for the difference in altitude between the RCM grid point (H_{RCM}) and the

Table 1 Geographical position and altitude of the considered locations

Location	Longitude (°:')	Latitude (°:')	Altitude (masl)	Season	$\overline{T}_{min}$(°C)	S (°C)[1]	S_{sm} (°C)[2]
Helsinki	24:57 E	60:10 N	4	December–February	−7.55	7.21	3.20
				March–May	0.29	6.10	1.39
				June–August	12.39	3.00	0.93
				September–November	3.82	5.66	1.25
Copenhagen	12:32 E	55:41 N	9	December–February	−0.92	3.92	2.01
				March–May	3.83	4.30	0.95
				June–August	12.90	2.49	0.65
				September–November	7.21	4.15	0.69
Potsdam	13:04 E	52:23 N	81	December–February	−2.66	5.24	2.40
				March–May	3.75	4.87	0.97
				June–August	12.42	2.94	0.55
				September–November	5.78	4.80	0.76
Oxford	1:16 W	51:46 N	63	December–February	1.75	4.08	1.55
				March–May	4.87	3.53	0.58
				June–August	11.69	2.66	0.60
				September–November	7.32	4.34	0.73
Paris	2:20 E	48:49 N	75	December–February	2.50	4.19	1.52
				March–May	7.08	3.89	0.74
				June–August	14.41	2.79	0.81
				September–November	9.06	4.36	0.64
Zurich	8:34 E	47:23 N	556	December–February	−1.83	4.24	1.68
				March–May	4.25	4.42	0.89
				June–August	12.34	2.89	0.61
				September–November	6.25	4.76	0.81
Madrid	3:39 W	40:25 N	667	December–February	3.13	3.06	1.15
				March–May	7.63	3.74	0.89
				June–August	16.87	3.11	0.94
				September–November	10.42	4.86	0.95
Athens	23:45 E	37:54 N	15	December–February	7.75	3.42	0.81
				March–May	11.97	3.91	0.84
				June–August	21.82	2.52	0.86
				September–November	15.74	4.22	0.75

Notes: Data are long-term mean values, $\overline{T}_{min}$; the standard deviation of daily values, S; and the standard deviation of seasonal mean values, S_{sm}, of the daily minimum temperature for winter (December–February), spring (March–May), summer (June–August) and autumn (September–November) (ECA data, 1961–90).

[1] S is defined as follows:

$$S = \left(\frac{1}{2700 - 1} \sum_{y=1961}^{1990} \sum_{d=1}^{90} (T_{\min,y,s,d} - \overline{T}_{\min,s})^2 \right)^{1/2}$$

[2] S_{sm} is defined as follows:

$$S_{sm} = \left(\frac{1}{30 - 1} \sum_{y=1961}^{1990} (\overline{T}_{\min,y,s} - \overline{T}_{\min,s})^2 \right)^{1/2}$$

measurement station (H_{Obs}) using a standard atmosphere temperature lapse rate:

$$\gamma = -0.0065\,\mathrm{K/m}.$$

The following error measures were considered:

$$\delta\overline{T} = \overline{T}_{\min,Ctrl} + \gamma(H_{RCM} - H_{Obs}) - \overline{T}_{\min,Obs} \quad (1)$$

$$\delta S = \frac{S_{Ctrl}}{S_{Obs}}. \quad (2)$$

Formal statistical testing of the above differences did not prove to be very helpful due to the very large sample sizes of the data sets compared ($n = 2700$). As a consequence, even very small deviations that were neither physically meaningful nor relevant for the present application proved to be highly significant. Therefore, the following criteria were considered instead: data from an RCM for a given season and location were only used if $|\delta\overline{T}| \leq 2K$ and $|\delta S - 1| \leq 20\%$.

The choice of the above threshold values was based on the consideration of the climate change 'signals'. These

were defined as follows:

$$\Delta\overline{T} = \overline{T}_{\mathrm{min,Scen}} - \overline{T}_{\mathrm{min,Ctrl}} \quad (3)$$

$$\Delta S = \frac{S_{\mathrm{Scen}}}{S_{\mathrm{Ctrl}}}, \quad (4)$$

where the subscript 'Scen' denotes a statistic derived from an RCM scenario data set. The control and scenario run pairs used are shown in Table A1.

The threshold value of 2 K for model selection was chosen based on the assumption that in order to be able to 'trust' a given scenario, the model error $\delta\overline{T}$ should be smaller than the signal $\Delta\overline{T}$. In 95% of the n_{Scen} cases considered $\Delta\overline{T}$ was larger than +2 K

In contrast to the changes in the mean, which always increased, the standard deviation decreased or increased depending on seasons and locations, with 90% of all ΔS values falling within the range 0.79–1.26. The threshold value of 20% used for model selection corresponded to the requirement that model errors for S should not be larger than the changes 'typically' simulated for this statistic.

Figure 1 shows by way of example the $\Delta\overline{T}$ signal for summer as modelled by the RCM of the Danish Meteorological Institute (DMI) based on driving data from an A2 scenario integration with the HadAM3H AOGCM (Table A1: Scenario S1). The trend is particularly marked in Southern Europe, totalling 5.0–6.5 K for Central Spain. A similarly pronounced shift emerges in the Baltic Sea region. In Northern, Central and Eastern Europe too the shift in summer mean daily minimum temperature simulated by this model still reaches 2.5–5.0 K. Similarly, complex change patterns were also found for the other scenario simulations and seasons.

Construction of temperature scenarios

Two types of scenarios for possible changes in T_{min} were considered: (1) scenarios describing possible future distributions of T_{min} for 2071–2100 ('static scenarios'); and (2) scenarios describing possible time-dependent changes in the distribution of T_{min} for 1990–2100 ('transient scenarios'). The following procedures were applied separately for each RCM scenario data set, season and location.

For the static scenarios future ('projected', subscript 'Proj') temperature values for all days ($1 \le d \le 2700$) of a given season, $T_{\mathrm{min,Proj}(d)}$, were constructed by adjusting the mean and standard deviation of the measured ECA data according to the respective climate change signals:

$$T_{\mathrm{min,Proj}(d)} = \overline{T}_{\mathrm{min,Obs}} + (T_{\mathrm{min,Obs}(d)} - \overline{T}_{\mathrm{min,Obs}}) \cdot \Delta S + \Delta\overline{T}. \quad (5)$$

The construction of transient scenarios was based on the assumption that the climate change signals $\Delta\overline{T}$ and ΔS for a given future time-point to a first approximation scale linearly with the change in the expected value of the globally and annually averaged near-surface temperature, $\Delta\overline{T}_g$, for that time-point ('pattern scaling' technique; e.g. Mitchell, 2003). Daily data for a given future time point ($1990 \le t \le 2100$) were thus constructed according to:

$$T_{\mathrm{min,Proj}(t,d)} = \overline{T}_{\mathrm{min,Obs}} + (T_{\mathrm{min,Obs}(d)} - \overline{T}_{\mathrm{min,Obs}}) \cdot (1 + \kappa \cdot \Delta\overline{T}_{g(t)}) + \lambda \cdot \Delta\overline{T}_{g(t)} \quad (6)$$

The coefficients $\kappa = \partial\Delta S/\partial\overline{T}_g$ and $\lambda = \partial\Delta\overline{T}/\partial\overline{T}_g$ were estimated separately for each RCM, season and location as follows:

$$\kappa = \left(\frac{S^*_{\mathrm{Scen}}}{S_{\mathrm{Ctrl}}} - 1\right)/\Delta\overline{T}_{\mathrm{GCM}} \quad (7)$$

$$\lambda = \Delta\overline{T}/\Delta\overline{T}_{\mathrm{GCM}}, \quad (8)$$

where S^*_{Scen} is the standard deviation of the linearly detrended (see below) T_{min} scenario data; and $\Delta\overline{T}_{\mathrm{GCM}}$ is the 2071–2100 mean value of ΔT_g, as simulated by the (AO-)GCM used to drive the respective RCM scenario run. Only models with available values of $\Delta\overline{T}_{\mathrm{GCM}}$ (Table A1) were considered for the construction of transient scenarios.

The need to use S^*_{Scen} instead of S_{Scen} arose from the fact that T_{min} showed an upward trend in the 2071–2100 period due to ongoing climate change in the driving GCMs. This trend was considered as an integral part of the static scenarios used to describe the climate of the entire 2071–2100 period. The situation was different with regard to the transient scenarios, since these aimed at describing the statistics of T_{min} for distinct time points. Using non-detrended data would have inflated the standard deviation estimate for the period's central time point ($t = 2085$), thus also leading to a systematic overestimation of κ.

Detrending was performed as follows: first, seasonal means of T_{min} were computed for each year in the 2071–2100 period. The trend was then estimated as the slope of the linear regression of the 30 seasonal means from the year number. Finally, each daily value for a given year was adjusted by subtracting the linear trend component of the corresponding year. S^*_{Scen} was found to be always smaller than S_{Scen}, in

10% of all n_{scen} cases the difference amounted to more than 2% (a maximum of 8%).

For $\Delta\overline{T}_g$ an 'upper' and a 'lower' scenario as provided by Cubasch *et al.* (2001, figure 9.14, 'several models, all SRES envelope') were considered. These $\Delta\overline{T}_g$ trajectories accounted for a much broader range of radiative forcing scenarios and possible $\Delta\overline{T}_g$ responses to a given forcing (climate sensitivities) than was represented in the original PRUDENCE scenarios. The $\Delta\overline{T}_g$ for 2090–99 relative to 1980–99 for the 'upper' ('lower') scenario was 1.3°C (5.5°C). However, it should be noted that these upper and lower bounds still did not account for the full range of possible future developments (Cubasch *et al.*, 2001).

Transient scenarios were constructed by evaluating the $\Delta\overline{T}_g$ data at every five years within the period 1990–2100, and by using the κ and λ values derived from all selected RCM simulations for a given season and location.

Definition of the 'climatic cooling potential'

The potential for passive cooling of buildings by night-time ventilation was assessed based on a degree-hour method that evaluates the difference between the building and the ambient temperature. The method has been presented, extensively tested, and used to assess present-day cooling potentials (Artmann *et al.*, 2007). Therefore, it is described only very briefly here.

The method requires temperature data at an hourly time step as an input and gives the climatic cooling potential in degree hours (Kh). The daily climatic potential for ventilative night cooling, $CCP_{(d)}$, is defined as a summation of products between building/external air temperature difference, $T_b - T_e$ and time interval, m:

$$CCP_{(d)} = \sum_{h=h_i}^{h_f} m_{(d,h)}\left(T_{b(d,h)} - T_{e(d,h)}\right) \qquad (9)$$

$$\begin{cases} m = 1\,\text{h} & \text{if} \quad T_b - T_e \geq \Delta T_{crit} \\ m = 0 & \text{if} \quad T_b - T_e < \Delta T_{crit} \end{cases}$$

where d is the day; h is the time of day, where $h \in \{0, \ldots, 23\}$, h_i; h_f is the initial and final time of night-time ventilation; and ΔT_{crit} is a threshold value specifying a minimum temperature difference that is required for effective convection. Throughout all calculations $h_i = 19$, $h_f = 7$ and $\Delta T_{crit} = 3$K were assumed.

Because heat gains and night-time ventilation typically do not coincide in time, energy storage is an inherent part of the passive cooling concept. As building structures are almost always made of materials which are suitable for sensible energy storage only, such as concrete or brick, the temperature of the building structure varies when energy is stored or released. To take this fact into account, a variable building temperature was used for the calculation of the climatic cooling potential. In order to obtain a model which is as general as possible, no building-specific parameters were employed. Instead, the building temperature, T_b, was assumed to oscillate harmonically:

$$T_{b(d,h)} = 24.5°\text{C} + 2.5°\text{C}\cos\left(2\pi\frac{h - h_i}{24}\right)\forall d. \qquad (10)$$

According to this simple model, the maximum building temperature occurs at the initial time of night-ventilation, h_i, and as the ventilation time is 12 hours, the minimum building temperature occurs at the final time, h_f (Figure 2). In real buildings, depending on the direction of the building facade and the ratio of internal and solar gains, the maximum building temperature typically occurs between 14.00 hours ($h = 14$) and 18.00 hours ($h = 18$). Especially for high thermal mass buildings with high internal gains, a shift of the maximum to later hours is typical.

The choice of the building temperature range was based on CEN report CR 1752 (1998), which distinguishes three different categories of summertime thermal comfort, each based on a mean temperature of 24.5°C: category A ±1.0°C, category B ±1.5°C, category C ±2.5°C. International standard ISO 7730 (International Standards Organization (ISO), 1994) also recommends a temperature range of $T = 24.5 \pm 1.5$°C as summer conditions. However, recent studies confirm that broader temperature ranges are acceptable in non-air-conditioned buildings (Olesen and Parsons, 2002).

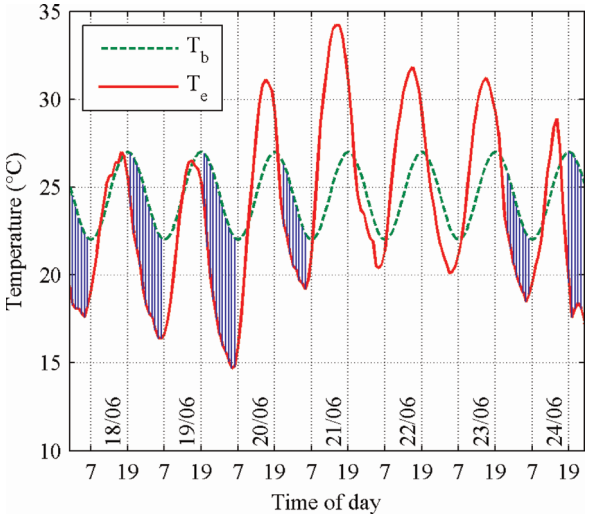

Figure 2 Building temperature, T_b, and external air temperature, T_e, during one week in summer 2003 for Zurich SMA (ANETZ data). Shaded areas illustrate the Climatic Cooling Potential (after Artmann *et al.*, 2007)

Category C of CR 1752 was therefore employed, i.e. $T_b = 24.5 \pm 2.5$°C was assumed for all calculations.

An example of the practical significance of the defined potential showed that a *CCP* of about 80 Kh per night is needed to discharge heat gains of 50 W/m^2 during 8 h using a ventilation rate of 6 air changes per hour (ACH) (Artmann *et al.*, 2007). However, as building parameters as well as heat gains can vary significantly, this value should be seen as a rough indication only.

In this study the following were considered for each season and location: (1) the distribution of $CCP_{(d)}$ and (2) the long-term mean values:

$$\overline{CCP} = \frac{1}{N}\sum_{d=1}^{N} CCP_{(d)}, \qquad (11)$$

where $N = 2700$.

Estimation of the 'climatic cooling potential' from daily minimum temperature

Because no hourly temperature data were available from the PRUDENCE simulations, $CCP_{(d)}$ had to be estimated from daily minimum temperatures, $T_{\min(d)}$. This was done based on the following equation:

$$CCP_{(d)} = \begin{cases} (T_0 - T_{\min(d)} \cdot \mathrm{C} & \text{if } T_{\min(d)} < T_0 \\ 0 & \text{if } T_{\min(d)} \geq T_0 \end{cases} \qquad (12)$$

The threshold temperatures, T_0, and the coefficients, C, were determined separately for each location by linearly regressing the $CCP_{(d)}$ values as calculated from hourly Meteonorm data (equations 9 and 10) with the corresponding $T_{\min(d)}$ data, i.e. the minima of the 24-hourly values per day. T_0 was defined as the temperature at which the regression line intersects the x-axis.

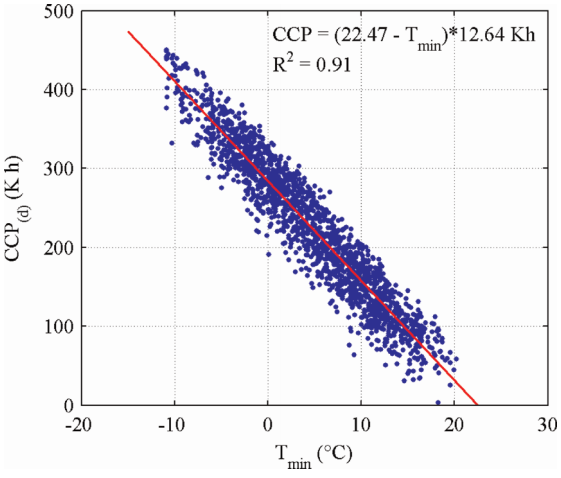

Figure 3 Correlation between daily climatic cooling potential ($CCP_{(d)}$) and daily minimum temperature (T_{min}) based on Meteonorm data for location Zurich SMA

Table 2 Threshold temperatures, T_0, and coefficients, C, for the eight case study locations

Location	T_0 (°C)	C (Kh/K)	R^2
Helsinki	24.11	12.17	0.91
Copenhagen	22.87	12.31	0.88
Potsdam	22.20	12.21	0.85
Oxford	24.07	11.23	0.78
Paris	22.25	12.22	0.83
Zurich	22.47	12.64	0.91
Madrid	19.67	12.92	0.87
Athens	21.86	12.82	0.89

An example for the location Zurich SMA is given in Figure 3. The results for all locations are summarized in Table 2.

Results

Figure 4 shows the seasonal $\overline{CCP}$ values found at the eight locations (arranged from left to right by latitude) under present-day (1961–90) and possible future conditions (2071–2100) for the two forcing scenarios A2 and B2 (for numerical values, see the Appendix, Table A2). Unsurprisingly, the potential is highest in winter and lowest in summer, and it clearly increases from South to North. A significant reduction of the potential for cooling by night-time ventilation is displayed for all locations, seasons and both forcing scenarios. Differences in the response between the two scenarios were found to be comparatively small, but, as expected, scenario A2 with higher concentrations of radiatively active gases yielded generally lower $\overline{CCP}$ values than scenario B2.

Figure 5 shows the absolute and relative reduction in $\overline{CCP}$ based on forcing scenario A2 for all seasons as a function of latitude. Except in Athens, where the mean potential in summer is currently only 13 Kh per night, the absolute reduction based on forcing scenario A2 amounted to about 30–60 Kh (B2 = 20–45 Kh) (Table A2). No clear trends depending on latitude or season were found for the absolute changes (Figure 5 (left)).

Considering the relative change in $\overline{CCP}$, a clear gradient from North to South can be recognized (Figure 5 (right)). The potential for night-time cooling during the summer months (June–August) was found to decrease by about 28–51% (B2 = 21–41%) (Table A2) in Central and Northern Europe. Very high values of relative reduction in $\overline{CCP}$ of up to 94% (B2 = 86%) were detected for the two Southern European locations. It should be noted

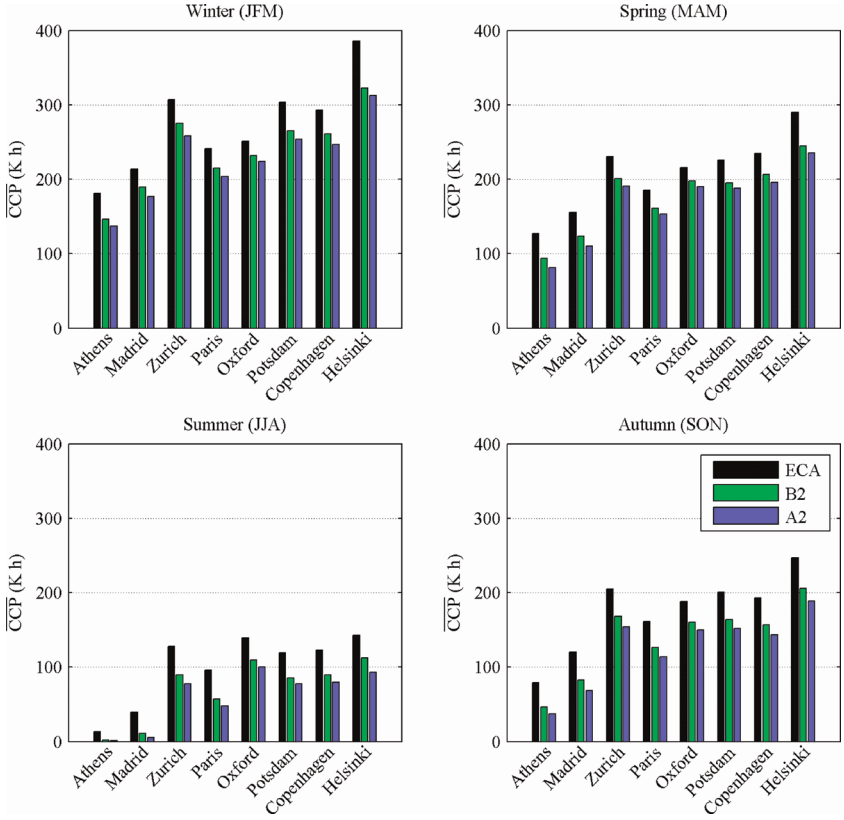

Figure 4 Estimated mean climatic cooling potential ($\overline{CCP}$) per season under current (1961–90, ECA data) and possible future (2071–2100, scenarios 'A2' and 'B2') climatic conditions at eight European locations. Future estimates present averages obtained from all selected climate scenario data sets (see 'Model-simulated temperature data') for that particular location, season and forcing scenario

that these high values are relative to the current summertime potential, which is, in fact, already insufficient for effective night-time cooling. However, in Southern Europe the potential during spring (March–May) and autumn (September–November) was also found to decrease by 29–53% (B2 = 20–42%). For all locations, the largest relative reductions occurred in summer.

Figure 6 illustrates the uncertainty of future summertime $\overline{CCP}$ estimates due to the choice of alternative

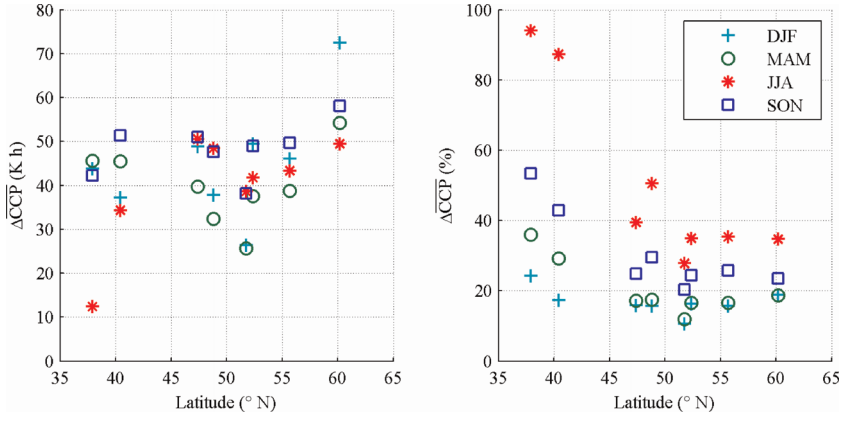

Figure 5 Absolute (left) and relative (right) changes in mean climatic cooling potential, $\Delta\overline{CCP}$ per season for 2071–2100 based on forcing scenario 'A2'. Results from eight European locations relative to the 1961–90 baseline are shown as a function of latitude. Each datum point represents the average from all selected climate scenario data sets (see 'Model-simulated temperature data') for that particular location, season and forcing scenario

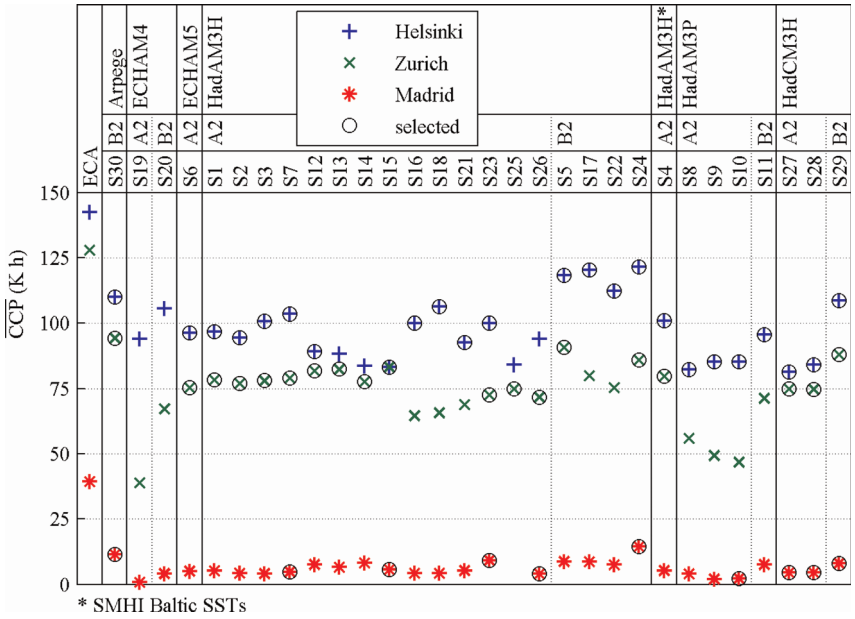

Figure 6 Mean climatic cooling potential, $\overline{CCP}$, for summer (June–August) at three selected European locations based on measured T_{min} data for 1961–90 (ECA, left column) and 30 T_{min} scenario data sets (scenarios S1–S30; see the Appendix, Table A1) for 2071–2100. All scenario data sets were constructed from regional climate model data provided by the PRUDENCE project. A2, B2: radiative forcing scenarios; Arpege, ECHAM4, ECHAM5, HadAM3H, HadAM3P and HadCM3H: global climate models used to drive the regional models; circles denote global/regional climate model configurations selected for further analysis based on an evaluation of model performance under present-day conditions (see 'Model-simulated temperature data')

forcing scenario (A2 versus B2) and GCM/RCM configuration. Results for the three locations Helsinki, Zurich and Madrid, representative for climates of Northern, Central and Southern Europe, respectively, are shown. The first column represents the $\overline{CCP}$ values based on ECA data. For ease of comparison, the results from the 30 PRUDENCE runs were sorted by forcing scenario and GCM. Figure 6 shows some interesting features in addition to what can already be discerned from Figures 4 and 5.

First, simulation runs under A2 conditions always resulted in lower $\overline{CCP}$ values than the respective B2 simulations using the same RCM/GCM configuration (compare, for example, S19 and S20). Second, differences in projected values due to the use of different RCMs under one and the same GCM simulation were often found to be of the same order as the differences due to the choice of forcing scenario. Compared with these uncertainties, the reduction in the cooling potential between current climate (1961–90) and predictions for future climate (2071–2100) was still significant. For example, at Helsinki the difference in the average $\overline{CCP}$ value from all selected (see 'Model-simulated temperature data') RCM/GCM configurations under the A2/HadAM3H boundary conditions as compared with the B2/HadAM3H boundary conditions amounted to 21 Kh. This compares with the inter-RCM range for the two boundary conditions of 23 and 9 Kh, respectively. The reduction in $\overline{CCP}$ during summer, however, amounted to 47 Kh under A2 and 29 Kh under B2 conditions. In addition, it can be seen that RCM/GCM configurations that were excluded due to poor performance under present-day conditions (data points not enclosed within a circle in Figure 6) often showed outlying $\overline{CCP}$ values (e.g. Zurich: S8, S9, S10 and S19). This also applied to other locations and seasons.

Figure 7 shows for Zurich and Madrid the percentage of nights per season under present-day and possible future conditions when the daily cooling potential $CCP_{(d)}$ exceeds a certain value. (Each curve corresponds to 1 minus the cumulative distribution function (CDF) of a $CCP_{(d)}$ data set; note also the reversal of the x- and y-axes as compared with the usual representation of CDFs). Additional charts for the other case study locations are presented in the Appendix (Figure A1).

Figure 7 suggests significant and highly variable changes in exceedance probabilities depending on location, season, and the threshold of minimum CCP necessary in a particular case. For example, at Zurich (Figure 7 (left)), under current climate conditions $CCP_{(d)}$ is higher than 80 Kh (roughly necessary to remove heat gains of 50 W/m^2; Artmann *et al.*, 2007) throughout most of the year, except for about 10% of summer nights. Under scenario A2 $CCP_{(d)}$ was found to fall below 80 Kh in more than 50% (B2 = 45%) of summer

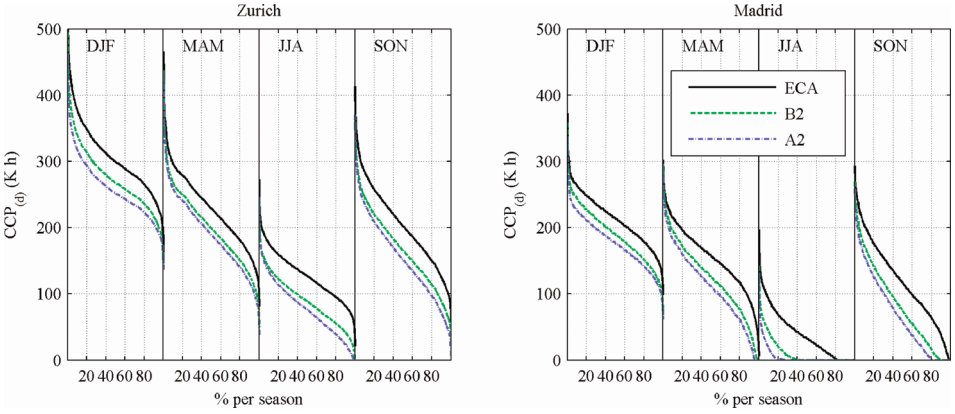

Figure 7 Percentage of nights per season under present day (ECA data, 1961–90) and possible future conditions (forcing scenarios A2 and B2, 2071–2100) during which the daily cooling potential $CCP_{(d)}$ exceeds a certain value at Zurich (left) and Madrid (right). For future conditions average percentages of nights are shown as computed from all selected climate scenario data sets (see section two) per location, season and forcing scenario

nights. Similar results were also found for Potsdam and Copenhagen. Even at the most northern location, Helsinki, under A2 conditions, 35% (B2 = 18%) of all summer nights were found to exhibit a cooling potential of less than 80 Kh per night (Figure A1).

Under present climatic conditions $CCP_{(d)}$ values at the studied locations in Southern Europe were found to be below 80 Kh throughout almost the entire summer. However, a considerable cooling potential was revealed in the transition seasons, such that the 80 Kh threshold was exceeded in 70% of all days in the year at Madrid (Athens = 57%). Under A2 conditions $CCP_{(d)}$ was found to be below 80 Kh for 48% of the year in Madrid (Figure 7 (right)) and 61% in Athens (Figure A1).

A further feature that can be discerned from Figure 7 is the changes in the variability of $CCP_{(d)}$. Significant increases in $CCP_{(d)}$ variability were typically found at the Central and Northern European locations during the summer (more stretched CDFs across the *y*-axis, e.g. Zurich in Figure 7). In contrast, large decreases in variability were found in cases with a low $\overline{CCP}$ under present-day conditions (e.g. Madrid in June–August and September–November) (Figure 7).

The diagram on the left in Figure 8 shows a range of the possible development of the mean climatic cooling potential, $\overline{CCP}$ during the summer (June–August) from 1990 to 2100. The lower limit indicated a rapid decrease in night cooling potential, especially after 2030. In the case of Madrid the slope of the lower limit tailed out as it approached zero. The upper limit showed a flatter slope and levelled to a constant value at the end of the 21st century.

The diagram on the right-hand side gives the time-dependent percentage of nights when $CCP_{(d)}$ exceeds

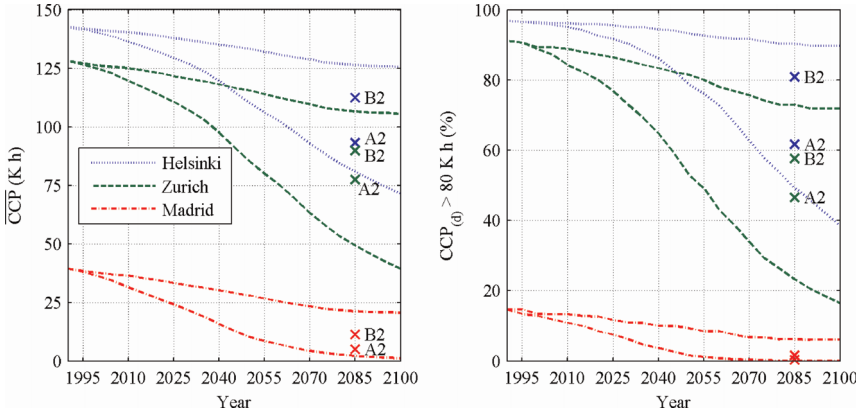

Figure 8 Time-dependent change in mean climatic cooling potential, $\overline{CCP}$ (left) and percentage of nights when $CCP_{(d)}$ exceeds 80 Kh (right) during the summer (June–August); upper and lower scenarios are based on mean global temperature scenarios (Cubash *et al.*, 2001, figure 9.14, 'several models, all SRES envelope') and mean values of selected PRUDENCE models for 'A2' and 'B2'

80 Kh. In the most extreme scenario the percentage of nights with $CCP_{(d)}$ exceeding 80 Kh in Madrid was found to decrease from 15% at present to below 1% by 2060. Until 2100 the same percentage decreased from 91% currently to 17% in Zurich and from 97 to 38% in Helsinki.

The range given by the upper and lower limits was found to be much wider than indicated by the mean values of the selected PRUDENCE models based only on forcing scenarios A2 and B2. Additionally, the position of the A2 and B2 mean values within the full range was not symmetric, and varied with location.

Discussion

The results presented here suggest that future warming will have a significant impact on the night-time ventilative cooling potential across Europe. This finding is generally in line with an earlier scenario-based analysis by Roaf *et al.* (1998), with empirical evidence for the exceptionally hot summer of 2003 (Eicker *et al.* 2006), as well as with the studies of Geros *et al.* (2005) and Kolokotroni *et al.* (2006), who concluded that in urban areas increased temperatures of a few degrees significantly lower the performance of night-time ventilation.

To the present authors' knowledge, this is the first study to provide a more in-depth assessment of possible climate change impacts on the potential for passive cooling by night-time ventilation. Unlike Roaf *et al.* (1998), who merely used a crude, threshold-based approach and coarse climate change scenarios, the present study is based upon a well-tested climatic cooling potential index (CCP; Artmann *et al.* 2007, equations 9 and 10), and explicitly accounts for temperature variations at the diurnal to century time scales. Moreover, by studying changes in probabilities at which $CCP_{(d)}$ exceeds a particular threshold value (Figures 7, 8 (right), and A1), information that is of immediate use for planning is provided.

For locations in Northern Europe, such as Copenhagen or Helsinki, the ventilative cooling potential was found to be currently sufficient throughout the entire year, whereas by 2071–2100 under conditions A2 or B2 the calculations in the present study yielded 19–48% of summer nights with a $CCP_{(d)} < 80$ Kh (Figures 8 (right) and A1). Considering that high minimum temperatures tend to coincide with generally warm days, these figures suggest an increased risk of thermal discomfort for two to six weeks per year.

Even stronger warming impacts were found for the Central European locations (Figures 7 (left), 8 and A1). For example, in Zurich the disproportionately great change in CCP during warm summer nights under scenario A2 resulted in some nights per year with zero potential, and a considerable extension of the period with less than 80 Kh (Figure 7 (left)). It seems that in decades to come summertime thermal comfort is unlikely to be achieved by night-time ventilation alone, and that eventually additional cooling systems, e.g. earth-to-air heat exchangers, will become necessary.

In Southern Europe summer cooling potential was found to be low already under present conditions (Figures 7 (right), 8 and A1), and according to the calculations in the present study it could be reduced by around 2050 to as little as 10–30 Kh, and later to zero (Figure 8). Note that by 2071–2100 for Madrid and Athens the RCMs used showed an increase in summer mean $T_{\min(d)}$ of over 5.0 and 3.6 K (data not shown) under the A2 and B2 scenarios, respectively. The additional cooling demand due to this warming in combination with the projected decrease in ventilative night cooling potential will make it particularly difficult to meet thermal comfort expectations. In order to avoid heavily increased energy consumption by mechanical cooling systems there is a great need for additional passive cooling techniques, such as radiant or evaporative cooling, and/or hybrid approaches. However, it should be noted that although cooling by night-time ventilation is expected to become increasingly ineffective during summer, it is likely to remain an attractive option in the transition seasons (Figures 7 (right) and A1). This will be even more the case if it is considered that under general warming the cooling season will tend to start earlier in spring and end later in autumn.

It should be pointed out that CCP values below about 40 Kh are increasingly sensitive to the threshold temperature ΔT_{crit} in equation (9) (Artmann *et al.*, 2007, figure 4). The value of $\Delta T_{\text{crit}} = 3$K was chosen for practical reasons. Especially in mechanically ventilated buildings night-time ventilation becomes ineffective if the temperature difference is too low. In naturally ventilated buildings a higher cooling potential might be useable by applying a lower ΔT_{crit} value. However, simulations performed during a follow-up study (Artmann *et al.*, submitted) showed that such low temperature differences can only be utilized at very high air change rates which are hardly achievable by natural forces. Therefore, the impact of ΔT_{crit} on the presented results seems small compared with other uncertainties.

A somewhat surprising result was that the estimated absolute changes in $\overline{CCP}$ were rather independent of location (Figures 4 and 5 (left)). This was first due to the linear dependence of $CCP_{(d)}$ on $T_{\min(d)}$ perturbations over a wide temperature range (equation 12 and Figure 3) in combination with the relatively small variability of the associated temperature

thresholds and coefficients (Table 2). Second, this result is also related to the fact that Figures 4 and 5 report average changes in $\overline{CCP}$ from all selected RCM simulations per location and forcing scenario. Apparently, although the climate change signal, $\Delta\overline{T}$, of individual RCMs typically shows large spatial variability (e.g. Figure 1), the use of multi-model means tended to blur inter-RCM differences, thus yielding roughly similar average responses for $\overline{CCP}$. As a consequence, relative changes in $\overline{CCP}$ were found to be largest in situations where the current $\overline{CCP}$ is smallest, i.e. at the southern-most locations and during summer (Figure 5 (right)).

The results further suggest that the uncertainty in the $\overline{CCP}$ signal due to the use of different radiative scenarios and the estimation of the associated local temperature signals by means of RCMs are of a similar magnitude (Figure 6). Similar results were also found for other locations and seasons (data not shown). This indicates that robust assessments should be based on the use of as many RCMs as possible, with the aim to cancel out errors simulated by individual RCMs.

At the same time the present analysis showed that RCMs cannot be trusted blindly. In several cases the models were found to show large biases in the simulation of present-day local $T_{\min(d)}$ (authors' analyses, cf. equations 1–4, results not shown) (also Kjellström *et al.*, 2007). Moreover, these problematic cases frequently yielded outlying $\overline{CCP}$ change values (Figure 6, e.g. for Zurich: S8, S9, S10 and S19), and using these would have introduced a strong bias in the $\overline{CCP}$ scenarios. This was also found to be the case for other seasons and locations (results not shown) and underlines the need for careful RCM evaluation and selection, as done in the present study.

The analysis at the daily time-scale revealed that future warming will have a strong impact on the cumulative distribution functions for $CCP_{(d)}$. Figure 8 illustrates the need for, and added value of, an analysis using daily data: for Helsinki and Zurich the $\overline{CCP}$ values start at a high level and show a relatively smooth, inconspicuous decrease over the first half of the 21st century (Figure 8 (left)). Yet, if exceedance probabilities for the relevant 80 Kh threshold are considered (Figure 8 (right)), practical implications would follow for the same period that could not be readily deduced from the $\overline{CCP}$ signal alone.

Also noteworthy are the great changes in the variability of $CCP_{(d)}$ – in particular during summer (Figures 7 and A1). The variability changes on the one hand reflected the generally increasing number of cases with zero potential (cf. equation 12) under a warmer climate. On the other hand, the future $CCP_{(d)}$ variability was also affected by a general increase in the variability of summertime $T_{\min(d)}$ in most RCM scenario simulations (on average 15% across all summer scenario data sets and locations; data not shown). The variability changes in the RCMs can be traced to land–atmosphere interactions that are expected to become increasingly important for the Central and Eastern European climate (Seneviratne *et al.*, 2006), and they had a significant effect on the results of the present study. For example, in Zurich it was estimated that under the A2 scenario 5% of future summer nights will have a cooling potential below 12 Kh; without changes in variability the corresponding value would have been about 21 Kh.

The increasing uncertainty range of the estimates with time (Figure 8) reflected the associated uncertainty in the evolution of the future global radiative forcing (Nakicenovic *et al.*, 2000). The 'upper' and 'lower' CCP trajectories shown in Figure 8 should by no means be considered as definitive. Rather, they present the current best estimates, given the scenarios, models and data available for this study. However, there are at least three reasons why the authors believe that the 'lower' CCP trajectories in Figure 8 might still be too optimistic.

First, the global temperature scenarios (input to equation 6) used to produce the CPP scenarios depend critically on assumptions regarding the equilibrium climate sensitivity, i.e. the equilibrium response of global mean temperature to a doubling of atmospheric CO_2 concentrations relative to the pre-industrial level. The global temperature scenarios used in this study assumed that the climate sensitivity is in the range 1.7–4.2 K (Cubasch *et al.*, 2001). More recent studies suggest, however, a 5–95% interval of 1.5–6.2 K for the equilibrium climate sensitivity (Hegerl *et al.*, 2006), or even a 95% upper limit as high as approximately 8 K (Stainforth *et al.*, 2005). The IPCC Fourth Assessment Report states a likely (>66% probability) range of 2.0–4.5 K (Meehl *et al.*, 2007), i.e. +0.3 K as compared with the bounds assumed here. Clearly, larger climate sensitivities for any given forcing scenario result in higher global temperature change rates, implying stronger local temperature signals, and consequently a more rapid decrease in cooling potential.

Second, the IPCC Fourth Assessment Report states for $\Delta\overline{T}_g$ a possible increase in the range 1.1–6.4°C in 2090–99 relative to 1980–99 (Meehl *et al.*, 2007), as opposed to the 1.3–5.5°C assumed in the present work (see 'Model-simulated temperature data'). One reason for the larger $\Delta\overline{T}_g$ range is that the new estimates incorporate the effect of carbon cycle uncertainties. However, note too that the new range was based on a set of six marker emissions scenarios that all assume that no climate change mitigation policies will be implemented. Hence, it might be argued that

the implementation of such policies would result in generally lower estimates for $\Delta\overline{T}_g$. Yet, it is unclear whether this would suffice to reduce the upper bound to below the 5.5°C assumed in the present work.

Third, this study did not account for the heat island effect that is present in many urban environments. Geros *et al.* (2005) analysed this effect for ten urban canyons situated in the extended region of Athens. Their measurements suggested a mean increase in outdoor air temperatures during the night of 0.6–2.9 K. For London, Kolokotroni *et al.* (2006) state for summer a mean heat island effect of 3.2 K. These numbers compare with the mean temperature signal for 2071–2100 in the present study that amounted to 3.8 K (2.8 K) for the A2 (B2) forcing scenario (averages across all RCMs, seasons and locations). As the heat island effect has not been considered in the present study, the true potential for night-time cooling in large urban areas could be considerably lower than stated in the given results.

Conclusions

Future climate warming will have a significant impact on the potential for cooling by night-time ventilation in Europe. Under an A2 or B2 radiative forcing scenario the authors estimate that by 2071–2100 the decrease in mean cooling potential will be in the order of 20–60 Kh, depending on season, location and forcing scenario, as compared with 80 Kh roughly necessary to remove heat gains of 50 W/m^2. Relative decreases in mean cooling potential are expected to be largest at low latitudes and for summer, i.e. cases where there is typically the highest cooling demand.

This study clearly demonstrated that any assessment of possible changes in the future ventilative night cooling potential (and probably also in any other indices related to the energy demand of buildings) is subject to large and partially irreducible uncertainties. Nevertheless, the amplitude and rate of the expected climatic changes and the longevity of buildings make planning necessary. The authors believe that it is neither possible nor desirable to establish any rigid guidelines. Instead, it is suggested that planning basics should be updated on a regular basis in order to reflect the latest developments from climate science and building physics.

The authors believe to have shown that this can be accomplished by linking high-resolution meteorological data sets, state-of-the-art climate model simulations, and applications-orientated climate scenarios with a simplified building model. More specifically, the results of the present study suggest that useful analyses of building energy balance scenarios should: (1) consider a high (e.g. daily) temporal resolution, (2) rely on as many global/regional climate models as possible, (3) account for the regionally and seasonally varying quality of these models, (4) consider changes in daily to inter-annual climate variability, in particular during summer, and (5) take into consideration the uncertainty of transient climate developments, e.g. by considering a wide range of radiative forcing scenarios and global climate sensitivities.

The decreases found in mean cooling potential have regionally varying implications. In Northern Europe (Helsinki, Copenhagen) the risk of thermal discomfort for buildings that use exclusively ventilative night cooling is expected to increase steadily up to possibly critical levels in the second half of the 21st century. In Central Europe (Zurich, Paris, London, Potsdam) extended periods with very low night cooling potential – where thermal comfort cannot be assured based on night-time ventilation only – could already become more frequent in the next few decades if a strong warming scenario became real. For Southern Europe (Athens, Madrid) the potential for ventilative night cooling will eventually become negligible during summer and will decrease to critical levels in the transition seasons.

In order to prevent a massive increase in energy consumption by mechanical cooling systems, at least three further strategies will have to be investigated: the reduction of external and internal heat gains, alternative passive cooling techniques, and the use of hybrid systems. The latter approach might be particularly attractive for Central Europe during summer, where a substantial potential for night-time cooling is likely to remain throughout the 21st century. In Southern Europe the hybrid approach could be attractive at least during the transition seasons due to the expected prolongation of the cooling season in combination with a generally increased cooling demand throughout the year.

In any case, in view of the need to abate global warming and to reduce dependency on fossil fuels, the authors believe that building design should be based on energy-efficient passive cooling techniques whenever possible.

Acknowledgements

This work was partially funded by the Hybrid Ventilation Centre, Department of Civil Engineering, Aalborg University, and the Swiss Federal Office of Energy (Project No. 101'308). The project was also supported by the private sector (WindowMaster, Belimo, SZFF). The authors acknowledge with thanks all financial support. Data were provided through the PRUDENCE data archive, funded by the European Union through Contract No. EVK2-CT2001-00132.

References

Allard, F. (1998) *Natural Ventilation in Buildings*, James & James, London.

Artmann, N., Manz, H. and Heiselberg, P. (2007) Climatic potential for passive cooling of buildings by night-time ventilation in Europe. *Applied Energy*, **84**, 187–201.

Artmann, N., Manz, H. and Heiselberg, P. (submitted) Parameter study on performance of building cooling by night-time ventilation. *Renewable Energy*.

CEN (1998) *Ventilation for Buildings: Design Criteria for the Indoor Environment*. CR 1752, CEN, Brussels.

Chandra, S. (1989) Ventilative cooling, in J. Cook (ed.): *Passive Cooling*, MIT Press, Cambridge, MA, p. 70.

Chartered Institution of Building Services Engineers (CIBSE) (2005) *TM36, Climate Change and the Indoor Environment: Impacts and Adaptation*. Technical Memorandum No. 36, CIBSE, London.

Christensen, J.H., Carter, T.R. and Giorgi, F. (2002) PRUDENCE employs new methods to assess European climate change. *EOS, Transactions of the American Geophysical Union*, **83**(13), 147.

Christensen, J.H., Carter, T.R., Rummukainen M. and Amanatidis, G. (2007) Evaluating the performance and utility of climate models: the PRUDENCE project. *Climatic Change*, **81**(Suppl. 1), 1–6.

Christenson, M., Manz, H. and Gyalistras, D. (2005) Climate warming impact on degree-days and building energy demand in Switzerland. *Energy Conversion and Management*, **47**, 671–686.

Cubasch, U., Meehl, G.A., Boer, G.J., Stouffer, R.J., Dix, M., Noda, A., Senior, C.A., Raper, S., Yap, K.S. *et al.* (2001) Projections of future climate change, in J.T. Houghton, Y. Ding, D.J. Griggs, M. Noguer, P.J. van der Linden, X.D. Dai, K. Maskell and C.A. Johnson (eds): *Climate Change 2001: The Scientific Basis*. Contribution of Working Group I to the Third Assessment Report of the Intergovernmental Panel on Climate Change (IPCC), Cambridge University Press, Cambridge, pp. 525–582 (available at: http://www.grida.no/climate/ipcc_tar/wg1/338.htm).

Eicker, U., Huber, M., Seeberger, P. and Vorschulze, C. (2006) Limits and potentials of office building climatisation with ambient air. *Energy and Buildings*, **38**, 574–581.

Engineering and Physical Sciences Research Council (EPSRC) (2003) *Building Knowledge for a Changing Climate – The Impacts of Climate Change on the Built Environment*, UK Climate Impacts Programme, Oxford.

Frank, T. (2005) Climate change impacts on building heating and cooling energy demand in Switzerland. *Energy and Buildings*, **37**, 1175–1185.

Geros, V., Santamouris, M., Karatasou, S., Tsangrassoulis, A. and Papanikolaou, N. (2005) On the cooling potential of night ventilation techniques in the urban environment. *Energy and Buildings*, **37**, 243–257.

Giorgi, F., Hewitson, B., Christensen, J., Hulme, M., Von Storch, H., Whetton, P., Jones, R., Mearns, L., Fu, C. *et al.* (2001) Regional climate information – evaluation and projections, in J.T. Houghton, Y. Ding, D.J. Griggs, M. Noguer, P.J. van der Linden, X.D. Dai, K. Maskell and C.A. Johnson (eds): *Climate Change 2001: The Scientific Basis*. Contribution of Working Group I to the Third Assessment Report of the Intergovernmental Panel on Climate Change (IPCC), Cambridge University Press, Cambridge, pp. 583–638.

Gyalistras, D., Schär, C., Davies, H.C. and Wanner, H. (1998) Future Alpine climate, in P. Cebon, U. Dahinden, H.C. Davies, D. Imboden, C.G. Jäger (eds): *Views from the Alps: Regional Perspectives on Climate Change*, MIT Press, Boston, pp. 171–223.

Hegerl, G.C., Crowley, T.J., Hyde, W.T. and Frame, D.J. (2006) Constraints on climate sensitivity from temperature reconstructions of the past seven centuries. *Nature*, **440**, 1029–1032.

Intergovernmental Panel on Climate Change (IPCC) (2006) (available at: http://www.ipcc.ch) (accessed May 2006).

International Standards Organization (ISO) (1994) *Moderate Thermal Environments – Determination of the PMV and PPD Indices and Specification of the Conditions for Thermal Comfort*. ISO 7730, ISO, Geneva.

Kjellström, E., Bärring, L., Jacob, D., Jones, R.J., Lenderink, G. and Schär, C. (2007) Modelling daily temperature extremes: recent climate and future changes over Europe, *Climatic Change*, **81**, 249–265.

Klein Tank, A.M.G. *et al.* (2002) Daily data set of 20th-century surface air temperature and precipitation series for the European Climate Assessment, International Journal of Climatology, **22**, 1441–1453 (data and metadata available at: http://eca.knmi.nl).

Kolokotroni, M., Giannitsaris, I. and Watkins, R. (2006) The effect of the London urban heat island on building cooling demand and night ventilation strategies. *Solar Energy*, **80**, 383–392.

Manz, H. (2004) Total solar energy transmittance of glass double façades with free convection, *Energy and Buildings*, **36**, 127–136.

Manz, H. and Frank, T. (2005) Thermal simulation of buildings with double-skin façades, *Energy and Buildings*, **37**, 1114–1121.

Mearns, L.O., Hulme, M., Carter, T.R., Leemans, R., Lal, M., Whetton, P. *et al.* (2001) Climate scenario development, in J.T. Houghton, Y. Ding, D.J. Griggs, M. Noguer, P.J. van der Linden, X.D. Dai, K. Maskell and C.A. Johnson (eds): *Climate Change 2001: The Scientific Basis*. Contribution of Working Group I to the Third Assessment Report of the Intergovernmental Panel on Climate Change (IPCC), Cambridge University Press, Cambridge, pp. 739–768.

Meehl, G.A., Stocker, T.F., Collins, W.D., Friedlingstein, P., Gaye, A.T., Gregory, J.M., Kitoh, A., Knutti, R., Murphy, J.M., Noda, A., Raper, S.C.B., Watterson, I.G., Weaver, A.J. and Zhao, Z.-C. (2007) Global climate projections, in S. Solomon, D. Qin, M. Manning, Z. Chen, M. Marquis, K.B. Averyt, M. Tignor and H.L. Miller (eds): *Climate Change 2007: The Physical Science Basis*. Contribution of Working Group I to the Fourth Assessment Report of the Intergovernmental Panel on Climate Change, Cambridge University Press, Cambridge, pp. 747–845.

Meteonorm (2005) *Global Meteorological Database for Engineers, Planners and Education*, Version 5.1 (available at: http://www.meteonorm.com).

Mitchell, T.D. (2003) Pattern scaling: an examination of the accuracy of the technique for describing future climates. *Climatic Change*, **60**(3), 217–242.

Nakicenovic, N., Alcamo, J., Davis, G., De Vries, B., Fenhann, J., Gaffin, S., Gregory, K., Grübler, A., Jung, T.Y., Kram, T., La Rovere, E.L., Michaelis, L., Mori, S., Morita, T., Pepper, W., Pitcher, H., Price, L., Raihi, K., Roehrl, A., Rogner, H.-H., Sankovski, A., Schlesinger, M., Shukla, P., Smith, S., Swart, R., Van Rooijen, S., Victor, N. and Dadi, Z. (2000) *IPCC Special Report on Emissions Scenarios*, Cambridge University Press, Cambridge.

Olesen, B.W. and Parsons, K.C. (2002) Introduction to thermal comfort standards and to the proposed new version of EN ISO 7730. *Energy and Buildings*, **34**, 537–548.

PRUDENCE (2005) *Prediction of Regional scenarios and Uncertainties for Defining European Climate Change Risks and Effects*. Final Report 2005 (available at: http://prudence.dmi.dk).

PRUDENCE (2006) (available at: http://prudence.dmi.dk) (accessed April 2006).

Roaf, S., Haves, P. and Orr, J. (1998) Climate change and passive cooling in Europe, in *Proceedings of 'Environmentally Friendly Cities'*, PLEA '98 (Passive and Low Energy Architecture) Conference, Lisbon, Portugal, June 1998, pp. 463–466.

Santamouris, M. and Asimakopoulos, D. (1996) *Passive Cooling of Buildings*. London, UK: James & James.

Schaer, C., Vidale, P.L., Luethi, D., Frei, C., Haeberli, C., Liniger, M.A. and Appenzeller, C. (2004) The role of increasing temperature variability in European summer heatwaves. *Nature*, **427**, 332–336.

Seneviratne, S.I., Lüthi, D., Litschi, M. and Schär, Ch. (2006) Land–atmosphere coupling and climate change in Europe. *Nature*, **443**, 205–209.

Stainforth, D.A., Aina, T., Christensen, C., Collins, M., Faull, N., Frame, D.J., Kettleborough, J.A., Knight, S., Martin, A., Murphy, J.M., Piani, C., Sexton, D., Smith, L.A., Spicer, R.A., Thorpe, A.J. and Allen, M.R. (2005). Uncertainty in predictions of the climate response to rising levels of greenhouse gases. *Nature*, **433**, 403–406.

Trenberth, K.E., Jones, P.D., Ambenje, P. Bojariu, R., Easterling, D., Klein Tank, A., Parker, D., Rahimzadeh, F., Renwick, J.A., Rusticucci, M., Soden, B. and Zhai, P. (2007) Observations: surface and atmospheric climate change, in S. Solomon, D. Qin, M. Manning, Z. Chen, M. Marquis, K.B. Averyt, M. Tignor and H.L. Miller (eds): *Climate Change 2007: The Physical Science Basis*. Contribution of Working Group I to the Fourth Assessment Report of the Intergovernmental Panel on Climate Change, Cambridge University Press, Cambridge, pp. 235–336.

Appendix

Table A1 PRUDENCE scenario and corresponding control data sets

Institute	Model	Scenario					Control	
		Number	Driving data	Forcing	$\Delta\bar{T}_{GCM}$	Acronym	Number	Acronym
DMI	HIRHAM	S1	HadAM3H	A2	3.2	HS1	C1	HC1
DMI	HIRHAM	S2	HadAM3H	A2	3.2	HS2	C2	HC2
DMI	HIRHAM	S3	HadAM3H	A2	3.2	HS3	C3	HC3
DMI	HIRHAM	S4	HadAM3H (SMHI Baltic SSTs)	A2	–	HS4	C1	HC1
DMI	HIRHAM	S5	HadAM3H	B2	2.3	HB1	C1	HC1
DMI	HIRHAM	S6	ECHAM5	A2	–	ECS	C4	ECC
DMI	HIRHAM h. r.	S7	HadAM3H	A2	3.2	S25	C5	F25
HC	HadRM3P	S8	HadAM3P	A2	–	Adhfa	C6	adeha
HC	HadRM3P	S9	HadAM3P	A2	–	Adhfe	C7	adehb
HC	HadRM3P	S10	HadAM3P	A2	–	Adhff	C8	adehc
HC	HadRM3P	S11	HadAM3P	B2	–	Adhfd	C6	adeha
ETH	CHRM	S12	HadAM3H	A2	3.2	HC_A2	C9	HC_CTL
GKSS	CLM	S13	HadAM3H	A2	3.2	SA2	C10	CTL
GKSS	CLM impr.	S14	HadAM3H	A2	3.2	SA2sn	C11	CTLsn
MPI	REMO	S15	HadAM3H	A2	3.2	3006	C12	3003
SMHI	RCAO	S16	HadAM3H	A2	3.2	HCA2	C13	HCCTL
SMHI	RCAO	S17	HadAM3H	B2	2.3	HCB2	C13	HCCTL
SMHI	RCAO h. r.	S18	HadAM3H	A2	3.2	HCA2_22	C14	HCCTL_22
SMHI	RCAO	S19	ECHAM4/OPYC	A2	3.4	MPIA2	C15	MPICTL
SMHI	RCAO	S20	ECHAM4/OPYC	B2	2.6	MPIB2	C15	MPICTL
UCM	PROMES	S21	HadAM3H	A2	3.2	a2	C16	control
UCM	PROMES	S22	HadAM3H	B2	2.3	b2	C16	control
ICTP	RegCM	S23	HadAM3H	A2	3.2	A2	C17	ref
ICTP	RegCM	S24	HadAM3H	B2	2.3	B2	C17	ref
met.no	HIRHAM	S25	HadAM3H	A2	3.2	HADCN	C18	HADCN
KNMI	RACMO	S26	HadAM3H	A2	3.2	HA2	C19	HC1
CNRM	Arpege	S27	HadCM3H	A2	–	DE6	C20	DA9
CNRM	Arpege	S28	HadCM3H	A2	–	DE7	C20	DA9
CNRM	Arpege	S29	HadCM3H	B2	–	DE5	C20	DA9
CNRM	Arpege	S30	Arpege/OPA	B2	–	DC9	C20	DA9

Table A2 Mean climatic cooling potential per season (Kh/night) under current (1961–90) and future (2071–2100 A2 and B2) climatic conditions, absolute and relative reduction at different locations

Location	Season	1961–90	2071–2100 A2			2071–2100 B2		
		CCP (Kh)	CCP (Kh)	ΔCCP (Kh)	ΔCCP (%)	CCP (Kh)	ΔCCP (Kh)	ΔCCP (%)
Helsinki	December–February	385	312	73	19.0	321	64	16.7
	March–May	290	236	54	18.5	245	45	15.6
	June–August	143	96	47	32.8	114	29	20.3
	September–November	247	189	58	23.5	206	41	16.7
Copenhagen	December–February	293	246	47	16.1	255	38	12.9
	March–May	234	195	39	16.8	204	30	12.8
	June–August	123	81	42	34.3	90	33	26.8
	September–November	193	144	49	25.2	157	36	18.6
Potsdam	December–February	304	255	49	16.0	265	38	12.6
	March–May	225	187	38	16.9	196	29	13.0
	June–August	119	77	42	35.5	87	33	27.5
	September–November	201	153	48	23.9	164	37	18.4
Oxford	December–February	251	224	26	10.6	232	18	7.4
	March–May	216	189	27	12.4	196	20	9.3
	June–August	139	102	37	26.8	111	28	19.8
	September–November	188	150	38	20.1	161	27	14.2
Paris	December–February	241	203	38	15.8	216	25	10.5
	March–May	185	154	32	17.2	161	24	13.0
	June–August	96	48	48	49.7	52	44	45.5
	September–November	161	115	46	28.6	126	35	21.8
Zurich	December–February	307	260	48	15.5	280	27	8.9
	March–May	230	193	37	16.3	208	22	9.7
	June–August	128	78	50	39.2	88	40	31.0
	September–November	205	154	51	24.8	167	38	18.7
Madrid	December–February	214	176	38	17.6	190	24	11.3
	March–May	156	110	46	29.4	124	31	20.2
	June–August	39	5	34	86.5	12	28	70.6
	September–November	120	70	49	41.3	83	36	30.4
Athens	December–February	181	137	44	24.5	148	32	18.0
	March–May	127	82	45	35.5	94	33	25.9
	June–August	13	1	12	94.2	2	11	86.4
	September–November	79	36	43	54.5	46	33	42.2

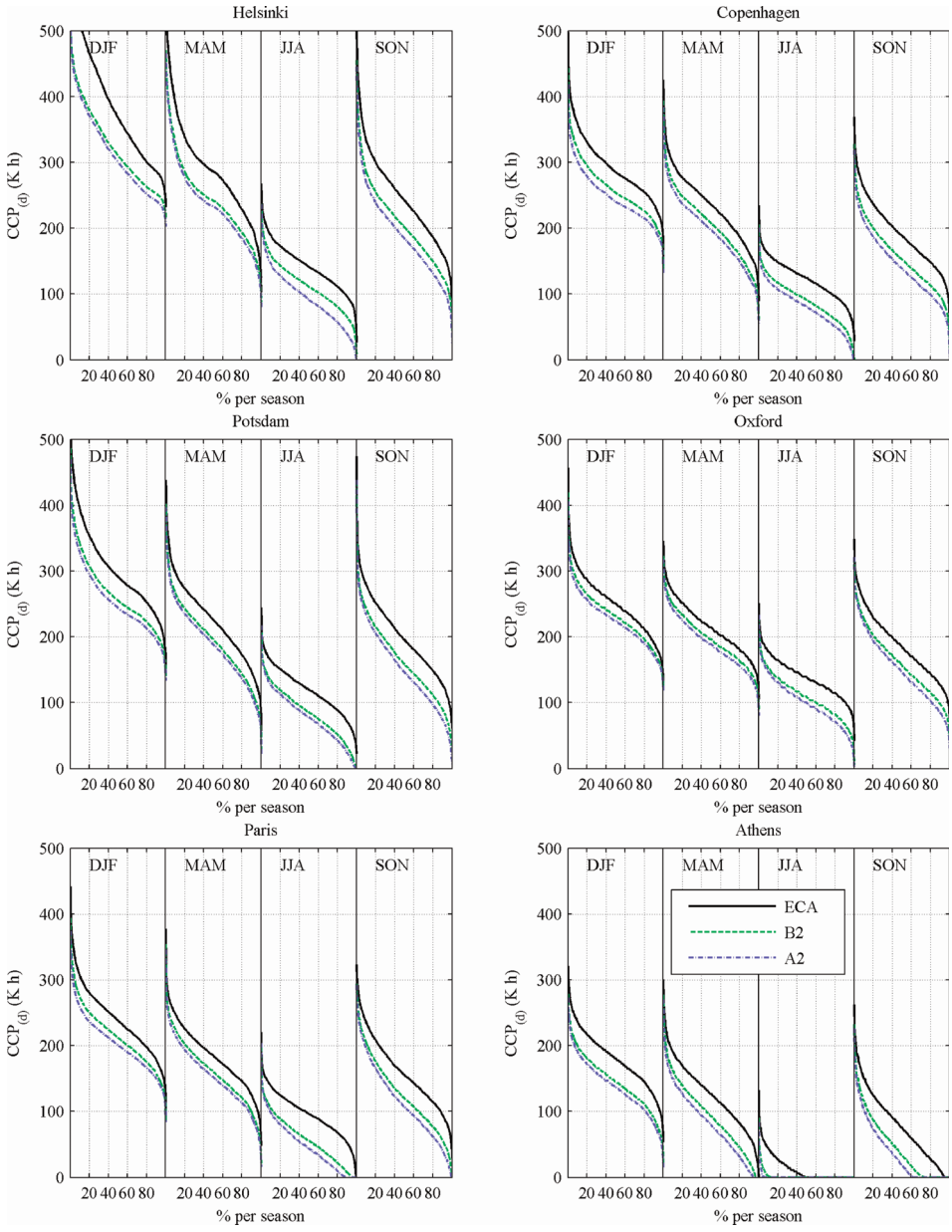

Figure A1 Seasonal cumulative distributions of CCP at different locations under current climatic conditions (ECA data) and projections based on forcing scenarios A2 and B2

Renewable Energy 33 (2008) 2589–2598

Contents lists available at ScienceDirect

Renewable Energy

journal homepage: www.elsevier.com/locate/renene

Parameter study on performance of building cooling by night-time ventilation

N. Artmann [a,*], H. Manz [a], P. Heiselberg [b]

[a] Empa, Swiss Federal Laboratories for Materials Testing and Research, Laboratory for Building Technologies, CH-8600 Duebendorf, Switzerland
[b] Department of Civil Engineering, Aalborg University, Hybrid Ventilation Centre, DK-9000 Aalborg, Denmark

ARTICLE INFO

Article history:
Received 31 May 2007
Accepted 19 February 2008
Available online 7 April 2008

Keywords:
Passive cooling
Night-time ventilation
Parameter study
Thermal mass
Heat transfer
Climate

ABSTRACT

Especially for commercial buildings in moderate climates, night-time ventilation seems to be a simple and energy-efficient approach to improve thermal comfort in summer. However, due to uncertainties in the prediction of thermal comfort in buildings with night-time ventilation, architects and engineers are still hesitant to apply this technique. In order to reduce the uncertainties, the most important parameters affecting night ventilation performance need to be identified. A typical office room was therefore modelled using a building energy simulation programme (HELIOS), and the effect of different parameters such as building construction, heat gains, air change rates, heat transfer coefficients and climatic conditions including annual variations on the number of overheating degree hours (operative room temperature $>26\,^{\circ}C$) was evaluated. Climatic conditions and air flow rate during night-time ventilation were found to have the largest effect. But thermal mass and internal heat gains also have a significant effect on cooling performance and the achievable level of thermal comfort. Using this modelling approach, significant sensitivity to heat transfer was found only for total heat transfer coefficients below about $4\,W/m^2\,K$.

1. Introduction

Considering the increasing demand for building cooling even in moderate and cold climates, night-time ventilation could bear significant potential for energy savings. Whenever the night-time outdoor air temperature is low enough, natural or mechanical ventilation can be used to cool the exposed thermal mass of a building in order to provide a heat sink during the following day. Despite the simplicity of the concept, the effectiveness of night-time cooling is affected by many parameters, which makes predictions uncertain. Therefore architects and engineers continue to be hesitant to apply low-energy techniques such as night ventilation in commercial buildings [1].

Numerous studies have been undertaken to investigate the effect of different parameters on the efficiency of night-time ventilation.

Using an hourly simulation model, Shaviv et al. [2] analysed the maximum indoor temperature in a residential building in the hot humid climate of Israel as a function of night ventilation air change rate, thermal mass and daily temperature difference. In a heavy mass building, the maximum indoor temperature was found to be reduced by 3–6 °C compared to the outdoor maximum.

The suitability of night ventilation for cooling offices in moderate climates such as that of the UK has been studied by Kolokotroni et al. [3]. Parametric analysis regarding thermal mass, heat gains and air change rates was used to develop a pre-design tool. Kolokotroni and Aronis [4] also studied the potential for energy savings by applying night ventilation in air-conditioned offices.

Finn et al. [5] investigated the effect of design and operational parameters on the performance of a night ventilated library building in the moderate maritime climate of Ireland. Increasing thermal mass by changing construction materials (from 887 to 1567 kg/m^2, per unit floor area) was observed to lower peak daily temperature by up to 3 °C. Internal gains (20–40 W/m^2) and ventilation rates up to 10 ACH were also found to have a significant effect on internal comfort, with a change in peak temperature of up to 1.0 °C. However, increasing ventilation rates beyond 10 ACH did not lead to significant improvement.

The effect of convective heat transfer on the efficiency of night ventilation was not considered in these studies, even though other studies showed the importance of this parameter for thermal energy storage in building elements. Akbari et al. [6] used an analytical model and numerical simulations to evaluate the effectiveness of massive interior walls. The effectiveness—defined as the ratio of the wall's total diurnal heat storage capacity for a given convective heat transfer coefficient to the maximum storage

* Corresponding author. Tel.: +41 44 823 4620; fax: +41 44 823 4009.
E-mail addresses: nikolai.artmann@empa.ch (N. Artmann), heinrich.manz@empa.ch (H. Manz), ph@civil.aau.dk (P. Heiselberg).

0960-1481/$ - see front matter © 2008 Elsevier Ltd. All rights reserved.
doi:10.1016/j.renene.2008.02.025

Nomenclature

A_{floor}	floor area
c	heat capacity
c_{dyn}	dynamic heat capacity
CCP_{JJA}	mean climatic cooling potential in June July and August
d	thickness
h	heat transfer coefficient
ODH_{26}	overheating degree hours above 26 °C
T_S	average room surface temperature
ΔT_{crit}	critical temperature difference

Greek symbols

λ	thermal conductivity
ρ	density

capacity of the same wall when the coefficient is infinite—of a 0.305 m thick concrete wall was found to be almost doubled by increasing the convective heat transfer coefficient from 2.84 to 5.68 $W/m^2 K$.

Several authors point out the importance of this finding for the efficiency of night-time ventilation, especially as increased convective heat transfer coefficients (HTCs) are expected at high air change rates [7–9]. However, Blondeau et al. [10] did not observe any significant difference in predicted indoor air temperature due to various increased convective coefficients during the night-time in their simulation study.

Lomas [11] found considerable discrepancies on comparison of the number of overheating hours predicted by different simulation programs. However, different algorithms for calculating convective heat transfer were found to be an unlikely explanation of the large variations in overheating predictions.

A sensitivity analysis conducted by Breesch and Janssens [12] gives a ranking of 14 most influential parameters on the uncertainty in thermal comfort in a single occupancy office in a moderate climate, cooled by single-sided natural night ventilation. The three parameters identified as having the most significant effect were, in this order: Internal heat gains, local outdoor temperature and internal heat transfer by day. It should be noted that increased convection due to high air change rates during night ventilation was not considered in this study.

The objective of the present study is to assess the effect of climate, thermal mass, heat gains, air change rates and heat transfer coefficient on the effectiveness of night-time ventilation. In contrast to other studies a wide range of HTCs at the internal surfaces is considered, and their effect on the night cooling performance is compared to the effect of other parameters.

2. Method

The HELIOS [13] building energy simulation programme was used to model a standard office room. Starting from a base case, different parameters were varied to assess their effect on night ventilation performance. Performance was rated by evaluating overheating degree hours of the operative room temperature above 26 °C.

Table 1
Main parameters of modeled office room

Floor area	20 m^2
Room height	2.6 m
Volume	52 m^3
Facade area	10.4 m^2
Facade area/volume ratio	0.2 m^{-1}
Internal surface area	86.8 m^2
Ceiling area	20 m^2
Internal wall area	36.4 m^2
External wall area	4.8 m^2
Window area	5.6 m^2
Glazed area (aperture)	4.05 m^2
Glazed area/facade area ratio	38.9%

2.1. Simulation model

A typical office room occupied by two persons was modelled applying the main characteristics as given in Table 1. In the base case, the external façade including two windows was oriented to the south. Assuming similar conditions in all adjacent rooms, the remaining boundaries were considered to be adiabatic. Therefore, only one floor slab (20.0 m^2) was modelled, representing the ceiling and the floor of the room by connecting both surfaces to the internal air node. Likewise, the internal walls were represented by an element with half the area (18.2 m^2), and both surfaces were connected to the internal air node.

2.1.1. Thermal mass models

Three different levels of thermal mass were defined, representing a light-weight (suspended ceiling, gypsum board walls), medium-weight (exposed concrete ceiling, gypsum board walls), and heavy-weight (exposed concrete ceiling, solid sand–lime brick[1] walls) construction. The detailed composition of the building elements and the thermal properties of the building materials are given in Table 2. The last column in Table 2 contains the dynamic heat capacity c_{dyn} of the building elements, i.e. the amount of energy stored per area if its surface is exposed to a varying temperature. The values give the dynamic heat capacity at the internal surfaces according to EN ISO 13786 [14], assuming a sinusoidal temperature variation with a 24 h time-period, excluding surface resistance. Fig. 1 illustrates the resulting dynamic heat capacity for the three different levels of thermal mass itemised by building elements. Dynamic heat capacity per unit floor area, c_{dyn}/A_{floor}, was 193, 432 and 692 $kJ/m^2 K$ for light-, medium-, and heavy-weight construction, respectively.

2.1.2. Windows and sun screen model

The windows were modelled as double-glazed with a 16 mm Argon fill and a low-emissivity coating ($\varepsilon = 5\%$) on the external surface of the internal glass pane ($U_{Glazing} = 1.2\ W/m^2 K$) and a wooden frame ($U_{Window} = 1.45\ W/m^2 K$).

The model included an external sun screen ($\tau_{Solar} = 19.2\%$) which was used for shading whenever solar irradiation was above 300 $W/m^2 K$ and internal air temperature was above 20 °C. The resulting total solar energy transmittance (*g*-value) was 66% or 16% with the sun screen opened and closed, respectively.

2.1.3. Internal heat gain models

Three different levels of internal heat gains were defined, representing low (159 $W h/m^2 d$), medium (229 $W h/m^2 d$) and high gains (313 $W h/m^2 d$). In all cases the office was occupied by

[1] Sand–lime brick: Bricks made from sand and slaked lime.

Table 2
Composition of building elements and thermal properties of building materials

	d (m)	λ (W/mK)	ρ (kg/m^3)	c (kJ/kg K)	c_{dyn} (kJ/m^2 K)
Floor slab (light, medium, heavy)[a]					
Carpet	0.005	0.050	80	930	99.9
Plaster Floor	0.080	1.500	2200	1080	
Sound insulation	0.040	0.040	30	1404	
Concrete	0.180	1.800	2400	1080	287.1
Suspended ceiling (light)[a]					
Air gap	0.250	$R = 0.160$ m^2 K/W			
Acoustic panel	0.020	0.210	800	900	51.1
Internal wall (light, medium)[a]					
Gypsum board	0.025	0.400	1000	792	21.7
Mineral wool	0.070	0.036	90	612	
Gypsum board	0.025	0.400	1000	792	21.7
Internal wall (heavy)[a]					
Plaster	0.015	0.700	1400	936	144.7
Sand–lime	0.150	1.100	2000	936	
Plaster	0.015	0.700	1400	936	144.7
External wall (light, medium)[a]					
Concrete	0.180	1.800	2400	1080	
Exp. polystyrene	0.120	0.035	40	1200	
Gypsum board	0.025	0.400	1000	792	24.0
External wall (heavy)[a]					
Plaster ext.	0.020	0.870	1600	1000	
Exp. polystyrene	0.120	0.035	40	1200	
Sand–lime	0.150	1.100	2000	936	
Plaster	0.015	0.700	1400	936	172.8

[a] Light-, medium-, and heavy-weight building construction.

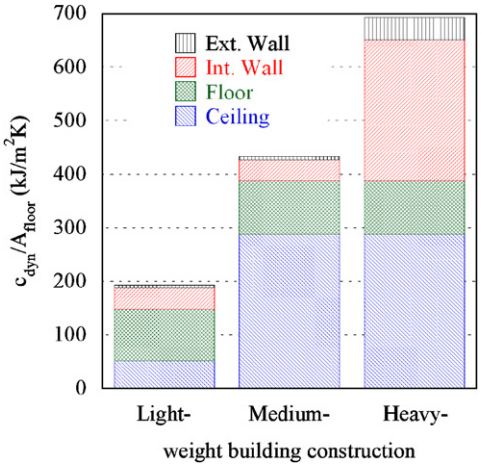

Fig. 1. Dynamic heat capacity (EN ISO 13786 [14]; excluding surface resistance) of building elements for three different levels of thermal mass.

two people, with a heat gain of 126 W/person (60% conv./40% rad.). Heat gains from equipment (80% conv./20% rad.) were assumed to be 50 W/person (low) or 150 W/person (medium and high). Lighting power was 10 W/m^2 (40% conv./60% rad.) with different schedules representing an office with (low and medium) and without (high) daylight utilisation. The lighting power in the case with daylight utilisation was defined according to measurements by Loutzenhiser et al. [15]. In the case without daylight utilisation, lighting power was 10 W/m^2 during the entire occupied period.

The resulting heat gains over the course of a day are shown in Fig. 2 and the values per unit floor area and day are given in Table 3. No internal heat gains were assumed during weekends.

2.1.4. Ventilation model

Night-time ventilation was applied from 7 p.m. to 7 a.m. at a fixed air change rate (base case: 6 ACH) if the external temperature was at least $\Delta T_{crit} = 3$ K below the average room surface temperature, T_S. To prevent over-cooling, night ventilation was applied only if the 24-h running average external temperature was above a certain cooling setpoint temperature, and terminated as soon as the average room surface temperature, T_S fell below 20 °C. Even if the room air temperature could drop well below the minimum comfort level, it was found to quickly approach the temperature of the walls after the end of the night ventilation period. Therefore the operative room temperature was within the comfort range at the beginning of the occupied period.

During the occupied period (7 a.m.–7 p.m.) the air change rate was set to 2 air changes per hour (1.4 l/m^2 s), according to prEN 15251 [16] category II for a building with low contamination levels. When night-time ventilation was not applied during unoccupied periods an infiltration rate of 0.5 ACH was accounted for. During weekends, the same settings as during the night were applied.

2.1.5. Heat transfer coefficients

HELIOS uses combined HTCs for convection and radiation, i.e. radiative heat transfer between internal surfaces is not computed explicitly, but is accounted for by increased HTCs which couple the internal surfaces to the indoor air node. The combined HTCs can be defined separately for each internal surface (ceiling, floor and walls). To allow for increased convective heat transfer during night-time ventilation, a step function model for the HTCs was integrated in HELIOS as a function of air change rate. In the base case, all HTCs were set to $h = 7.7$ W/m^2 K in accordance with DIN 4701 [17]. Values for combined [18] and convective [19] HTC are given in Table 4.

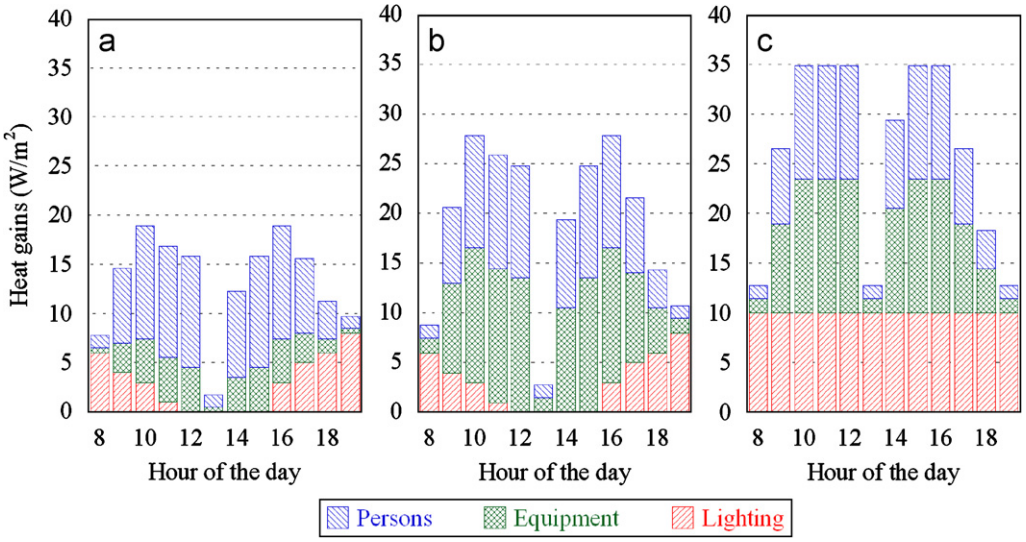

Fig. 2. (a) Low (159 W h/m²d), (b) medium (229 W h/m²d) and (c) high (313 W h/m²d) internal heat gains over the course of a day.

Table 3
Internal heat gains per unit floor area and day

	Persons (W h/m² d)	Equipment (W h/m² d)	Lighting (W h/m² d)	Total (W h/m² d)
Low	88	35	36	159
Medium	88	105	36	229
High	88	105	120	313

Table 4
Standard heat transfer coefficients (HTC)

	Combined HTC (W/m² K)	Convective HTC (W/m² K)
Vertical	7.7	2.5
Horizontal (upward)	10	5.0
Horizontal (downward)	5.9	0.7

2.2. Climatic data

HELIOS requires meteorological input data on an hourly basis. Three different sources of climatic data were used:

For Switzerland, the National Weather Service (MeteoSwiss) provides high-quality long-term series of measured hourly meteorological data. The automatic measurement network (ANETZ) was launched in the early 1980s and consists of 72 stations. Data from the Zurich SMA station from the period of 1981–2005 were used in this study.

The commercial Meteonorm [20] database contains measurements from 7400 stations around the world. The database includes software to generate semi-synthetic 1-year data sets of hourly weather data from measured long-term monthly mean values of weather variables (mainly representative for the period 1961–1990) by means of stochastic generation. In addition to long-term mean weather data 10-year maximum and 10-year minimum monthly mean values are available as a basis to generate hourly weather data. Meteonorm data sets were applied for 8 different case study locations, Helsinki, Copenhagen, Potsdam, London, Paris, Zurich, Madrid and Athens.

The third source of meteorological data was the design reference year (DRY) for Zurich SMA. The Zurich SMA DRY is a semi-synthetic hourly data set generated at Empa (Swiss Federal Laboratories for Materials Testing and Research) using the DRY method [21] based on measurements from the period 1981–1990.

2.3. Thermal comfort evaluation

Thermal comfort depends on the indoor environmental conditions, which are air temperature, mean radiant temperature, air velocity and humidity, as well as on the activity and the clothing of the occupants [22,23]. As the model used in this study predicts only temperatures, the operative room temperature—the mean value of air and average surface temperature—is used to evaluate thermal comfort. The cumulative distribution function of the operative room temperature (as shown in Fig. 3a in Section 3) gives the percentage of working hours when a certain temperature is exceeded. This provides complete information on the extent of overheating.

Overheating degree hours above 26 °C (ODH_{26}) are also used for simplified representation of thermal comfort evaluation in this study. Overheating degree hours are defined as the number of office hours (7 a.m.–7 p.m.) during which the temperature exceeds 26 °C, weighted by degrees by which 26 °C is exceeded. According to the German DIN 4108 [24], a maximum 10% of working hours with an operative room temperature above 26 °C can be accepted. In most cases this corresponds to about 400–600 Kh above 26 °C per year. Stricter limits with 100 h/a (3.2%) above 26 °C and 25 h/a (0.8%) above 27 °C, which corresponds to about 100–200 Kh/a above 26 °C, are given in the Danish standard DS474 [25]. The European standard prEN 15251 [16] gives the limit for the operative temperature in office buildings in 3 categories, I: 25.5 °C, II: 26 °C and III: 27 °C. For buildings without mechanical cooling systems higher limits are defined depending on the exponentially weighted running mean of the daily mean outdoor temperature. A building can be classified as a certain category, when at least 95% of occupancy time the operative temperature stays within the category limits. For the different categories this approximately corresponds to I: 100 Kh, II: 200 Kh and III: 400 Kh. It should be noted, that ODH values describe overheating in a integrated form, and therefore do not provide all information given by the cumulative distribution function.

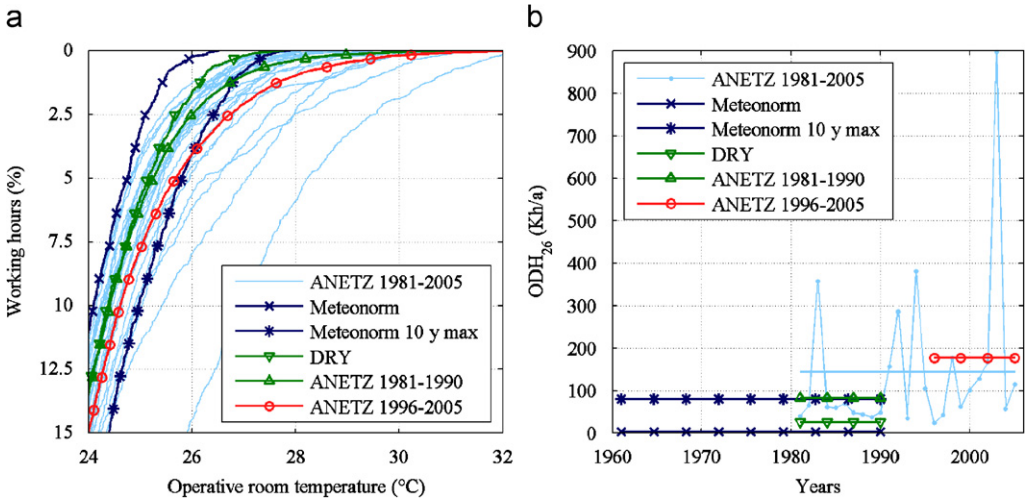

Fig. 3. (a) Cumulative distribution function of operative room temperature and (b) overheating degree hours (ODH) above 26 °C based on different climatic data for Zurich SMA: ANETZ 1981–2005, Meteonorm (standard and 10-year maximum), DRY, ANETZ 1981–1990 (mean) and ANETZ 1996–2005 (mean); medium thermal mass, high level of internal heat gains, air change rate 6 ACH, all heat transfer coefficients $h = 7.7\ W/m^2\,K$.

3. Results

3.1. Influence of climate data on building overheating

Fig. 3a shows the cumulative distribution function of the operative room temperature and Fig. 3b shows the ODH_{26} in a medium thermal mass office with high internal heat gains based on different climatic data for Zurich SMA. In the period from 1981 to 2005 (excluding 2003), the percentage of working hours exceeding 26 °C varied over the range of 1.2–8% if annual weather site data (ANETZ) was used. In 2003, exceptionally high summer temperatures resulted in 14.5% of working hours or nearly 900 Kh above 26 °C, while the mean value from 1981 to 2005 was 142 Kh/a.

Simulations based on Meteonorm or DRY data resulted in a far lower extent of overheating. The operative room temperature exceeded 26 °C only during 0.2% of working hours or 2.3 Kh/a if the Meteonorm standard data were applied, and 4.1% ($ODH_{26} = 79$ Kh/a) when Meteonorm data based on 10-year maximum monthly mean values were used. Applying DRY data (based on measurements from 1981 to 1990) resulted in 1.7% overheating hours ($ODH_{26} = 25$ Kh/a), while ANETZ data averaged over the same period yielded 2.5% of working hours above 26 °C ($ODH_{26} = 82$ Kh/a). ANETZ data from the period 1996 to 2005 resulted in 4.1% of working hours or 177 Kh per year above 26 °C.

3.2. Influence of climate conditions at different locations

ODH_{26} in an office with a medium level of thermal mass and high internal heat gains at different locations based on Meteonorm standard and 10-year maximum data are given in Table 5. Standard Meteonorm data resulted in very good thermal comfort with a maximum of 20 Kh per year for all considered locations in Northern and Central Europe except Paris, where a level of 99 Kh/a was calculated. Applying the Meteonorm data based on 10-year maximum values still yielded good thermal comfort with less than 100 overheating degree hours for Helsinki, Copenhagen, London and Zurich and 186 Kh for Potsdam. For Paris, the 10-year maximum data resulted in 434 Kh, which is at the limit for acceptable thermal comfort (prEN 15251 [16]: category III). Simulations based on Zurich ANETZ data from 1996 to 2005 yielded 177 Kh/a. For the same case (medium thermal mass and high heat gains) extensive overheating was found under Southern European climatic conditions such as in Madrid or Athens with more than 1500 Kh/a for both standard and 10-year maximum data.

Table 5 also gives the values of the mean climatic cooling potential during June, July and August (CCP_{JJA}) as defined by Artmann et al. [26]. The mean daily CCP (in Kh/d) is evaluated from the useable temperature difference between building and outdoor temperature during the night. It is defined as the number of night-time hours during which the outdoor temperature is below the building temperature, weighted by the temperature difference (detailed definition in [26]). Generally, the extent of overheating corresponded to the CCP during summer at the different locations. However, more overheating degree hours resulted for Potsdam than for London, for example, despite the higher cooling potential.

Table 5
Mean climatic cooling potential in June, July and August (CCP_{JJA}) and overheating degree hours above 26 °C (ODH_{26}) at different locations for Meteonorm standard and 10-year maximum data (including ANETZ 1996–2005 for Zurich)

Location	Climatic data	CCP_{JJA} (Kh/d)	ODH_{26} (Kh/a)
Helsinki	Meteonorm	142	1.6
	Meteonorm 10 yr max	118	54
Copenhagen	Meteonorm	137	0
	Meteonorm 10 yr max	116	18
Potsdam	Meteonorm	125	20
	Meteonorm 10 yr max	105	186
London	Meteonorm	116	10
	Meteonorm 10 yr max	97	90
Paris	Meteonorm	100	99
	Meteonorm 10 yr max	80	434
Zurich	Meteonorm	124	2.3
	Meteonorm 10 yr max	102	79
	ANETZ 1996–2005	104	177
Madrid	Meteonorm	51	1563
	Meteonorm 10 yr max	41	2293
Athens	Meteonorm	11	4200
	Meteonorm 10 yr max	3	6399

ODH_{26} for medium-weight building construction and high internal heat gains, air change rate 6 ACH, all heat transfer coefficients $h = 7.7\ W/m^2\,K$.

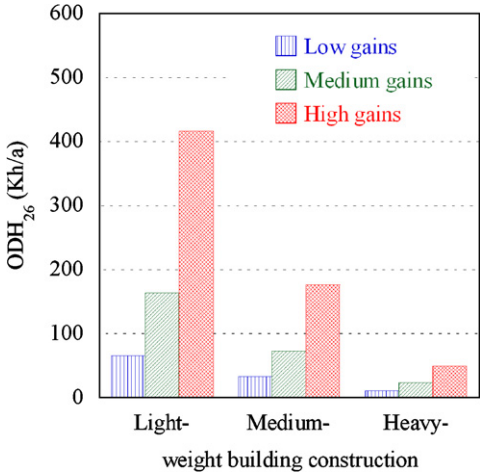

Fig. 4. Overheating degree hours (ODH) above 26 °C for different levels of internal heat gains (low, medium and high gains) and different building constructions (light-, medium- and heavy-weight); Zurich (ANETZ 1996–2005), 6 ACH, all heat transfer coefficients $h = 7.7\,W/m^2\,K$.

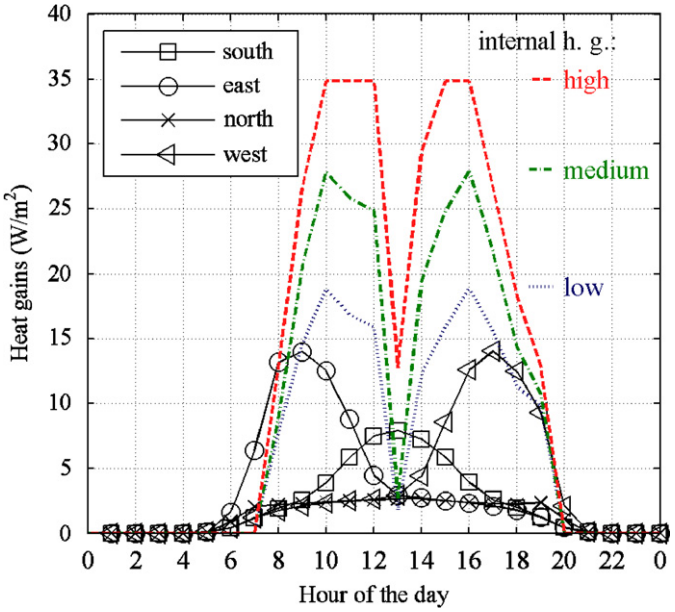

Fig. 5. Internal (low, medium and high) and solar (south, east, north and west orientation of the façade) heat gains on a sunny day, July 11, 2003.

3.3. Influence of thermal mass and heat gains

Significant effects of both different building constructions (thermal mass) and different levels of internal heat gains are shown in Fig. 4. Increasing thermal mass from $c_{dyn}/A_{floor} = 193\,kJ/m^2\,K$ (light-weight) to $c_{dyn}/A_{floor} = 692\,kJ/m^2\,K$ (heavy-weight) reduced overheating in an office with medium heat gains from 164 to 23 Kh/a. In a medium thermal mass office, overheating increased from 33 to 177 Kh/a if internal heat gains were changed from low ($159\,Wh/m^2\,d$) to high level ($313\,Wh/m^2\,d$). Four hundred and sixteen overheating degree hours resulted for the extreme case of a light-weight office with high internal loads.

The effect of solar heat gains was analysed by changing the orientation of the external façade. As an example, Fig. 5 shows the solar heat gains on a sunny day (July 11, 2003) for different façade orientations compared to the internal heat gains. As solar heat gains were generally low compared to internal heat gains, the effect of façade orientation on overheating degree hours was relatively small. In an office with a medium level of internal heat gains in south, east and west orientation, 74, 79 and 85 Kh/a above 26 °C resulted, respectively. A clear difference was found only for an office oriented to the north, where overheating was reduced to 42 Kh/a.

3.4. Night ventilation air change rate and heat transfer coefficients

Fig. 6 shows the ODH_{26} as a function of air change rate (0.5–32 ACH) during night-time ventilation and different HTCs ($5.9–10\,W/m^2\,K$; all surfaces, day and night). In most cases, a relatively low air change rate of 1–4 ACH was sufficient to maintain the limit of thermal comfort (prEN 15251 [16], category III; about 400 Kh). The greatest extent of overheating always occurred in light-weight buildings with about 370 Kh/a at 1 ACH in the case of low internal heat gains ($159\,W\,h/m^2\,d$), up to 350 Kh/a at 3 ACH in the case of medium heat gains ($229\,W\,h/m^2\,d$) and 400 Kh/a at 8 ACH in a office with high heat gains ($313\,W\,h/m^2\,d$).

Increasing the night ventilation air change rate improved thermal comfort significantly. For the example of a light-weight building with medium internal heat gains, overheating was reduced from 466 to 138 Kh/a when the air change rate was increased from 2 to 8 ACH ($h = 7.7\,W/m^2\,K$). In the same range of air change rate, overheating was reduced from 419 to 32 Kh/a in a heavy-weight office with high heat gains. In most cases, applying a higher air change rate than 8 ACH did not improve thermal comfort significantly. Overheating was only reduced by about 100 Kh/a in a light-weight office with high heat gains when the air change rate was increased from 8 to 32 ACH.

Variation of the combined HTC in the range from 5.9 to $10\,W/m^2\,K$ generally had a minor effect on overheating degree hours. The most significant effect was found for high heat gains, where at 6 ACH overheating degree hours were in the range from 147 to 215 Kh/a in a medium-weight office and from 377 to 464 Kh/a in a light-weight office.

For the case of high internal heat gains, more detailed information on the effect of combined HTCs is shown in Fig. 7. In Fig. 7a, the HTCs at all internal surfaces were changed during day and night, while in Fig. 7b HTCs were changed only during night-time ventilation, and in Fig. 7c only the HTC at the ceiling was changed during night-time ventilation.

When all HTCs were increased from $h = 5.9$ to $10\,W/m^2\,K$ during day and night, overheating degree hours were reduced from 464 to 377 Kh/a in a light-weight, 215 to 147 Kh/a in a medium-weight and 57 to 45 Kh/a in a heavy-weight office. The effect was smaller when the HTCs were varied in the same range, but only during night-time ventilation. While increasing the HTCs during night ventilation to $h = 22\,W/m^2\,K$ reduced overheating to 362, 138 and 41 Kh/a, respectively, the effect was more significant for lower HTCs. Increasing the HTC at the ceiling during night ventilation affected overheating only slightly. The largest effect occurred in the medium-weight building, where ODH_{26} decreased to 145 Kh/a. However, decreasing the HTC to $0.7\,W/m^2\,K$ increased overheating to 322 Kh/a.

3.5. Influence of the air change rate during the day

Changing the air flow rate during the day mainly affected thermal comfort in cases where night-time ventilation is not very effective, i.e. in light or medium-weight buildings together with a high or medium level of internal heat gains (Fig. 8). In such cases, overheating decreased with increasing air change rate. In contrast, overheating increased slightly in cases with very good thermal comfort ($ODH_{26} < 50$ Kh/a), when the air flow rate during the day was increased.

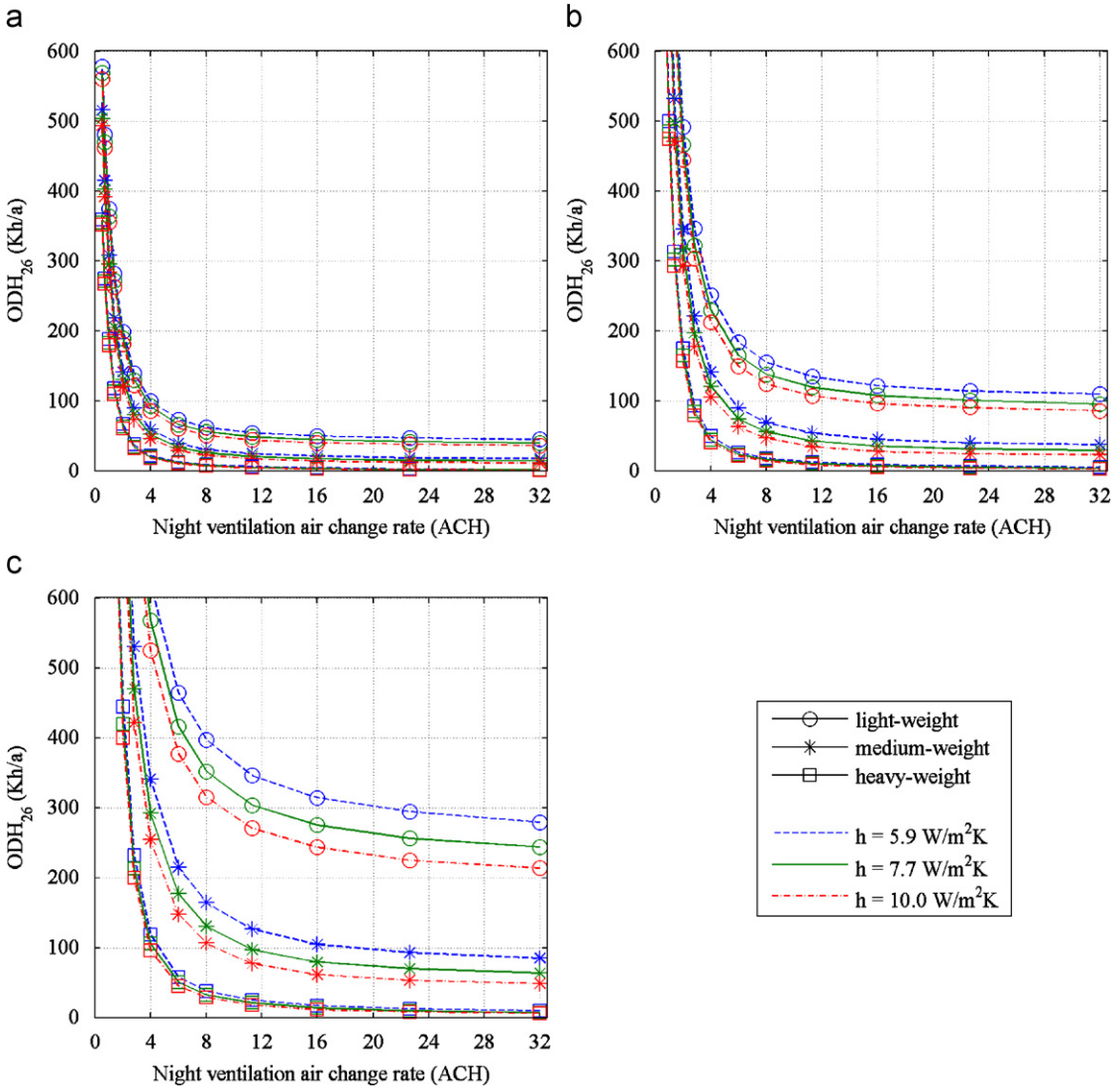

Fig. 6. Overheating degree hours (ODH) above 26 °C as a function of air change rate for different heat transfer coefficients (all surfaces, day and night) and different building constructions: (a) low, (b) medium and (c) high internal heat gains; Zurich, ANETZ 1996–2005.

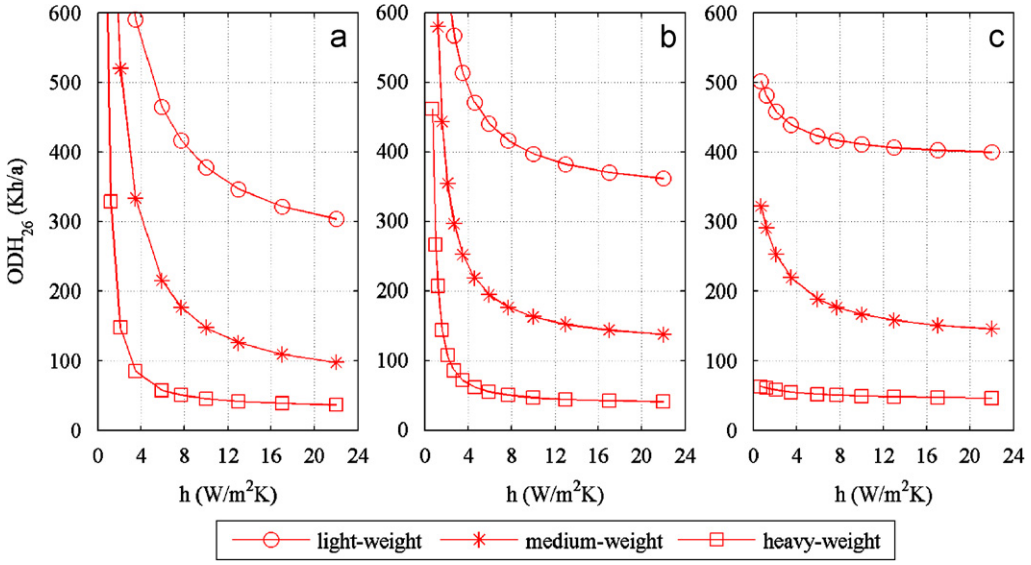

Fig. 7. Overheating degree hours (ODH) above 26 °C as a function of heat transfer coefficients for different building constructions (light-, medium- and heavy-weight): (a) all surfaces, day and night, (b) all surfaces, during night ventilation and (c) only ceiling, during night ventilation; high internal heat gains; 6 ACH; Zurich, ANETZ 1996–2005.

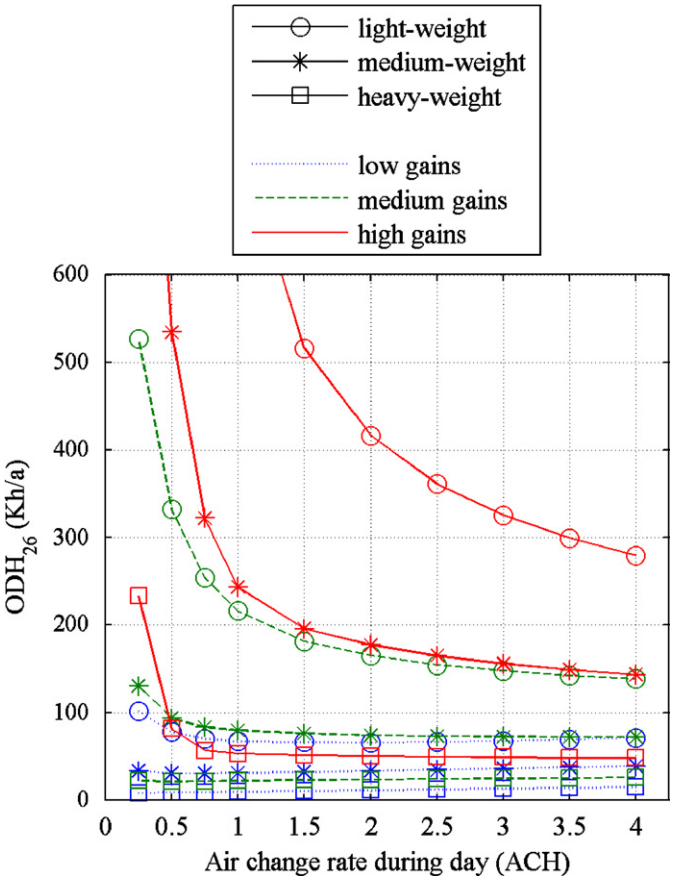

Fig. 8. Overheating degree hours (ODH) above 26 °C as a function of air change rate during the day for different building constructions and different levels of internal heat gains; 6 ACH; heat transfer coefficients $h = 7.7\ W/m^2\ K$ (all surfaces, day and night); Zurich, ANETZ 1996–2005.

4. Discussion

The external climatic conditions were found to have a very large impact on overheating. While good thermal comfort was achieved in a medium-weight office with high heat gains under Central and Northern European conditions, overheating degree hours clearly exceeded the comfort limit in Southern European climate. This generally agrees with the findings of our previous study on the potential for night-time ventilation in different climatic zones of Europe [26]. Furthermore, not only local, but also annual climatic variability largely affects overheating. While good thermal comfort conditions with max 400 Kh above 26 °C were usually achieved in a medium-weight office with high heat gains under climatic conditions measured at Zurich SMA during the period 1981–2005, a very high value of 900 Kh was calculated for 2003, with summer temperatures more than 3 K above the average. This clearly demonstrates the climatic limitations of building cooling by night-time ventilation.

In contrast, simulations of the same case based on semi-synthetic 1 year data sets such as Meteonorm or DRY resulted in very much lower values of ODH_{26}. Even applying Meteonorm data based on 10-year maximum values yielded ODH_{26} values far below the average of measured data for the period 1981–2005 (Fig. 3). This clearly shows that simulations based on commonly used climatic data do not always allow reliable predictions of thermal comfort in summer. Simulations in this study were therefore based on measured weather data from a 10-year period (1996–2005). As annual variability is greater than local variability, the results for Zurich SMA are believed to be representative for most locations in Central and Northern Europe, at least qualitatively.

Depending on comfort expectations, a certain number of overheating degree hours might be acceptable under extreme weather conditions. Thereby the tolerated extent of overheating also depends on the occupants' possibilities to adapt themselves, (e.g. by changing clothing) and control their environment (operation of windows, access to building controls, etc.). In order to account for this ability to adaptation the concept of adaptive thermal comfort has been proposed (see e.g. [27]), which relates the comfort temperature to the external temperature. In cases where abilities for adaptation are limited (e.g. dress code policy) and night-time ventilation is not sufficient to achieve the expected level of thermal comfort, additional cooling systems—preferably other energy-efficient systems, such as earth-to-air heat exchangers or solar absorption cooling—will be necessary.

Night-time ventilation was also found to depend clearly on building construction and heat gains (Fig. 4). A 180 mm thick concrete ceiling in direct contact with the room air reduced overheating by a factor of two compared to a suspended ceiling. Additionally, the application of solid sand–lime brick walls instead of gypsum board walls reduced overheating by a factor of three. As the ratio of wall to floor area depends on room geometry, these factors change with room size. In a large open plan office, the ratio of wall to floor area is smaller and the construction of the walls thus becomes less important.

Internal heat gains have an effect of similar magnitude. Both increasing the heat gains of office equipment from 50 to 150 W per person and using artificial light instead of daylight, respectively, increased overheating degree hours by a factor of 2–2.5. These factors depended on thermal mass, with a smaller sensitivity in heavier buildings.

Simulations with different orientations of the external façade showed the effect of solar heat gains. In the summer, solar irradiation is highest on the east and west façades. West-oriented rooms tend to overheat most because there is a coincidence in the afternoon between high ambient temperature and high solar irradiation. As good sun protection with a total solar energy transmittance (g-value) of 16% was considered in this study, solar gains were generally low compared to the internal gains (Fig. 5). The difference between south, east or west orientation was therefore not very pronounced. However, overheating degree hours were almost halved in an office oriented to the north. It must also be considered that peak solar gains coincide with a high temperature by day and a low cooling potential during night. An adequate solar shading system is therefore important to ensure thermal comfort in office buildings with night ventilation.

Evaluation of thermal comfort as a function of the night ventilation air change rate clearly demonstrated the effectiveness of night cooling (Fig. 6), as night-time ventilation even at relatively moderate air change rates significantly reduced overheating degree hours. This agrees with the analysis by Finn et al. [5] of a library building with night ventilation. For this case, they found a significant cooling effect for night ventilation with 4–10 ACH, but no further improvement for higher air change rates. In our simulations, the critical air change rate beyond which no significant improvement in absolute OHD_{26} values occurred was between 4 and 20 ACH, increasing with increasing heat gains and with decreasing thermal mass. This dependence on heat gains and thermal mass might be the reason for contradictory findings regarding the critical air flow rate in different studies [28–30], as discussed by Blondeau et al. [10].

The very high sensitivity to night ventilation air change rate in the range of 0.5–4 ACH makes predictions of thermal comfort very uncertain. This is especially true for buildings using natural night ventilation, where the air change rate depends on ambient

temperature and wind conditions. If natural ventilation depends mainly on buoyancy forces, low air flow rates coincide with high temperatures, and the cooling effect is smallest during warm periods. Additionally, sensitivity to the air change rate is enhanced even more if the dependency of heat transfer on the flow rate is considered. Therefore, in cases where air change rates in the range of high sensitivity are to be expected, the application of a hybrid ventilation system should be considered. In hybrid ventilation, a mechanical system is used whenever natural forces are not sufficient to ensure a certain ventilation rate. A shortfall of the critical air flow rate can thus be prevented and the risk of overheating reduced.

The effect of the air change rate during the day is relatively small compared to the night ventilation air change rate. Only if the indoor air temperature is higher than the ambient temperature—as is the case in light-weight offices with high heat gains—higher air change rates during the day can reduce the indoor temperature. In cases with good night ventilation performance with daytime indoor air temperatures below the ambient temperature, an increased air flow rate during the day causes additional heat gains. It should be noted that air motion enhances thermal comfort due to the increased convective heat transfer (comfort ventilation). However, this can also be achieved by a ceiling or portable room fan without exchanging cooler indoor air with warmer air from outside. Still, a sufficient air change rate for maintaining indoor air quality needs to be applied.

Compared with other parameters such as climatic conditions, the night ventilation air change rate, internal heat gains and building construction, the effect of the combined HTCs at the internal surfaces was relatively small, even if all HTCs during day and night were varied in the range from $h = 5.9$ to $10\,W/m^2K$ (Figs. 6 and 7a). This range represents the values given for downward ($h = 5.9\,W/m^2K$) and upward ($h = 10\,W/m^2K$) heat transfer at internal room surfaces in EN ISO 6946 [18].

During night-time ventilation, a higher heat transfer is expected due to the increased air flow rate and the possibility of a cold air jet flowing along the ceiling. However, increasing the HTCs during night-time ventilation to $22\,W/m^2K$ did not significantly affect the number of overheating degree hours (Fig. 7b). The effect was even smaller if only the HTC at the ceiling was increased (Fig. 7c). In this case, the largest effect occurred in the medium-weight building where 66% of the dynamic heat capacity was comprised by the ceiling.

On the other hand, it must be considered that combined HTCs are a very simplified representation of the real situation. In this model, heat can only be exchanged between wall surfaces and the room air, but not directly between surfaces. Heat transfer by radiation is accounted for by applying increased HTCs, and radiative heat flows therefore depend on the temperature difference between the surfaces and room air. If all surfaces have a similar temperature which is higher than the room temperature—this is a typical situation during night-time ventilation—the model overestimates the radiative heat flow.

Particularly at surfaces with downward heat flow, the coefficients for convective heat transfer alone are considerably lower than the coefficients for combined heat flow (Table 4). While the combined HTC for a downward heat flow is $h = 5.9\,W/m^2K$ [18], the convective HTC alone is only $h = 0.7\,W/m^2K$ [19]. Therefore during night-time cooling in particular heat transfer at the ceiling might be overestimated by a combined heat flow model. With decreasing HTCs below about $h = 4\,W/m^2K$, the effectiveness of night-time ventilation becomes increasingly sensitive (Fig. 7).

The effect of radiation, indoor air temperature distribution and near-surface velocities on heat transfer must be investigated in more detail, in order to determine the predominant effect and to decide whether the resulting combined HTC is within a range of high sensitivity. While radiation could be investigated using a more detailed building energy simulation programme (e.g. EnergyPlus [31] or ESP-r [32]), a detailed simulation of the indoor air flow patterns with computational fluid dynamics (CFD) is needed to clarify the effect of indoor air temperature and velocity distribution.

5. Conclusions and recommendations

Building energy simulation was used to investigate the effect of different parameters on the performance of building cooling by night-time ventilation. The climatic ambient conditions and the air flow rate during night-time ventilation mode were identified to have the most significant effect. However, building construction (thermal mass) and heat gains also have a considerable effect on thermal comfort in summer. Therefore, as much thermal mass as possible should be placed in contact with the room air (e.g. avoidance of suspended ceilings) and heat gains should be limited by applying energy-efficient office equipment, daylight utilisation, and the installation of an effective sun protection system.

The high sensitivity to climatic conditions demonstrates the significance of high-quality climatic data for building energy simulations. Simulations based on commonly used semi-synthetic 1 year data sets such as DRY or Meteonorm data tend to underestimate the extent of overheating compared to measured weather data. We therefore recommend the application of climatic data from long-term measurements including extreme weather conditions. Because of the gradually warming global climate, continuous updating of weather data for building simulation is also needed, as was also stated by Christenson et al. [33] and Artmann et al. [34].

Simulations with different night ventilation air change rates clearly demonstrate the effectiveness of night-time ventilation, as increased flow rates significantly reduce overheating degree hours. However, increasing the air flow rate above a certain value—a critical air flow rate depending on building construction and heat gains—does not lead to further improvement. If natural forces are not sufficient to achieve this critical flow rate, a hybrid ventilation system might be reasonable.

Heat transfer between the internal surfaces and the room air was found to have only a minor effect if the HTCs vary in the range from 5.9 to $10\,W/m^2K$ given for combined (convection and radiation) heat transfer in the European standard EN ISO 6946 [18]. Further increases also do not significantly improve night ventilation performance. Higher sensitivity was found only for HTCs below about $h = 4\,W/m^2K$. However, more detailed work on the effect of convective and radiative heat transfer is needed in order to improve the basic understanding of the cooling processes.

Acknowledgements

This work was partially funded by the Hybrid Ventilation Centre, the Department of Civil Engineering at Aalborg University and the Swiss Federal Office of Energy (Project no. 101'308). The project is also supported by the private sector (WindowMaster, Belimo, SZFF). We acknowledge with thanks all financial support. We also like to thank Stefan Carl for support with the HELIOS simulations.

References

[1] Breesch H, Bossaer A, Janssens A. Passive cooling in a low-energy office building. Sol Energy 2005;79:682–96.
[2] Shaviv E, Yezioro A, Capeluto IG. Thermal mass and night ventilation as passive cooling design strategy. Renewable Energy 2001;24:445–54.

[3] Kolokotroni M, Webb BC, Hayes SD. Summer cooling with night ventilation for office buildings in moderate climates. Energy Buildings 1998;27:231–7.
[4] Kolokotroni M, Aronis A. Cooling energy reduction in air-conditioned offices by using night ventilation. Appl Energy 1999;63:241–53.
[5] Finn D, Connolly D, Kenny P. Sensitivity analysis of a maritime located night ventilated library building. Sol Energy 2007;81:697–710.
[6] Akbari H, Samano D, Mertol A, Bauman F, Kammerud R. The effect of variations in convective coefficients on thermal energy storage in buildings: Part I—interior partition walls. Energy Buildings 1986;9:195–211.
[7] Chandra S, Kerestecioglu AA. Heat transfer in naturally ventilated rooms data from fullscale measurements. ASHRAE Transform 1984;90(1):211–24.
[8] Clark G. Passive cooling systems. In: Cook J, editor. Passive cooling. Cambridge, MA: MIT Press; 1989. p. 347–538.
[9] Givoni B. Performance and applicability of passive and low-energy cooling systems. Energy Buildings 1991;17:177–99.
[10] Blondeau P, Sperandio M, Allard F. Night ventilation for building cooling in summer. Sol Energy 1997;61:327–35.
[11] Lomas KJ. The UK applicability study: an evaluation of thermal simulation programs for passive solar house design. Building Environ 1996;31:197–206.
[12] Breesch H, Janssens A. Uncertainty and sensitivity analysis of the performances of natural night ventilation. In: Roomvent 2004 conference, Coimbra, Portugal, 5–8 September 2004, ISBN 972-97973-2-3.
[13] HELIOS Software. Building energy simulation code. Swiss Federal Laboratories for Materials Testing and Research (Empa). Switzerland: Duebendorf; 2007.
[14] EN ISO 13786. Thermal performance of building components—dynamic thermal characteristics—calculation methods, 1999.
[15] Loutzenhiser PG, Maxwell GM, Manz H. Empirical validation of the daylighting algorithms and associated interactions in building energy simulation programs using various shading devices and windows. Energy [available online 17 April 2007].
[16] prEN 15251. Indoor environmental parameters for assessment of energy performance of buildings- addressing indoor air quality, thermal environment, lighting and acoustics. European Standard, 2006.
[17] DIN 4701. Energy efficiency of heating and ventilation systems in buildings. Berlin, Germany: German Institute of Standardization; 2003.
[18] EN ISO 6946. Building components and building elements—thermal resistance and thermal transmittance—calculation method, 1997.
[19] EN ISO 13791. Thermal performance of buildings—internal temperatures in summer of a room without mechanical cooling—general criteria and calculation procedures, 2004.
[20] Meteonorm. Global meteorological database for engineers, planners and education, version 5.1—edition 2005, software incl. manual. 〈www.meteonorm.com〉.
[21] Skartveit A, Lund H, Olseth JA. The design reference year, recent advances in solar radiation resource assessment, seminar, Denver, CO, 1992.
[22] Fanger PO. Thermal comfort. Copenhagen, Denmark: Danish Technical Press; 1970.
[23] ISO 7730. Moderate thermal environments—determination of the PMV and the PPD indices and specifications of the conditions for thermal comfort, 1994.
[24] DIN 4108. Thermal protection and energy economy in buildings. German Standard, Beuth Verlag, 2003.
[25] DS474. Specifikation af termisk indeklima. Danish Standard, 1995 [in Danish].
[26] Artmann N, Manz H, Heiselberg P. Climatic potential for passive cooling of buildings by night-time ventilation in Europe. Appl Energy 2007;84:187–201.
[27] Nicol JF, Humphreys MA. Adaptive thermal comfort and sustainable thermal standards for buildings. Energy Buildings 2002;34:563–72.
[28] Ducrotoy H, Hutter E. Refraîchissement d'été sans Groupe Frigorifique par Évaporation d'eau dans les Immeubles de Bureaux Chauffage, Ventilation et Conditionnement d'Air (CVC), vol. 3, 1989. p. 15–20 [in French].
[29] Agas G, Matsaggos T, Santamouris M, Argyriou A. On the use of the atmospheric heat sinks for heat dissipation. Energy Buildings 1991;17:321–9.
[30] Blondeau P, Spérandio M, Sandu L. Potentialités de la ventilation nocturne pour le refraîchissement des bâtiments du Sud de l'Europe. In: Guarracino G, editor. Proceedings of the European conference on energy performance and indoor climate in buildings, vol. 3. Lyon, France: Ecole Nationale des Travaux Publics de l'Etat; 1994. p. 854–9 (in French).
[31] EnergyPlus program, 〈http://www.eere.energy.gov/buildings/energyplus/〉, 2007.
[32] ESRU ESP-r program, 〈http://www.esru.strath.ac.uk〉, 2007.
[33] Christenson M, Manz H, Gyalistras D. Climate warming impact on degree-days and building energy demand in Switzerland. Energy Convers Manage 2006;47:671–86.
[34] Artmann N, Gyalistras D, Manz H, Heiselberg P. Impact of climate warming on passive night cooling potential. Build Res Inform 2008;36(2):111–28.

Experimental investigation of heat transfer during night-time ventilation

N. Artmann [a, b, *], R. L. Jensen [b], H. Manz [a] and P. Heiselberg [b]

[a] *Empa, Swiss Federal Laboratories for Materials Testing and Research, Laboratory for Building Technologies, CH-8600 Duebendorf, Switzerland*

[b] *Hybrid Ventilation Centre, Department of Civil Engineering, Aalborg University, DK-9000 Aalborg, Denmark*

Manuscript submitted to Energy and Buildings, October 2008

Abstract

Night-time ventilation is seen as a promising approach for energy efficient cooling of buildings. However, uncertainties in the prediction of thermal comfort restrain architects and engineers from applying this technique. One parameter essentially affecting the performance of night-time ventilation is the heat transfer at the internal room surfaces. Increased convection is expected due to high air flow rates and the possibility of a cold air jet flowing along the ceiling, but the magnitude of these effects is hard to predict. In order to improve the predictability, heat transfer during night-time ventilation in case of mixing and displacement ventilation has been investigated in a full scale test room. The results show that for low air flow rates displacement ventilation is more efficient than mixing ventilation. For higher airflow rates the air jet flowing along the ceiling has a significant effect, and mixing ventilation becomes more efficient. A design chart to estimate the performance of night-time cooling during an early stage of building design is proposed.

Keywords: Passive cooling, Night-time ventilation, Experiments, Heat transfer, Temperature efficiency, Mixing ventilation, Displacement ventilation

---

* *Corresponding author:* Tel.: +41 44 823 4620; fax: +41 44 823 4009

E-mail addresses: nikolai.artmann@empa.ch (N. Artmann), rlj@civil.aau.dk (R. L. Jensen), heinrich.manz@empa.ch (H. Manz), ph@civil.aau.dk (P. Heiselberg)

Nomenclature

A	Surface area	(m^2)
ACR	Air change rate	(ACH)
Ar	Archimedes Number	(-)
c, c_p	Heat capacity	(J/kgK)
CCP	Climatic cooling potential	(Kh)
F	View factor	(-)
H	Room height	(m)
h	Heat transfer coefficient	(W/m^2K)
$\dot{m}$	Mass flow	(kg/s)
Q	Heat	(Wh)
$\dot{Q}$	Heat flow	(W)
$\dot{Q}_0$	Reference heat flow	(W)
$\dot{q}$	Heat flux	(W/m^2)
T	Temperature	(K), (°C)
ΔT	Temperature difference	(K)
ΔT_0	Initial temperature difference	(K)
t	Time	(s)
$\dot{V}$	Flow rate	(m^3/s)

Greek symbols

γ	Convection ratio	(-)
ε	Emissivity	(-)
η	Temperature efficiency	(-)
λ	Thermal conductivity	(W/mK)
ρ	Density	(kg/m^3)
σ	Stefan-Boltzmann constant	(W/m^2K^4)
τ	Dimensionless time	(-)

Subscripts

cond	Conduction
conv	Convection
d	Day
rad	Radiation
tot	Total
vent	Ventilation

Introduction

In many countries, a trend towards increasing cooling demand has been observed especially in commercial buildings in the last few decades [1], [2]. More extreme summertime weather conditions [3], [4], higher internal and solar heat gains and increased comfort expectations give rise to an increase in building cooling demand. One possibility to face the increasing energy demand of air conditioning systems is the passive cooling of buildings by night-time ventilation. The basic idea of the concept is to ventilate a building during the night with relatively cold outdoor air. In the simplest case this can be done by opening windows or, if necessary, by using a mechanical ventilation system. By night-time ventilation heat accumulated in the thermal mass of building elements is being removed. During the next day the cool building elements absorb heat gains, which prevents an extensive increase in indoor temperature.

Krausse et al. [5] recorded the energy consumption and the internal temperatures and CO_2 levels in the naturally ventilated Lanchester Library at Coventry University, UK. Due to the exposed thermal mass and the night ventilation strategy the building meets thermal comfort criteria even during prolonged hot spells, using 51 % less energy than a typical air-conditioned office. Another example for a passively cooled building is the KfW office building in Frankfurt, Germany. A monitoring study conducted in this building by Wagner et al. [6] showed, that even under extreme climate conditions acceptable thermal comfort conditions can be reached with passive cooling.

Despite many successful examples, architects and engineers continue to be hesitant to apply this technique in commercial buildings because of high uncertainties in thermal comfort predictions [7]. One parameter obviously affecting the efficiency of night-time ventilation is the heat transfer at the internal room surfaces [8]. In a previous study [9] a high sensitivity was found for combined (convection and radiation) heat transfer coefficients below about 4 W/m^2K. Depending on the direction of the heat flow, standard heat transfer coefficients for combined heat transfer are in the range from 5.9 to 10 W/m^2K [10]. However, during night-time ventilation radiation does not contribute to the heat transfer from room surfaces to the air (as air is virtually transparent for infrared radiation), but in fact transfers heat from one surface to another. For convective heat transfer standard coefficients are 2.5 W/m^2K for vertical walls, 5.0 W/m^2K for upward heat flow and 0.7 W/m^2K for downward heat flow [11]. This means that, especially at the ceiling – a concrete ceiling often represents a significant share of the thermal mass of a room – the convective heat transfer can be very limited (downward heat flow during night-time ventilation). On the other hand a higher convective heat transfer is expected due to the increased air flow rate and the possibility of a cold air jet flowing along the ceiling [12], [13], [14].

Several studies deal with the heat transfer at internal room surfaces. Different correlations were proposed for natural (e.g. Alamdari and Hammond [15], Khalifa and Marshall [16], Awbi and Hatton [17]) and mixed convection (e.g. Chandra and Kerestecioglu [12], Spitler et al. [18], Awbi and Hatton [19]) from horizontal and vertical surfaces. Based on such empirical correlations Beausoleil-Morrison developed an adaptive algorithm for the simulation of the convective heat transfer at internal building surfaces [20]. However, many of these correlations are based on experiments on small heated plates. A review comparing natural convective heat transfer at isolated surfaces and surfaces in enclosures revealed clear discrepancies [21], [22]. This demonstrates the necessity of considering a room as a whole.

Geros et al. [23] compared monitoring data from a very heavy, massive and free floating building, where night ventilation was applied by natural cross-ventilation with thermal simulations. When the measured air flow rate was used as an input, the simulation model overestimated the performance of the night ventilation. The authors attribute this mainly to the non-efficient coupling of the air flowing through the building to the thermal mass (short circuit air flow). The effective flow rate was then found by adjusting the simulation model

to result in the measured indoor air temperature. The ratio between the measured and the effective flow rate was found to be close to 0.3.

The effect of different flow patterns on the storage efficiency during night-time ventilation has been investigated by Salmerón et al. [24] using a 2-dimensional computational fluid dynamics model. A variation by a factor of 6 was found between different configurations of air in- and outlet openings. However, radiation between internal room surfaces was not considered. Furthermore, the impact of the air flow rate on the storage efficiency was not investigated.

This study provides a detailed analysis of convection and radiation during night-time ventilation depending on the air flow rate and the initial temperature difference between the inflowing air and the room. Heat transfer in case of mixing and displacement ventilation has been investigated in a full scale test room.

Setup of the test room

A test room at Aalborg University – a wooden construction insulated with 100 mm rock wool – was rebuilt for the experimental investigation of the heat transfer during night-time ventilation. For increased thermal mass a heavy ceiling element consisting of 7 layers of 12.5 mm gypsum boards was installed [25]. The walls and the floor were insulated with 160 mm (floor: 230 mm) expanded polystyrene (EPS). After installation of the insulation the internal dimensions were 2.64 m x 3.17 m x 2.93 m (width x length x height) resulting in a volume of 24.52 m^3. A vertical section of the test room is shown in Figure 1, a detailed description can be found in [26].

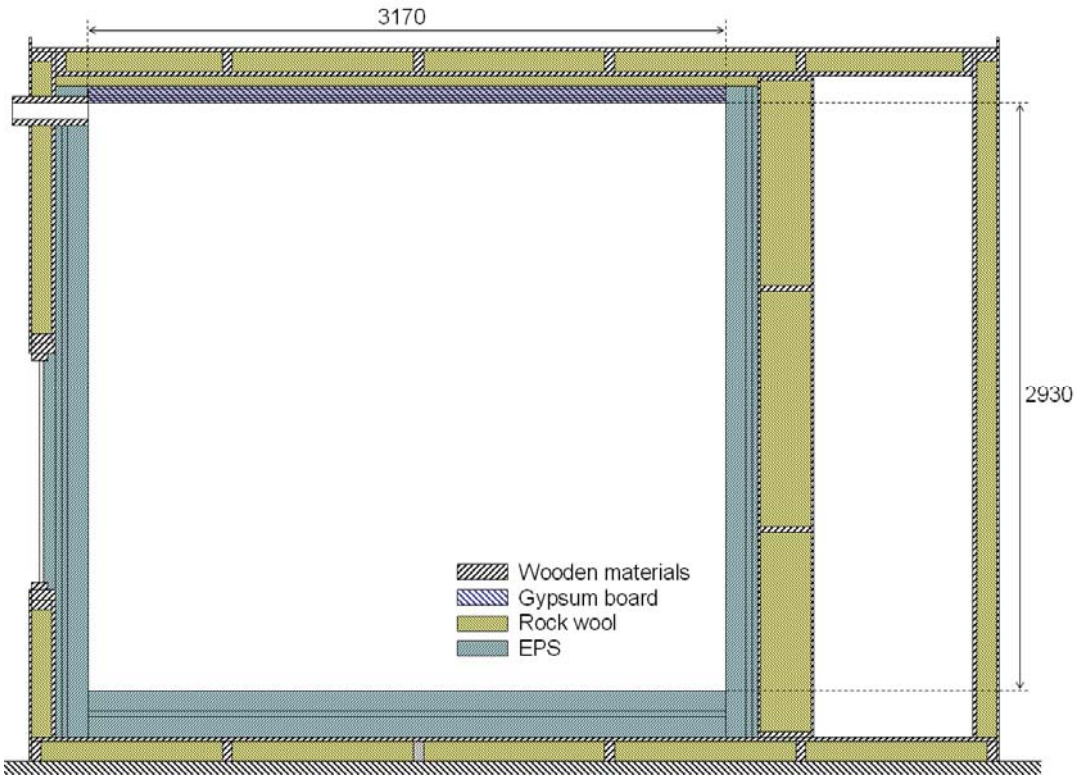

Figure 1. Vertical section of the test room.

The thermal properties of the materials used at the internal surfaces of the test room were measured or taken from literature (see [26] for details). The values used for calculations including estimated uncertainties are summarised in Table 1.

Table 1. Properties of the materials used at the internal surfaces of the test room.

	λ (W/mK)	ρ (kg/m^3)	c (J/kgK)	ε (-)
Gypsum board	0.28 ± 0.01	1127 ± 10	1006 ± 100	-
Expanded polysteren (EPS)	0.037 ± 0.001	16.0 ± 0.1	1450 ± 100	0.73 ± 0.05
White paint (Ceiling)	-	-	-	0.90 ± 0.05

A mechanical ventilation system was installed to supply air at a defined temperature to the test room. The ventilation system was capable of providing an air flow rate of about 56 - 330 m^3/h, corresponding to 2.3 - 13 air changes per hour (ACH). For measuring the air flow rate, an orifice was installed in the supply air pipe to the test room. The pressure difference over the orifice was measured using a micro-manometer. The accuracy of the air flow measurement was about ± 5 %.

Two different configurations of the air in- and outlet openings of the test room representing mixing and displacement ventilation were investigated (Figure 2). In case of mixing ventilation the air inlet to the test room was a rectangular opening of 830 mm width and 80 mm height located directly below the ceiling (Figure 3). To obtain a more uniform velocity profile, two fleece filters were placed approximately 25 and 35 cm before the opening. For the air outlet there were two circular openings with a diameter of 110 mm close to the floor.

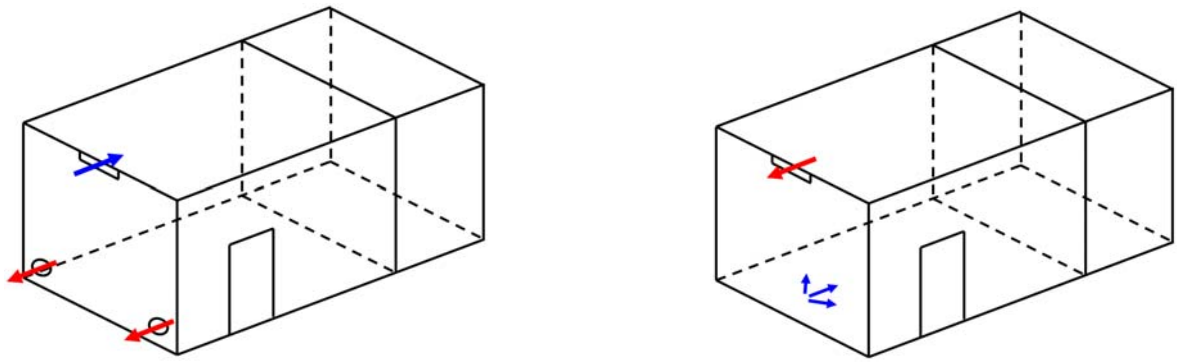

Figure 2. Configurations of the air in- and outlet openings of the test room for mixing (left) and displacement ventilation (right).

Figure 3. Opening used as air inlet for mixing ventilation and outlet for displacement ventilation.

For displacement ventilation the same rectangular opening below the ceiling was used as outlet and a semicircular displacement inlet device was placed at the floor on the same side of the test room (Figure 4).

Figure 4. Inlet device for displacement ventilation.

Measurement instrumentation and location of sensors

For temperature measurements type K thermocouples connected to two Fluke Helios Plus 2287A data loggers with 100 channels each were used. The setup of the Helios data loggers using 178 channels for temperature measurement and 17 channels for temperature difference measurement is described in detail in [27]. The accuracy of the measurement system using the Helios data loggers was estimated to be ± 0.086 K. The data loggers were configured to record temperatures at a sampling rate of 0.1 Hz.

The ceiling was divided into 22 sections (Figure 5). At each of the 22 positions 5 thermocouples were installed in different layers (see Figure 7). Additional thermocouples were installed 30 mm below the ceiling to measure the local air temperature.

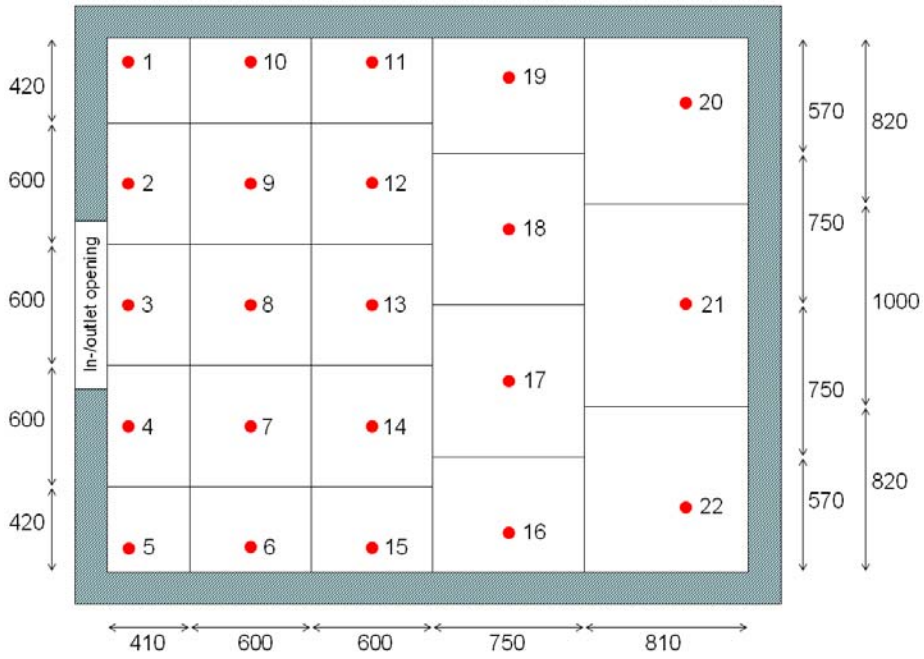

Figure 5. Subdivision of the ceiling into 22 sections and location of sensors (top view).

The walls and the floor were divided into 3 sections each, and sensors were located in the centre of each section (Figure 6). At all positions indicated in Figure 6 thermocouples were installed to measure the internal surface and the local air temperature at a distance of 30 mm from the surface. To determine the heat flow through the walls and the floor the temperature difference over a 30 mm layer of EPS (100 - 130 mm from the surface) was measured.

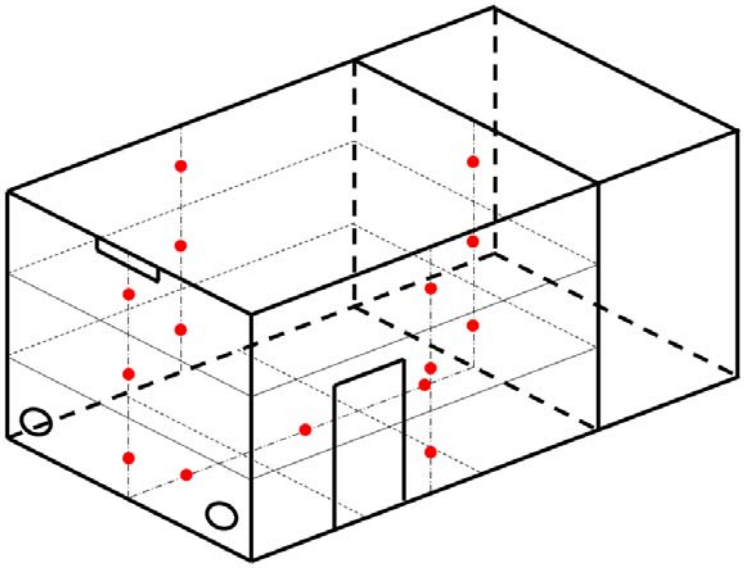

Figure 6. Subdivision of the walls and the floor into 3 sections and location of sensors.

To measure the air temperature distribution in the room 3 columns of thermocouples were installed in the vertical symmetry plane. The columns were located below the 2nd, 3rd and 4th row of sensors at the ceiling, i.e. positions 8, 13, and in the middle between 17 and 18 (Figure 5). In these columns thermocouples were at heights 0.1, 1.1, 1.7, 2.6 and 2.9 m above the floor. The height 2.9 m above the floor is equal to 30 mm below the ceiling (sensors for local air temperature at the ceiling).

For determination of the total heat flow removed from the test room by ventilation, the inlet and outlet air temperatures were measured. In case of mixing ventilation, sensors were placed in the centre of the inlet and both outlet openings. In case of displacement ventilation the sensors for the inlet air temperature measurement were installed where the pipe enters the room and in the inlet device (Figure 4). The former was used for calculations regarding the heat balance of the room.

Procedure for experiments

In each experiment the response of the test room to a step in the air flow rate (inflow temperature below room temperature) was measured for at least 12 hours. In total 16 experiments with different ventilation modes, air change rates (*ACR*) and initial temperature differences (ΔT_0) were conducted (Table 2). The experiments were started with the test room having a homogeneous temperature equal to the lab temperature. As it took some time until the temperature measured at the inlet was constant (cf. Figure 7), the initial temperature difference, ΔT_0 was defined as the difference between the mean temperature of the ceiling element before the experiment and the mean inlet air temperature measured during the last 10 hours of the experiment.

Table 2. List of experiments.

No	Ventilation mode	*ACR* (ACH)	ΔT_0 (K)
1	Mixing ventilation	2.3	7.9
2	Mixing ventilation	3.3	4.3
3	Mixing ventilation	3.3	10.2
4	Mixing ventilation	6.7	2.9
5	Mixing ventilation	6.8	6.1
6	Mixing ventilation	6.6	8.9
7	Mixing ventilation	13.1	2.9
8	Mixing ventilation	13.2	4.0
9	Mixing ventilation	13.1	5.3
10	Mixing ventilation	13.3	9.2
11	Displacement ventilation	3.1	10.1
12	Displacement ventilation	6.7	5.8
13	Displacement ventilation	6.7	11.3
14	Displacement ventilation	12.6	3.6
15	Displacement ventilation	12.6	6.0
16	Displacement ventilation	12.7	12.7

Data evaluation

For the evaluation of the heat transfer at the internal room surfaces, first the total surface heat flow (conduction in the material) for each section was calculated from the measured temperatures. Also the radiative heat flow between the surfaces was determined from the measured surface temperatures. The difference between conduction and radiation then yielded the convective heat flow for each section.

By way of example, Figure 7 shows the measured temperatures of the inlet air, and for position 8, the local air and 5 different layers of the ceiling. For the calculation of the conduction the temperatures measured at the internal (A) and external (E) surface of the gypsum boards were used as boundary condition for a transient 1-dimensional finite difference model using an explicit scheme. To reduce the noise in the measurement signals the moving average of 15 values (2.5 min) was applied. Running the model resulted in the spatial temperature profile for each time step. For each section, *i* the conductive heat flux, $\dot{q}_{cond,i}$ at the surface was calculated from the spatial temperature gradient.

The heat flows through the walls and the floor were calculated from the measured temperature difference over a 30 mm layer of EPS. In order to account for the thermal mass of the EPS, the heat flux at the internal wall and floor surfaces, $\dot{q}_{cond,i}$ was calculated using the same method as at the ceiling. Here the internal surface temperature and the external heat flux were used as boundary condition for the finite difference model.

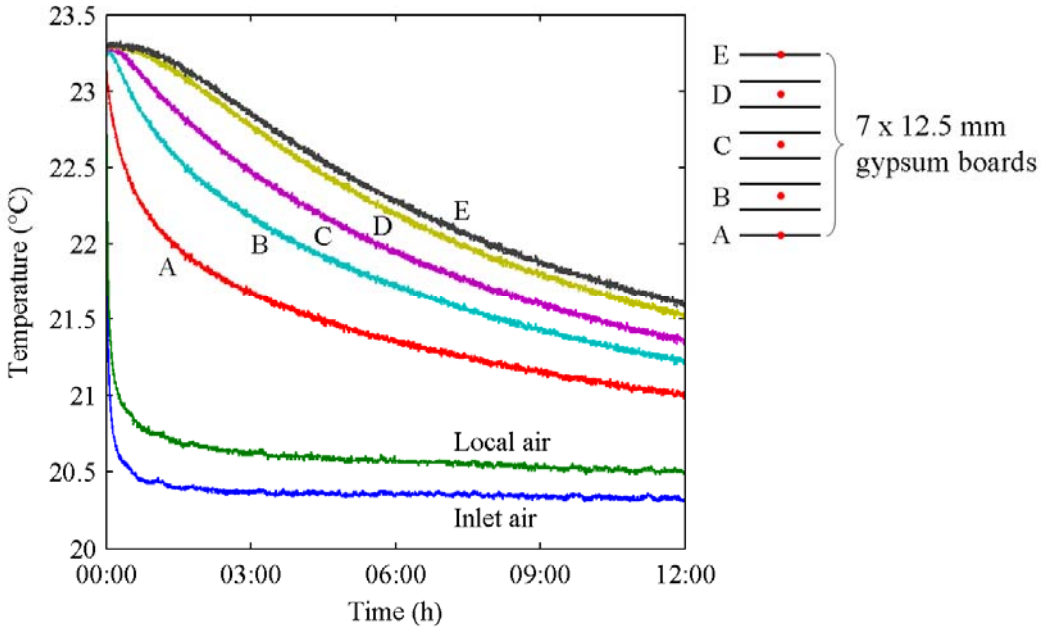

Figure 7. Temperatures measured at position 8 during the experiment no. 4 with mixing ventilation with 6.7 ACH and an initial temperature difference of ΔT_0 = 2.9 K (A-E: different layers of the ceiling, A: internal surface, E: external surface).

For the calculation of the radiative heat flows the view factors $F_{i,j}$ between all 22 sections of the ceiling and 3 sections of each wall and the floor were determined according to [28]. The radiative heat flux, $\dot{q}_{rad\,i}$ from the surface, A_i was obtained as sum of the heat fluxes to all surfaces, A_j applying the measured surface temperatures:

$$\dot{q}_{rad,\,i} = \sum_j \frac{\sigma \cdot \varepsilon_i \cdot \varepsilon_j \cdot F_{i,\,j}}{1-(1-\varepsilon_i)(1-\varepsilon_j)\cdot F_{i,\,j} \cdot F_{j,\,i}} \left(T_i^4 - T_j^4\right)$$

Where $\sigma = 5.67 \cdot 10^{-8}\, W/\left(m^2 K^4\right)$ is the Stefan-Boltzmann constant, and ε_i and ε_j are the emissivities of the surfaces.

The convective heat flux, $\dot{q}_{conv,\,i}$ for each section, *i* was then obtained from the difference between the conductive and radiative heat fluxes. Integrating the convective heat flux over all room surfaces results in the total heat flow removed from the test room, $\dot{Q}_{conv,\,tot}$:

$$\dot{Q}_{conv,\,tot} = \sum_i A_i \cdot \dot{q}_{conv,\,i}$$

It should be noted, that the total convective heat flow, $\dot{Q}_{conv,\,tot}$ equals the total conductive heat flow, $\dot{Q}_{cond,\,tot}$, as by radiation heat is only transported from one surface to another ($\dot{Q}_{rad,\,tot} = 0$).

Alternatively, the total heat flow removed from the room can also be determined from the flow rate, $\dot{V}_{Air}$, the density, ρ_{Air}, the heat capacity, $c_{p,\,Air}$ and the temperature difference between the in- and outflowing air.

$$\dot{Q}_{vent,\,tot} = \dot{V}_{Air} \cdot \rho_{Air} \cdot c_{p,\,Air} \cdot \left(T_{Outlet} - T_{Inlet}\right)$$

Figure 8 compares the total heat flow obtained by the two different methods. The difference visible at the beginning of the experiment results from the thermal capacity of the air in the room. In the experiment shown in Figure 8 the two methods are in very good agreement. In other cases a difference up to 18 % was found due to measurement uncertainties. The uncertainties in $\dot{Q}_{vent,\,tot}$ and $\dot{Q}_{conv,\,tot}$ were estimated as ± 12 % and ± 16 %, respectively [26]. Considering these uncertainties, results in overlapping bands of uncertainty in all experiments.

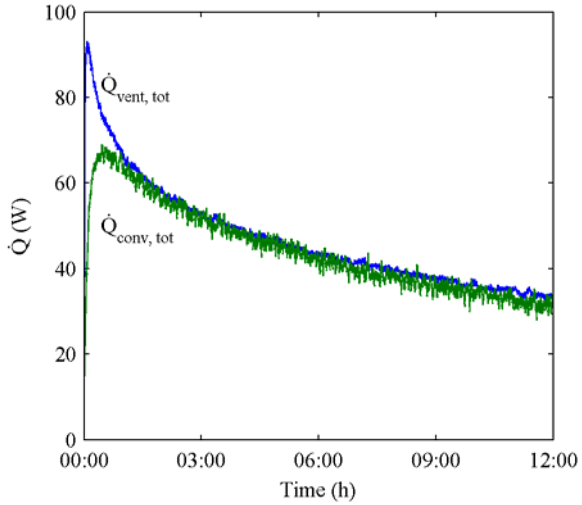

Figure 8. Total heat flow removed from the room obtained from direct measurements ($\dot{Q}_{vent,\,tot}$) and from integrating the convective heat flows over all surfaces ($\dot{Q}_{conv,\,tot}$); experiment no. 4: mixing ventilation, ACR = 6.7 ACH, ΔT_0 = 2.9 K. Uncertainty estimates: $\dot{Q}_{vent,\,tot}$: ± 12 %, $\dot{Q}_{conv,\,tot}$: ± 16 % [26].

Results

The total heat flow from all surfaces obtained in different experiments with an initial temperature difference of approximately 10 K (experiments no. 3, 6, 10, 11, 13 and 16) is shown in Figure 9. For better comparison the total convective heat flow from all surfaces, $\dot{Q}_{conv,\,tot}$ was normalised by the reference heat flow $\dot{Q}_0$, defined as $\dot{Q}_0 = \dot{m}_{Air} \cdot c_{p,\,Air} \cdot \Delta T_0$. Additionally the timescale was multiplied by the air change rate, yielding a dimensionless time, $\tau = t \cdot ACR$. Applying this normalisation, heat flows obtained in experiments with the same air flow rate but different initial temperature differences are almost congruent (not shown in Figure 9).

In all cases the heat flow quickly reaches a peak. After the peak the heat flow decreases over time as the temperature difference between the room and the inlet air temperature decreases. Comparing experiments with different flow rates shows that the normalised heat flow is higher for lower flow rates. This difference is more distinct for displacement ventilation than for mixing ventilation.

The increase before the peak is due to the delayed drop in the inflow air temperature (cf. Figure 7) and the heat capacity of the room air. To exclude this initial transient effect, the first hour of each experiment was not considered in the following diagrams. Later the room air is in a quasi steady state, i.e. the change in room (surface and air) temperature is slow compared to the time constant of the room air.

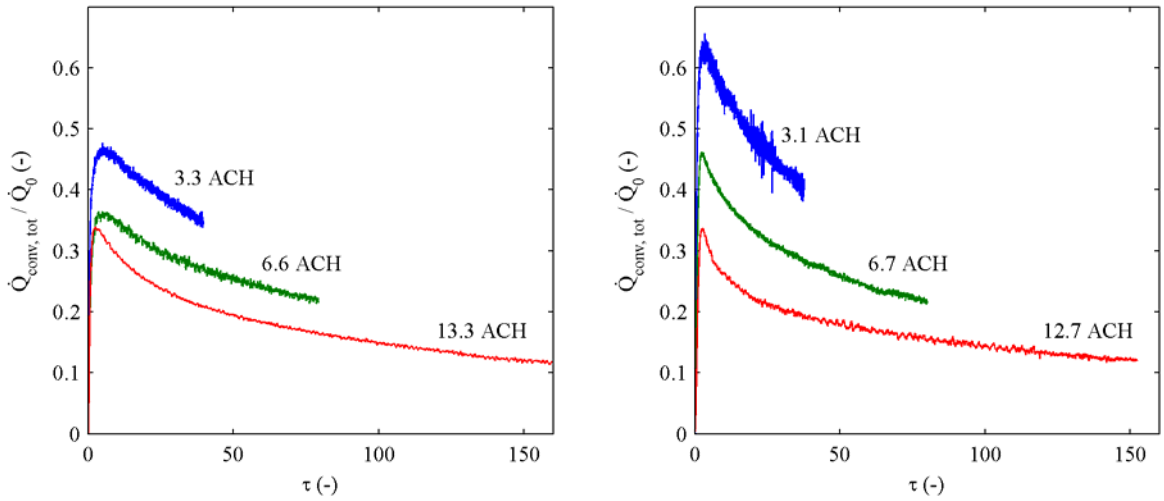

Figure 9. Normalised total convective heat flow from all surfaces comparing experiments with different air flow rates and ventilation modes (left: mixing ventilation, experiments no. 3, 6 and 10; right: displacement ventilation, experiments no. 11, 13 and 16). Initial temperature difference, ΔT_0 between 8.9 and 12.7 K. Uncertainty estimate for $\dot{Q}_{conv,tot}$: ± 16 % [26].

Figure 10 shows the mean convective heat flux $\dot{q}_{conv,tot}$ from all room surfaces depending on the difference between the mean surface temperature, $\overline{T}_{Surface}$ and the inlet air temperature, T_{Inlet} . During each experiment the temperature difference decreases over time and consequently the heat flux also decreases. This relation is very close to linear. Furthermore, experiments with the same airflow rate but different initial temperature differences follow the same line. The gradients of these lines can be interpreted as average heat transfer coefficients, $h' = \dot{q}_{conv,tot} / \left(\overline{T}_{Surface} - T_{Inlet}\right)$.

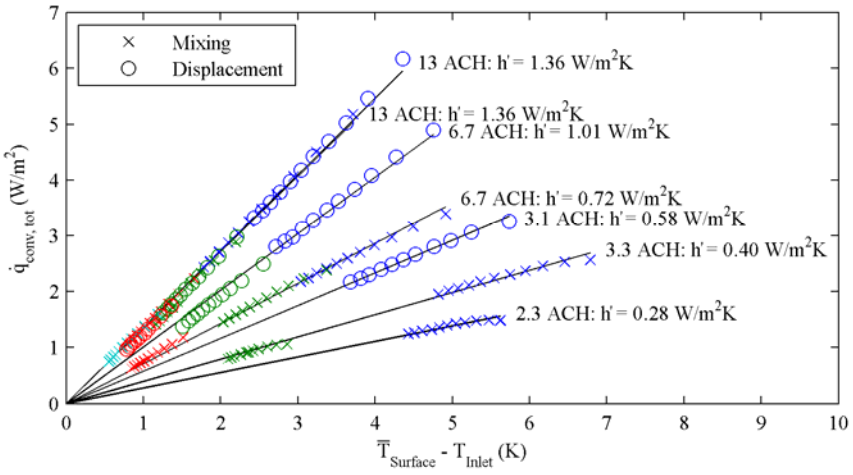

Figure 10. Mean heat flux from all surfaces depending on the difference between the mean surface temperature and the inlet air temperature; hourly values, first hour excluded; different colours relate to different experiments. Uncertainty estimate for $\dot{Q}_{conv,tot}$: ± 16 % [26].

It should be noted, that the average heat transfer coefficients, *h'* given in Figure 10 are defined using the inlet air temperature instead of the room air temperature as reference. Therefore, these values can not be

compared to standard heat transfer coefficients. The inlet air temperature was applied as reference, because the room air temperature is difficult to determine, especially in the case of displacement ventilation.

The average heat transfer coefficient, *h'* mainly depends on the air flow rate. At 13 ACH it is the same for mixing and displacement ventilation. At lower flow rates *h'* is higher for displacement ventilation than for mixing ventilation.

For the evaluation of the impact of the air jet on the heat transfer at the ceiling, the ratio of the convective and the total heat flow from the ceiling was defined as:

$$\gamma = \frac{\dot{Q}_{conv,\,Ceiling}}{\dot{Q}_{cond,\,Ceiling}}$$

The air flow pattern in mixing ventilation is characterised by the dimensionless Archimedes number. To avoid an arbitrary definition of a characteristic length scale, only the temperature difference and the air flow rate, $\dot{V}$ (m^3/s) were used to define *Ar'*:

$$Ar' = \frac{\overline{T}_{Surface} - T_{Inlet}}{\dot{V}^2} \qquad \left(Ks^2/m^6\right).$$

Figure 11 shows the convection ratio γ depending on *Ar'*. During experiments with mixing ventilation, for small Archimedes numbers the inlet air jet is attached to the ceiling and the convection ratio is large. For higher Archimedes numbers the jet tends to drop down. In this case a smaller proportion of the total heat flow is due to convection and radiation becomes dominant.

In displacement ventilation, the air flow pattern does not change depending on buoyancy effects and the impact of *Ar'* is small. In all experiments with displacement ventilation less than 32 % of the heat flow from the ceiling is due to convection. The convection ratio increases slightly with increasing air flow rate.

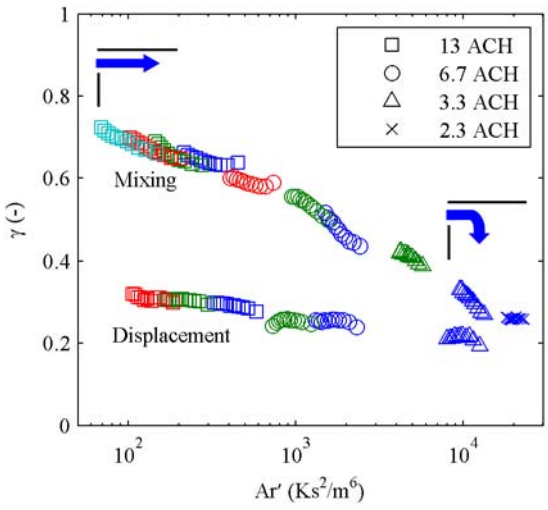

Figure 11. Ratio, γ of convective to total heat flow from the ceiling depending on Ar' for mixing and displacement ventilation; hourly values, first hour excluded; different colours relate to different experiments. Uncertainty estimate for γ : ± 0.11 [26].

During all experiments the temperature difference decreases over time (*Ar'* decreasing). Especially for mixing ventilation the convection ratio tends to increase during the experiment.

The performance of night-time ventilation can be described by the temperature efficiency of the ventilation:

$$\eta = \frac{T_{Outlet} - T_{Inlet}}{\overline{T}_{Surface} - T_{Inlet}}$$

The temperature efficiency yielded from the measurements mainly depends on the ventilation mode and the air change rate (Figure 12). During each experiment (excluding the first hour) and for different inlet air temperatures the efficiency is almost constant.

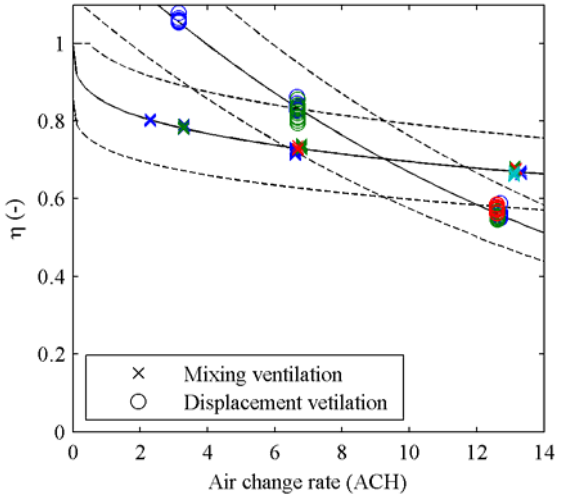

Figure 12. Temperature efficiency, η depending on the air change rate for mixing and displacement ventilation; hourly values, first hour excluded; different colours relate to different experiments. Fitted curves with estimated uncertainty bands (± 14 % [26]).

For mixing ventilation the efficiency decreases slightly with increasing air change rate. Values between 0.8 and 0.65 were found for air change rates between 2.3 and 13.3 ACH. In a perfectly mixed room, during night-time cooling ($T_{Inlet} < \overline{T}_{Surface}$ and without internal heat sources) the temperature efficiency is limited to 1. In contrast, in displacement ventilation the temperature stratification can result in an efficiency exceeding 1. In the experiment with displacement ventilation at 3.1 ACH the temperature efficiency was 1.06. For higher air change rates, the decrease in the efficiency is more distinct for displacement ventilation than for mixing ventilation. At 12.7 ACH the efficiency was decreased to about 0.56.

Discussion

The congruence of the normalised total heat flow during experiments with varying initial temperature difference, ΔT_0 suggests that the total heat transfer scales linearly with the temperature difference. The mean heat flux from all surfaces also increases linearly with the difference between the mean surface temperature and the inlet air temperature. This results in a constant average heat transfer coefficient, $h' = \dot{q}_{conv,tot} / \left(\overline{T}_{Surface} - T_{Inlet}\right)$ during each experiment. Additionally, the average heat transfer coefficient is the same for experiments with the same airflow rate and ventilation mode.

However, looking at the ratio of the convective to the total heat flow from the ceiling reveals, that the flow characteristic changes depending on the temperature difference. During experiments with mixing ventilation and an air change rate of about 6.7 ACH, depending on the temperature difference, the convection ratio varies between 43 and 60 %, and at 3.3 ACH between 27 and 42 %. The variation in the convection ratio is

caused by the characteristic of the inflowing air jet. Depending on the Archimedes number – the ratio between buoyancy and momentum forces – the cold inlet air flows along the ceiling or drops down into the room. For small Archimedes numbers (small temperature difference, high flow rate) the cold air jet is attached to the ceiling and a large proportion of the heat flow from the ceiling is due to convection. For higher Archimedes numbers (high temperature difference, low flow rate) the jet covers a smaller part of the ceiling surface and the convection ratio decreases.

In the case of displacement ventilation, high local air temperatures (stratification) and low air flow velocities (no jet) result in a small convective heat transfer at the ceiling. On the other hand the radiative heat transfer from the ceiling to the floor (and the lower parts of the walls) is increased because of the large surface temperature difference. Comparing mixing and displacement ventilation at high air flow rates shows very different convection ratios but similar total heat flows. This means that in displacement ventilation the increased radiation compensates for the lower convection.

At low air flow rates the inlet air jet is not strong enough to be attached to the ceiling and the convection ratio in mixing ventilation is as low as in displacement ventilation. The total heat flow is, however, higher in displacement ventilation than in mixing ventilation. One reason for this is probably the location of the outlet opening close to the ceiling, which allows the warm air to flow out of the room instead of accumulating below the ceiling.

The positive effect of the outlet opening being located close to the ceiling, also becomes evident in the high temperature efficiency of displacement ventilation at low air flow rates. In this case the stratification results in an outlet temperature higher than the mean surface temperature (temperature efficiency, $\eta > 1$). With increasing air change rate the efficiency decreases. As the heat flow from the surfaces is limited by conduction in the material and heat transfer at the surface, the difference between inlet and outlet air temperature decreases with increasing mass flow rate. In mixing ventilation the decrease in the temperature efficiency is smaller than in displacement ventilation, since the effect of the jet increases with the air flow rate. In both cases, despite the decrease in efficiency, the total heat flow still increases, as it is proportional to the effective air flow rate, $\eta \cdot ACR$.

It should be noted that there is a discrepancy between the total convective heat flow from all surfaces (Figure 10) and the temperature efficiency (Figure 12) when comparing experiments with mixing and displacement ventilation at 13 ACH. Figure 10 displays the same average heat transfer coefficient, h' for mixing and displacement ventilation. As both, h' and η are proportional to $\dot{Q}/\left(\overline{T}_{Surface} - T_{Inlet}\right)$ the efficiency should also be the same. Figure 12, however, shows a higher efficiency for mixing ventilation. This discrepancy is probably due to a systematic error in the measurement of the temperature difference between the in and outflowing air. Therefore, the exact air flow rate, at which mixing ventilation becomes more (or as) efficient as displacement ventilation, can not be determined.

The temperature efficiency can be applied for a simple model to estimate the performance of night-time ventilation. Together with the daily climatic cooling potential, CCP_d (Kh) and the temperature efficiency, η , the amount of heat removed per day and unit floor area, Q_d / A_{Floor} (Wh/m^2) can be estimated:

$$\frac{Q_d}{A_{Floor}} = H \cdot \rho_{Air} \cdot c_{p,\,Air} \cdot \eta \cdot \frac{ACR}{3600\,s/h} \cdot CCP_d \,,$$

where H is the room height, ρ_{Air} the density and $c_{p,\,Air}$ the heat capacity of air. CCP is defined as the number of night-time hours during which the outdoor temperature is below the building temperature, weighted by the temperature difference (detailed definition in [29]). If the total internal and solar heat gains

per day and unit floor area are smaller than the estimated heat Q_d / A_{Floor} , the building temperature will stay within the thermal comfort range. A precondition for the application of this method is that the thermal mass is sufficient to store the daily heat gains.

Figure 13 shows the amount of heat discharged during night-time ventilation per unit floor area and *CCP* depending on the air change rate. Such a diagram can be used as design chart to estimate the performance of night-time cooling during an early stage of building design. As room geometry and construction (distribution of thermal mass) might substantially affect the heat transfer mechanisms and the temperature efficiency, the diagram in Figure 13 is valid only for cases similar to the experiments. The test room represented a typical situation in an office building with a raised floor and light-weight partition walls, where the exposed concrete ceiling is the main contribution to thermal mass. For a more generally applicable design chart, the temperature efficiency should be determined for various room geometries, constructions (amount and location of thermal mass) and ventilation systems (location of inlet and outlet openings).

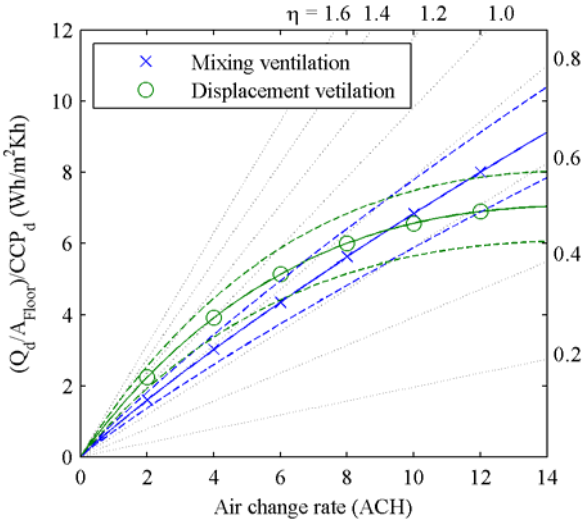

Figure 13. Heat discharged during night-time ventilation per unit floor area and CCP depending on the air change rate; experimental results for mixing and displacement ventilation (including range of uncertainty) and lines of constant efficiency; room height H = 2.93 m.

Considering a temperature efficiency $\eta > 1$ reveals limitations of a model assuming a homogeneous room air temperature to describe the heat transfer during displacement ventilation. In such a model the outflowing air temperature equals the room air temperature. Due to the temperature stratification during displacement ventilation, some of the internal room surfaces (e.g. the floor) can be colder than the outflowing air. As the temperature of this surface, $T_{Surface,i}$ is still higher than the air close to it, the surface releases heat to the air ($\dot{q}_{conv,i} > 0$). For a one-air-node model this results in a negative heat transfer coefficient:

$$h_i = \frac{\dot{q}_{conv,i}}{T_{Surface,i} - T_{Room\ air}} = \frac{\dot{q}_{conv,i}}{T_{Surface,i} - T_{Outlet}} < 0$$

An alternative approach could be to use the temperature efficiency, η to calculate the total heat flow removed from a room in a dynamic model. In this model, the efficiency represents the heat transfer at all room surfaces (including radiation), which supersedes the definition of heat transfer coefficients for single surfaces. However, such a model does not give the heat flows from different room surfaces separately. Therefore the entire thermal mass of the room needs to be modelled as one element with a homogeneous

surface temperature. A possible approach for representing the thermal mass of a room (or building) using a virtual sphere model has been proposed by Li and Yam [30].

Conclusions and outlook

The experimental results clearly demonstrate the interaction of convective and radiative heat flows contributing to the total heat flow removed from a room during night-time ventilation. For mixing ventilation, different flow characteristics significantly affect the ratio of the convective to the total heat flow from the ceiling. In cases with low convective heat transfer at the ceiling (mixing ventilation at high Archimedes number or displacement ventilation) large differences in surface temperatures cause higher radiative heat flows from the ceiling to the floor.

Nonetheless, it is beneficial to prevent warm air from accumulating below the ceiling. In displacement ventilation this is achieved through the location of the outlet opening close to the ceiling. At low air flow rates, the temperature stratification and the high location of the outlet opening results in a very high temperature efficiency ($\eta > 1$). In mixing ventilation warm air should be removed from the ceiling by the inflowing air jet. However, only at a relatively high air change rate (above about 10 ACH) the effect of the air jet flowing along the ceiling becomes significant and mixing ventilation is more efficient. Therefore, if a low air flow rate is expected, the outlet opening should be placed as close to the ceiling as possible.

The temperature efficiency can be used to estimate the total heat flow removed from a room. Based on this, a design chart to estimate the performance of night-time cooling during an early stage of building design is proposed. Further work is needed to determine the temperature efficiency for various room geometries, constructions (amount and location of thermal mass) and ventilation systems (location of inlet and outlet openings), in order to develop a more generally applicable design chart. Additionally the presence of furniture might have a significant impact on the air flow, the heat transfer, and the resulting temperature efficiency. A possible approach to investigate a large number of different cases could be the application of computational fluid dynamics (CFD).

Acknowledgements

This work was partially funded by the Hybrid Ventilation Centre, the Department of Civil Engineering at Aalborg University and the Swiss Federal Office of Energy (Project no. 101’308). The project is also supported by the private sector (WindowMaster, Belimo, SZFF). We acknowledge with thanks all financial support. We would also like to thank R. Vonbank for support with the measurement equipment and T. Christensen, P. Knudsen, K. E. Olesen and M. Olsen for their help during construction of the test room.

References

[1] Energy Efficiency and Certification of Central Air Conditioners (EECCAC). D.G. Transportation-Energy (DGTREN) of the Commission of the E.U. Final report. Co-ordinator: J. Adnot. Armines, France, 2003.

[2] A. Kirchner, P. Hofer, A. Kemmler, M. Keller, B. Aebischer, M. Jakob, G. Catenazzi, W. Baumgartner. Analyse des schweizerischen Energieverbrauchs 2000-2006 nach Verwendungszwecken. Bundesamt für Energie (Swiss Federal Office of Energy), Bern, 2008 (in German).

[3] T. Frank. Climate change impacts on building heating and cooling energy demand in Switzerland. Energy and Buildings 2005, 37, pp. 1175-1185.

[4] M. Christenson, H. Manz, D. Gyalistras. Climate warming impact on degree-days and building energy demand in Switzerland. Energy Conversion and Management 2006, 47, pp. 671-686.

[5] B. Krausse, M. Cook, K. Lomas. Environmental performance of a naturally ventilated city centre library. Energy and Buildings 2007, 39, pp. 792-801.

[6] A. Wagner, M. Kleber, C. Parker. Monitoring results of a naturally ventilated and passively cooled office building in Frankfurt, Germany. International Journal of Ventilation 2007, 6 (1), pp. 3-20.

[7] H. Breesch, A. Janssens. Uncertainty and sensitivity analysis to evaluate natural night ventilation design in an office building. 26th AIVC conference 2005, Brussels, Belgium.

[8] H. Akbari, D. Samano, A. Mertol, F. Bauman, R. Kammerud. The effect of variations in convective coefficients on thermal energy storage in buildings: Part I – interior partition walls, Energy and Buildings 1986; 9, pp. 195-211.

[9] N. Artmann, H. Manz, P. Heiselberg. Parameter study on performance of building cooling by night-time ventilation. Renewable energy 2008, 33, pp. 2589-2598.

[10] EN ISO 6946. Building components and building elements – thermal resistance and thermal transmittance – calculation method. European Standard, CEN, Brussels, 1997.

[11] EN ISO 13791. Thermal performance of buildings – internal temperatures in summer of a room without mechanical cooling – general criteria and calculation procedures. European Standard, CEN, Brussels, 2004.

[12] S. Chandra, A. A. Kerestecioglu. Heat transfer in naturally ventilated rooms: Data from fullscale measurements. ASHRAE Transformation 1984, 90 (1), pp. 211-224.

[13] G. Clark. Passive cooling systems. In: Cook J. (ed.). Passive Cooling. MIT Press, 1989, pp. 347-538.

[14] B. Givoni. Performance and applicability of passive and low-energy cooling systems. Energy and Buildings 1991, 17, pp. 177-199.

[15] F. Alamdari, G. P. Hammond. Improved data correlations for buoyancy driven convection in rooms, Building Services Engineering Research & Technology 1983, 4, pp. 106-112.

[16] A. J. Khalifa, R. H. Marshall. Validation of heat transfer coefficients on interior building surfaces using a real-sized indoor passive test cell. International Journal of Heat and Mass Transfer 1990, 33, pp. 2219-2236.

[17] H. B. Awbi, A. Hatton. Natural convection from heated room surfaces, Energy and Buildings 1999, 30, pp. 233-244.

[18] J. D. Spitler, C. O. Pedersen, D. E. Fisher, Interior convective heat transfer in buildings with large ventilative flow rates, ASHRAE Transactions 1991, 97, pp. 505-515.

[19] H. B. Awbi, A. Hatton. Mixed convection from heated room surfaces, Energy and Buildings 2000, 32, pp. 153-166.

[20] I. Beausoleil-Morrison. The adaptive simulation of convective heat transfer at internal building surfaces, Building Environment 2002, 37, pp. 791-806.

[21] A. J. Khalifa. Natural convective heat transfer coefficient – a review I. Isolated vertical and horizontal surfaces. Energy Conversion and Management 2001, 42, pp. 491-504.

[22] A. J. Khalifa. Natural convective heat transfer coefficient – a review II. Surfaces in two- and three-dimensional enclosures. Energy Conversion and Management 2001, 42, pp. 505-517.

[23] V. Geros, M. Santamouris, A. Tsangrasoulis, G. Guarracino. Experimental evaluation of night ventilation phenomena. Energy and Buildings 1999, 29, pp. 141–154.

[24] J. M. Salmerón, J. A. Sanz, F. J. Sánchez, S. Álvarez, Á. Pardo. Flow pattern effects on night cooling ventilation. International Journal of Ventilation 2007, 6 (1), pp. 21-30.

[25] R. L. Jensen. Modelling of natural ventilation and night cooling – by the loop equation method. PhD-thesis, Aalborg University, Department of Civil Engineering, Hybrid Ventilation Centre, 2005 (in Danish).

[26] N. Artmann, R. L. Jensen. Night-time ventilation experiments – Setup, data evaluation and uncertainty assessment. DCE Technical Report No. 053, Aalborg University, Department of Civil Engineering, 2008.

[27] N. Artmann, R. Vonbank, R. L. Jensen. Temperature measurements using type K thermocouples and the Fluke Helios Plus 2287A data logger. DCE Technical Report No. 052, Aalborg University, Department of Civil Engineering, 2008.

[28] J. R. Ehlert, T. F. Smith. View factors for perpendicular and parallel rectangular plates. Journal of thermophysics and heat transfer 1993, 7 (1), pp. 173-174.

[29] N. Artmann, H. Manz, P. Heiselberg. Climatic potential for passive cooling of buildings by night-time ventilation in Europe. Applied Energy 2007; 84, pp. 187-201.

[30] Y. Li, J. C. W. Yam. Designing thermal mass in naturally ventilated buildings. International Journal of Ventilation 2004, 2 (4), pp. 313-324.

Potential for passive cooling of buildings by night-time ventilation in present and future climates in Europe

Nikolai Artmann[1], Heinrich Manz[1] and Per Heiselberg[2]

[1] Swiss Federal Laboratories for Materials Testing and Research (EMPA), Laboratory for Building Technologies, Ueberlandstr. 129, CH-8600 Duebendorf, Switzerland
[2] Hybrid Ventilation Centre, Department of Civil Engineering, Aalborg University, Sohngaardsholmsvej 57, DK-9000 Aalborg, Denmark

ABSTRACT: Given the general shift in recent decades towards a lower heating and higher cooling demand for buildings in many European countries, passive cooling by night-time ventilation has come to be seen as a promising option, particularly in the moderate or cold climates of Central, Eastern and Northern Europe. The basic concept involves cooling the building structure overnight in order to provide a heat sink that is available during the occupancy period. In this study, the potential for the passive cooling of buildings by night-time ventilation is evaluated by analysing climatic data, irrespective of any building-specific parameters. An approach for calculating degree-hours based on a variable building temperature — within a standardized range of thermal comfort — is presented and applied to climatic data from 259 stations throughout Europe. The results show a very high potential for night-time ventilative cooling over the whole of Northern Europe and a still significant potential in Central, Eastern and even some regions of Southern Europe. However, given the inherent stochastic properties of weather patterns, series of warmer nights can occur at some locations, where passive cooling by night-time ventilation alone might not suffice to guarantee thermal comfort. It should also be remembered that climatic cooling potential is likely to have fallen appreciably by the end of the 21st century due to climate warming.

Keywords: Passive Cooling; Night-time Ventilation; Climate Change; Climatic Cooling Potential

1. INTRODUCTION

In Europe, commercial buildings in particular have experienced an uptrend in cooling demand over the last few decades. An increase in internal loads coupled with higher solar gains — especially in modern, highly glazed buildings — has fed the demand for air-conditioning systems, even in moderate and cold climates such as in Central or Northern Europe. Additionally, increased comfort expectations in summertime and the gradual warming of our climate are pushing up the cooling demand. While the heating requirement can be effectively reduced by installing thermal insulation, cooling plays a more significant role in the overall energy demand of buildings.

Particularly in moderate climates, such as in Switzerland, Germany or the UK, and cold climates such as in Scandinavia, with relatively low night-time temperatures even in summer, passive cooling of buildings by night-time ventilation appears to hold considerable potential. The basic concept involves cooling the building structure overnight in order to provide a heat sink that is available during occupancy periods [1]-[4]. Such a strategy could guarantee the daytime thermal comfort of building occupants without mechanical cooling or, at least, with a lower daytime cooling energy requirement.

However, this concept is highly dependent on climatic conditions, as a sufficiently high temperature difference between ambient air and the building structure is needed during the night to achieve efficient convective cooling of the building mass.

The purpose of this study is to evaluate the climatic potential for the passive cooling of buildings by night-time ventilation in present and future climates in Europe.

2. METHOD

A method was developed, verified and applied which is basically suitable for all building types, regardless of building-specific parameters. This was achieved by basing the approach solely on a building temperature variable within a temperature band given by summertime thermal comfort.

2.1 Definition of the 'Climatic Cooling Potential'

Degree-days or degree-hours methods are often used to characterise a climate's impact on the thermal behaviour of a building. In this study, the climatic potential for ventilative cooling, *CCP*, is defined as the sum of degree-hours for the difference between building and external air temperature (Fig. 1). In the numerical analysis, it was assumed that night-time

ventilation starts at $h_i = 19h$ and ends at $h_f = 7h$. As a certain temperature difference is needed for effective convection, night ventilation is only applied if the difference between building temperature, T_b and external temperature, T_e is greater than $\Delta T_{crit} = 3K$.

2.2 Building temperature

As heat gains and night-time ventilation are not simultaneous, energy storage is an integral part of the concept. In the case of sensible energy storage, this is associated with a variable temperature of the building structure. This aspect is included in the model by defining building temperature as a sine oscillation around *24.5°C* with an amplitude of *2.5 K*. The maximum building temperature occurs at the initial time of night ventilation, h_i, and, given a ventilation time of 12 hours, the minimum building temperature occurs at the final time, h_f (Fig. 1). The temperature range $T_b = 24.5°C \pm 2.5°C$ is equivalent to that recommended for thermal comfort in offices [5] [6]. The exact definition of CCP and building temperature can be found in [7].

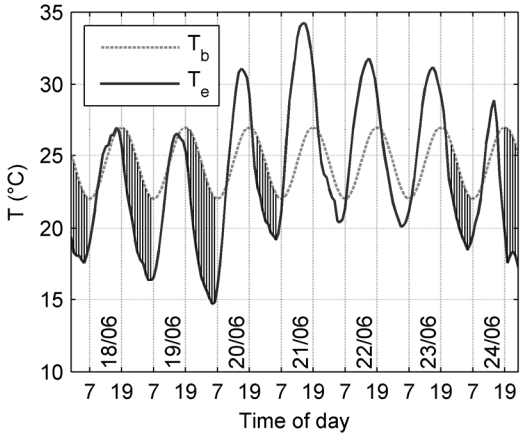

Figure 1: Shaded areas illustrate graphically the Climatic Cooling Potential during one week in summer 2003 for Zurich SMA (ANETZ data).

2.3 Climatic data

Hourly air temperature data are needed to analyse the climatic potential for the passive cooling of buildings by night-time ventilation using the presented approach. For Switzerland, the National Weather Service (MeteoSwiss) provides high-quality long time series of measured hourly temperature data. In addition to air temperature *2 m* above ground level, the automatic measurement network (ANETZ) measures a range of meteorological parameters.

The commercial database Meteonorm [8] provides semi-synthetic meteorological data for 7400 stations around the world. Hourly air temperature data are generated on the basis of measured long-term monthly mean values (mainly 1961-1990). For analysis of the climatic cooling potential in Europe, data were selected from 259 meteorological stations at densely populated locations.

2.4 Practical Significance of CCP

The following example should give an idea of the practical significance of the calculated degree-hours. This simple calculation should be seen only as a rough analysis. It is not intended to replace a detailed simulation for a specific building at a given location by means of a building energy simulation code.

The thermal capacity of the building mass is assumed to be sufficiently high so as not to limit the heat storage process. If the building is in the same state after one cycle, the heat which charges the building structure, Q_{charge}, during the occupancy period, t_{occ}, is equal to the heat released through night ventilation, $Q_{release}$. The mean heat flux during the storage process, $\dot{q}$, per room area, *A*, can then be calculated as follows:

$$\dot{q} = \frac{Q_{charge}}{At_{occ}} = \frac{Q_{release}}{At_{occ}} = \frac{\dot{m}c_p}{At_{occ}} CCP \qquad (1)$$

The effective mass flow rate, $\dot{m}$, is written as $\dot{m} = AHR\eta\rho$, where *H* is the room height, *R* the air change rate and η a temperature efficiency, defined as $\eta = (T_{out} - T_e)/(T_b - T_e)$, that takes account of the fact that the temperature of the outflowing air, T_{out}, is lower than the building temperature, T_b. The density and specific heat of the air are taken as $\rho = 1.2\,kg/m^3$ and $c_p = 1000\,J/(kg\,K)$.

Assuming a room height of $H = 2.5\,m$, a constant effective air change rate of $R\eta = 6\,h^{-1}$, and an occupancy time of $t_{occ} = 8\,h$, the heat flux, $\dot{q}$, absorbed per degree-hour of the cooling potential *CCP*, can be calculated as:

$$\frac{\dot{q}}{CCP} = \frac{2.5\,m \cdot 6h^{-1} \cdot 1.2\frac{kg}{m^3} \cdot 1000\frac{J}{kg\,K}}{8 \cdot 3600\,s} = 0.625\frac{W/m^2}{K\,h} \qquad (2)$$

The solar and internal gains of an office space can vary substantially depending on the local climate, orientation and total solar energy transmittance of the façade, building geometry and type of building. Assuming e.g. internal heat gains of $20\,W/m^2$ and solar gains of $30\,W/m^2$ — with both values referring to the time period of *8 h* — a climatic cooling potential of about *80 K h* per day is needed to discharge the stored heat.

3. VERIFICATION OF THE METHOD

To verify the applicability of the presented method, the climatic cooling potential was calculated on the basis of measured hourly temperature data for Zurich SMA. ANETZ data downloaded from the National Weather Service (MeteoSwiss) data centre were employed. The data for 2003, which witnessed

exceptionally high temperatures in July and August, were used [9].

3.1 Building temperature

Figure 1 shows the building temperature as defined in section 2.2, the measured external air temperature at Zurich SMA and the resulting climatic cooling potential (shaded area) for one week in June. In most cases, the theoretical building temperature appears reasonable in that it correlates quite well with the outdoor temperature. However, in the two nights between June 21st to 23rd, the building temperature drops to the same level, even without night ventilation, which is physically implausible. A cooling potential might exist during the later hours of the night-time period where the building temperature remains at a constant level. While a more 'realistic', building temperature could obviously be obtained using a building energy simulation code, the associated drawback of having to define numerous building parameters would entail a loss of generality.

3.2 Sensitivity of *CCP*

The sensitivity of *CCP* to different parameters was examined. Especially for nights with a high cooling potential, *CCP* was not found to be very sensitive to either the building temperature amplitude, ΔT_b, or the critical temperature difference, ΔT_{crit}. A slightly higher sensitivity was found in respect of the selected ventilation period, where a shift of $\pm 1h$ results in a variation of maximum $\pm 10Kh$ in *CCP* [7].

3.3 Cooling potential in different time intervals

For the comparison of different climates, the cooling potential can be averaged over a certain time period. It must, however, be remembered that nightly values exhibit wide fluctuations within a bandwidth of up to *200 K h* within a few days; weekly mean values still vary by about *50-100 K h* within a month. For example, although August 2003 witnessed a whole week without any notable potential for night cooling, the monthly mean value still exceeded *50 K h*. This warrants close attention, especially given that low night cooling potential is associated with a high cooling demand.

Not only does cooling potential per night differ within a month, the monthly mean values also vary over the years. The standard deviation, minimum and maximum of monthly mean values were computed for all calendar months for the period 1981-2002. Figure 2 also shows the impact of the exceptionally hot summer of 2003 [9] on the climatic potential for night cooling; mean values for June and August lie far below all the data from the previous 22 years. This might help to estimate the impact of a warmer climate on night cooling potential.

3.4 Applicability of semi-synthetic climatic data

The hourly temperature data provided by the meteorological database Meteonorm [8] are semi-synthetic values generated from monthly mean values. The applicability of Meteonorm data for calculating cooling potential was verified for two locations, Zurich SMA and Copenhagen Vaerlose [7].

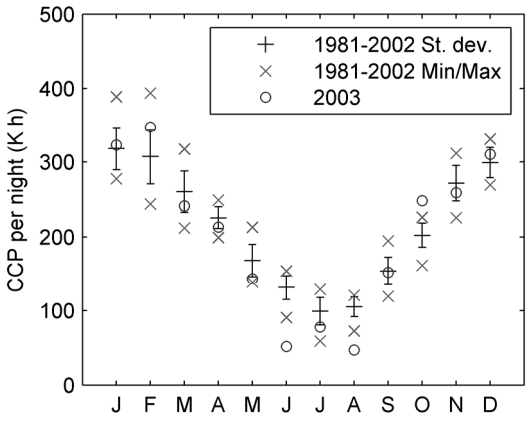

Figure 2: Mean value and standard deviation, minimum and maximum of monthly mean *CCP* for Zurich SMA 1981-2002 and monthly mean *CCP* for 2003 (ANETZ data).

4. RESULTS

To give a general picture of the climatic potential for night-time cooling in Europe, the July mean values for *CCP* were plotted on a map (Fig. 3). As expected, a clear gradation from north to south emerges. Even in the hottest month of the year, Northern Europe (including the British Isles) exhibits a very high cooling potential of *120* to *180 K h*. In Central and Eastern Europe, but also in the northern parts of Portugal, Spain, Greece and Turkey, the cooling potential is still *60* to *140 K h*.

Cumulative frequency distributions allow a more detailed analysis of cooling potential by showing the number of nights per year when cooling potential exceeds a certain value. Two cumulative frequency charts for 20 different locations showing the climatic *potential* for night-time cooling in maritime and continental climates are presented in the Appendix.

A usable potential during the colder periods can be observed at locations for which Figure 3 indicates only very low potential. For example, in Lisbon, where the July mean value is about *40-60 K h*, there are more than 200 nights per year with over *100 K h*. On the other hand, some 15 nights per year offer no cooling potential at all.

The cumulative frequency charts also illustrate the difference between continental and maritime climates. While the lines for maritime climates are flatter, the curves for continental climates cover a wider range of *CCP* and display a steadier gradient.

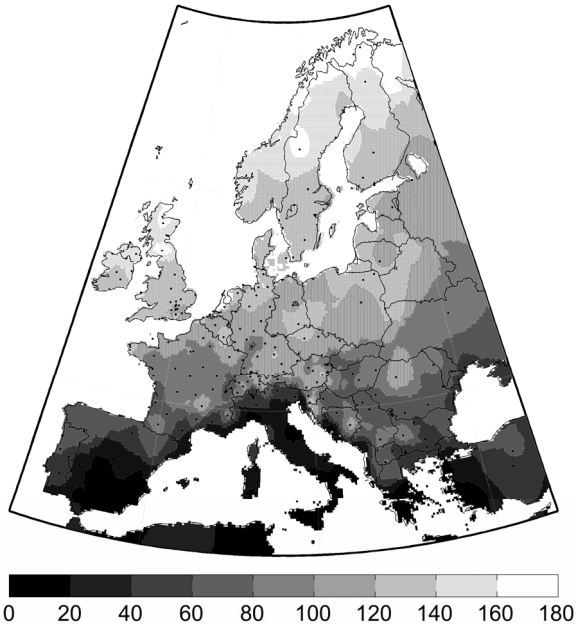

Figure 3: Map of mean Climatic Cooling Potential (K h / night) in July based on Meteonorm data [8].

5. OUTLOOK

As significant gradual global warming in consequence of increasing greenhouse gas concentrations is expected to occur within the service life of buildings constructed at the present time, the impact of rising temperatures on the potential of passive cooling by night-time ventilation warrants investigation. The temperatures observed during the exceptionally hot summer of 2003 could well serve as a preview of a typical summer at the end of this century [9]. The monthly mean *CCP* values in Zurich for June and August of that year are about *50 K h*, compared to *100 – 150 K h* in the years before. Given the wide variation in nightly values and the fact that warm nights are associated with a high daily cooling demand, this shift may cause periods of high thermal discomfort in buildings designed for cooling by night-time ventilation in present-day climatic conditions. It is clear that a more detailed analysis is needed of the night cooling potential in a warmer climate and, accordingly, the presented method will also be applied to climate projections for the end of this century.

The PRUDENCE project [10] provides climatic data for the period 2070-2100. These data were obtained by using Regional Climate Models (RCMs) for downscaling the results of Atmosphere Ocean General Circulation Models (AOGCMs) to a finer grid over Europe. Figure 4 shows the shift in the mean daily minimum temperatures in June to August, modelled by the Danish Meteorological Institute (DMI) and based on a HadAM3H A2 AOGCM simulation run. The trend is particularly marked in Southern Europe, totalling *5* to *6.5 K* for central Spain. A similarly pronounced shift emerges in the Baltic Sea region. In Northern, Central and Eastern Europe too, the shift in summer mean daily minimum temperature simulated by this model still reaches *2.5* to *5 K*. However, future climate simulation models — forcing scenarios, AOGCMs and RCMs — are subject to a high level of uncertainty, and a detailed analysis of data from different models plus related effect on cooling potential is needed.

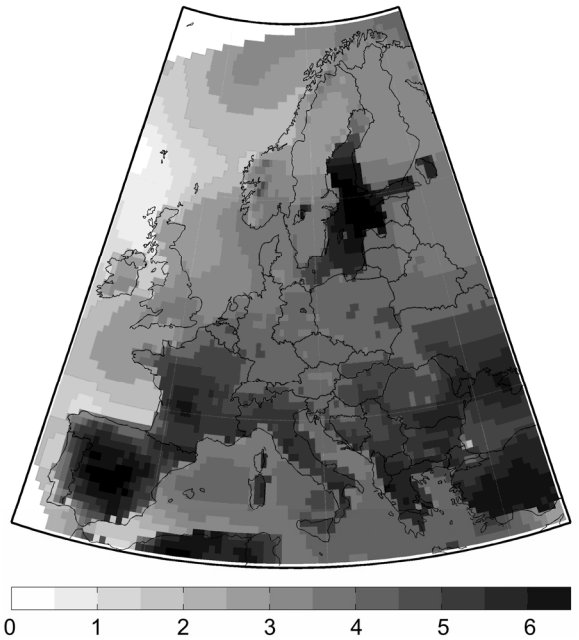

Figure 4: Map of shift in mean daily minimum temperature in June to August, modelled by DMI [10].

6. DISCUSSION

Under current climatic conditions, the whole of Northern Europe (including the British Isles) exhibits a mean *CCP* per night in July of roughly *120* to *180 K h*. Even allowing for variations in nightly values around the monthly mean value, this region appears to hold sufficient cooling potential to assure thermal comfort throughout the year in most cases.

Central, Eastern and some regions of Southern Europe offer a mean monthly *CCP* of *60* to *140 K h*. In these regions, cooling by night-time ventilation is a promising technique for most applications. Still, it must be remembered that nightly values can fall far below the monthly mean and that very low cooling potential may be experienced on a few nights per year. In the wake of climate change, the incidence of higher temperatures with high cooling demand and low night cooling potential is very likely to increase. The acceptability of the resulting discomfort needs to be examined for each specific case.

In regions such as southern Spain, Italy and Greece with mean *CCP* per night for July of less than *60 K h*, night-time ventilation alone might not suffice the whole year round. Other passive cooling techniques, such as radiant or evaporative cooling, might therefore prove useful for buildings requiring a high level of thermal comfort. Hybrid systems should be considered wherever passive systems cannot provide the required cooling duty. For example, even

in air-conditioned buildings, night-time ventilation could service to cut the energy demand for the mechanical cooling system.

Some buildings, mainly commercial facilities with high internal and/or solar loads, need to be cooled even if the outdoor temperature is well below the thermal comfort limit. Thus, especially in the warmer climates of Southern Europe, cooling may also be required during spring and autumn, and even, for some buildings, in winter. Hybrid systems incorporating night-time ventilative cooling can be used in such cases to reduce the energy demand of air-conditioned buildings. Night-time ventilation would be exploited whenever the outside air temperature is significantly below the building temperature, with mechanical cooling serving as a backup to safeguard thermal comfort.

The information provided by cumulative frequency charts might be of particular interest for design engineers seeking to estimate the potential for cooling by night-time ventilation.

7. CONCLUSIONS

In this study, a method was developed to compute the climatic potential for the passive cooling of buildings by night-time ventilation. This method is based on a variable building temperature, which is intrinsic to this passive cooling concept. The building temperature varies within a range of thermal comfort as specified in international standards and is defined independently of any building-specific parameters. The robustness of the degree-hours approach was tested and the impact of the assumed building temperature function and the threshold value for the temperature difference between building and external air investigated. This method was employed for a systematic analysis of European climate with regard to passive cooling by night-time ventilation using 259 stations.

Considerable potential for the passive cooling of buildings by night-time ventilation was shown to exist throughout Northern Europe (including the British Isles), where the technique seems generally applicable. Climatic cooling potential is still significant in Central, Eastern and even in some regions of Southern Europe, though, given the inherent stochastic properties of weather patterns, series of warmer nights can occur at some locations, where passive cooling by night-time ventilation might not suffice to guarantee thermal comfort. If short periods of lower thermal comfort are not acceptable, additional cooling systems would be required. Climatic cooling potential is limited in regions such as southern Spain, Italy and Greece. Nevertheless, the passive cooling of buildings by night-time ventilation might be useful for hybrid systems.

The presented method provides a valuable aid in assessing the cooling potential offered by a particular climate and could be of greatest assistance during the initial design phase of a building at a given location. It must, however, be stressed that a more thorough analysis of the summertime transient thermal behaviour of a building needs to be based on a building energy simulation that factors in all building-specific parameters such as time-dependent internal and solar gains, active building thermal mass, thermal insulation of building envelope, along with air flow rates and patterns. The latter may even require a computational fluid dynamics analysis given that room geometry, window type and positioning may significantly affect the air flow rate and, hence, the cooling effect.

For a better understanding of the long-term potential of this technology, the impact of future gradual climate warming on cooling potential needs closer investigation. Also required is a more fundamental grasp of air exchange and the resulting cooling effect, backed by improved modelling algorithms in building energy simulation codes.

ACKNOWLEDGEMENTS

This work was partially funded by the Hybrid Ventilation Centre, the Department of Civil Engineering at Aalborg University and the Swiss Federal Office of Energy (Project No. 101'308). The project is also supported by the private sector (WindowMaster, Belimo, SZFF). We acknowledge with thanks all financial support. We also acknowledge the use of data from the PRUDENCE project.

REFERENCES

[1] Allard F. Natural Ventilation in Buildings. London: James & James; 1998.
[2] Chandra S. Ventilative cooling. In: Cook J editor. Passive cooling. Cambridge, Massachusetts: The MIT Press; 1989. p. 70.
[3] Santamouris M, Asimakopoulos D, Passive cooling of buildings. London, UK: James & James; 1996.
[4] Givoni B. Passive and low energy cooling of buildings. Van Nostrand Reinhold; 1994
[5] CR 1752 Ventilation for buildings: Design criteria for the indoor environment. CEN, Brussels, 1998
[6] ISO 7730 Moderate thermal environments – Determination of the PMV and PPD indices and specification of the conditions for thermal comfort. International Standard, 1994
[7] Artmann N, Manz H, Heiselberg P. Climatic potential for passive cooling of buildings by night-time ventilation in Europe. (accepted for publication in Applied Energy, May 29th, 2006)
[8] Meteonorm, Global meteorological database for engineers, planners and education. Version 5.1 – Edition 2005, Software incl. Manual (www.meteonorm.com)
[9] Schaer C, Vidale P L, Luethi D, Frei C, Haeberli C, Liniger M A, Appenzeller C. The role of increasing temperature variability in European summer heatwaves, Nature Vol 427, 2004, pp. 332-336
[10] http://prudence.dmi.dk

APPENDIX

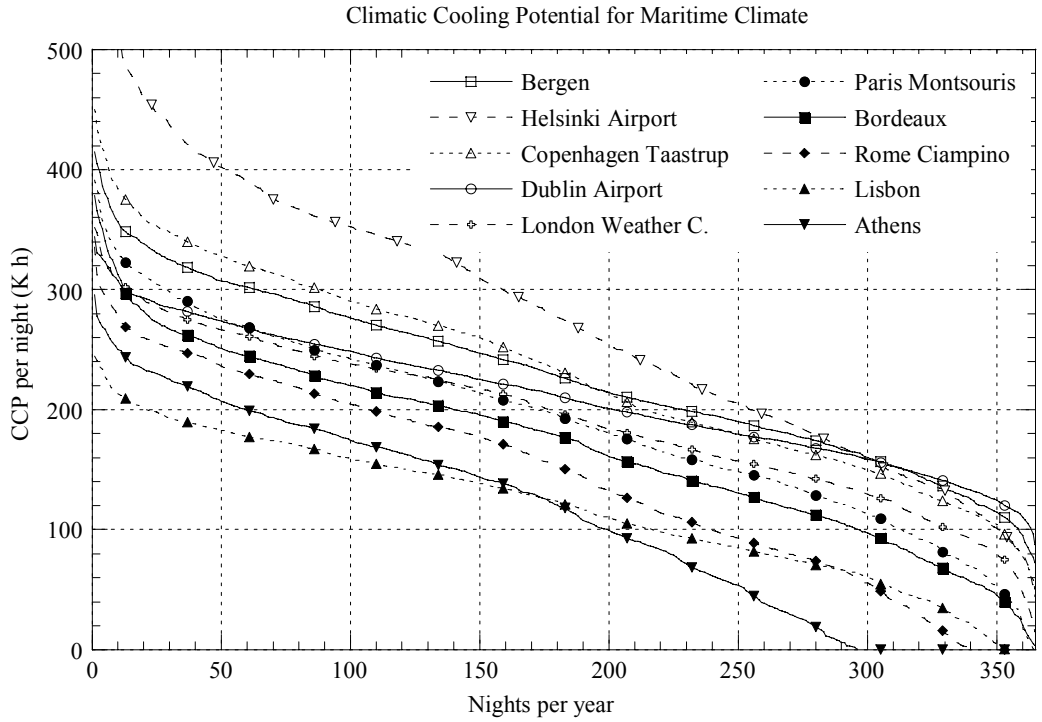
Climatic Cooling Potential for Maritime Climate
CCP per night (K h)
Nights per year
0
100
200
300
400
500
0
50
100
150
200
250
300
350
Bergen
Helsinki Airport
Copenhagen Taastrup
Dublin Airport
London Weather C.
Paris Montsouris
Bordeaux
Rome Ciampino
Lisbon
Athens

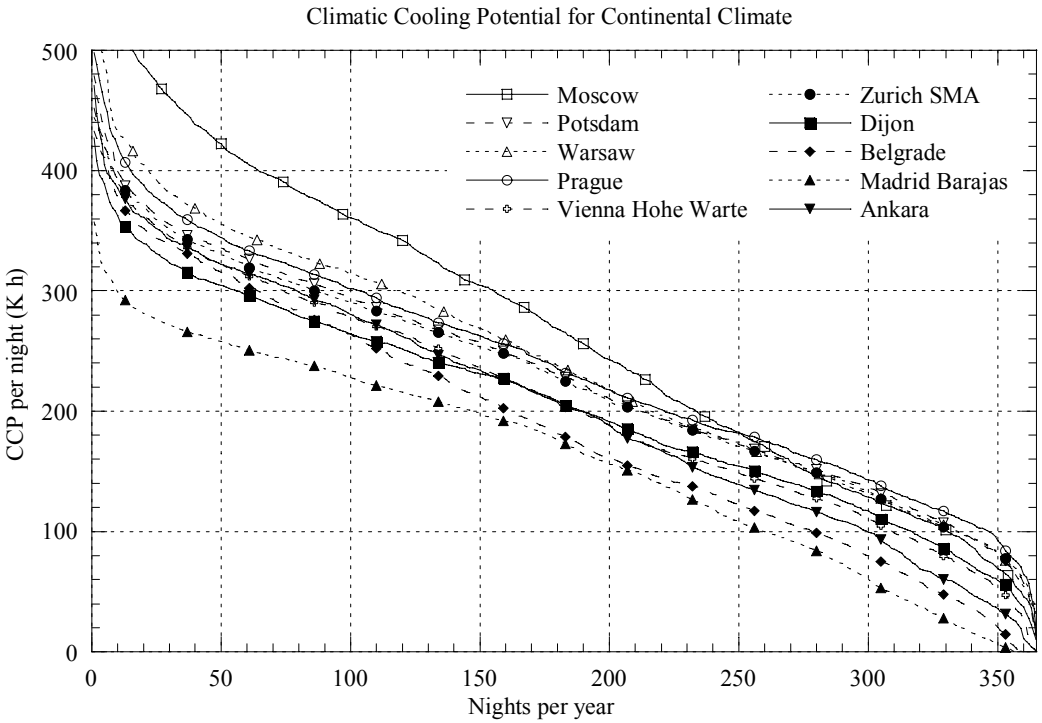
Climatic Cooling Potential for Continental Climate
CCP per night (K h)
Nights per year
0
100
200
300
400
500
0
50
100
150
200
250
300
350
Moscow
Potsdam
Warsaw
Prague
Vienna Hohe Warte
Zurich SMA
Dijon
Belgrade
Madrid Barajas
Ankara

Parametric study on the dynamic heat storage capacity of building elements

N. Artmann, H. Manz
Swiss Federal Laboratories for Materials Testing and Research, Switzerland

P. Heiselberg
Hybrid Ventilation Centre, Aalborg University, Denmark

ABSTRACT

In modern, extensively glazed office buildings, due to high solar and internal loads and increased comfort expectations, air conditioning systems are often used even in moderate and cold climates. Particularly in this case, passive cooling by night-time ventilation seems to offer considerable potential. However, because heat gains and night ventilation periods do not coincide in time, a sufficient amount of thermal mass is needed in the building to store the heat. Assuming a 24 h-period harmonic oscillation of the indoor air temperature within a range of thermal comfort, the analytical solution of one-dimensional heat conduction in a slab with convective boundary condition was applied to quantify the dynamic heat storage capacity of a particular building element. The impact of different parameters, such as slab thickness, material properties and the heat transfer coefficient was investigated, as well as their interrelation. The potential of increasing thermal mass by using phase change materials (PCM) was estimated assuming increased thermal capacity. The results show a significant impact of the heat transfer coefficient on heat storage capacity, especially for thick, thermally heavy elements. The storage capacity of a 100 mm thick concrete slab was found to increase with increasing heat transfer coefficients as high as 30 W/m²K. In contrast the heat storage capacity of a thin gypsum plaster board was found to be constant when the heat transfer coefficient exceeded 3 W/m²K. Additionally, the optimal thickness of an element depended greatly on the heat transfer coefficient. For thin, light elements a significant increase in heat capacity due to the use of PCMs was found to be possible. The present study shows the impact and interrelation of geometrical and physical parameters which appreciably influence the heat storage capacity of building elements.

1. INTRODUCTION

During the last few decades various factors have caused a trend towards increasing cooling demand in buildings. Particularly in modern commercial buildings with extensive glazing, higher solar gains and higher internal loads are contributing to the rise in cooling demand. Additionally, due to gradual climate warming and increased comfort expectations in summertime the installation of air-conditioning systems is becoming more common, and cooling plays a more significant role in the overall energy demand of buildings even in moderate and cold climates such as in Central or Northern Europe. Particularly in moderate climates, passive cooling of buildings by night-time ventilation appears to be a promising technique. If night-time temperatures are relatively low even in summer, the building can be cooled by ventilation with outdoor air. The ventilation can be achieved by mechanically forcing air through ventilation ducts, but also by natural ventilation through the windows. Hybrid systems combining the two methods are often also used. Thereby fans are only used if natural forces – thermal buoyancy and wind – are not strong enough to ensure sufficient ventilation rates.
As heat gains and night ventilation periods do not coincide in time, the energy of daily heat gains needs to be stored until it can be discharged by ventilation during the following night. A sufficient amount of thermal mass is therefore needed for a successful application of night-time ventilation. For effective utilisation of the thermal mass both a sufficient heat transfer to the surface and sufficient conduction within the element are needed. The purpose of this study is to evaluate the impact of different parameters such as material properties, slab thickness and heat transfer coefficient on the heat storage capacity of building elements.

2. MODEL OF A BUILDING ELEMENT

In this study a building element is represented by an infinite homogeneous slab with half-thickness d. One surface of the slab (x = 0) is exposed to a varying temperature, while the other surface (x = d) is considered adiabatic. Because of the symmetry this also represents a slab with thickness 2d with both surfaces exposed to the same conditions (surfaces at x = 0 and x = 2d, symmetry at x = d). The solution to the one-dimensional conduction problem in a slab with a sinusoidal surface temperature is given in Carslaw and Jaeger (1959).

Based on this solution Akbari et al. (1986) provided an analytical solution to the heat transfer problem in a slab with convective boundary condition and sinusoidally varying air temperature. The analytical solution gives both the temperature and heat flow profiles within the slab. Integrating the positive (charging) or negative (discharging) heat flow at the surface over one periodic cycle yields the dynamic heat storage capacity q of the element. This corresponds to the dynamic heat storage capacity as defined in European standard EN ISO 13786. A method to calculate the dynamic heat storage capacity of an element composed of layers with different thermal properties is also presented in EN ISO 13786.

The dynamic heat storage capacity can be calculated for different time intervals t, e.g. short term variations (t = 1 h), diurnal variations (t = 24 h) or seasonal variations (t = 8760 h). In this study the capacity was calculated based on a 24 h temperature variation, as the performance of night-time ventilation mostly depends on the diurnal heat storage.

The used model includes the following parameters:

- Heat transfer coefficient, h (W/m^{2}K)
- Half thickness of the slab, d (mm)
- Thermal conductivity, λ (W/mK)
- Volumetric heat capacity, ρc (J/m^{3}K)
- Time period, t (h)

These parameters completely describe the heat storage capacity of a building element exposed to a sinusoidally varying temperature. However, the model does not include internal and solar heat gains, the ventilation air change rate or climatic conditions, which certainly also influence the performance of night-time ventilation.

3. TEMPERATURE PROFILES

The analytical solution given by Akbari et al. (1986) was used to plot the temperature profiles in a 100 mm thick concrete slab (material properties are given in Table 1) with a convective boundary condition (h = 10 W/m^{2}K) and a sinusoidally varying air temperature, T_{Air} = 24.5±2.5 °C (Fig. 1).

Even at a relatively high heat transfer of h = 10 W/m^{2}K the amplitude of the surface temperature is reduced to 44 % of the air temperature amplitude. Compared to the surface temperature the amplitude of the core temperature is still 92 %. This indicates that even for a fairly thick element and a high heat transfer at the surface the thermal conductivity of concrete (λ = 1.8 W/mK) is sufficient to utilise the whole thickness of the slab.

4. HEAT STORAGE CAPACITY

The heat storage capacity of building elements exposed to a sinusoidal temperature variation with a periodic time of 24 h was evaluated depending on different parameters.

Table 1: Material properties

	λ	ρ	c
	W/mK	kg/m^3	kJ/kgK
Concrete	1.80	2400	1.1
Lime sand	1.10	2000	0.9
Gypsum	0.40	1000	0.8
MDF	0.18	800	1.7

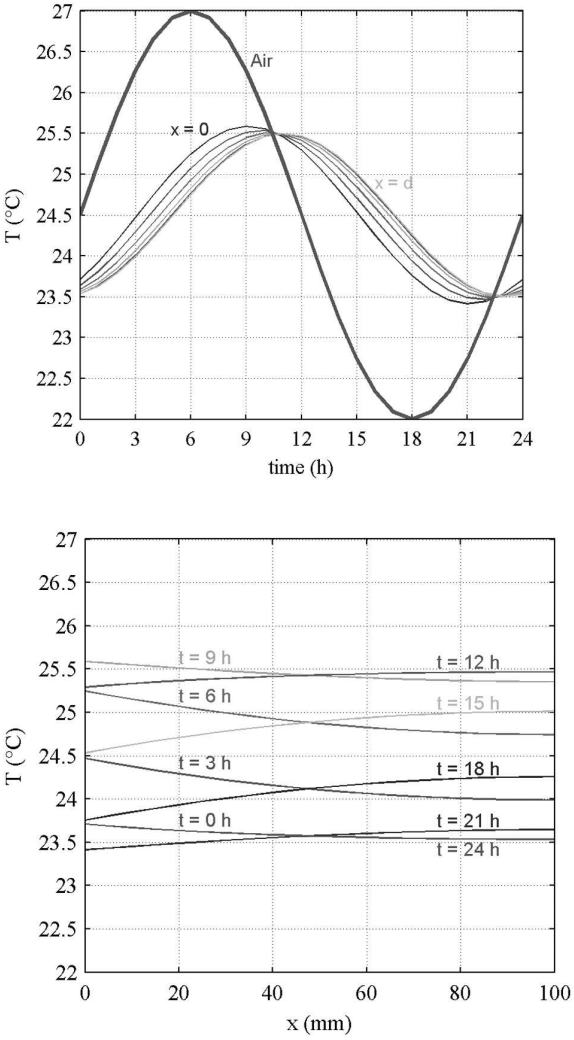

Figure 1: Temperature profile in a 100 mm thick concrete slab with convective boundary condition (h = 10 W/m^{2}K), exposed to a sinusoidal air temperature (24.5±2.5 °C) on one side (x = 0) and adiabatic boundary condition on the other side (x = 100 mm). Temporal profile at different layers of the slab, Δx= 20 mm (left) and spatial profile at different time-steps, Δt = 3 h (right).

4.1 Heat Transfer Coefficient

Figure 2 shows the diurnal heat storage capacity depending on the heat transfer coefficient for different materials and slab thicknesses. The properties of the

different materials are given in Table 1.
The impact of the heat transfer coefficient depends greatly on slab thickness and the thermal properties of the material. For thin slabs (d = 15 mm) the heat storage capacity is almost constant for heat transfer coefficients higher than h = 3 W/m²K. In contrast, for thick slabs increasing the heat transfer coefficient up to h = 30 W/m²K significantly increases the diurnal heat storage capacity. Generally, the storage capacity of thin elements, such as gypsum boards used for light-weight wall constructions or medium density fibreboards (MDF) used for furniture is rather small compared to thick and heavy elements such as a concrete ceiling or lime sand brick walls. However, especially at a low heat transfer coefficient and in consideration of its large surface area, furniture might still make a notable contribution to the total heat storage capacity of a room.

4.2 Slab Thickness

Increasing the slab thickness clearly raises the diurnal heat storage capacity until a maximum is reached. Beyond the maximum the capacity decreases slightly and converges to a constant value as the thickness approaches infinity (Fig. 3). This somewhat surprising effect has been described previously (e.g. Gruber and Toedtli, 1989) and is explained by the superposition of an incident wave and a reflected wave. With increasing heat transfer coefficient the maximum becomes more distinct. Additionally the optimum thickness of a concrete slab increases from about d = 90 mm to 140 mm if the heat transfer coefficient increases from h = 5 W/m²K to h = 30 W/m²K.The most significant decrease between the maximum capacity and the capacity of an infinite slab also occurs at the highest heat transfer coefficient and amounts to about 12 % for h = 30 W/m²K.

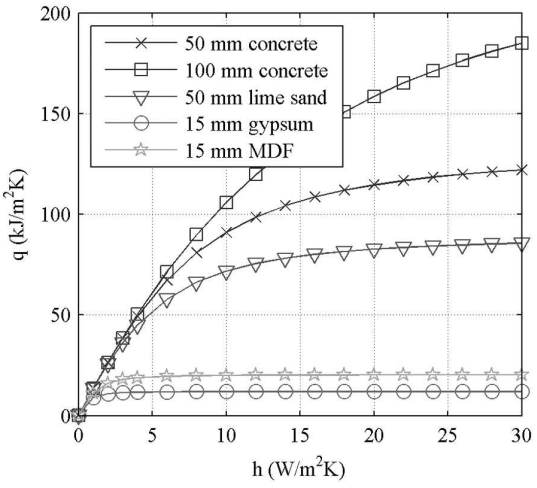

Figure 2: Diurnal heat storage capacity, q depending on the heat transfer coefficient, h for different materials and slab thicknesses.

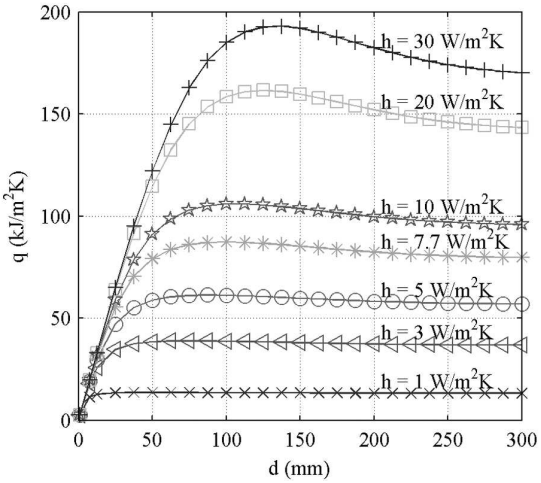

Figure 3: Diurnal heat storage capacity, q of a concrete slab depending on the thickness, d for different heat transfer coefficients, h.

4.3 Volumetric Heat Capacity

The impact of the volumetric heat capacity, ρc is displayed in Figure 4. The heat storage capacity of very light materials such as insulation materials with ρc < 0.1 MJ/m³K is generally very small. Even for a slab with half-thickness d = 100 mm and a high heat transfer coefficient, h = 20 W/m²K, the heat storage capacity is only 10 kJ/m²K. Increasing the thermal capacity to the value of concrete (ρc = 2.6 MJ/m³K) significantly improves the storage capacity, especially at high heat transfer coefficients (h= 10 to 20 W/m²K) to maximum 158 kJ/m²K. Further improvement for capacities above ρc = 2.6 MJ/m³K is only achieved for thin slabs (d = 15 mm) or at very high heat transfer coefficients (h = 20 W/m²K). These are the cases in which the use of phase change materials appears to be promising.

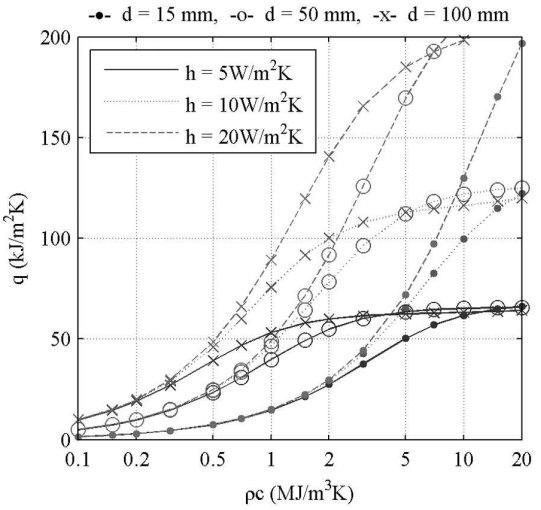

Figure 4: Diurnal heat storage capacity, q depending on the heat

capacity, ρc for different heat transfer coefficients, h and slab thicknesses, d; λ = 1.8 W/mK.

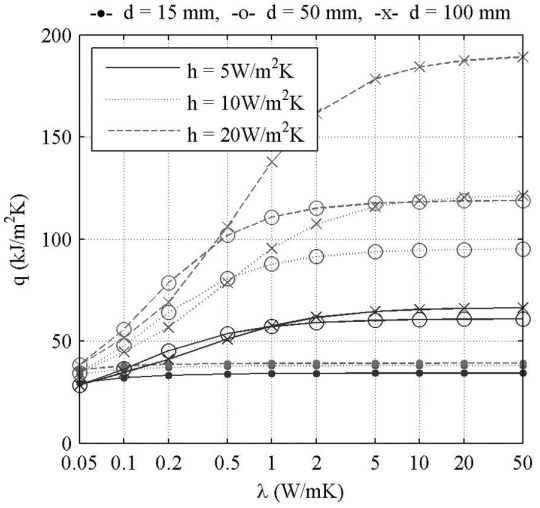

Figure 5: Diurnal heat storage capacity, q depending on the thermal conductivity, λ for different heat transfer coefficients, h and slab thicknesses, d; ρc = 2.6 MJ/m3K.

4.4 Thermal Conductivity

Figure 5 shows the impact of the thermal conductivity, λ of the slab material. For thin slabs (d = 15 mm) there is almost no impact of the conductivity in the range from λ = 0.05 W/mK and λ = 50 W/mK. For thicker slabs the heat storage capacity increases with increasing conductivity. However, in most cases the storage capacity increases only slightly for conductivities above 1.8 W/mK (concrete). Only in the case of a very thick slab (d = 100 mm) in combination with a high heat transfer coefficient (h = 20 W/m²K) does the storage capacity increase with conductivities up to 50 W/mK.

5. PHASE CHANGE MATERIALS

A well known possibility for increasing the thermal heat capacity of building elements is the integration of phase change materials (PCM). PCMs, like paraffins or salt hydrides, absorb and release a considerable amount of heat during the melting and solidification process. If the melting temperature of the PCM lies in the range of thermal comfort, the latent heat can be utilised to increase the heat storage capacity of a building element. A possible approach is the integration of micro-encapsulated PCMs into gypsum plaster boards or plaster (Schossig et al. 2005). PCMs are characterised by an increased heat capacity at melting temperature, as the heat of fusion needs to be applied for a further temperature increase. Ultra-pure materials show a sharp melting temperature, but typically the heat of fusion is introduced within a certain temperature range. The thermal conductivity also depends on the temperature and especially differs for the solid and liquid phase. These non-linear thermal properties complicate the representation of PCMs in physical models.

For a rough estimation of the effect of PCMs on the heat storage capacity a very simple model was used in this study. Assuming that the heat of fusion, ΔH_{fusion} is introduced continuously over the range of the temperature fluctuation, ΔT, the PCM was considered by applying an increased heat capacity:

$$c_{PCM} = c_{sensible} + \frac{\Delta H_{fusion}}{\Delta T} \quad (1)$$

The temperature fluctuation ΔT was set to 5 K, according to the comfort range given in prEN 15251 (2006), category III. For a building material with integrated PCM, the resulting volumetric heat capacity, ρc and the conductivity, λ were calculated according to the weight proportions. The values yielded for gypsum with 20 % and 40 % PCM (λ = 0.2 W/mK, ρ = 800 kg/m³, $c_{sensible}$ = 2.0 kJ/kgK, ΔH_{fusion} = 200 kJ/kg) are given in Table 2.

Table 2: Properties of gypsum including PCM

	λ	ρc
	W/mK	MJ/m³K
Gypsum, 20 % PCM	0.36	8.7
Gypsum, 40 % PCM	0.32	15.9

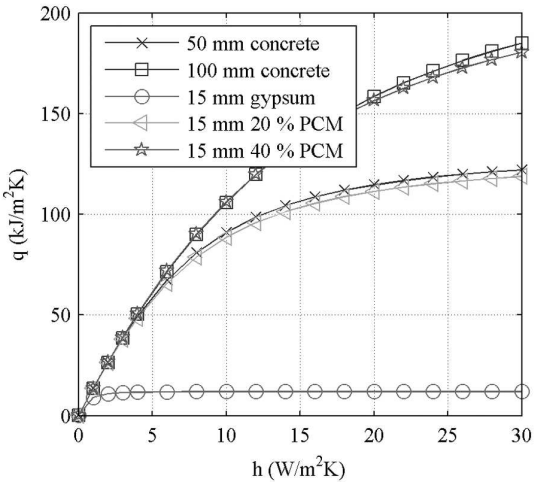

Figure 6: Effect of integrated PCM on the diurnal heat storage capacity, q depending on the heat transfer coefficient, h. Gypsum plaster board with different PCM contents compared to concrete slabs.

The heat storage capacity of a 15 mm thick gypsum plaster board with different PCM contents compared to concrete slabs is shown in Figure 6. Even at relatively

low heat transfer coefficients, h< 5 W/m²K, a significant effect of the PCM can be recognised. While the heat capacity of the plain gypsum plaster board is constant for heat transfer coefficients above 3 W/m²K, the capacity of the boards with integrated PCM continuously increase with increasing heat transfer coefficients up to 30 W/m²K. The plaster boards with 20 % and 40 % PCM content show similar performance to a 50 mm and 100 mm thick concrete slab, respectively. This clearly shows the feasibility of PCM integration for improving the thermal performance of light-weight wall constructions. However, considering the simplicity of the PCM model, the presented results should be seen as a rough indication only. The heat of fusion was divided by the maximum temperature range expected for the operative room temperature, although the temperature variation inside the building element might be significantly smaller (cp. Fig. 1). This leads to an underestimation of the heat storage effect of the PCM. On the over hand if the melting range of the PCM lies partly outside the material's temperature fluctuation, the latent heat capacity might not be utilised. For a more detailed PCM model the dynamic melting and solidification processes and the temperature dependency of the material properties need to be considered. A possible approach for the numerical modelling of PCMs has been presented by Egolf and Manz (1994).

6. CONCLUSIONS

An analytical solution to the heat transfer problem in a slab with convective boundary condition and sinusoidally varying air temperature was used to investigate the impact of different parameters on the heat storage capacity of building elements. The following effects were found:

- The heat storage capacity of thick thermally heavy elements significantly increases with an increasing heat transfer coefficient up to 30 W/m²K.
- The heat storage capacity of thin thermally light elements is almost constant for heat transfer coefficients higher than 3 W/m²K.
- The optimum thickness of an element depends on the heat transfer coefficient; the optimum half-thickness of a concrete slab increases from about 90 mm to 140 mm if the heat transfer coefficient increases from 8 W/m²K to 30 W/m²K.
- In most cases the thermal conductivity of concrete (λ = 1.8 W/mK) is sufficient; only at a high heat transfer coefficient (h = 20 W/m²K) does the storage capacity of a very thick slab (d = 200 mm) increase with conductivities up to 50 W/mK.
- The integration of phase change materials can significantly increase the heat storage capacity of building elements. A 15 mm gypsum plaster board with 40 % PCM content shows similar performance to a 100 mm thick concrete slab.

The heat storage capacity of building elements is an important precondition for the application of night-time ventilation. However, the effectiveness of night-time ventilation also depends on other parameters such as internal and solar heat gains, outdoor air temperature and ventilation air change rate, which were not considered in the model used in this study. Additionally, several building elements with different properties are typically present in a real room. If the different elements have different surface temperatures, energy is not only transferred by convection to the room air, but also by radiation between the elements. The impact of the heat storage capacity compared to other parameters, the interaction of different building elements and the impact of convective and radiative heat transfer needs to be investigated in more detail e.g. by building energy simulation.

ACKNOWLEDGEMENTS

This work was partially funded by the Hybrid Ventilation Centre, the Department of Civil Engineering at Aalborg University and the Swiss Federal Office of Energy (Project No. 101'308). The project is also supported by the private sector (WindowMaster, Belimo, SZFF). We acknowledge with thanks all financial support.

REFERENCES

Akbari H, Samano D, Mertol A, Baumann F and Kammerud R (1986). The effect of variations in convection coefficients on thermal energy storage in buildings Part I – Interior Partition Walls. Energy and Building Vol. 9, pp. 195-211.

Carslaw H S and Jaeger J C (1959). Conduction of heat in solids. Oxford University Press, Oxford, UK, 2nd edn.

Egolf P W and Manz H (1994). Theory and modelling of phase change materials with and without mushy regions. Int. J. Heat Mass Transfer Vol. 37, No. 18, pp. 2917-2924.

EN ISO 13786 (1999). Thermal performance of building components – Dynamic thermal characteristics – Calculation methods.

Gruber P and Toedtli J (1989). On the optimal thermal storage capacity of a homogeneous wall under sinusoidal excitation. Energy and Buildings, 13, pp. 177-186.

prEN 15251 (2006). Indoor environmental parameters for assessment of energy performance of buildings- addressing indoor air quality, thermal environment, lighting and acoustics. European Standard.

Schossig P, Henning H-M, Gschwander S and Haussmann T (2005). Micro-encapsulated phase-change materials integrated into construction materials. Solar Energy Materials & Solar Cells, 89, pp. 297-306.

Temperature measurements using type K thermocouples and the Fluke Helios Plus 2287A data logger

N. Artmann
R. Vonbank
R. L. Jensen

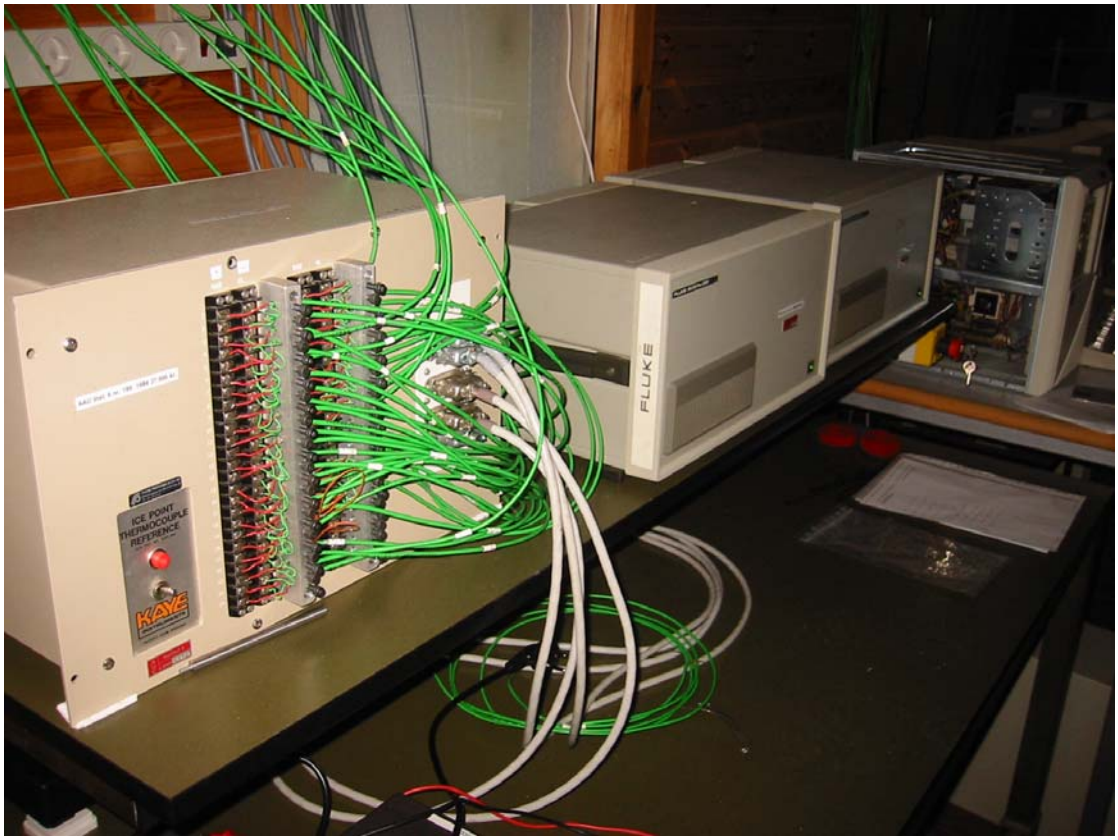

ISSN 1901-726X
DCE Technical Report No. 052

AALBORG UNIVERSITY
Department of Civil Engineering

Aalborg University
Department of Civil Engineering
Indoor Environmental Engineering Research Group

DCE Technical Report No. 052

Temperature measurements using type K thermocouples and the Fluke Helios Plus 2287A data logger

by

N. Artmann
R. Vonbank
R. L. Jensen

October 2008

Scientific Publications at the Department of Civil Engineering

Technical Reports are published for timely dissemination of research results and scientific work carried out at the Department of Civil Engineering (DCE) at Aalborg University. This medium allows publication of more detailed explanations and results than typically allowed in scientific journals.

Technical Memoranda are produced to enable the preliminary dissemination of scientific work by the personnel of the DCE where such release is deemed to be appropriate. Documents of this kind may be incomplete or temporary versions of papers—or part of continuing work. This should be kept in mind when references are given to publications of this kind.

Contract Reports are produced to report scientific work carried out under contract. Publications of this kind contain confidential matter and are reserved for the sponsors and the DCE. Therefore, Contract Reports are generally not available for public circulation.

Lecture Notes contain material produced by the lecturers at the DCE for educational purposes. This may be scientific notes, lecture books, example problems or manuals for laboratory work, or computer programs developed at the DCE.

Theses are monograms or collections of papers published to report the scientific work carried out at the DCE to obtain a degree as either PhD or Doctor of Technology. The thesis is publicly available after the defence of the degree.

Latest News is published to enable rapid communication of information about scientific work carried out at the DCE. This includes the status of research projects, developments in the laboratories, information about collaborative work and recent research results.

Published 2008 by
Aalborg University
Department of Civil Engineering
Sohngaardsholmsvej 57,
DK-9000 Aalborg, Denmark

Printed in Aalborg at Aalborg University

ISSN 1901-726X
DCE Technical Report No. 052

Table of contents

Functional principle of thermocouples [1]

In 1821, the German–Estonian physicist Thomas Johann Seebeck discovered that when any conductor (such as a metal) is subjected to a thermal gradient, it will generate a voltage. This is now known as the thermoelectric effect or Seebeck effect. Any attempt to measure this voltage necessarily involves connecting another conductor to the "hot" end. This additional conductor will then also experience the temperature gradient, and develop a voltage of its own which will oppose the original. Fortunately, the magnitude of the effect depends on the metal in use. Using a dissimilar metal to complete the circuit creates a circuit in which the two legs generate different voltages, leaving a small difference in voltage available for measurement (Figure 1). That difference increases with temperature, and can typically be between one and seventy micro-volts per Kelvin (µV/K) for the modern range of available metal combinations. Certain combinations have become popular as industry standards, driven by cost, availability, convenience, melting point, chemical properties, stability, and output. This coupling of two metals gives the thermocouple its name.

It is important to note that thermocouples measure the temperature difference between two points, not absolute temperature. In traditional applications, one of the junctions – the cold junction – was maintained at a known (reference) temperature, while the other end was attached to a probe. An ice bath made of finely crushed ice and air saturated water (0 °C) was used as reference.

Having available a known temperature cold junction, while useful for laboratory calibrations, is simply not convenient for most directly connected indicating and control instruments. They incorporate into their circuits an artificial cold junction using some other thermally sensitive device, such as a thermistor or diode, to measure the temperature of the input connections at the instrument, with special care being taken to minimize any temperature gradient between terminals. Hence, the voltage from a known cold junction can be simulated, and the appropriate correction applied. This is known as cold junction compensation.

Figure 1. Functional principle of thermocouples

Type K thermocouples

The type K thermocouple consists of two different nickel alloys called Chromel (90 % nickel and 10 % chromium) and Alumel (95% nickel, 2% manganese, 2% aluminium and 1% silicon). In the following the abbreviations CHR for Chromel and AL for Alumel are used. The sensitivity of the type K thermocouple is approximately 41 µV/K. Different colour codes exist for type K thermocouple wires (Table 1).

Deviations in the alloys can affect the accuracy of thermocouples. For type K thermocouples the tolerance class one is given as ± 1.5 K between -40 and 375 °C. However, deviations between thermocouples coming from the same production are very small and a much higher accuracy can be achieved by individual calibration.

Table 1. Different colour codes for type K thermocouple wires

Colour code	Chromel (+)	Alumel (-)
IEC	Green	White
DIN	Red	Green
BS	Purple	Blue
ANSI	Yellow	Red

Additionally, local changes of the alloys at the junction of the two thermocouple wires can affect the thermoelectric potential. This kind of local changes can occur if heat is applied during the joining process, e.g. during welding or soldering.

All thermocouples used in these experiments were made of type K thermocouple wires. Aluminium tips were used to make the junctions (Figure 2). Using a special tool the aluminium tips were pressed to the wires without applying heat.

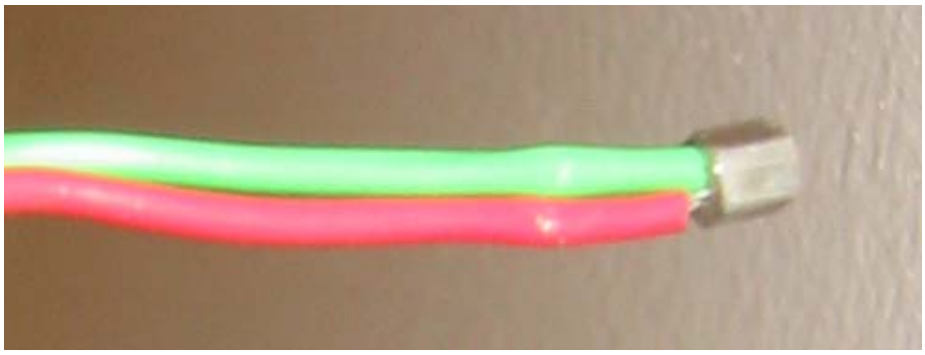

Figure 2. Thermocouple with aluminium tip.

Basic thermocouple circuits

Figures 3 and 4 show two different basic thermocouple circuits. In the first one (Figure 3) the potentiometer is included in one of the thermocouple wires. In this case a possible temperature difference between the input terminals of the potentiometer could affect the measurement. In order to exclude this error, both thermocouple wires can be connected to copper transmission lines (Figure 4). In this case the reference is the temperature of these two junctions.

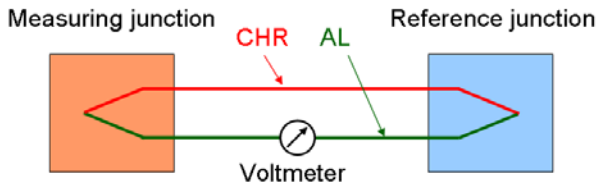

Figure 3. Basic thermocouple circuit.

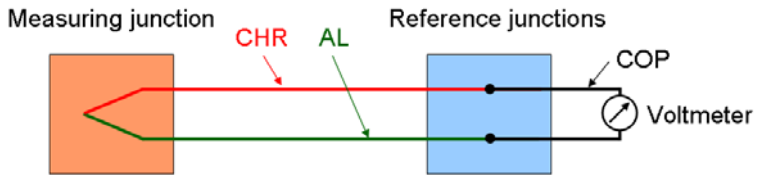

Figure 4. Basic thermocouple circuit with copper transmission lines.

Measurement of temperature differences

If the quantity of interest is not an absolute temperature but a temperature difference, no reference junction is needed. In this case several thermocouples can be connected in series with each other to form a thermopile, where all the hot junctions are exposed to the higher temperature and all the cold junctions to the lower temperature (Figure 5). Thus, the voltages of the individual thermocouples add up, which allows for a larger signal and higher accuracy.

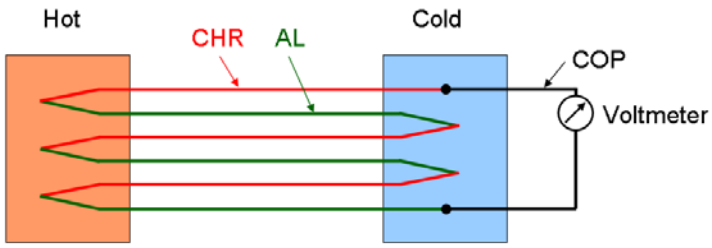

Figure 5. Three thermocouples connected in series with each other forming a thermopile.

Fluke Helios Plus 2287A data logger

The Helios Plus 2287A is a modular data acquisition system for measuring voltage, current, resistance, temperature etc. The Helios data loggers used are equipped with a High Accuracy A/D Converter (161) and 5 Thermocouple/DCV Scanners (162) each of which sequentially switches 20 channels to the A/D converter. Therefore 100 channels are available at each Helios data logger. The resolution of the data logger is 0.488 μV. Using type K thermocouples this corresponds to about 0.012 K. For all experiments, the data logger was configured to measure every 10 seconds.

Two different types of connectors are available for measuring temperature and voltage. The Thermocouple/DCV Connector (175) and the DC Voltage Input Connector (176) both provide 20 channels with 3 screw terminals, ‘High’, ‘Low’ and ‘Shield’ for each channel. The screw terminals of the Thermocouple/DCV Connector (Figure 6) are embedded in an aluminium block to keep them isothermal. Additionally there is a thermistor measuring the temperature of the aluminium block. The Thermocouple/DCV Connector can be used to connect thermocouples directly. If configured for temperature measurement, the measured voltage signal is converted to an absolute temperature (in °C or °F) using the temperature measured by the thermistor as reference. The Thermocouple/DCV Connector can also be configured to measure voltage without applying the thermistor. The DC Voltage Input Connector provides the same terminals, but without the aluminium block and the thermistor. It can only be used for voltage measurement.

Figure 6. FLUKE Thermocouple/DCV Connector (175), cover removed to show the aluminium block and the thermistor.

As all channels are switched to the same A/D converter, the difference in the measured voltage between different channels is very small. Small differences can be caused by thermoelectric potentials generated in the electric circuits of the scanners. This offset can be measured if the input terminals are short-circuited. The offsets measured for all channels were between 1.7 and 7.9 μV. For type K thermocouples this corresponds to a maximum error of ± 0.075 K. However, the accuracy of the measurements was not found to be improved when the offsets were subtracted from the measured signals. The reason for this might be that the offsets are not constant over time.

Ice point reference

Instead of using the temperature of the input terminals measured by the thermistor as reference, an ice point reference can be applied. By definition the temperature of an ice bath made of finely crushed ice and air saturated water is 0 °C, the reference point for most thermocouple tables. Automatic ice bath reference systems follow the same principle.

One KAYE K170-6 with 6 channels and one KAYE K 170-50 (Figure 7) with 50 channels were used. Both instruments contain a sealed cell filled with pure water. A sensitive bellows is an integral part of the cell. When power is turned on, the cell is chilled by a Peltier cooler. As ice is formed, there is an increase in volume which causes the bellows to extend. When a sufficient amount of ice is formed, the extending bellows will actuate a micro-switch, causing the power supply to turn off. Ambient heat will then melt a small amount of ice, which results in a decrease in volume, ultimately turning the power supply on again, and the cycle repeats. A pilot light is connected in parallel to the Peltier cooler. A cycling condition of the pilot light

gives a positive indication that the system is functioning properly. Utilizing only the volume change of water at its freezing temperature for control offers an inherent stability of the temperature in the cell. The Kaye Automatic Ice Bath is capable of operating continuously with an error less than 0.02 K [2].

Figure 7. KAYE 170-50 ice point reference with 50 channels.

The wiring setup for measurements using an ice point reference and copper transmission lines is shown in Figure 8. The junctions connecting the thermocouple wires to copper wires are placed within the water and ice cell of the ice point reference. In order not to introduce additional thermocouples it is important, that the entire connections from the measuring junctions to the reference junctions, including the screw terminals are made from the same material. Therefore no wire end sleeves or the like should be used to connect the thermocouples to the ice point reference. In the configuration shown in Figure 8 the measured voltage signal corresponds to the temperature difference between the measuring junctions and the reference junctions. As the temperature of the reference junctions is 0 °C, the temperature of the measuring point can be found directly from a standard thermocouple table.

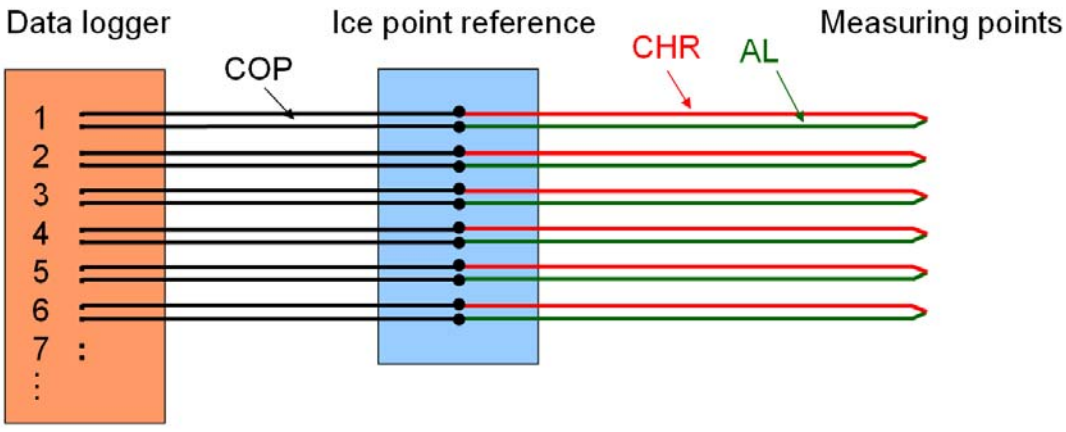

Figure 8. Wiring setup for temperature measurements using an ice point reference and copper transmission lines.

Accuracy of measurements using the Thermocouple/DCV Connector

As the number of channels of the ice point reference is limited, the accuracy of measurements using the Thermocouple/DCV Connector and the thermistor as reference (Figure 9) should be examined. If thermocouples are connected directly to the Thermocouple/DCV Connector, the measured voltage signal corresponds to the temperature difference between the measuring point and the input terminals of the connector (reference junctions). As the reference temperature is only measured at one point (thermistor in the centre of the connector), any temperature difference between the input terminals and the reference point will have a direct impact on the accuracy of the measurement.

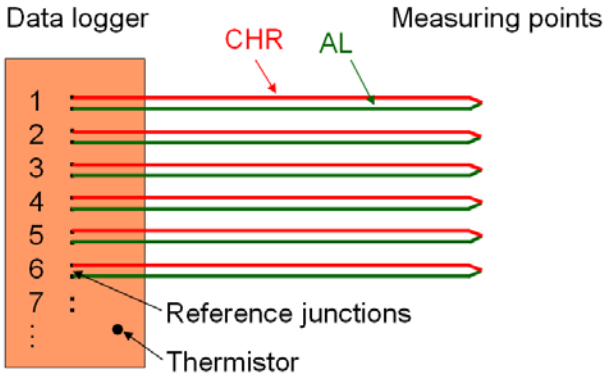

Figure 9. Setup for measurements using the thermistor to determine the reference temperature.

In order to test the temperature gradient across the Thermocouple/DCV Connectors (Figure 6) six channels were connected to the KAYE K170-6 ice point reference. For the connection of the ice point reference to the data logger thermocouple wires were used according to the ice point terminals CHR and AL, and the copper outputs of the ice point reference were short-circuited by copper (COP) wires (Figure 12). The 6 channels of the ice point reference were connected to the terminals 0 (left), 10 (centre), and 19 (right) of two Thermocouple/DCV Connectors, respectively. The two connectors were placed in the first and second slot of the Helios data logger (Figure 11). These correspond to the channels 1, 11, 20, 21, 31 and 40.

In this configuration (Figure 12) the data logger measures the thermoelectric potential corresponding to the temperature difference between the ice point and the respective terminals of the Thermocouple/DCV Connectors. As all junctions in the ice point reference have the same temperature, differences in the measured voltage are caused by temperature differences of the input terminals.

Figure 10. KAYE K170-6 ice point reference with thermocouples connected to the CHR/AL inputs and COP outputs short-circuited.

Figure 11. Fluke Helios Plus 2287A data logger (back view).

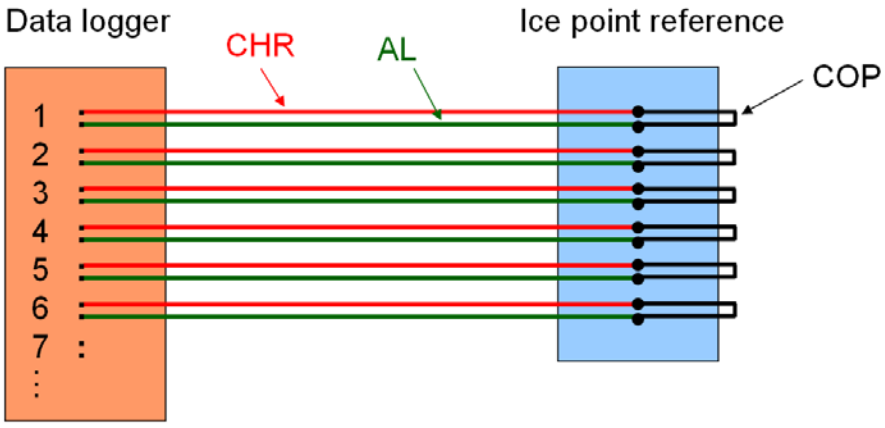

Figure 12. Setup for testing the temperature gradients across the Thermocouple/DCV Connectors.

The measured voltage signals (Figure 13) clearly show that the upper connector (channels 1 to 20) is warmer than the lower one (channels 21 to 40). The difference in voltage of about 40 μV corresponds to

about 1 K temperature difference. At the upper connector the input terminal 0 (channel 1) is clearly warmer than the other two. At the lower input block the temperature increases from the left (channel 21) to the right (channel 40). Within the connectors the differences are about 10 μV or 0.25 K.

These temperature differences between different input terminals are added to the temperatures measured at the different channels. If the differences between different channels are constant over time, these errors can be excluded by calibration. However, considering variations of the air temperature in the lab and possibly sun irradiation, considerable errors may remain.

The measurement shown in Figure 13 was started immediately after the data logger was turned on. The large gradient in the voltage signal in the beginning of the measurement shows that the temperature of the input terminals is affected by the heat production of the data logger and the air movement caused by the cooling fan. Therefore, in any case, the data logger should be turned on at least 2 h before a measurement is started.

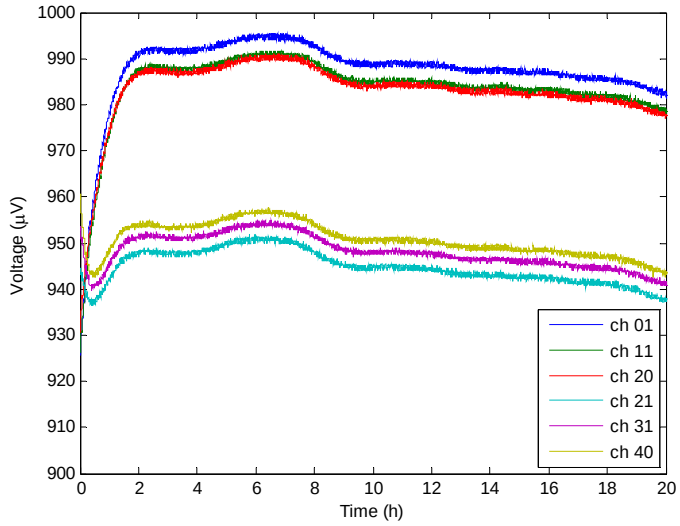

Figure 13. Measured voltage corresponding to the temperature difference between the ice point reference and different input terminals of two FLUKE Thermocouple/DCV Connectors.

Compensation box

Another alternative is to use an external compensation box, where the thermocouples are connected to copper wires. The copper wires are then connected to the data logger. In this case the measurement is independent of the temperatures of the input terminals of the data logger. The measured thermoelectric potential corresponds to the temperature difference between the measuring point and the junctions in the compensation box. In an insulated box these junctions can be well protected from ambient conditions.

For the evaluation of the measured voltage signal the temperature of the junctions in the compensation box needs to be known. The temperature of the reference junction can be measured by an additional temperature sensor, e.g. a resistance temperature sensor (PT 100). Alternatively, one channel can be connected to an ice point reference, while the other channels are used for measuring. The voltage signal of the reference channel then corresponds to the temperature difference between the compensation box and the ice point, and the temperature of the compensation box can be calculated.

In order to test this method, copper wires were used to connect the thermocouples to the data logger. The other ends of the thermocouples were connected to the ice point reference with the copper outputs short-circuited (Figure 14). The junctions of the thermocouples to the copper wires were attached to a massive metal block which was insulated with EPS (Figure 15). The voltage signals measured during the experiment with this configuration are shown in Figure 16. The maximum difference in the mean values between different channels is 2 μV corresponding to about 0.05 K.

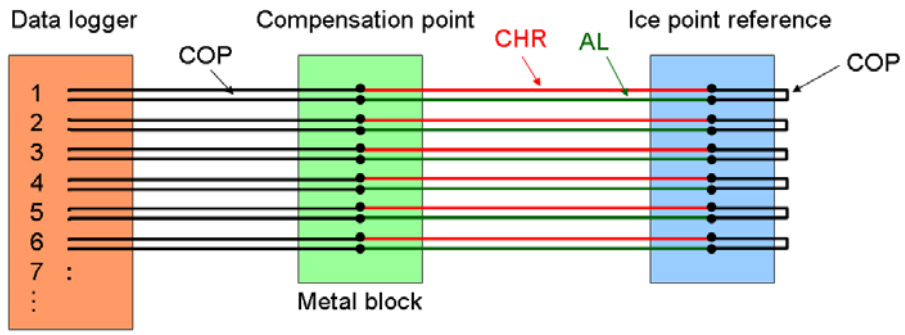

Figure 14. Setup for testing an external compensation box.

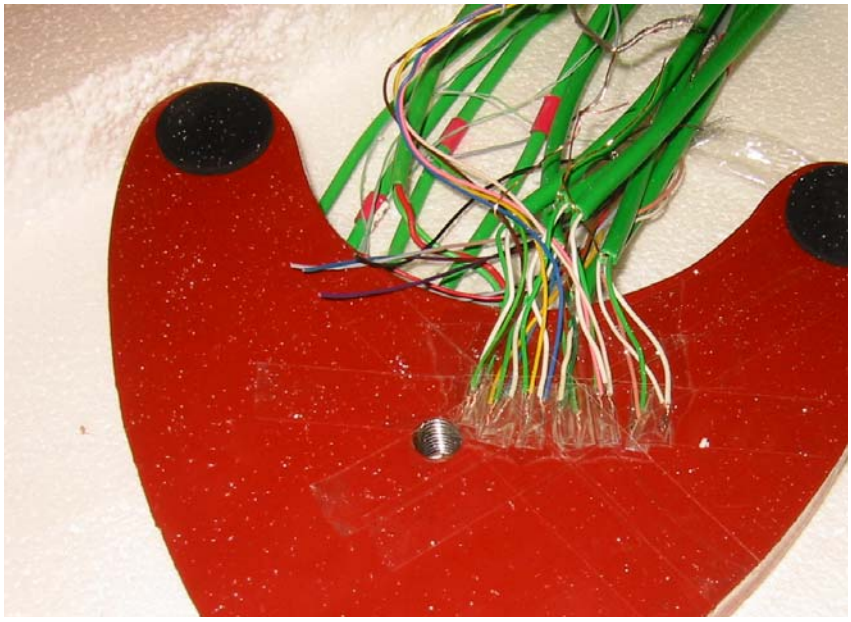

Figure 15. CHR/COP and AL/COP junctions attached to a massive metal block, insulated with EPS.

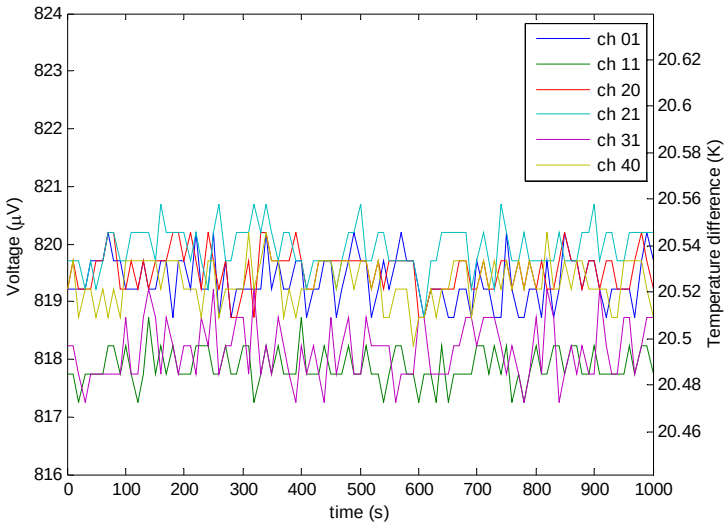

Figure 16. Voltage measured during preliminary test using an external compensation point.

For the final setup a more advanced compensation box developed at Empa was used (Figure 17). It consists of 16 terminal blocks with 20 terminals (10 channels) each. Thus in total 160 thermocouples can be connected. The terminal blocks are embedded in an aluminium block to maintain a homogeneous temperature. Resistance temperature sensors (PT 100) are placed in the centre line of the aluminium block to measure the reference temperature.

The box containing the aluminium block including the circuit boards is made of XPS for thermal insulation. Additionally the terminals are shielded by an aluminium sheet to reduce radiation heat exchange. The performance of the compensation box was estimated by applying a temperature step of 2 K in a climatic chamber. The maximum temperature difference measured between different channels was 0.005 K.

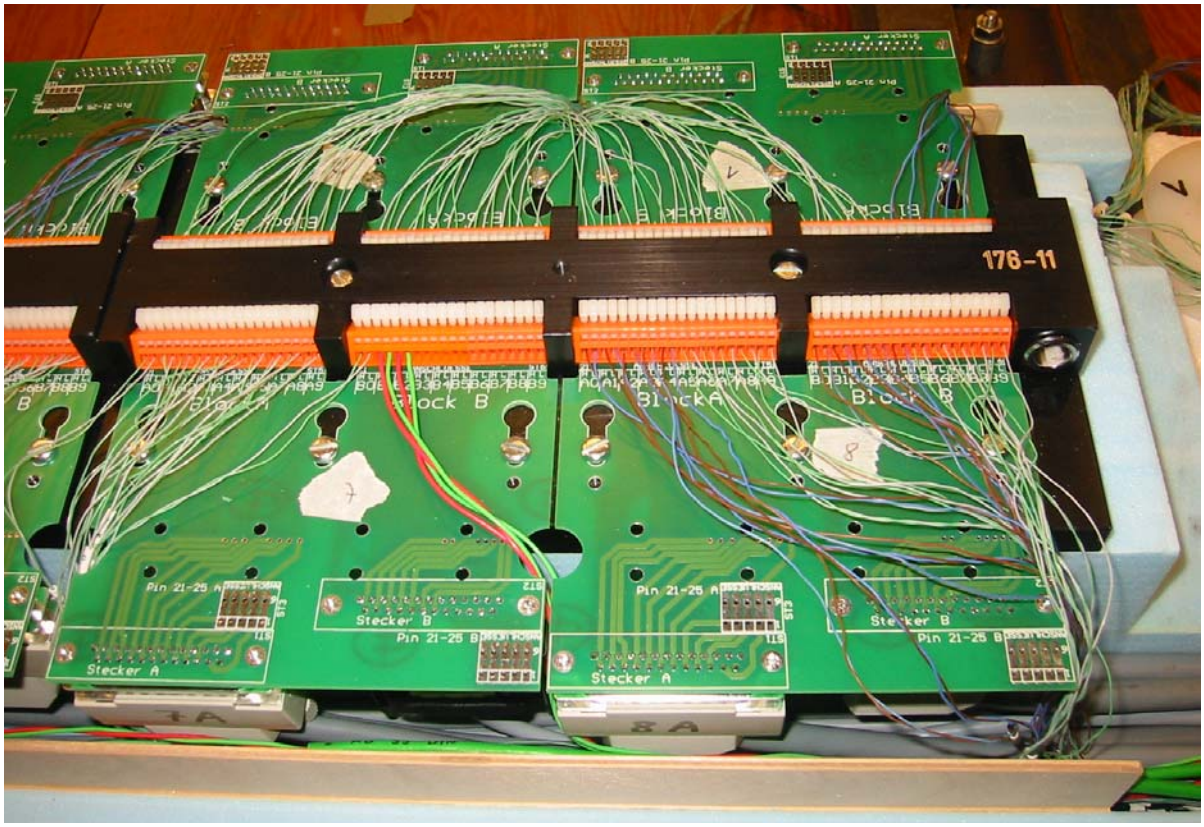

Figure 17. Compensation box with 160 channels. Cover and radiation shield removed.

Calibration

As deviations in the thermocouple alloys can affect the thermoelectric potential, the used thermocouple wires were calibrated. The thermoelectric potential does not only depend on the temperature difference between the two junctions but also on the temperature level, i.e. if T_{ref} = 0 °C and T_{mp} = 20 °C does not give exactly the same voltage as if T_{ref} = 10 °C and T_{mp} = 30 °C. Therefore calibration needs to be done at a defined reference temperature. Normally 0 °C is used as reference temperature.

Because of the dependency on the temperature level, the slope of the calibration curve is not constant and a linear interpolation would cause an error. For the small temperature range between 8 and 30 °C this error amounts to about ± 0.04 K. A 3rd order polynomial was found to be sufficient to exclude this error.

The non-linearity of the calibration curve also affects the evaluation of the measured data (Figure 18). If the reference temperature during the measurement is not the same as during the calibration, the measured voltage signal can not be converted to the temperature difference directly. In this case, first the reference voltage corresponding to the known reference temperature needs to be determined. The measured voltage is then added to the reference voltage. The temperature at the measuring point is yielded by applying the resulting voltage to the calibration curve.

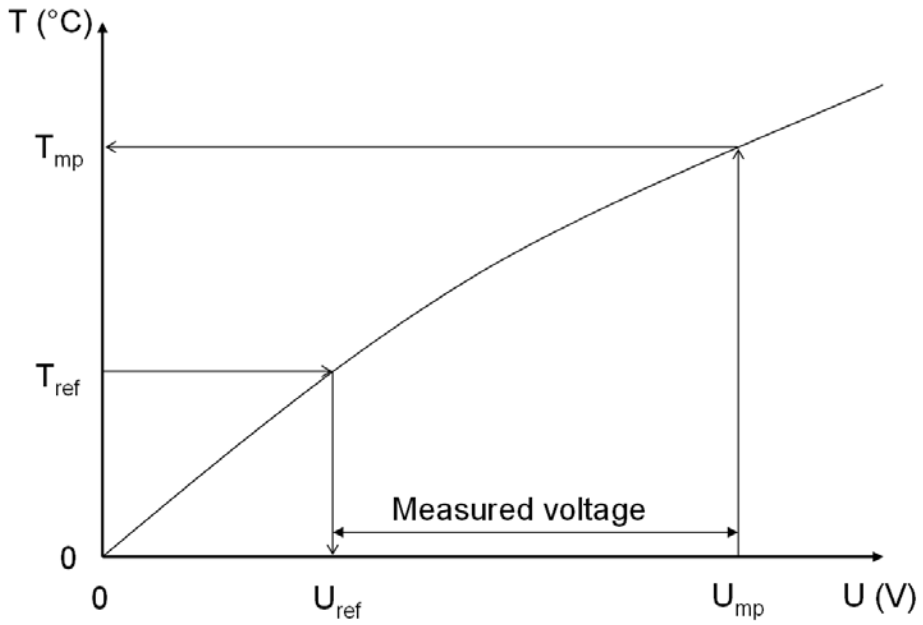

Figure 18. Data evaluation for the case when the reference temperature, T_{ref} is not 0 °C

Two different types of wires were calibrated:

1. Thin wires without additional insulation. 1/0.2 mm TYPE K PFA TW-PR, Class 1, 1/2 Tolerance, -40 to 375 °C, Batch No 2912 01+02, IEC colour code.

2. Thick wires with shield and insulation. Thermocoax 2 AB 35 DIN

For calibration of the thin wires two thermopiles, each composed of two thermocouples were used. Two isothermal calibration devices were used to maintain the junctions at defined temperatures. The cold junctions were maintained at 0 °C, while the temperature of the hot junctions was varied between 8 and 30 °C. The temperature difference was measured with a high precision thermometer and the voltage was measured by a high precision voltmeter. To compensate for the two thermocouples per thermopile the measured voltage was divided by 2. The calibration data for the two thermopiles is given in Table 2.

A third order polynomial ($\Delta T = p_1(U)$) was fitted to the mean value of the two series of data points. To improve the numerical properties of both the polynomial and the fitting algorithm a centring and scaling transformation was applied (see Matlab function ‘polyfit’ [3]). Figure 19 shows the difference between the values obtained by this polynomial and the measured values. The error is less than ± 0.023 K.

Table 2. Calibration data for thin thermocouple wires.

ΔT_1 (K)	U_1 (V)	ΔT_2 (K)	U_2 (V)
8.128	321.1	8.124	319.1
10.091	399.7	10.091	398.3
12.080	479.5	12.072	478.3
14.050	558.9	14.047	557.8
16.023	638.5	16.016	637.4
18.008	718.7	17.988	718.2
19.981	799.0	19.979	799.0
21.957	879.1	21.958	879.3
23.912	958.3	23.910	958.9
25.887	1038.8	25.890	1039.5
27.851	1118.8	27.857	1120.1
29.842	1200.2	29.857	1202.0

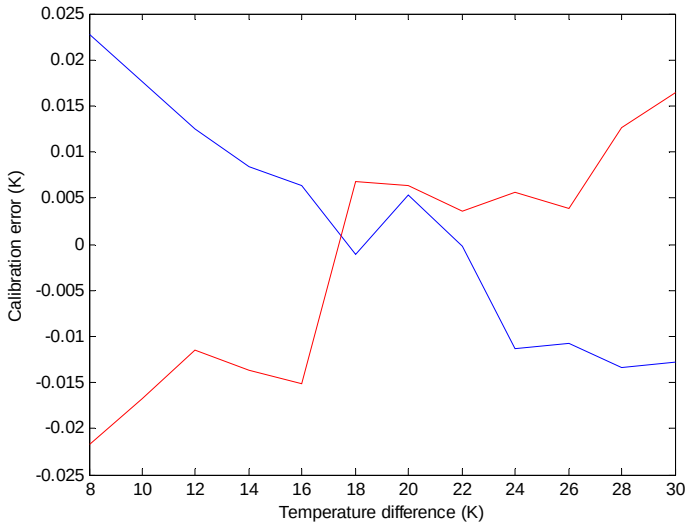

Figure 19. Calibration error for two thermopiles made of the thin thermocouple wires.

The thick thermocouples were only used in combination with the ice point reference and were therefore calibrated together with the KAYE 170-50 ice point reference and the Helios data logger. By calibrating the entire system together, the total error can be minimised. Four thick thermocouples were calibrated using the KAYE 170-50 as reference and an isothermal calibration device for the hot junctions. A high precision thermometer was used to measure the temperature of the isothermal calibration device (Isocal-6, Venus 2140 B Plus) and the Helios data logger was used to read the voltage. The calibration data is given in Table 3.

A third order polynomial ($\Delta T = p_2(U)$) was fitted to the mean value of the four series of data points. To improve the numerical properties of both the polynomial and the fitting algorithm a centring and scaling transformation was applied (see Matlab function 'polyfit' [3]). Figure 20 shows the difference between the

values obtained by this polynomial and the measured values. The error is less than ± 0.028 K. This error also includes possible deviations between different channels of the ice point reference and the Helios data logger.

Figure 21 shows the two calibration curves p_1 and p_2 obtained for the thin and thick thermocouples, respectively. The difference between the two curves amounts to maximum ± 0.125 K.

Table 3. Calibration data for thick thermocouples.

ΔT (K)	U_1 (V)	U_2 (V)	U_3 (V)	U_4 (V)
8.111	317.2	317.0	317.9	318.8
10.091	396.1	395.8	396.6	397.2
12.058	474.3	474.1	475.0	475.3
14.034	553.0	552.7	553.6	553.7
16.028	632.8	632.7	633.5	633.4
18.734	741.5	741.4	742.1	741.9
20.746	822.2	822.1	823.0	822.4
22.757	903.3	902.9	904.0	903.2
24.759	984.0	983.7	984.6	983.6
26.768	1065.2	1064.9	1065.8	1064.6
28.769	1146.3	1145.9	1146.9	1145.5
30.772	1227.4	1226.8	1227.9	1226.3

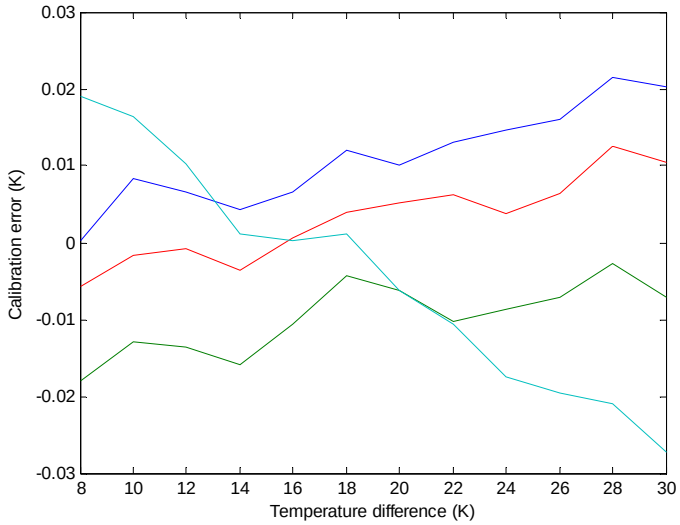

Figure 20. Calibration error for 4 different thick thermocouples.

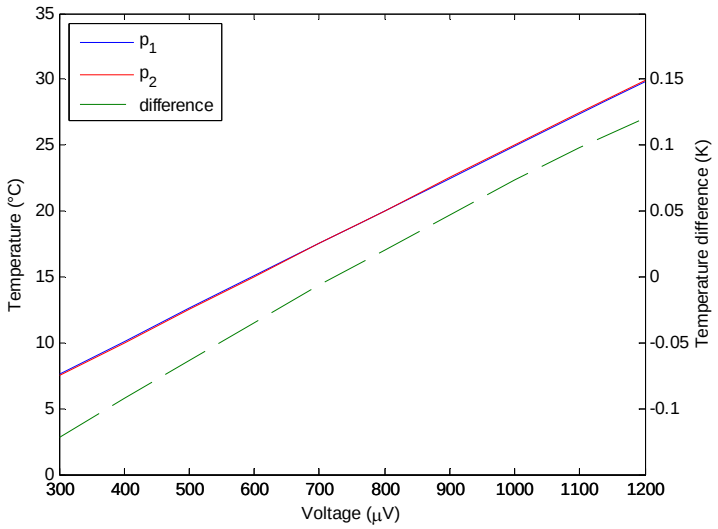

Figure 21. Calibration curves for two different types of thermocouple wires (p1: thin and p2: thick) and their difference.

Final setup and data evaluation

For the final setup two Helios data loggers, the KAYE 170-50 ice point reference and the compensation box with 160 channels were used (Figure 22). 37 thick thermocouples were connected to the ice point reference and the Helios data logger No. 233. In total 141 thin thermocouples were connected to the compensation box, 60 to the data logger No. 233 and 81 to the data logger No. 283. Two channels of each data logger were applied as reference for the compensation box. As the thick thermocouples were calibrated together with the ice point reference, thick thermocouples were used to connect the four reference channels from the compensation box to the ice point reference. The corresponding outputs of the ice point reference were short-circuited. Additionally 17 channels of the data logger No. 283 were applied for direct temperature difference measurements.

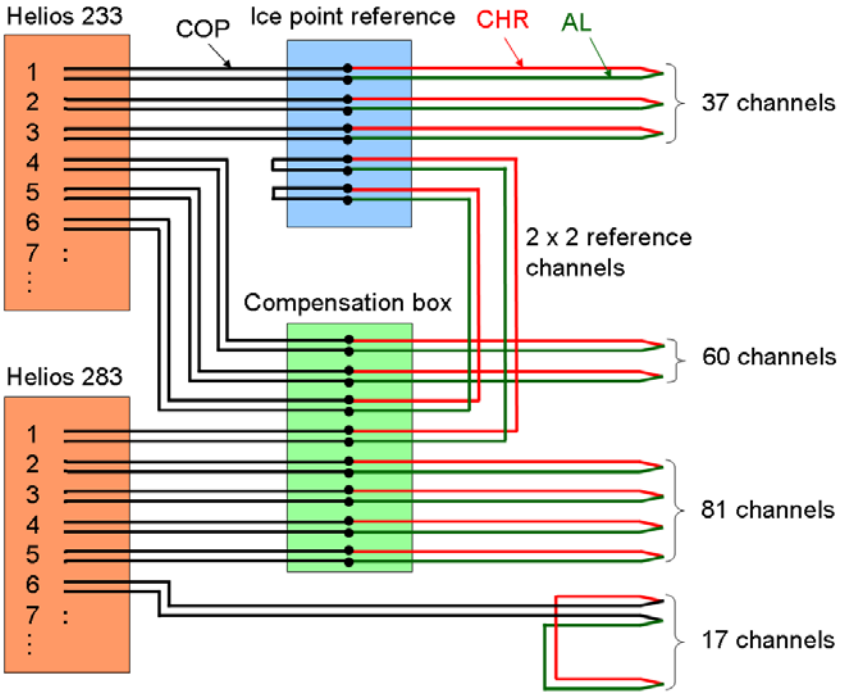

Figure 22. Setup with two Helios data loggers, a KAYE ice point reference and a compensation box providing 178 channels for temperature measurement and 17 channels for direct temperature difference measurement.

For the 37 channels of the data logger no. 233 with thick thermocouples connected to the ice point reference the calibration curve p_2 was applied.

For the thermocouples connected to the compensation box the data evaluation was more complicated. In order to exclude the difference between the two calibration curves the reference temperature (temperature in the compensation box, T_{ref}) was calculated from the voltage, U_{ref} measured at the reference channels applying the calibration curve p_2: $T_{ref} = p_2(U_{ref})$. The inverse function of the other calibration curve, p_1' was then applied to calculate the reference voltage corresponding to the temperature of the compensation box for the thin thermocouples. This reference voltage was then added to the signal, U measured at the remaining channels. The temperature, T at the measuring points was obtained from the resulting voltage using the calibration curve p_1: $T = p_1(p_1'(T_{ref}) + U)$

All sensors for temperature difference measurements were made of the thin thermocouple wires. As the exact reference temperature was not known, a linear calibration was used. The reference temperature was expected to be in the range from 14 to 22 °C. The gradient of the calibration curve p_1 between 14 and 22 °C was therefore used to calculate the temperature difference from the measured voltage signals ($\Delta T = U$ 0.02464 K/μV).

Noise / grounding problems

In order to prevent noise in the voltage signals it is important that all measurement devices including the computers and monitors used for data logging are properly grounded without creating any ground loops. Ground loops are formed if there are several ground connections between different parts of the system. If

radiation from external noise sources penetrates the setup, currents are generated in the loop and transformed into the signal lines.

To prevent ground loops each device needs to be connected to the ground at only one point. The shield of data cables or the like might connect the ground potential of two devices. In this case only one of the devices should be connected to the ground by the power supply cable.

Furthermore, devices like a frequency transformer used to control the speed of a fan might generate noise which can be transferred to the measurement system by the power cables. If this is the case, the device causing the noise should be connected to a different power plug.

Estimation of accuracy

The accuracy of the temperature measurement is affected by many different factors. The sources of uncertainty are:

- Voltage measurement of the data logger (resolution: 0.012 K, maximum offset between different channels ± 0.075 K)
- Cell temperature of the ice point reference (± 0.02 K)
- Composition of the thermocouple alloys (± 1.5 K, after calibration, thick: ± 0.028 K, thin: ± 0.023 K)
- Local changes of the alloys at the junction (minimised by cold joining)
- Material of wires and terminals of the ice point reference (included in calibration of the thick thermocouples)
- Temperature difference between different channels of the compensation box (± 0.005 K)

The total uncertainty is estimated by quadrature addition. For the thick thermocouples connected to the ice point reference follows:

$$\delta_{thick} = \sqrt{0.075^2 + 0.02^2 + 0.028^2} = 0.083\,\mathrm{K}$$

And for the thin thermocouples connected to the compensation box:

$$\delta_{thin} = \sqrt{0.075^2 + 0.02^2 + 0.028^2 + 0.005^2 + 0.023^2} = 0.086\,\mathrm{K}$$

When measuring air or surface temperatures the accuracy is also affected by radiation from surrounding surfaces.

To give an impression of the accuracy achieved, Figure 23 shows the temperatures measured in 5 different layers of the ceiling element 30 minutes before and after night-time ventilation was started. Before the experiment was started the difference between the internal (A) and the external (E) surface of the ceiling element is about 0.1 K. The results from the sensors in the intermediate layers (B C and D) lie in between and form a reasonable gradient.

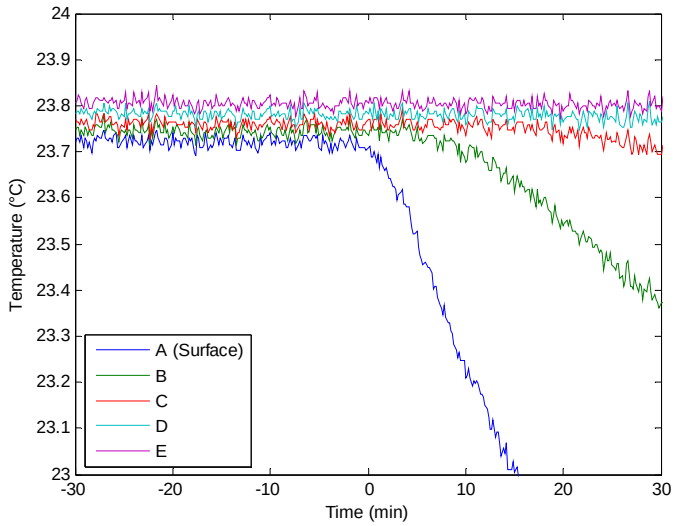

Figure 23. Temperatures measured in 5 different layers of the ceiling element 30 minutes before and after night-time ventilation was started.

References

[1] http://en.wikipedia.org/wiki/Thermocouple

[2] KAYE Instruments. Thermocouple Reference Systems. KAYE INSTRUMENTS, INC., 15 De Angelo Drive, Bedford, Massachusetts, US

[3] Matlab. The language of technical computing. Copyright 1984-2007, The MathWorks, Inc.

Night-time ventilation experiments

Setup, data evaluation and uncertainty assessment

N. Artmann
R. L. Jensen

ISSN 1901-726X
DCE Technical Report No. 053

AALBORG UNIVERSITY
Department of Civil Engineering

Aalborg University
Department of Civil Engineering
Indoor Environmental Engineering Research Group

DCE Technical Report No. 053

Night-time ventilation experiments

Setup, data evaluation and uncertainty assessment

by

N. Artmann
R. L. Jensen

October 2008

Scientific Publications at the Department of Civil Engineering

Technical Reports are published for timely dissemination of research results and scientific work carried out at the Department of Civil Engineering (DCE) at Aalborg University. This medium allows publication of more detailed explanations and results than typically allowed in scientific journals.

Technical Memoranda are produced to enable the preliminary dissemination of scientific work by the personnel of the DCE where such release is deemed to be appropriate. Documents of this kind may be incomplete or temporary versions of papers—or part of continuing work. This should be kept in mind when references are given to publications of this kind.

Contract Reports are produced to report scientific work carried out under contract. Publications of this kind contain confidential matter and are reserved for the sponsors and the DCE. Therefore, Contract Reports are generally not available for public circulation.

Lecture Notes contain material produced by the lecturers at the DCE for educational purposes. This may be scientific notes, lecture books, example problems or manuals for laboratory work, or computer programs developed at the DCE.

Theses are monograms or collections of papers published to report the scientific work carried out at the DCE to obtain a degree as either PhD or Doctor of Technology. The thesis is publicly available after the defence of the degree.

Latest News is published to enable rapid communication of information about scientific work carried out at the DCE. This includes the status of research projects, developments in the laboratories, information about collaborative work and recent research results.

Published 2008 by
Aalborg University
Department of Civil Engineering
Sohngaardsholmsvej 57,
DK-9000 Aalborg, Denmark

Printed in Aalborg at Aalborg University

ISSN 1901-726X
DCE Technical Report No. 053

Table of contents

Setup of the test room

Originally, 'DET LILLE HUS PÅ PRÆRIEN' (Figure 1 to Figure 3) was a wooden construction insulated with 100 mm rock wool. The internal surfaces were covered with 19 mm plywood. Externally the walls were covered with 16 mm wooden boards and the roof with 22 mm plywood. In previous experiments the chamber was used to simulate a room with an external facade. Therefore a small part was separated to simulate the outdoor climate. The separation wall was insulated with 240 mm rock wool and covered with 12 mm chipboards on both sides.

For a previous PhD study on night time ventilation by Jensen [1] a massive ceiling element made of 7 layers of 12.5 mm gypsum boards was installed. For additional insulation, a layer of 50 mm rock wool between wooden beams was placed between the ceiling element and the former roof. In total 110 thermocouples were installed in 5 different layers of the ceiling element.

For the experiments described here, additional insulation was installed at the internal surfaces in order to improve the boundary conditions. The insulation was installed in 3 layers, so that sensors could be placed in-between. The total thickness of the insulation made of expanded polystyrene (EPS) was 160 mm (30 + 30 + 100) at the walls and 230 mm (100 + 30 + 100) at the floor. Along the edge of the ceiling the gypsum boards were cut, so that the new insulation could be extended to the rock wool layer (Figure 3).

After installation of the insulation the internal dimensions were 2.64 m x 3.17 m x 2.93 m (width x length x height) resulting in a volume of 24.52 m^3.

Figure 1. The test room 'DET LILLE HUS PÅ PRÆRIEN'

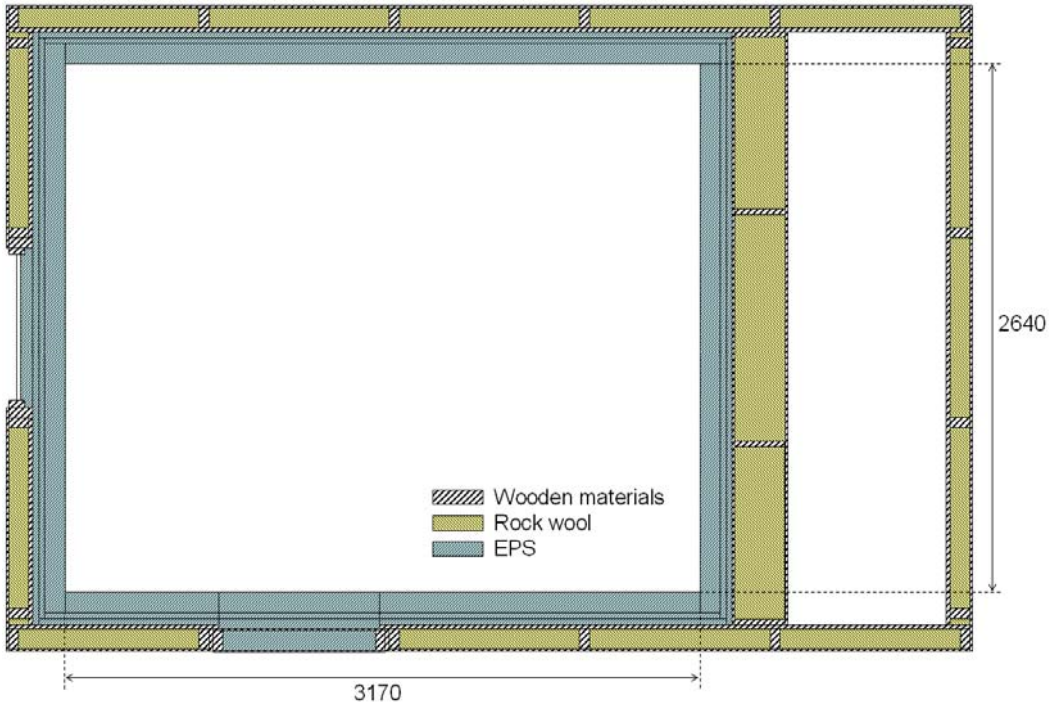

Figure 2. Plan view of the test room.

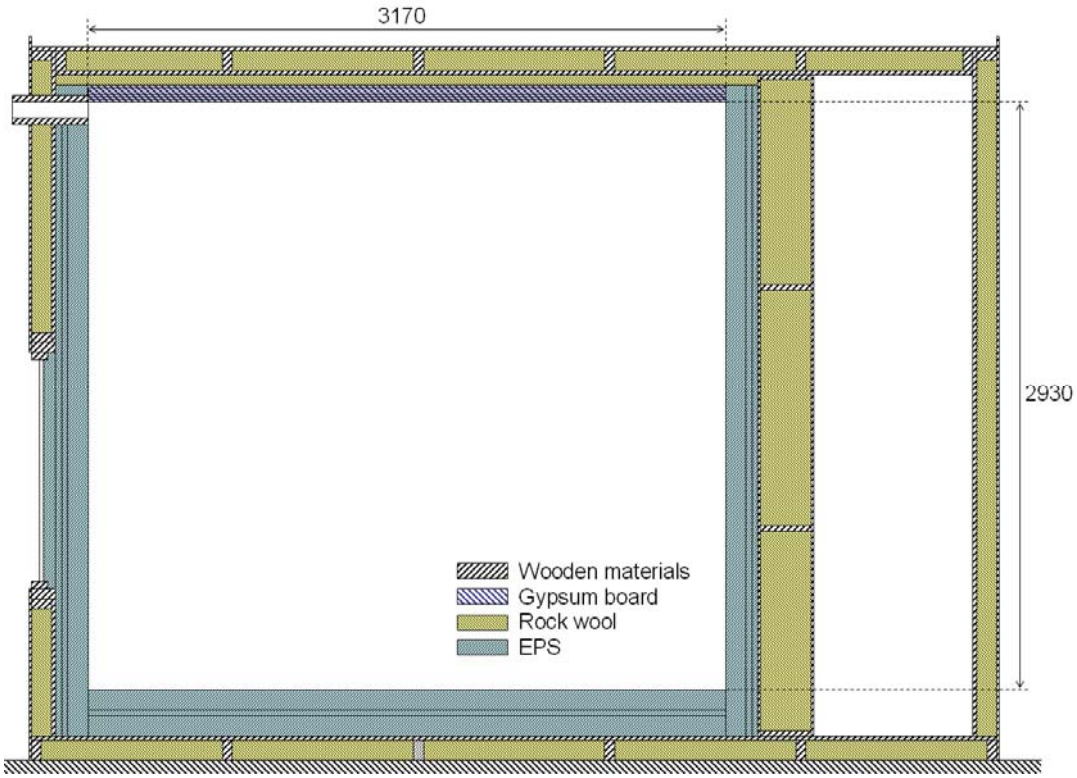

Figure 3. Vertical section of the test room

Ventilation system

A mechanical ventilation system was installed to supply air at a defined temperature to the test room. A schematic diagram of the ventilation system is shown in Figure 4. Air is taken from the lab and flows through

a filter and two heat exchangers for cooling and heating. The heating and cooling power is controlled by motor-operated valves and a PID controller. The temperature sensor for the controller is placed after the fan. The fan speed can be controlled by a frequency transformer to set the air flow rate. The ventilation system was capable of providing an air flow rate of about 56 - 330 m^3/h, corresponding to 2.3 - 13 air changes per hour (ACH).

In order to obtain stable supply air conditions at the beginning of an experiment, a bypass valve was installed. By switching the bypass valve, ventilation of the test room can be started without changing the air flow rate through the air conditioning unit. In order to achieve the same flow rate through the bypass and the test room, the resistance of the bypass was adjusted by a control valve at the end of the bypass. Orifices for measuring the flow rate were installed in the supply air pipe to the test room and in the bypass. The pressure difference over the orifice was measured using a micro-manometer. Two different orifices with 100 mm and 160 mm diameter were used for low and high airflow rates, respectively. The accuracy of the air flow measurement was about ± 5 %.

Another fan with variable speed was installed in the exhaust pipe. To prevent air from flowing through leakages into the test room, the speed of the exhaust fan was adjusted aiming a very small overpressure (0.1 Pa) in the test room.

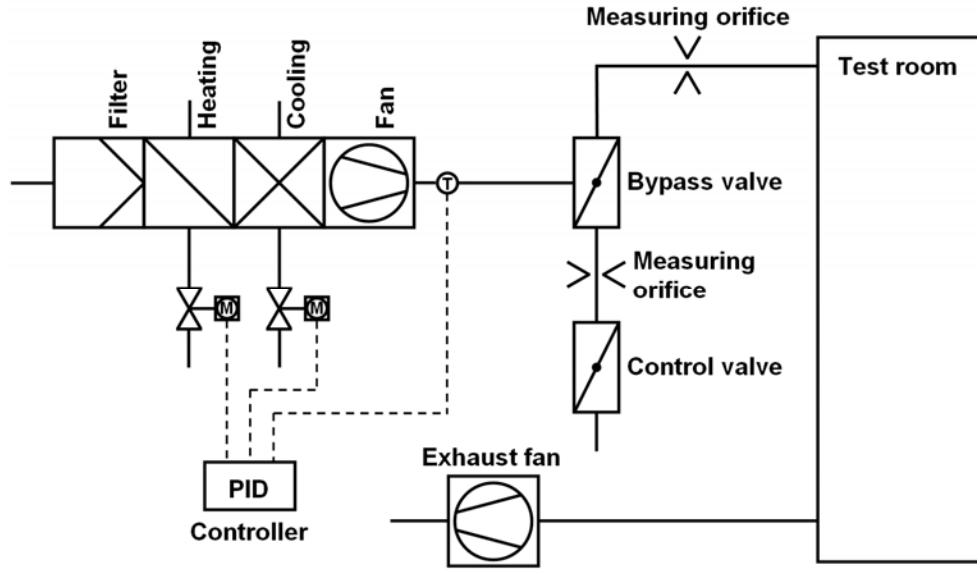

Figure 4. Schematic diagram of the ventilation system.

Two different configurations of the air in- and outlet openings of the test room representing mixing and displacement ventilation were investigated (Figure 5). In case of mixing ventilation, the air inlet to the test room was a rectangular opening of 830 mm width and 80 mm height located directly below the ceiling (Figure 6). To obtain a uniform velocity profile, two fleece filters were placed approximately 25 and 35 cm before the opening. For the air outlet there were two circular openings of 110 mm close to the floor.

For displacement ventilation the same rectangular opening below the ceiling was used as outlet and a semicircular displacement inlet device was placed at the floor on the same side of the test room (Figure 7).

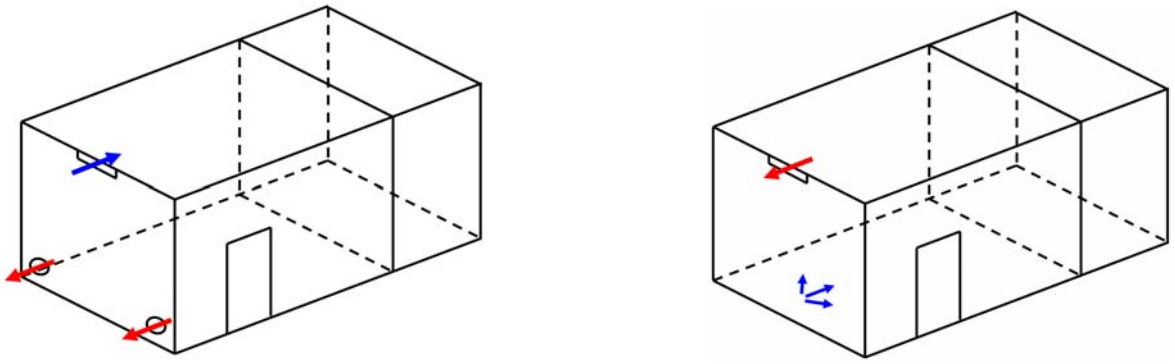

Figure 5. Configurations of the air in- and outlet openings of the test room for mixing (left) and displacement (right) ventilation

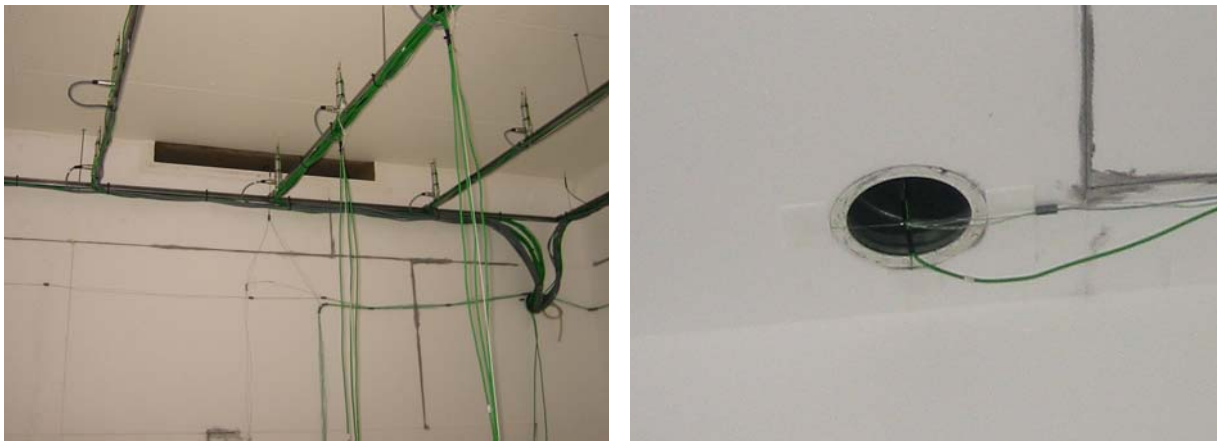

Figure 6. Ventilation openings. Left: Opening used as air inlet for mixing ventilation and outlet for displacement ventilation. Right: Outlet opening for mixing ventilation.

Figure 7. Inlet device for displacement ventilation.

Material properties

The thermal properties of the materials used at the internal surfaces of the test room are important for the data evaluation. The thermal conductivity, λ, the specific heat capacity, c and the density, ρ of the gypsum boards (Gyproc Gulvplank) used for the ceiling element were measured at Empa (Swiss federal laboratories

for materials testing and research). The thermal conductivity, λ and the density, ρ of the EPS (Sundolitt S80) used at the walls and the floor were also measured at Empa. For the specific heat capacity, *c* of the EPS the value given in the European standard EN 12524 [2] was used.

For the calculation of the radiative heat flows between the internal surfaces the emissivities need to be known. The ceiling was painted with white paint. The emissivity, ε of a sample painted with the same paint was measured at Empa using a calorimetric method. Because of the low thermal conductivity and the partial transparency the calorimetric method did not work for EPS. Therefore the emissivity of EPS was measured at ZAE Bayern using a Fourier-Transformation-InfraRed (FTIR) spectrometer and an integrating sphere [3].

The material properties including uncertainties are summarised in Table 1.

For the determination of the air flow rate the density of the air was calculated according to the temperature and the humidity in the lab and the atmospheric pressure. The heat capacity of the air was assumed to be constant, c_{Air} = 1005 J/kgK.

Table 1. Properties of the materials used at the internal surfaces of the test room.

	λ (W/mK)	ρ (kg/m^3)	c (J/kgK)	ε (-)
Gypsum board	0.28 ± 0.01	1127 ± 10	1006 ± 100	-
Expanded polysteren (EPS)	0.037 ± 0.001	16.0 ± 0.1	1450 ± 100	0.73 ± 5%
White paint (Ceiling)	-	-	-	0.90 ± 5%

Measurement instrumentation and location of sensors

For temperature measurements two Fluke Helios Plus 2287A data loggers with 100 channels each and one Grant Squirrel 2040 data logger with 32 channels were used. The setup of the Helios data loggers using 178 channels for temperature measurement and 17 channels for temperature difference measurement is described in detail in [4]. The accuracy of the measurement system using the Helios data loggers was estimated to be ± 0.086 K [4]. The accuracy of the Grant Squirrel 2040 for temperature measurements using type K thermocouples is given as ± 1.4 K [5]. All thermocouples needed for the data evaluation were connected to the more accurate Helios system (sensor configuration see Table A1). The Squirrel data logger was used to monitor the inlet air temperature, and the boundary conditions (sensor configuration see Table A2). The Helios and the Squirrel data loggers were configured to record temperatures at a sampling rate of 0.1 Hz.

For air flow velocity measurements a Dantec 54N10 Multichannel Flow Analyzer with 18 hot sphere anemometers was used. The anemometers were calibrated for horizontal flow in the range from 0 to 1 m/s. Velocity measurements were integrated over 120 s with 30 s pause between integration periods.

The ceiling was divided into 22 sections (Figure 8). Originally the sensors were placed in the centre of each section. Although this symmetry was broken after cutting the gypsum boards and installing the EPS, the size of the sections was still determined as shown in Figure 8. At each of the 22 positions 5 thermocouples were installed in different layers, totalling 110 thermocouples. Additional thermocouples were installed 30 mm below the ceiling to measure the local air temperature (Figure 9).

The anemometers were installed 30 mm below the ceiling at the same positions as the temperature sensors. As only 18 anemometers were available, no velocity sensors were installed at positions 1, 5, 6 and 10

(Figure 8). In order not to disturb the air flow measurements, the thermocouples for the air temperature measurement were installed in the back of the anemometers (Figure 10).

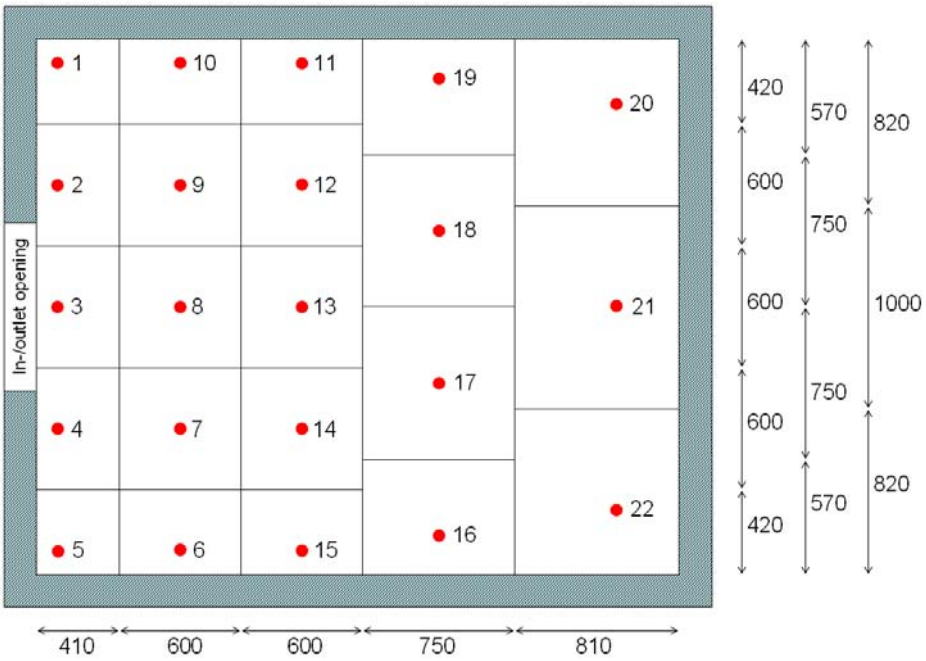

Figure 8. Subdivision of the ceiling into 22 sections and location of sensors (top view).

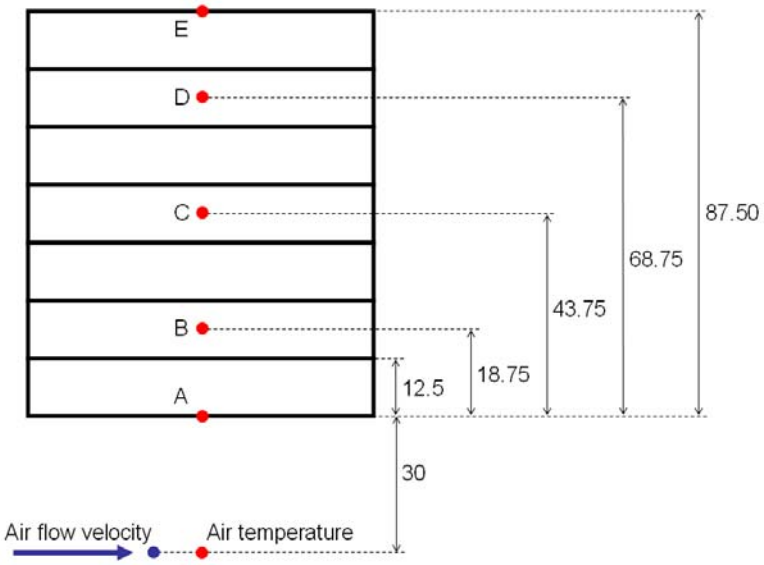

Figure 9. Vertical section of the ceiling element indicating the location of thermocouples for measuring the temperature in different layers (A - E) and the local air temperature; anemometer for air flow velocity measurement.

Figure 10. Anemometer and thermocouples for local air and ceiling surface temperature measurement.

The walls and the floor were divided into 3 sections each, and sensors were located in the centre of each section (Figure 11). At each position one thermocouple connected to the Squirrel data logger was installed at the internal surface of the plywood board. Then the first layer of insulation (walls: 30 mm, floor: 100 mm) was installed. The temperature difference over the second layer of EPS (30 mm) was measured with thermopiles made of 4 thermocouples (Figure 13, left). The temperature difference was used to calculate the heat flow through the walls and the floor. At all positions indicated in Figure 11 additional thermocouples were installed to measure the internal surface and the local air temperature at a distance of 30 mm from the surface (Figure 13, right).

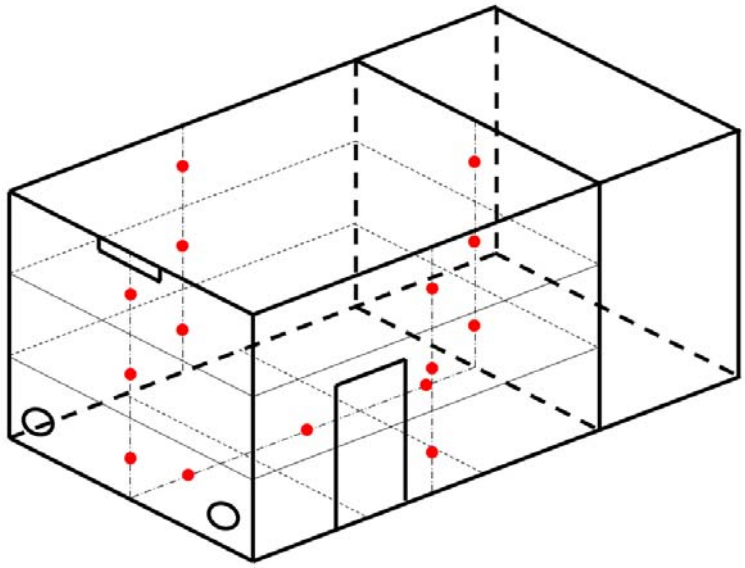

Figure 11. Subdivision of the walls and the floor into 3 sections and location of sensors.

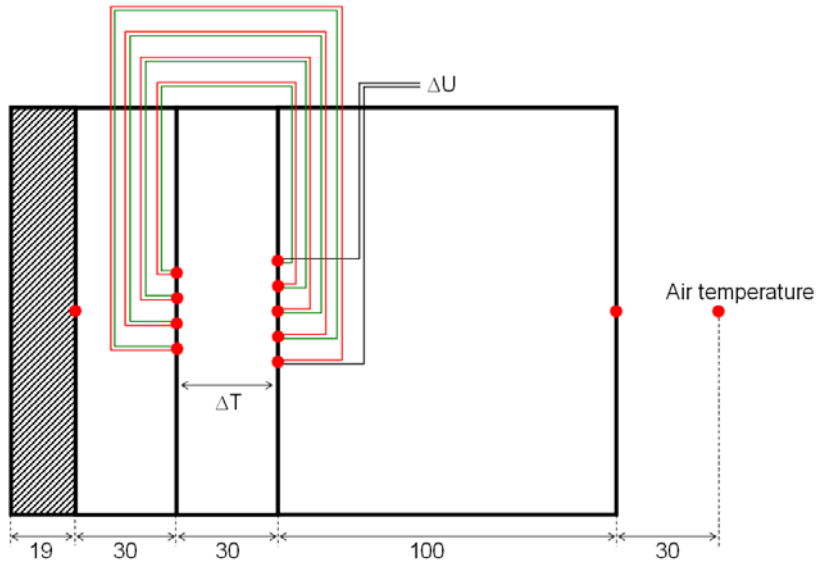

Figure 12. Location of thermocouples in different layers of the walls; thermopile for temperature difference (heat flow) measurement.

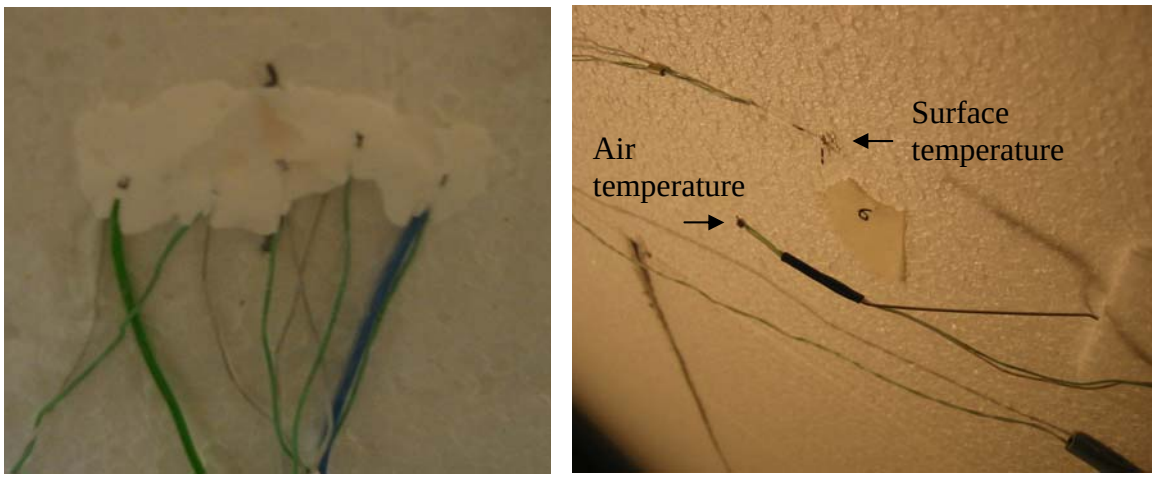

Figure 13. Internal junctions of the thermopile used for temperature difference measurement (left). Thermocouples for wall surface and local air temperature measurements (right).

To measure the air temperature distribution in the room 3 columns of thermocouples were installed in the vertical central plane. The columns were located below the 2nd, 3rd and 4th row of sensors at the ceiling, i.e. positions 8, 13, and between 17 and 18 (Figure 8). In these columns thermocouples were at heights 0.1, 1.1, 1.7, 2.6 and 2.9 m above the floor (Figure 14). The height 2.9 m above the floor is equal to 30 mm below the ceiling (sensors for local air temperature at the ceiling).

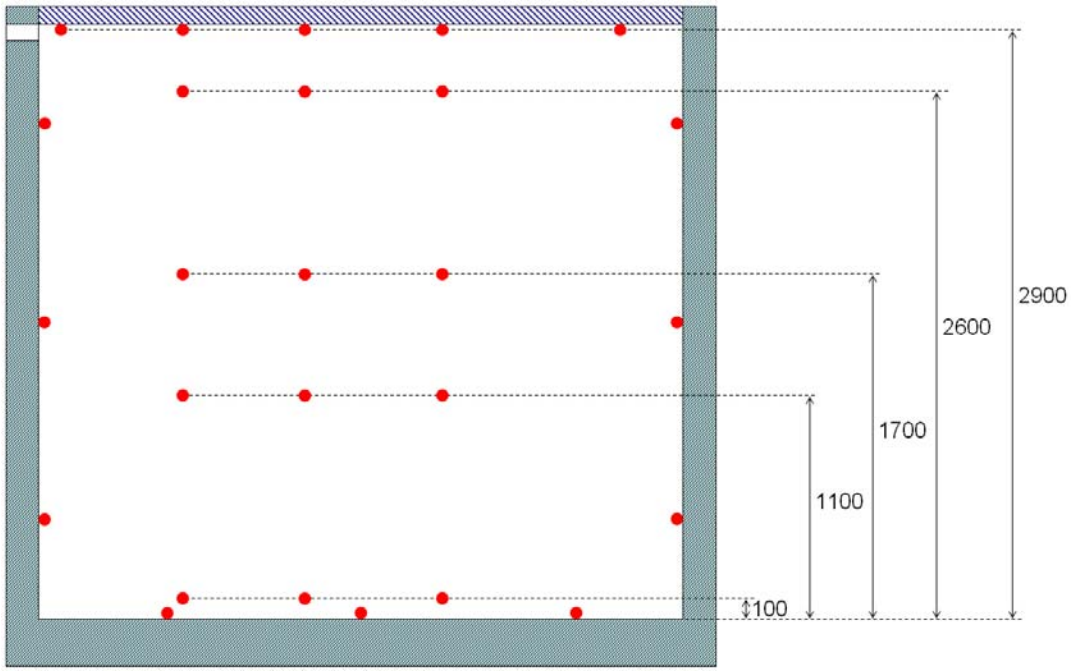

Figure 14. Thermocouples for air temperature measurements in the vertical central plane

For determination of the total heat flow removed from the test room by ventilation, the inlet and outlet air temperatures were measured. In case of mixing ventilation, sensors were placed in the centre of the inlet and both outlet openings (Figure 15). For higher accuracy, additionally, the temperature differences between the in- and outlet openings were measured using thermopiles made of 2 thermocouples. In case of displacement ventilation the sensors for the inlet air temperature measurement were installed where the pipe enters the room and in the inlet device (Figure 7). The outlet air temperature was measured using the same sensor as for the inlet during mixing ventilation (Figure 15, left).

Figure 15. Thermocouples for measuring inlet (left) and outlet (right) temperatures during mixing ventilation.

Procedure for experiments

In each experiment the response of the test room to a step in the air flow rate (inflow temperature below room temperature) was measured for at least 12 hours. In total 16 experiments with different ventilation modes, air change rates (*ACR*) and initial temperature differences (ΔT_0) were conducted (Table 2). The

experiments were started with the test room having a homogeneous temperature equal to the lab temperature. In order to obtain stable supply air conditions and a homogeneous temperature in the test room at the beginning of the experiment, the settings of the ventilation system (supply fan, exhaust fan, inflow set point, chiller set point) were adjusted about 36 hours before the experiment was started. During these 36 hours the air was piped through the bypass. The experiment was then started by switching the bypass valve to the test room. Because of the thermal mass of the pipe between the bypass valve and the test room, it still took some time until the temperature measured at the inlet was constant (cf. Figure 16). The initial temperature difference, ΔT_0 was therefore defined as the difference between the mean temperature of the ceiling element and the mean inlet air temperature measured during the last 10 hours of the experiment.

Table 2. List of experiments.

No	Ventilation mode	ACR (ACH)	ΔT_0 (K)	File No
1	Mixing ventilation	2.3	7.9	016
2	Mixing ventilation	3.3	4.3	014
3	Mixing ventilation	3.3	10.2	015
4	Mixing ventilation	6.7	2.9	010
5	Mixing ventilation	6.8	6.1	008
6	Mixing ventilation	6.6	8.9	006
7	Mixing ventilation	13.1	2.9	011
8	Mixing ventilation	13.2	4.0	009
9	Mixing ventilation	13.1	5.3	007
10	Mixing ventilation	13.3	9.2	002
11	Displacement ventilation	3.1	10.1	017
12	Displacement ventilation	6.7	5.8	019
13	Displacement ventilation	6.7	11.3	018
14	Displacement ventilation	12.6	3.6	022
15	Displacement ventilation	12.6	6.0	021
16	Displacement ventilation	12.7	12.7	020

Data evaluation

For the evaluation of the heat transfer at the internal room surfaces, first the total surface heat flow (conduction in the material) for each section was calculated from the measured temperatures. Also the radiative heat flow between the surfaces was calculated from the measured surface temperatures. The difference between conduction and radiation then yielded the convective heat flow.

By way of example, Figure 16 shows the measured temperatures of the inlet air and for position 8, the local air and 5 different layers of the ceiling. For the calculation of the conduction, the temperatures measured at the internal and external surface were used as boundary condition for a transient 1-dimensional finite difference model using an explicit scheme. To reduce the noise in the measurement signals the moving average of 15 values (2.5 minutes) was applied. Running the model resulted in the spatial temperature profile for each time step. For each section, *i* the conductive heat flux, $\dot{q}_{cond,i}$ at the surface was calculated from the temperature gradient.

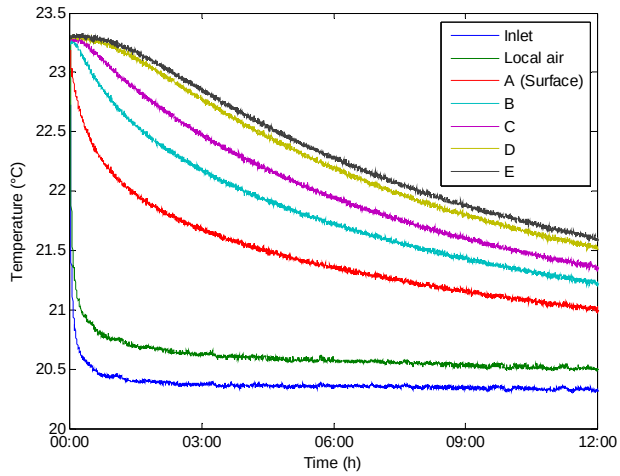

Figure 16. Temperatures measured at position 8 during experiment no. 4 with mixing ventilation with 6.7 ACH and an initial temperature difference of ΔT_0 = 2.9 K (A-E: 5 different layers of the ceiling).

The heat flows through the walls and the floor were calculated from the measured temperature difference over a 30 mm layer of EPS. In order to account for the thermal mass of the EPS, the heat flow at the internal wall and floor surfaces was calculated using the same method as at the ceiling. Here the internal surface temperature and the external heat flow were used as boundary condition for the finite difference model.

For calculation of the radiative heat flows, the view factors $F_{i,j}$ between all 22 sections of the ceiling and 3 sections of each wall and the floor were determined according to [6]. The radiative heat flux $\dot{q}_{rad\,i}$ from the surface A_i was obtained as sum of the heat fluxes to all surfaces A_j applying the measured surface temperatures:

$$\dot{q}_{rad,i} = \sum_j \frac{\sigma \cdot \varepsilon_i \cdot \varepsilon_j \cdot F_{i,j}}{1-(1-\varepsilon_i)(1-\varepsilon_j)\cdot F_{i,j} \cdot F_{i,j}} \left(T_i^{\,4} - T_j^{\,4}\right)$$

Where $\sigma = 5.67 \cdot 10^{-8}\, W/\left(m^2 K^4\right)$ is the Stefan-Boltzmann constant, and ε_i and ε_j are the emissivities of the surfaces.

The convective heat flux, $\dot{q}_{conv,\,i}$ for each section, *i* was then obtained from the difference between the conductive and radiative heat fluxes. Figure 17 shows the convective heat flux for different sections of the ceiling. The conductive, radiative and convective heat fluxes were integrated over all 22 sections of the ceiling to obtain the total heat flows at the ceiling surface. The total conductive, radiative and convective heat flows at the ceiling surface are displayed in Figure 18.

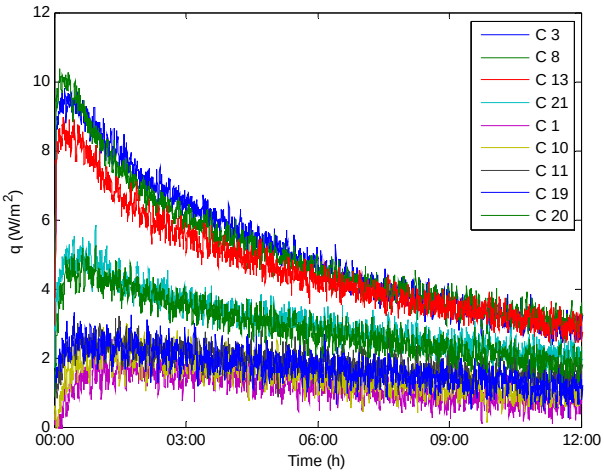

Figure 17. Convective heat flux for different sections of the ceiling during experiment no. 4 with mixing ventilation with 6.7 ACH and an initial temperature difference of ΔT_0 = 2.9 K.

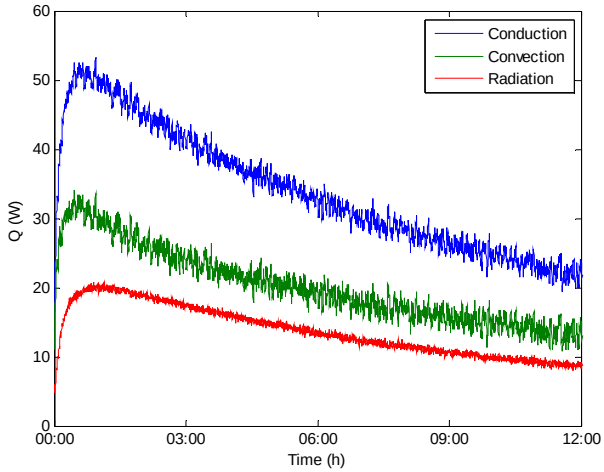

Figure 18. Total conductive, convective and radiative heat flows at the ceiling surface during experiment no. 4 with mixing ventilation with 6.7 ACH and an initial temperature difference of ΔT_0 = 2.9 K.

Integrating the convective heat flux over all room surfaces results in the total heat flow removed from the test room, $\dot{Q}_{conv,tot}$:

$$\dot{Q}_{conv,tot} = \sum_i A_i \cdot \dot{q}_{conv,i}$$

It should be noted, that the total convective heat flow, $\dot{Q}_{conv,tot}$ equals the total conductive heat flow, $\dot{Q}_{cond,tot}$, as by radiation heat is only transported from one surface to another ($\dot{Q}_{rad,tot} = 0$).

Alternatively, the total heat flow removed from the room can also be determined from the air flow rate, $\dot{V}_{Air}$, the density, ρ_{Air} , the heat capacity, $c_{p,Air}$ and the temperature difference between the in- and outflowing air.

$$\dot{Q}_{vent,tot} = \dot{V}_{Air} \cdot \rho_{Air} \cdot c_{p,Air} \cdot (T_{Outlet} - T_{Inlet})$$

Figure 19 compares the total heat flow obtained by the two different methods. The difference visible at the beginning of the experiment results from the thermal capacity of the air in the room. In the experiment shown in Figure 19, left the two methods are in very good agreement. In other cases a difference up to 18 % was found due to measurement uncertainties (Figure 19, right). It stands out, that in all experiments with mixing ventilation $\dot{Q}_{vent,\,tot}$ is larger than $\dot{Q}_{conv,\,tot}$, while in experiments with displacement ventilation $\dot{Q}_{vent,\,tot}$ is smaller than $\dot{Q}_{conv,\,tot}$ (excluding the first hour). Most probably this is due to a systematic error in the measurement of the temperature difference between the in- and outflowing air. The rectangular opening below the ceiling (and the temperature sensor placed in this opening) was used for the inlet air during mixing ventilation and for the outlet air during displacement ventilation. Accordingly the sensors used for the outlet air temperature during mixing ventilation were used for the inlet air during displacement ventilation. Therefore an error in this measurement might result in an increase in $\dot{Q}_{vent,\,tot}$ during mixing ventilation, but a decrease during displacement ventilation.

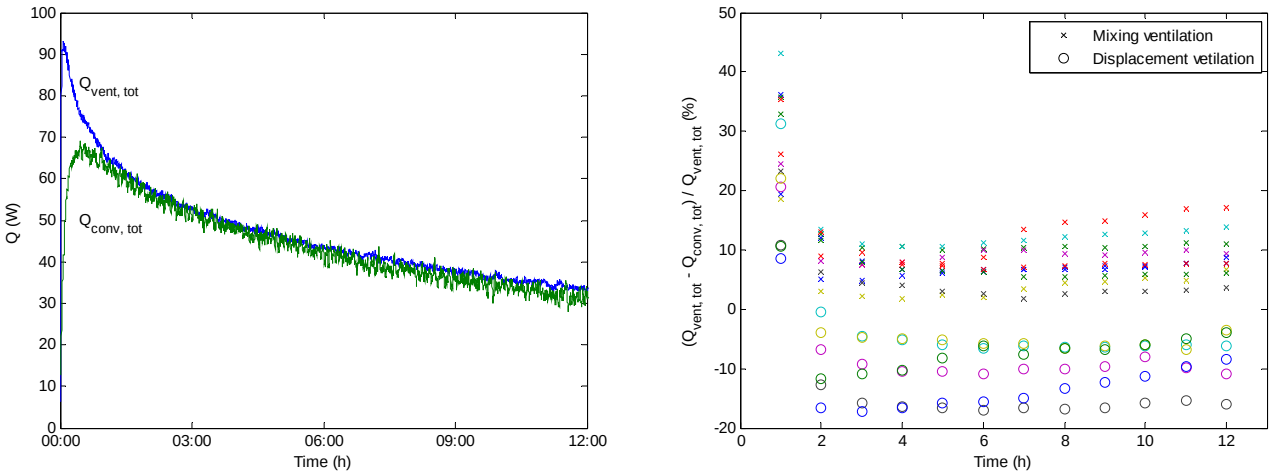

Figure 19. Total heat flow removed from the room obtained from direct measurements ($\dot{Q}_{vent,\,tot}$) and from integrating the convective heat flows over all surfaces ($\dot{Q}_{conv,\,tot}$); left: Heat flows during experiment no 4, mixing ventilation, ACR = 6.7 ACH, ΔT_0 = 2.9 K; right: Percentage of deviation, all experiments, hourly mean values.

Velocity measurements

In the first 5 experiments (no. 5, 6, 8, 9, 10 in Table 2) velocities were measured during the entire experiment. Later it turned out that the heat from the hot sphere anemometers affects the local air temperature measurements (see Figure 20). Therefore, in later experiments velocities were only measured during 10 minutes after the 12 hour measuring period.

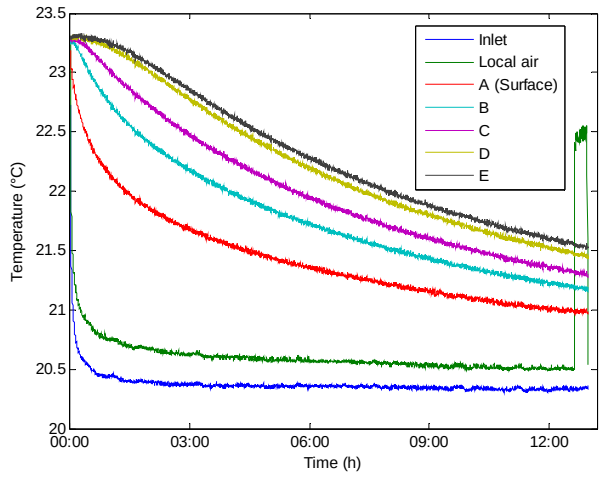

Figure 20. Increase in local air temperature during velocity measurement.

Figure 21 shows the velocities measured during experiment no. 5 with mixing ventilation with 6.8 ACH and an initial temperature difference of 6.1 K. The highest velocities occur in the centre line in front of the inlet opening (positions 3, 8, 13). The reason for the velocity at position 3 being lower than at position 8 is probably that the inlet temperature sensor partially shields the velocity sensor at position 3. The increase in the velocities at position 13 and 18 shows that the penetration of the jet changes as the room air temperature decreases. The velocity measurements also reveal that the air flow pattern is not symmetric. The velocity at position 18 is much higher than at position 17 and the velocity at position 20 is higher than at position 21. This indicates that the jet is directed to the left.

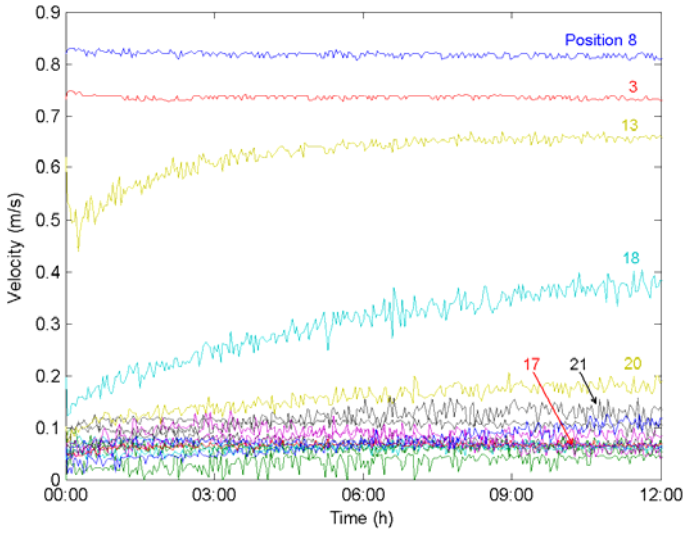

Figure 21. Velocities measured during experiment no. 5 with mixing ventilation with 6.8 ACH and an initial temperature difference of 6.1 K.

Uncertainty assessment

For each calculated quantity the uncertainty due to the uncertainty in each input parameter, *i* was calculated separately. Assuming that the uncertainties in each parameter are independent of each other, the total

uncertainty, δ was then calculated as the square root of the quadrature sum of the single uncertainties, δ_i (propagation of uncertainty):

$$\delta = \sqrt{\sum_i \delta_i^2}$$

The uncertainty in the conductive heat flux at the ceiling surfaces is estimated by variation of the input parameters of the finite difference model. Additionally to the uncertainty of the measurement equipment (± 0.086 K, [4]) the measurement of the surface temperature, *T* might be affected by radiation from other surfaces. At the ceiling this effect was assumed to be small, as the sensors were mounted before the ceiling was painted. The error was considered by adding an uncertainty depending on the radiative heat flux of ± 0.01 K/(W/m^2) (maximum ± 0.2 K for $q_{rad,max}$ = 20 W/m^2). The uncertainty in the thickness, *d* of the ceiling element was estimated as ± 3 mm and for the material properties the uncertainties given in Table 1 were used. Additionally uncertainties in the conductivity, λ and the volumetric heat capacity, ρc of the gypsum boards were considered (see Table 1).

Exemplarily, the results for two cases with a small and a high heat flux are shown in Figure 22. The cumulative distribution function of the uncertainty in the total heat flow from the ceiling during all experiments due to measurement errors is shown in Figure 23. During 95 % of the time, the uncertainty is below 10 %.

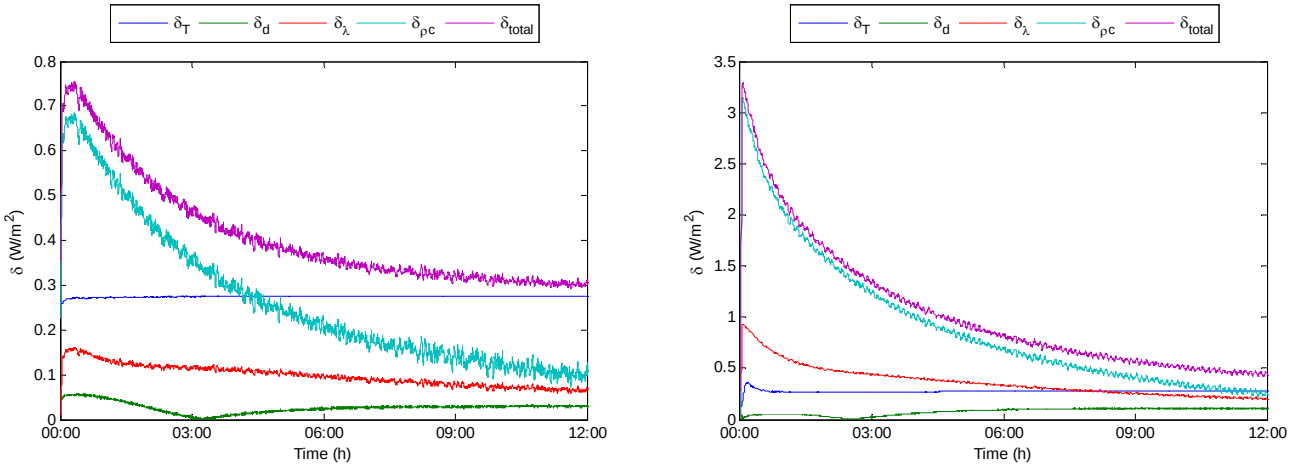

Figure 22. Uncertainty in the conductive heat flux at the ceiling due to different input parameters; left: small heat flux (experiment no. 4, position 8); right: high heat flux (experiment no. 10, position 8).

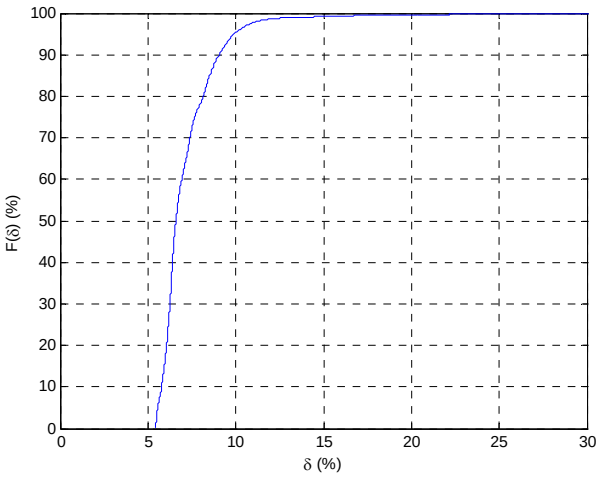

Figure 23. Cumulative distribution function of the uncertainty in the heat flux at the ceiling due to measurement errors.

An additional uncertainty is introduced by the integration of the heat flux over the ceiling surface. This error is largest for cases with an inhomogeneous heat flux, i.e. in cases with a jet flowing along the ceiling. In the base case the previously calculated heat flux at each measuring point was multiplied by the corresponding area as shown in Figure 8. This corresponds to a linear interpolation between the measuring points. To estimate the uncertainty, the profile in each row (positions 1 to 5, 6 to 10, 11 to 15, 16 to 19 and 20 to 22) was varied as shown in Figure 24 (left). For each section the minimum and maximum heat flux was calculated as follows:

$$\dot{q}_{\min,i} = \min\left(\frac{\dot{q}_{i-1}+\dot{q}_i}{2}, \dot{q}_i, \frac{\dot{q}_i+\dot{q}_{i+1}}{2}\right); \quad \dot{q}_{\max,i} = \max\left(\frac{\dot{q}_{i-1}+\dot{q}_i}{2}, \dot{q}_i, \frac{\dot{q}_i+\dot{q}_{i+1}}{2}\right)$$

The resulting uncertainty in the total conductive heat flux at the ceiling during experiment no. 10 is shown in Figure 24 (right). The uncertainty is largest in the beginning of the experiment and decreases as the heat flux becomes more homogeneous (cf. Figure 17). The cumulative distribution function of the uncertainty resulting from integrating the heat flux over the ceiling surface during all experiments is shown in Figure 25 (left). During 95 % of the time, the uncertainty is below ± 10 %.

For each time step the total uncertainty was calculated as the square root of the quadrature sum of the uncertainty due to measurement errors and the uncertainty resulting from the integration over the ceiling surface. The cumulative distribution function of the uncertainty in the total heat flow from the ceiling is shown in Figure 25 (right). During 95 % of the time, the uncertainty is below ± 13 %.

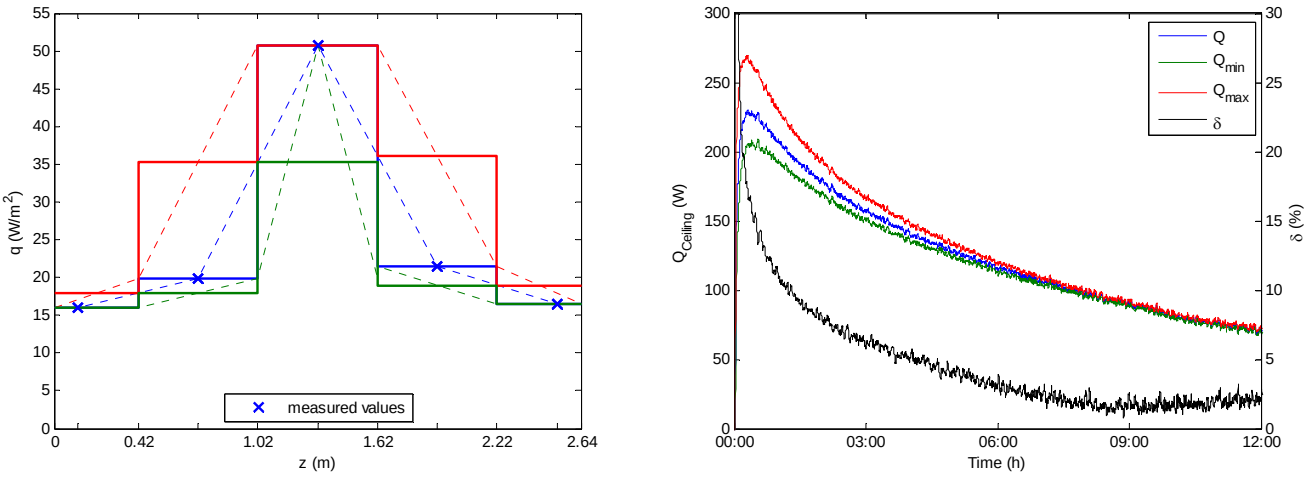

Figure 24. Uncertainty resulting from the integration of the heat flux over the ceiling surface; left: Different heat flux profiles (dotted lines give the same result as the step curves; congruent triangles); right: Resulting uncertainty in the total conductive heat flux at the ceiling during experiment no. 10.

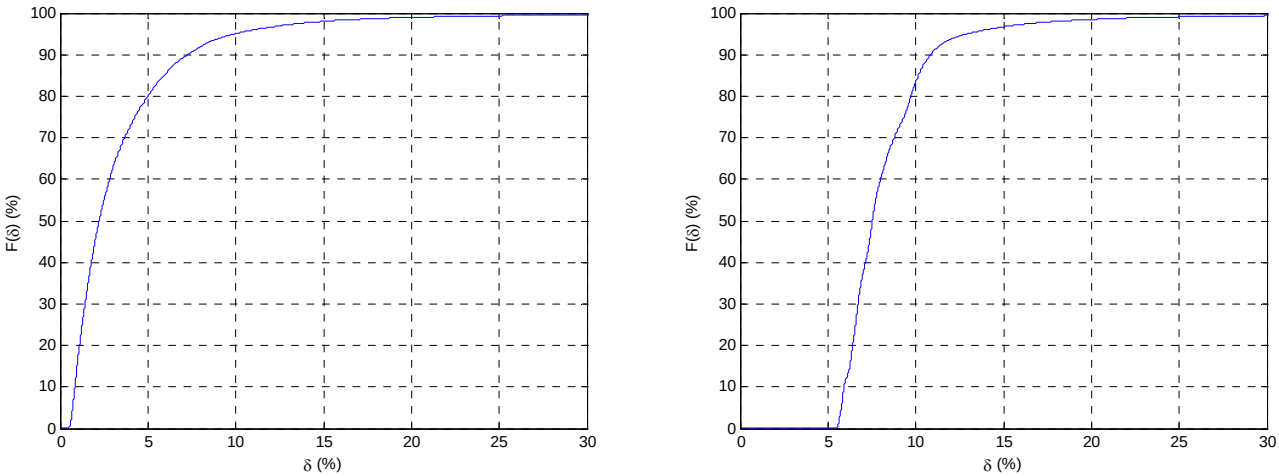

Figure 25. Cumulative distribution functions of the uncertainty resulting from integrating the heat flux over the ceiling surface (left) and the total uncertainty in the total heat flow from the ceiling (right).

Also the uncertainty in the conductive heat flux at the floor and wall surfaces was assessed by variation of the input parameters of the finite difference model. In this case the temperature at the internal surface and the heat flux at the external surface were used as boundary conditions. As the temperature difference ΔT, used to calculate the external heat flux, was measured with a thermopile made of 4 thermocouples, and radiation effects can be excluded, the uncertainty was estimated as ± 0.05 K. The uncertainty in the surface temperature, T_{Surf} due to radiation effects was assumed to be higher at the walls than at the ceiling. The error was considered by adding an uncertainty depending on the radiative heat flux of ± 0.042 K/(W/m^2) (maximum ± 0.5 K for $q_{rad,max}$ = 12 W/m^2). The uncertainty in the distance, d_1 between the two sensors measuring the temperature difference was estimated as ± 2 mm. The distance, d_2 was assumed to be 115 ± 15 mm (Figure 27). This also includes the uncertainty emerging from a non-linear temperature profile over d_1. The uncertainties in the conductivity, λ and the volumetric heat capacity, ρc of the EPS were assumed as given in Table 1.

Exemplarily, the results for two cases with a small and a high heat flux are shown in Figure 27. The cumulative distribution function of the uncertainty in the heat flow from the walls and the floor due to measurement errors is shown in Figure 28. Here in some cases a high relative uncertainty occurs due to small absolute heat flows. As the heat flows at the floor and walls are generally small compared to the heat flow from the ceiling, this uncertainty does not affect the total heat flow from the whole room too much. The uncertainty resulting from the integration of the heat flow over the floor and wall surfaces was estimated as ± 10 %.

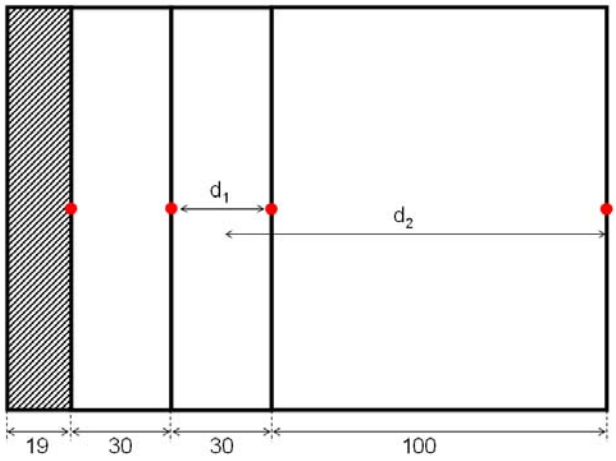

Figure 26. Distances d_1 and d_2 used for the calculation of the surface heat flux at the floor and walls.

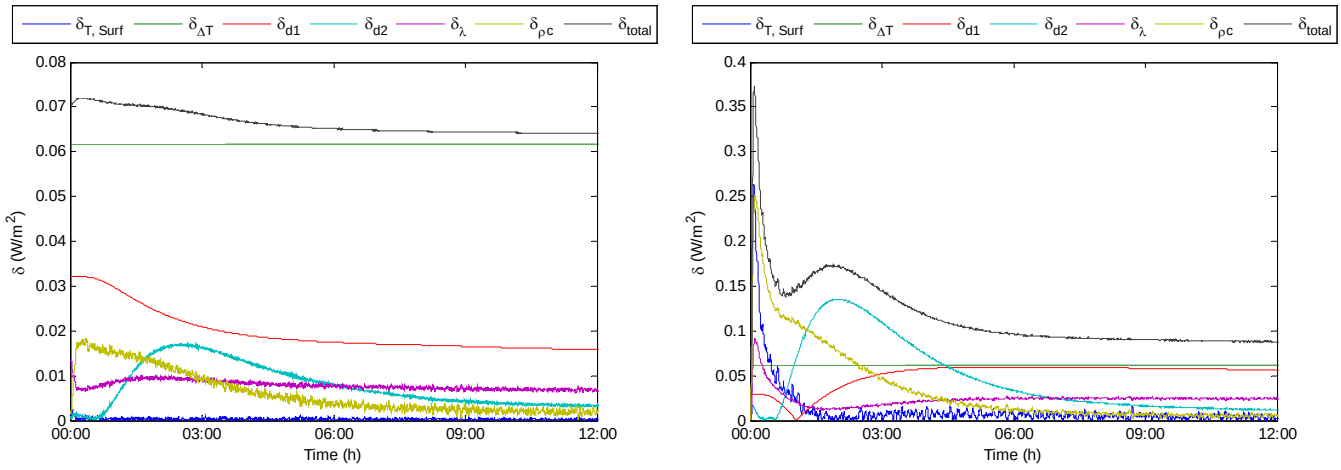

Figure 27. Uncertainty in the conductive heat flux at the floor due to different input parameters; left: small heat flux (experiment no. 4, central measuring point at the floor); right: high heat flux (experiment no. 16, central measuring point at the floor).

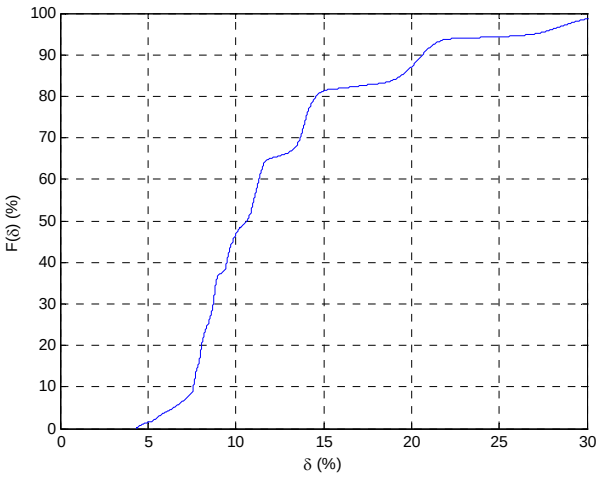

Figure 28. Cumulative distribution functions of the uncertainty in the conductive heat flux at the floor and wall surfaces due to measurement errors.

To assess the uncertainty in the total conductive heat flow at all room surfaces the absolute uncertainties in the heat flows at the ceiling and the other surfaces were summed up and put into relation to the total heat flow. The cumulative distribution function of the uncertainty in the total conductive heat flow from all room surfaces during all experiments is shown in Figure 29. During 95 % of the time, the uncertainty is below ± 16 %.

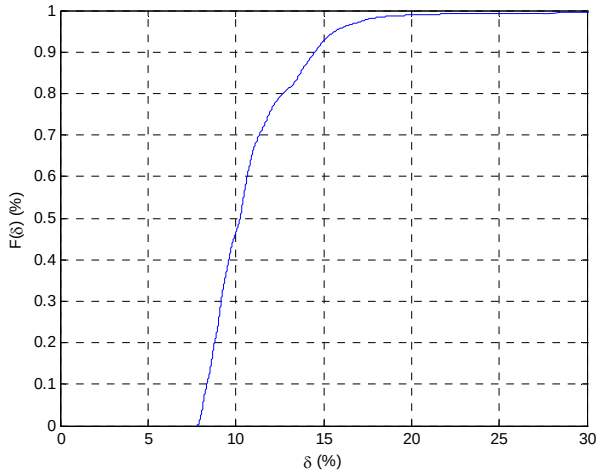

Figure 29. Cumulative distribution function of the uncertainty in the total conductive heat flow from all room surfaces.

For the calculation of the radiative heat flows it is assumed that the surface temperature is homogeneous in each section (22 sections at the ceiling and 3 sections at each wall and floor surface). To estimate the uncertainty introduced by this assumption, the error in averaging the ceiling surface temperature is assessed applying the same method as for the integration of the conduction heat flow (cf. Figure 24, left). The maximum error was ± 0.4 K corresponding to ± 5 % (relative to ΔT_0). The total uncertainty in the temperature difference was estimated as ± 10 %. The sensitivity of the radiative heat flow on uncertainties in the temperature difference and the emissivities (± 5 %) was assumed to be linear. The uncertainties in the

Stefan-Boltzmann constant and the geometric parameters were neglected. For the total uncertainty in the radiative heat flow follows:

$$\delta_{\dot{Q},rad} = \sqrt{\delta_{\varepsilon 1}{}^2 + \delta_{\varepsilon 2}{}^2 + \delta_{\Delta T}{}^2} = \sqrt{5^2 + 5^2 + 10^2} = \pm 12\%$$

As the sum of all radiative heat flows at all room surfaces is zero, the total convective heat flow from the room equals the total conductive heat flow and the uncertainty is also the same. The uncertainty in the convective heat flow from the ceiling was assessed as the square root of quadrature sum of the uncertainties in the conductive and radiative heat flows. The cumulative distribution functions of the absolute and relative uncertainty in the convective heat flow from the ceiling are shown in Figure 30. The calculation of the convective heat flow as difference between conduction and radiation, results in a high relative uncertainty (Figure 30, left). During 95 % of the time, the absolute uncertainty is below ± 2.2 W/m^2 (Figure 30, right).

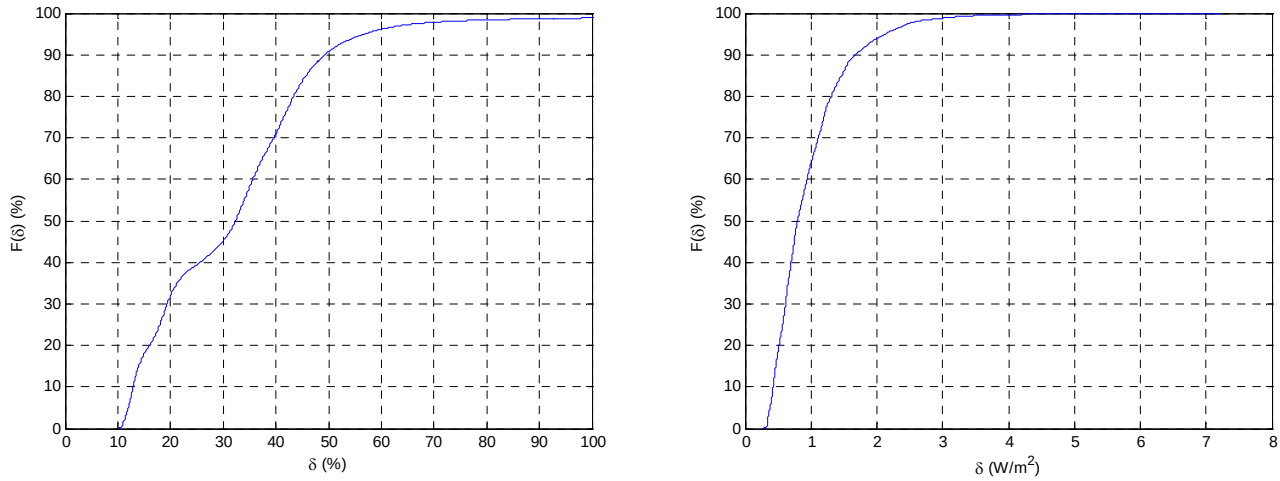

Figure 30. Cumulative distribution functions of the uncertainty in the mean convective heat flux from the ceiling; left: relative (%), right: absolute (W/m^2).

The ratio between the convective and the total heat flow from the ceiling, γ is defined as:

$$\gamma = \frac{\dot{Q}_{conv,Ceiling}}{\dot{Q}_{cond,Ceiling}} = 1 - \frac{\dot{Q}_{rad,Ceiling}}{\dot{Q}_{cond,Ceiling}}$$

The uncertainty in γ was calculated based on the uncertainties in $\dot{Q}_{rad,Ceiling}$ and $\dot{Q}_{cond,Ceiling}$. The cumulative distribution function of the absolute uncertainty in the convection ratio γ is shown in Figure 31. During 95 % of the time, the absolute uncertainty is below ± 0.11.

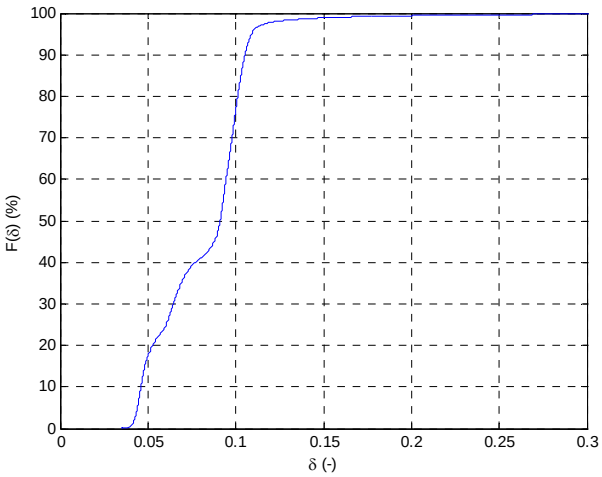

Figure 31. Cumulative distribution function of the absolute uncertainty in the convection ratio γ at the ceiling.

The total heat flow removed from the room was calculated based on the temperature difference between the in- and outflowing air and the air flow rate. The difference between the inlet and outlet air temperature was measured by a thermopile consisting of two thermocouples. Therefore the uncertainty is assumed to be dominated by radiation effects and was estimated as ± 10 %. The accuracy of the air flow measurement is given by the manufacturer of the orifice as ± 5 %. The uncertainties in the density and the thermal capacity of the air were estimated as ± 3 % and ± 1 %, respectively. For the uncertainty in the total heat flow removed by ventilation follows:

$$\delta_{\dot{Q},tot,vent} = \sqrt{\delta_{\dot{V},Air}{}^2 + \delta_{\rho,Air}{}^2 + \delta_{c_p,Air}{}^2 + \delta_{\Delta T}{}^2} = \sqrt{5^2 + 3^2 + 1^2 + 10^2} = \pm 12\,\%$$

The ventilation efficiency, η was defined as:

$$\eta = \frac{T_{Outlet} - T_{Inlet}}{\overline{T}_{Surface} - T_{Inlet}}$$

The uncertainty in the difference between the inlet and outlet air temperature was again estimated as ± 10 %. For the difference between the average room surface temperature and the inlet air temperature the uncertainty was estimated as ± 10 %. For the ventilation efficiency, η follows:

$$\delta_{\eta} = \sqrt{10^2 + 10^2} = \pm 14\,\%$$

Discussion and conclusion

A test room was equipped with temperature and air flow velocity sensors for a detailed analysis of heat transfer during night-time ventilation. Temperatures were measured at 22 points at the ceiling and at 3 points at each wall and floor surface. From the measured temperatures surface heat flows were calculated using a 1-dimensional finite difference model. The uncertainty in the conductive heat flow at the ceiling due to measurement errors was estimated as ± 10 %.

Additional uncertainty in the same order of magnitude is introduced by the integration of the heat flow over the ceiling surface (22 sections). Alternatively, a 3-dimensional finite difference model could be used to

determine the 3-dimensional temperature field in the ceiling element and thus the surface heat flow with a higher resolution. However, as the jet at the ceiling might cause a discontinuous surface temperature profile, the application of a 3-dimensional model is not expected to improve the accuracy significantly.

The radiative heat flows between different surfaces were determined from the measured surface temperatures. The difference between conduction and radiation then yielded the convective heat flow at each surface section. Integration over all surfaces results in the total heat flow discharged from the room.

The uncertainty in the total heat flow discharged from the room yielded from surface heat flow measurements was estimated as ± 16 %. The uncertainty in the heat flow resulting from in-/ outflowing air temperature and mass flow measurements was estimated as ± 12 %. Considering these uncertainties yielded overlapping uncertainty bands for all experiments.

Although there are considerable uncertainties, the presented method is regarded to be suitable to investigate surface heat transfer during night-time ventilation.

References

[1] Jensen R L. Modelling of natural ventilation and night cooling – by the Loop Equation Method. PhD-thesis, Aalborg University, Department of Civil Engineering, Hybrid Ventilation Centre, 2005 (in Danish).

[2] EN 12524:2000. Building materials and products - Hygrothermal properties - Tabulated design values. German version.

[3] Bavarian center for applied energy research (ZAE Bayern) Bestimmung des Emissionsgrades von einer EPS Probe. Report ZAE 2-0808-05, 2008 (in German).

[4] Artmann N, Vonbank R, Jensen R L. Temperature measurements using type K thermocouples and the Fluke Helios Plus 2287A data logger. Internal report, Aalborg University, 2008

[5] Grant Data Acquisition. Technical notes – Squirrel 2020 / 2040 Full Technical Specification and Accessories. Downloaded from http://www.grant.co.uk June 2008.

[6] Ehlert J R, Smith T F. View factors for perpendicular and parallel rectangular plates. Journal of thermophysics and heat transfer 1993, 7 (1), pp. 173-174.

Appendix

Table A1. Sensor configuration for Helios data loggers.

Logger	Channel	Inputblock		ch	Comp. Box		Cable Nr.	High	Low	Location
283	1	1	Isothermal	0	8A	A0	1A	brown	blue	Ceiling 1 A
283	2	1	Isothermal	1	8A	A1	1B	brown	blue	Ceiling 1 B
283	3	1	Isothermal	2	8A	A2	1C	brown	blue	Ceiling 1 C
283	4	1	Isothermal	3	8A	A3	1D	brown	blue	Ceiling 1 D
283	5	1	Isothermal	4	8A	A4	1E	brown	blue	Ceiling 1 E
283	6	1	Isothermal	5	8A	A5	2A	green	white	Ceiling 2 A
283	7	1	Isothermal	6	8A	A6	2B	green	white	Ceiling 2 B
283	8	1	Isothermal	7	8A	A7	2C	green	white	Ceiling 2 C
283	9	1	Isothermal	8	8A	A8	2D	green	white	Ceiling 2 D
283	10	1	Isothermal	9	8A	A9	2E	green	white	Ceiling 2 E
283	11	1	Isothermal	10	8B	B0	3A	brown	blue	Ceiling 3 A
283	12	1	Isothermal	11	8B	B1	3B	brown	blue	Ceiling 3 B
283	13	1	Isothermal	12	8B	B2	3C	brown	blue	Ceiling 3 C
283	14	1	Isothermal	13	8B	B3	3D	brown	blue	Ceiling 3 D
283	15	1	Isothermal	14	8B	B4	3E	brown	blue	Ceiling 3 E
283	16	1	Isothermal	15	8B	B5	4A	green	white	Ceiling 4 A
283	17	1	Isothermal	16	8B	B6	4B	green	white	Ceiling 4 B
283	18	1	Isothermal	17	8B	B7	4C	green	white	Ceiling 4 C
283	19	1	Isothermal	18	8B	B8	4D	green	white	Ceiling 4 D
283	20	1	Isothermal	19	8B	B9	4E	green	white	Ceiling 4 E
Logger	**Channel**	**Inputblock**		**ch**	**Comp. Box**		**Cable Nr.**	**High**	**Low**	**Location**
283	21	2	Isothermal	0	1A	A0	5A	brown	blue	Ceiling 5 A
283	22	2	Isothermal	1	1A	A1	5B	brown	blue	Ceiling 5 B
283	23	2	Isothermal	2	1A	A2	5C	brown	blue	Ceiling 5 C
283	24	2	Isothermal	3	1A	A3	5D	brown	blue	Ceiling 5 D
283	25	2	Isothermal	4	1A	A4	5E	brown	blue	Ceiling 5 E
283	26	2	Isothermal	5	1A	A5	6A	green	white	Ceiling 6 A
283	27	2	Isothermal	6	1A	A6	6B	green	white	Ceiling 6 B
283	28	2	Isothermal	7	1A	A7	6C	green	white	Ceiling 6 C
283	29	2	Isothermal	8	1A	A8	6D	green	white	Ceiling 6 D
283	30	2	Isothermal	9	1A	A9	6E	green	white	Ceiling 6 E
283	31	2	Isothermal	10	1B	B0	7A	green	white	Ceiling 7 A
283	32	2	Isothermal	11	1B	B1	7B	green	white	Ceiling 7 B
283	33	2	Isothermal	12	1B	B2	7C	green	white	Ceiling 7 C
283	34	2	Isothermal	13	1B	B3	7D	green	white	Ceiling 7 D
283	35	2	Isothermal	14	1B	B4	7E	green	white	Ceiling 7 E
283	36	2	Isothermal	15	1B	B5	8A	green	white	Ceiling 8 A
283	37	2	Isothermal	16	1B	B6	8B	green	white	Ceiling 8 B
283	38	2	Isothermal	17	1B	B7	8C	green	white	Ceiling 8 C
283	39	2	Isothermal	18	1B	B8	8D	green	white	Ceiling 8 D
283	40	2	Isothermal	19	1B	B9	8E	green	white	Ceiling 8 E
Logger	**Channel**	**Inputblock**		**ch**	**Comp. Box**		**Cable Nr.**	**High**	**Low**	**Location**
283	41	3	Isothermal	0	2A	A0	9A	green	white	Ceiling 9 A
283	42	3	Isothermal	1	2A	A1	9B	green	white	Ceiling 9 B
283	43	3	Isothermal	2	2A	A2	9C	green	white	Ceiling 9 C
283	44	3	Isothermal	3	2A	A3	9D	green	white	Ceiling 9 D
283	45	3	Isothermal	4	2A	A4	9E	green	white	Ceiling 9 E
283	46	3	Isothermal	5	2A	A5	10A	green	white	Ceiling 10 A
283	47	3	Isothermal	6	2A	A6	10B	green	white	Ceiling 10 B
283	48	3	Isothermal	7	2A	A7	10C	green	white	Ceiling 10 C
283	49	3	Isothermal	8	2A	A8	10D	green	white	Ceiling 10 D
283	50	3	Isothermal	9	2A	A9	10E	green	white	Ceiling 10 E
283	51	3	Isothermal	10	2B	B0	1	green	white	Surface Low X, bottom
283	52	3	Isothermal	11	2B	B1	2	green	white	Surface High X, bottom
283	53	3	Isothermal	12	2B	B2	3	green	white	Surface Low Z, bottom
283	54	3	Isothermal	13	2B	B3	4	green	white	Surface High Z, bottom
283	55	3	Isothermal	14	2B	B4	5	green	white	Surface Low X, centre
283	56	3	Isothermal	15	2B	B5	6	green	white	Surface High X, centre
283	57	3	Isothermal	16	2B	B6	7	green	white	Surface Low Z, centre
283	58	3	Isothermal	17	2B	B7	8	green	white	Surface High Z, centre
283	59	3	Isothermal	18	2B	B8	9	green	white	Surface Low X, top
283	60	3	Isothermal	19	2B	B9	10	green	white	Surface High X, top

Logger	Channel	Inputblock		ch	Comp. Box		Cable Nr.	High	Low	Location
283	61	4	Sullins	0	6B	B0	11	green	white	Surface Low Z, top
283	62	4	Sullins	1	6B	B1	12	green	white	Surface High Z, top
283	63	4	Sullins	2	6B	B2	13	green	white	Surface Floor, low x
283	64	4	Sullins	3	6B	B3	14	green	white	Surface Floor, centre
283	65	4	Sullins	4	6B	B4	15	green	white	Surface Floor, high x
283	66	4	Sullins	5	6B	B5	A1	green	white	Air Low X, bottom
283	67	4	Sullins	6	6B	B6	A2	green	white	Air High X, bottom
283	68	4	Sullins	7	6B	B7	A3	green	white	Air Low Z, bottom
283	69	4	Sullins	8	6B	B8	A4	green	white	Air High Z, bottom
283	70	4	Sullins	9	6B	B9	A5	green	white	Air Low X, centre
283	71	4	Sullins	10	7A	A0	A6	green	white	Air High X, centre
283	72	4	Sullins	11	7A	A1	A7	green	white	Air Low Z, centre
283	73	4	Sullins	12	7A	A2	A8	green	white	Air High Z, centre
283	74	4	Sullins	13	7A	A3	A9	green	white	Air Low X, top
283	75	4	Sullins	14	7A	A4	A10	green	white	Air High X, top
283	76	4	Sullins	15	7A	A5	A11	green	white	Air Low Z, top
283	77	4	Sullins	16	7A	A6	A12	green	white	Air High Z, top
283	78	4	Sullins	17	7A	A7	A13	green	white	Air Floor, low x
283	79	4	Sullins	18	7A	A8	A14	green	white	Air Floor, centre
283	80	4	Sullins	19	7A	A9	A15	green	white	Air Floor, high x
Logger	**Channel**	**Inputblock**		**ch**	**Comp. Box**		**Cable Nr.**	**High**	**Low**	**Location**
283	81	5	Voltage	0			1	blue	green	ΔT Low X, bottom
283	82	5	Voltage	1			2	blue	green	ΔT High X, bottom
283	83	5	Voltage	2			3	blue	green	ΔT Low Z, bottom
283	84	5	Voltage	3			4	blue	green	ΔT High Z, bottom
283	85	5	Voltage	4			5	yellow	orange	ΔT Low X, centre
283	86	5	Voltage	5			6	yellow	orange	ΔT High X, centre
283	87	5	Voltage	6			7	yellow	orange	ΔT Low Z, centre
283	88	5	Voltage	7			8	yellow	orange	ΔT High Z, centre
283	89	5	Voltage	8			9	red	brown	ΔT Low X, top
283	90	5	Voltage	9			10	red	brown	ΔT High X, top
283	91	5	Voltage	10			11	red	brown	ΔT Low Z, top
283	92	5	Voltage	11			12	red	brown	ΔT High Z, top
283	93	5	Voltage	12			13	blue	green	ΔT Floor, low x
283	94	5	Voltage	13			14	yellow	orange	ΔT Floor, centre
283	95	5	Voltage	14			15	red	brown	ΔT Floor, high x
283	96	5	Voltage	15			16	black	white	ΔT In- Outlet, low z
283	97	5	Voltage	16			17	grey	lilac	ΔT In- Outlet, high z
283	98	5	Voltage	17	7B	B0	In	green	white	Inlet
283	99	5	Voltage	18	7B	B1	43	red	green	Ice point 41
283	100	5	Voltage	19	7B	B2	44	red	green	Ice point 42
Logger	**Channel**	**Inputblock**		**ch**	**Comp. Box**		**Cable Nr.**	**High**	**Low**	**Location**
233	1	1	Isothermal	0	3A	A0	11A	green	white	Ceiling 11 A
233	2	1	Isothermal	1	3A	A1	11B	green	white	Ceiling 11 B
233	3	1	Isothermal	2	3A	A2	11C	green	white	Ceiling 11 C
233	4	1	Isothermal	3	3A	A3	11D	green	white	Ceiling 11 D
233	5	1	Isothermal	4	3A	A4	11E	green	white	Ceiling 11 E
233	6	1	Isothermal	5	3A	A5	12A	brown	blue	Ceiling 12 A
233	7	1	Isothermal	6	3A	A6	12B	brown	blue	Ceiling 12 B
233	8	1	Isothermal	7	3A	A7	12C	brown	blue	Ceiling 12 C
233	9	1	Isothermal	8	3A	A8	12D	brown	blue	Ceiling 12 D
233	10	1	Isothermal	9	3A	A9	12E	brown	blue	Ceiling 12 E
233	11	1	Isothermal	10	3B	B0	13A	brown	blue	Ceiling 13 A
233	12	1	Isothermal	11	3B	B1	13B	brown	blue	Ceiling 13 B
233	13	1	Isothermal	12	3B	B2	13C	brown	blue	Ceiling 13 C
233	14	1	Isothermal	13	3B	B3	13D	brown	blue	Ceiling 13 D
233	15	1	Isothermal	14	3B	B4	13E	brown	blue	Ceiling 13 E
233	16	1	Isothermal	15	3B	B5	14A	green	white	Ceiling 14 A
233	17	1	Isothermal	16	3B	B6	14B	brown	blue	Ceiling 14 B
233	18	1	Isothermal	17	3B	B7	14C	brown	blue	Ceiling 14 C
233	19	1	Isothermal	18	3B	B8	14D	brown	blue	Ceiling 14 D
233	20	1	Isothermal	19	3B	B9	14E	brown	blue	Ceiling 14 E

Logger	Channel	Inputblock		ch	Comp. Box		Cable Nr.	High	Low	Location
233	21	2	Isothermal	0	4A	A0	15A	green	white	Ceiling 15
233	22	2	Isothermal	1	4A	A1	15B	green	white	Ceiling 15
233	23	2	Isothermal	2	4A	A2	15C	green	white	Ceiling 15
233	24	2	Isothermal	3	4A	A3	15D	green	white	Ceiling 15
233	25	2	Isothermal	4	4A	A4	15E	green	white	Ceiling 15
233	26	2	Isothermal	5	4A	A5	16A	brown	blue	Ceiling 16
233	27	2	Isothermal	6	4A	A6	16B	brown	blue	Ceiling 16
233	28	2	Isothermal	7	4A	A7	16C	brown	blue	Ceiling 16
233	29	2	Isothermal	8	4A	A8	16D	brown	blue	Ceiling 16
233	30	2	Isothermal	9	4A	A9	16E	brown	blue	Ceiling 16
233	31	2	Isothermal	10	4B	B0	17A	brown	blue	Ceiling 17
233	32	2	Isothermal	11	4B	B1	17B	brown	blue	Ceiling 17
233	33	2	Isothermal	12	4B	B2	17C	brown	blue	Ceiling 17
233	34	2	Isothermal	13	4B	B3	17D	brown	blue	Ceiling 17
233	35	2	Isothermal	14	4B	B4	17E	brown	blue	Ceiling 17
233	36	2	Isothermal	15	4B	B5	18A	brown	blue	Ceiling 18
233	37	2	Isothermal	16	4B	B6	18B	brown	blue	Ceiling 18
233	38	2	Isothermal	17	4B	B7	18C	brown	blue	Ceiling 18
233	39	2	Isothermal	18	4B	B8	18D	brown	blue	Ceiling 18
233	40	2	Isothermal	19	4B	B9	18E	brown	blue	Ceiling 18
Logger	**Channel**	**Inputblock**		**ch**	**Comp. Box**		**Cable Nr.**	**High**	**Low**	**Location**
233	41	3	Isothermal	0	5A	A0	19A	brown	blue	Ceiling 19
233	42	3	Isothermal	1	5A	A1	19B	brown	blue	Ceiling 19
233	43	3	Isothermal	2	5A	A2	19C	brown	blue	Ceiling 19
233	44	3	Isothermal	3	5A	A3	19D	brown	blue	Ceiling 19
233	45	3	Isothermal	4	5A	A4	19E	brown	blue	Ceiling 19
233	46	3	Isothermal	5	5A	A5	20A	green	white	Ceiling 20
233	47	3	Isothermal	6	5A	A6	20B	green	white	Ceiling 20
233	48	3	Isothermal	7	5A	A7	20C	green	white	Ceiling 20
233	49	3	Isothermal	8	5A	A8	20D	green	white	Ceiling 20
233	50	3	Isothermal	9	5A	A9	20E	green	white	Ceiling 20
233	51	3	Isothermal	10	5B	B0	21A	brown	blue	Ceiling 21
233	52	3	Isothermal	11	5B	B1	21B	brown	blue	Ceiling 21
233	53	3	Isothermal	12	5B	B2	21C	brown	blue	Ceiling 21
233	54	3	Isothermal	13	5B	B3	21D	brown	blue	Ceiling 21
233	55	3	Isothermal	14	5B	B4	21E	brown	blue	Ceiling 21
233	56	3	Isothermal	15	5B	B5	22A	green	white	Ceiling 22
233	57	3	Isothermal	16	5B	B6	22B	green	white	Ceiling 22
233	58	3	Isothermal	17	5B	B7	22C	green	white	Ceiling 22
233	59	3	Isothermal	18	5B	B8	22D	green	white	Ceiling 22
233	60	3	Isothermal	19	5B	B9	22E	green	white	Ceiling 22
Logger	**Channel**	**Inputblock**		**ch**	**Comp. Box**		**Cable Nr.**	**High**	**Low**	**Location**
233	61	4	Isothermal	0	I. p. 1	1	1	red	green	Air Ceiling 1
233	62	4	Isothermal	1	I. p. 1	2	2	red	green	Air Ceiling 2
233	63	4	Isothermal	2	I. p. 1	3	3	red	green	Air Ceiling 3
233	64	4	Isothermal	3	I. p. 1	4	4	red	green	Air Ceiling 4
233	65	4	Isothermal	4	I. p. 1	5	5	red	green	Air Ceiling 5
233	66	4	Isothermal	5	I. p. 1	6	6	red	green	Air Ceiling 6
233	67	4	Isothermal	6	I. p. 1	7	7	red	green	Air Ceiling 7
233	68	4	Isothermal	7	I. p. 1	8	8	red	green	Air Ceiling 8
233	69	4	Isothermal	8	I. p. 1	9	9	red	green	Air Ceiling 9
233	70	4	Isothermal	9	I. p. 1	10	10	red	green	Air Ceiling 10
233	71	4	Isothermal	10	I. p. 2	11	11	red	green	Air Ceiling 11
233	72	4	Isothermal	11	I. p. 2	12	12	red	green	Air Ceiling 12
233	73	4	Isothermal	12	I. p. 2	13	13	red	green	Air Ceiling 13
233	74	4	Isothermal	13	I. p. 2	14	14	red	green	Air Ceiling 14
233	75	4	Isothermal	14	I. p. 2	15	15	red	green	Air Ceiling 15
233	76	4	Isothermal	15	I. p. 2	16	16	red	green	Air Ceiling 16
233	77	4	Isothermal	16	I. p. 2	17	17	red	green	Air Ceiling 17
233	78	4	Isothermal	17	I. p. 2	18	18	red	green	Air Ceiling 18
233	79	4	Isothermal	18	I. p. 2	19	19	red	green	Air Ceiling 19
233	80	4	Isothermal	19	I. p. 2	20	20	red	green	Air Ceiling 20

Logger	Channel	Inputblock		ch	Comp. Box		Cable Nr.	High	Low	Location
233	81	5	Isothermal	0	I. p. 3	21	21	red	green	Air Ceiling 21
233	82	5	Isothermal	1	I. p. 3	22	22	red	green	Air Ceiling 22
233	83	5	Isothermal	2	I. p. 3	23	23	red	green	Air A 0.1 m
233	84	5	Isothermal	3	I. p. 3	24	24	red	green	Air A 1.1 m
233	85	5	Isothermal	4	I. p. 3	25	25	red	green	Air A 1.7 m
233	86	5	Isothermal	5	I. p. 3	26	26	red	green	Air A 2.6 m
233	87	5	Isothermal	6	I. p. 3	27	27	red	green	Air B 0.1 m
233	88	5	Isothermal	7	I. p. 3	28	28	red	green	Air B 1.1 m
233	89	5	Isothermal	8	I. p. 3	29	29	red	green	Air B 1.7 m
233	90	5	Isothermal	9	I. p. 3	30	30	red	green	Air B 2.6 m
233	91	5	Isothermal	10	I. p. 4	31	31	red	green	Air C 0.1 m
233	92	5	Isothermal	11	I. p. 4	32	32	red	green	Air C 1.1 m
233	93	5	Isothermal	12	I. p. 4	33	33	red	green	Air C 1.7 m
233	94	5	Isothermal	13	I. p. 4	34	34	red	green	Air C 2.6 m
233	95	5	Isothermal	14	I. p. 4	35	35	red	green	Air C 2.9 m
233	96	5	Isothermal	15	I. p. 4	36	36	red	green	Outlet Low Z
233	97	5	Isothermal	16	I. p. 4	37	37	red	green	Outlet High Z
233	98	5	Isothermal	17	6A	A0	-			
233	99	5	Isothermal	18	6A	A1	43	red	green	Ice point 43
233	100	5	Isothermal	19	6A	A2	44	red	green	Ice point 44

Table A2. Sensor configuration for Grant Squirrel data logger.

Channel	Plug	Block	Pins	Type	Location	x (m) *	y (m) *	z (m) *
1	1	A	1-5	thin	Wall Low X, bottom	0.000	0.720	1.480
2	1	A	2-5	thin	Wall High X, bottom	3.490	0.720	1.480
3	1	A	3-5	thin	Wall Low Z, bottom	1.750	0.720	0.000
4	1	A	4-5	thin	Wall High Z, bottom	2.000	0.720	2.960
5	2	B	1-5	thin	Wall Low X, centre	0.000	1.700	1.480
6	2	B	2-5	thin	Wall High X, centre	3.490	1.700	1.480
7	2	B	3-5	thin	Wall Low Z, centre	1.750	1.700	0.000
8	2	B	4-5	thin	Wall High Z, centre	2.000	1.700	2.960
9	3	C	1-5	thin	Wall Low X, top	0.000	2.670	1.480
10	3	C	2-5	thin	Wall High X, top	3.490	2.670	1.480
11	3	C	3-5	thin	Wall Low Z, top	1.750	2.670	0.000
12	3	C	4-5	thin	Wall High Z, top	2.000	2.670	2.960
13	4	D	1-5	thin	Floor, low x	0.690	0.000	1.480
14	4	D	2-5	thin	Floor, centre	1.750	0.000	1.480
15	4	D	3-5	thin	Floor, high x	2.800	0.000	1.480
16	4	D	4-5	thin	Lab floor below house	1.470	-0.122	1.950
17	5	G	1-5	thick	Cold room, Wall, bottom	3.754	0.720	1.480
18	5	G	2-5	thick	Cold room, Wall, centre	3.764	1.700	1.480
19	5	G	3-5	thick	Cold room, Wall, top	3.764	2.670	1.480
20	5	G	4-5	thick	Cold room, Air	4.000	1.700	1.480
21	6	H	1-5	thick	Ext. wall Low X, bottom	-0.135	0.720	1.480
22	6	H	2-5	thick	Ext. wall Low X, centre	-0.135	1.700	1.480
23	6	H	3-5	thick	Ext. wall Low X, top	-0.135	2.670	1.480
24	6	H	4-5	thick	Ext. wall High Z, bottom	2.000	0.720	3.095
25	7	J	1-5	thick	Ext. wall High Z, centre	2.000	1.700	3.095
26	7	J	2-5	thick	Ext. wall High Z, top	2.000	2.670	3.095
27	7	J	3-5	thick	Ceiling, low x	0.690	3.439	1.480
28	7	J	4-5	thick	Ceiling, centre	1.750	3.439	1.480
29	8	K	1-5	thick	Ceiling, high x	2.800	3.439	1.480
30	8	K	2-5	thick	Lab air, bottom		0.720	
31	8	K	3-5	thick	Lab air, centre		1.700	
32	8	K	4-5	thick	Lab air, top		2.670	

* Coordinates from existing (before installation of EPS) internal wall surfaces, x from wall with inlet, y from floor, z from wall opposite door

ISSN 1901-7294

DCE Thesis No. 16

Department of Civil Engineering